An Investigation into the treatment and modelling of Municipal Solid Waste Incineration (MSWI) Air Pollution Control (APC) residues

Muhammad Umar Khalid

A thesis submitted in partial fulfilment of the requirements of the University of East London for the degree of Doctor of Philosophy

January 2019

Abstract:

Air Pollution Control (APC) residues from Municipal Solid Waste Incineration (MSWI) is considered a problematic hazardous waste, with no current viable reuse, within the UK. Therefore, it is often treated before being deposited into a landfill. This research explores a number of novel techniques to mitigate the hazardous properties of this waste by investigating thermal treatment and cold bonding. Thermal treatment was investigated to manufacture inert Light Weight Aggregate (LWA) by sintering APC residues with clay. The addition of 20% APC residue produced the highest fracture strength of 5.78MPa. Treatment through cold bonding was achieved using the geopolymerisation process. The developed material achieved a compressive strength of approximately 2.35 MPa. The data from the APC residues based geopolymer experimentation was used to develop a machine learning model to predict the compressive strength of the geopolymer.

In addition, it was observed through a comprehensive literature review, that complexities arising due to significant variations in the composition of the residue, makes it very difficult to produce a commercially stable product. Therefore, the research tackles this problem by developing an Artificial Neural Network (ANN) model to identify and classify different types of residues/ashes based on their chemical composition as determined by X-ray Fluorescence (XRF) spectroscopy. Overall this research showed that machine learning could be very beneficial to this field to determine the capabilities for various reuse applications for ash waste.

Keywords: Municipal Solid Waste (MSW), Air Pollution Control (APC) residue, Machine learning, geopolymerisation, sintering

Acknowledgement

I want to thank my parents for their great support.

I would also like to thank my director of studies Professor Darryl Newport and my supervisory team Dr Chloe Molineux and Dr Mihaela Anca Ciupala for their time, knowledge and invaluable guidance.

Muhammad Umar Khalid

January 2019

Table of Content

List of Figures

List of Tables

List of Equations

List of Abbreviations

Abbreviations	Definition
ADC	Analog to Digital converter
ANN	Artificial Neural Networks
APC	Air Pollution Control
APCFA	Air Pollution Control Fly Ash
AQC	Analytical Quality Control
CBA	Cost-Benefit Analysis
CBLA	Cold Bonded Light Weight Aggregates
CCIM	Cold Crucible Induction Melter
CLI	Command Line Interface
CNN	Convolutional Neural Network
CNS	Chinese National Standard
CPU	Central Processing Unit
CSH	Calcium Silicate Hydrate
DEFRA	Department for Environment, Food and Rural Affairs
DNA	Deoxyribonucleic acid
DNN	Deep Neural Network
ELU	Exponential Linear Unit

Abbreviations	Definition
ESP	Electrostatic Precipitator
FRP	Fibre Reinforced Plastic
GBFS	Ground Blast Furnace slag (GBFS)
GGBS	Ground Granulated Blast-furnace Slag
GUI	Graphical User Interface
HPC	High-Performance Concrete
IAWG	The International Ash Working Group
ICP-OES	Inductively Coupled Plasma Optical Emission Spectroscopy
IFA	Incineration Fly Ash
LED	Light Emitting Diode
LOI	Loss on Ignition
LWA	Lightweight Aggregate
MAE	Mean Absolute Error
MCA	Multi-Criteria Analysis
MEMS	Micro-Electro-Mechanical Systems
MIT	Massachusetts Institute of Technology
MLP	Multi-layer perceptron
MOSFET	Metal-Oxide-Semiconductor Field-Effect Transistors

Abbreviations	Definition
MSE	Mean Square Error
MSW	Municipal Solid Waste
MSWI	Municipal Solid Waste Incineration
NASH	Sodium Aluminosilicate Hydrate
OLS	Ordinary Least Squares
OPC	Ordinary Portland Cement
RMS	Root Mean Square
RMSE	Root Mean Square Error
RNN	Recurrent Neural Network
SAIL	Stanford Artificial Intelligence Laboratory
SELU	Scaled Exponential Linear Unit
SEM	Scanning Electron Microscopy
SGD	Stochastic Gradient Descent
SLP	Single Layer Perceptron
SVM	Support Vector Machine
TDS	Total Dissolved Solids
WAC	Waste Acceptance Criteria
XRD	X-Ray Diffraction

Abbreviations	Definition
XRF	X-Ray Fluorescence
ZVS	Zero-Voltage Switching

1 Introduction

This research will investigate the use of Air Pollution Control (APC) residues generated from the incineration of Municipal Solid Waste (MSW). MSW is generally defined as a waste produced within a municipality area, which is collected by local authorities (Periathamby, 2011). However, different countries have different definitions of MSW (Periathamby, 2011). In 2010, the definition of MSW was changed in the UK, from the one mentioned above to meet the EU Landfill Directive (Directive 2008/98/EC) requirements. The new definition states that MSW is household waste collected by local authorities as well as waste produced by businesses (commercial or industrial) of similar composition and nature, which may be or may not be collected by the local authorities (DEFRA, 2011, DEFRA, 2013). Generally, around the world, there has been an increase in MSW due to both increases in population and urbanisation (Periathamby, 2011, Chen, 2016); therefore it is critical to develop methodologies and strategies to deal with this problem. In Europe and the UK, waste is processed using a waste management hierarchy as defined by Directive 2008/98/EC to reuse, recycle, recover and then only it can be considered for landfill/disposal (Figure 1.1). This has had a positive influence on waste recycling in the UK, as in 2016, 45.2% of MSW was recycled (DEFRA, 2018b). In terms of recycling of packaging material, UK is exceeding the EU target by 11.4% as can be seen in Table 1.1.

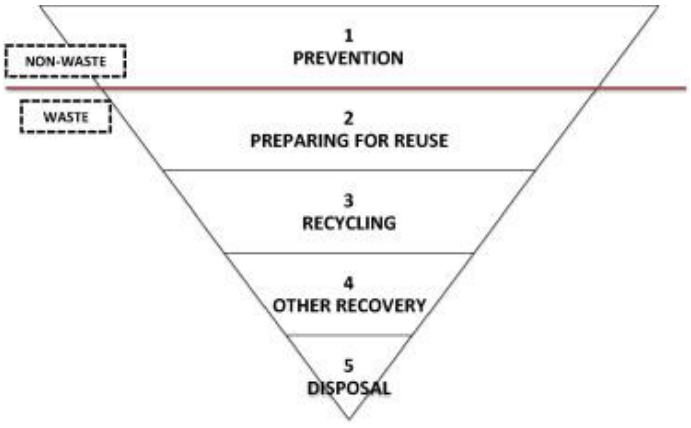

Figure 1.1: The waste hierarchy as defined by Directive 2008/98/EC (Gharfalkar et al., 2015)

Material	**Packaging waste arising (Thousand Tonnes)**	**Total recovered/ recycled (Thousand Tonnes)**	**Achieved recovery/ recycling rate (%)**	**EU target recovery/ recycling rate (%)**
Metal	736	506	68.7%	50.0%
of which: Aluminium	177	90	50.8%	NA
of which: Steel	559	416	74.4%	NA
Paper and cardboard	4,749	3,892	81.9%	60.0%
Glass	2,399	1,609	67.1%	60.0%
Plastic	2,260	1,015	44.9%	22.5%
Wood	1,310	405	30.9%	15.0%
Other materials	23	0	0.0%	NA
Total recycling	**11,476**	**7,427**	**64.7%**	**55.0%**
Energy from Waste	NA	767	6.7%	NA
Total recycling and recovery	**11,476**	**8,194**	**71.4%**	**60.0%**

Table 1.1: Shows the recycling rate in 2016 of packaging waste in the UK, (DEFRA, 2018b)

Increases in recycling have been a contributing factor to the reduction of disposal to landfill. However, the major factor influencing this decrease is the use of waste incineration plants. These plants can reduce waste by up to 90% by volume and 70% by weight (Li et al., 2017). Figure 1.2 shows that from 2001/02 to 2016/17 the rate of increase in waste incineration was much higher than the rate for recycling – hence supporting the above hypothesis.

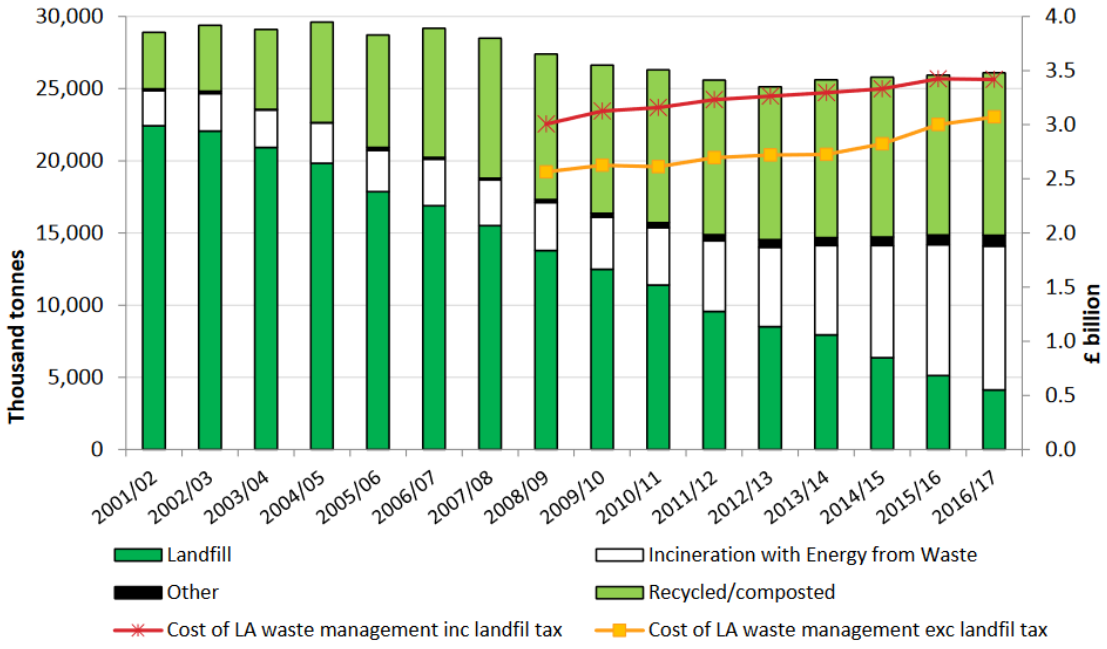

Figure 1.2: Waste management data for England from 2001/02 to 2016/17 (DEFRA, 2018a)

1.1 Incineration of Municipal Solid Waste (MSW)

Waste Incineration plants can exist with or without an energy recovery system. Incinerators with energy recovery systems are called Waste-to-Energy (WtE) plants (Malinauskaite et al., 2017). These plants recover heat energy from the incineration process and use it to generate electricity, and in a combined heat cycle it can heat water for industrial use as well as generating electricity. Incineration is one of the most widely used waste to energy (WtE) technology used for the treatment of Municipal Solid Waste (MSW) (Kumar and Samadder, 2017). It is the process of burning waste in the presence of excess oxygen in which carbon-based

compounds are decomposed into their inorganic mineral constituents by giving off heat (Malinauskaite et al., 2017). The first Municipal Solid Waste (MSW) incineration plant in England, U.K was built in 1876 (Yang et al., 2002). However, there were few challenges initially due to heterogeneous nature of the waste, as its composition varies greatly due to many different factors such as the origin of the waste, time of the year collected and even by the culture of the regional population (socio-economic) (Cheng and Hu, 2010). This variation in the composition can change the calorific value of the waste hence influence the energy output of the plant (Kathirvale et al., 2004, Komilis et al., 2012). After the initial challenges, incineration proved to be feasible (Rand et al., 2000).

A typical Waste to Energy (WtE) plant has a tank, furnace, gas cooling system, energy recovery system, flue gas treatment system, Air Population Control (APC) residue collection system and a chimney to discharge the fumes. Waste is stored in airtight tanks to stop oxidation of waste. This also stops dust and odour from escaping into the air. The waste from these large tanks is fed into the furnace. According to the European Directive 2010/75/EU incineration plants should be designed by taking into consideration that the combustion gases must at least reach the temperature of 850°C for 2 seconds to allow for the proper breakdown of organic toxins. The furnace aims to oxidise the waste using the combustion process. Formation of carbon monoxide and dioxin is prevented by ensuring the furnace is supplied with excess air to allow for at least 7% oxygen to ensure complete combustion of the waste (Celenza, 2000, Santoleri et al., 2000). The combustion of waste produces flue gases comprising of mainly Hydrogen Fluoride (HF), Nitrogen Oxides (NO_x), Carbon Monoxide (CO), Hydrogen Chloride (HCl), Sulphur Oxides (SO_x) and residual oxygen (O) (Williams, 1994, Beyene et al., 2018). These gases are produced due to waste comprising of compounds containing chlorine, hydrogen, carbon, nitrogen, sulphur and fluoride (Williams, 1994). The chemical equations of the process can be seen in Equation 1.1 and Equation 1.2.

$$C, H, Cl, F, S, N + O_2 \rightarrow CO + H_2O + HCl + HF + SO_2 + NO$$

Equation 1.1: Chemical reaction in an incinerator (Williams, 1994)

$$2SO_2 + O_2 \rightarrow 2SO_3$$

$$4HCl + O_2 \rightarrow 2H_2O + 2Cl_2$$

Equation 1.2: At lower temperatures, these reactions can take place through a catalyst or thermally (Williams, 1994)

The flue gases exiting the furnace reaches very high temperatures, but they must be cooled at the outlet of the furnace by the gas cooling system. This system consists of a heat exchanger, a water injection system and air dilution system. The heat exchanger allows the hot gases to heat the water or coolant in the heat exchanger which can be used to turn the turbines to generate electricity. After this, the temperature of the flue gases reaches between 400^{o}C which is further reduced to below 250^{o}C to 180^{o}C to reduce the formation of dioxins/furan (McKay, 2002). The cooling of the gases also allows condensation of most heavy metals and these can be collected in the form of finer particles by the filtration system (Zacco et al., 2014). The flue gases are filtered and treated before they are released into the atmosphere. A typical presentation of WtE incineration plant can be seen in Figure 1.3.

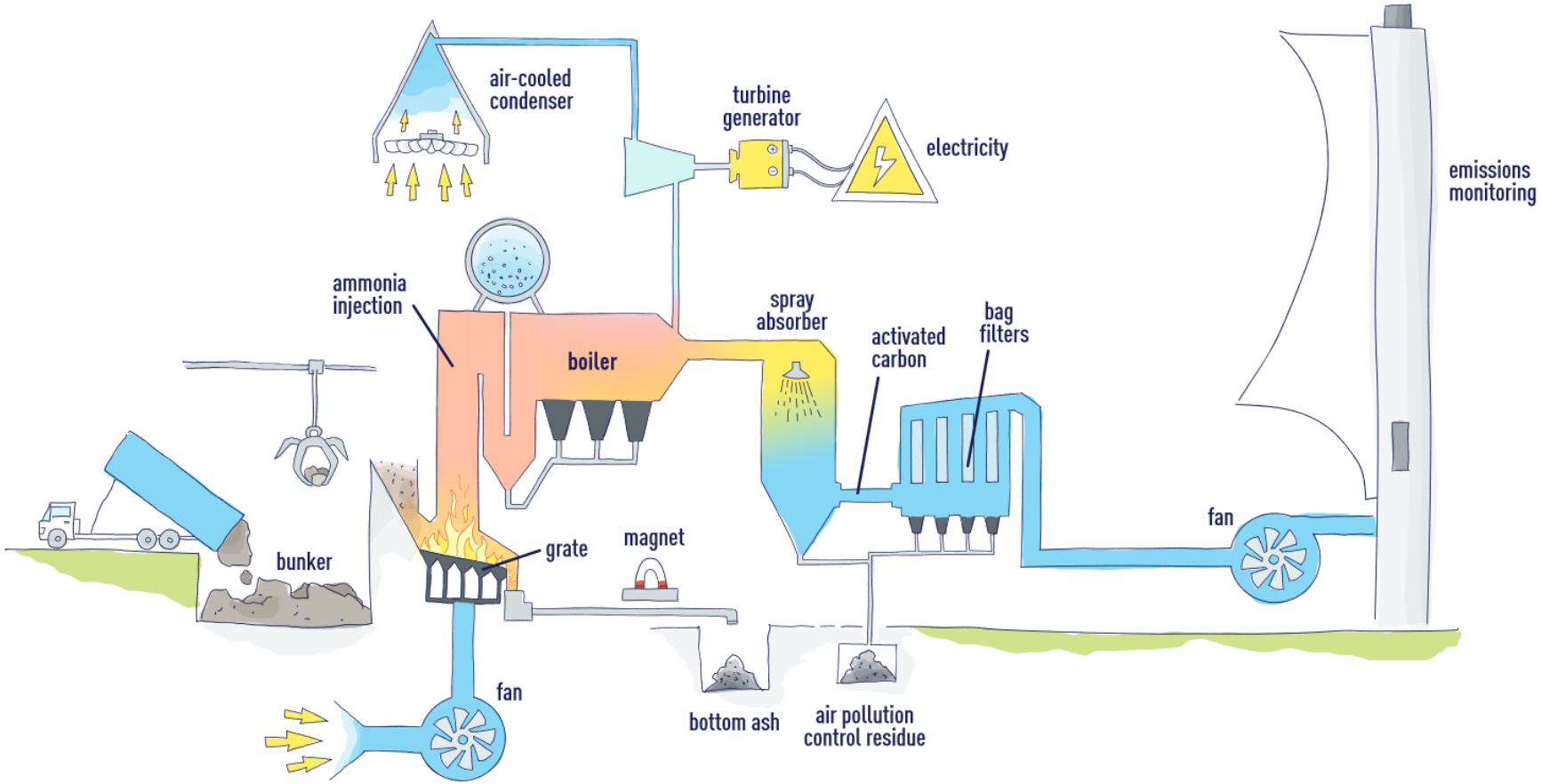

Figure 1.3: The incineration process (SUEZ Recycling and Recovery Isle of Man, 2018)

1.2 The waste output from the incineration of MSW

The incineration of MSW produces bottom ash that is a combination of grate ash and grate siftings from the furnace, heat recovery ash and Air Pollution Control (APC) residues that consist of fly ash and scrubber residue (Ecke et al., 2000). The graphical representation can be seen in Figure 1.4. However, bottom ash may also contain heat recovery ash depending on the design of the plant (Chimenos et al., 1999). APC residues are classified as hazardous waste according to the European Landfill Directive whereas bottom ash is classified as non-hazardous waste (Ginés et al., 2009, del Valle-Zermeño et al., 2013).

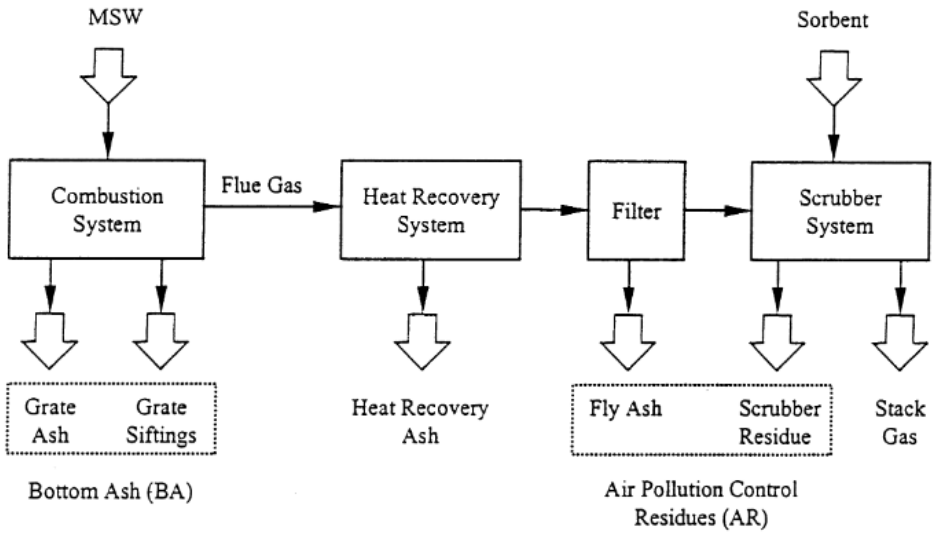

Figure 1.4: Types of Ashes produced by the MSW incineration process (Ecke et al., 2000)

1.3 Toxicity of MSW APC residues

APC residues are classified as hazardous and they can cause soil and water pollution if not managed properly and can have serious health risk to the environment and the humans (Amutha Rani et al., 2008a, Giusti, 2009, Lampris et al., 2009, Kumar and Samadder, 2017). The heavy metals, dioxins and furans present in MSW APC residues are very toxic to humans if ingested or inhaled as it can cause serious health issues (Rowat, 1999, Macleod et al., 2006, Kumar and

Samadder, 2017). The presence of heavy metals in APC residue can get into the bloodstream by coming in direct contact with the skin or can be transmitted through a cut (Plant et al., 2012). This can cause the formation of free radicals as heavy metal interaction in the body between free metal and the target cell, causing critical biomolecules (chromosomes, DNA, protein and lipids) oxidative damage (Ahamed and Siddiqui, 2007, Greim and Snyder, 2008). The effect of toxicity of these substances depends on many factors such as the absorption of the heavy metal compound, nature and duration of exposure (Aydın Ahmet and Aydın, 2016).

One of the major element that leach out from APC residues is lead (Jiao et al., 2016, Funari et al., 2017) and it can cause bladder, liver, heart and kidneys diseases (Miller, 2005). The central nervous system is also vulnerable to its exposure (Moon and Dermatas, 2007). Children are particularly very sensitive to lead as it can be effectively be absorbed into the bloodstream. The concentrations in the blood can affect the physical and mental development in children, which can cause difficulties in reading, learning and lower IQ. Low exposure of lead in blood levels (3.5 μg/dL) can increase the risk of heart diseases, and high exposure (23.4 μg/dL) can lead to prostate cancer (Ahamed and Siddiqui, 2007). At high concentrations of approximately 80 μg/dL, it can cause convulsions, coma and eventually death (Greim and Snyder, 2008). APC residues also contain other heavy metals, dioxins and furans those can be decremental to health as some are recognised as carcinogens, and its exposure can cause cancer (Allsopp et al., 2001). Therefore, it is very important to stabilise and dispose MSW APC residues properly.

1.4 Aims

This research aims to investigate treatment techniques to alter the physical and chemical properties of APC residues and also investigates the applicability of machine learning techniques to model APC residue-based material and to classify different types of ashes.

1.5 Objectives

- The research will investigate and characterise chemical composition of APC residue and conduct leaching test to compare it to Waste Acceptance Criteria (WAC) limits for hazardous waste within the UK.
- The change in physical and chemical properties can be achieved by using separation techniques, thermal treatments or solidification and stabilisation techniques (Chen et al., 2009, Gomez et al., 2009, Lam et al., 2010, Zacco et al., 2014, Lindberg et al., 2015, Sun et al., 2016, Toniolo and Boccaccini, 2017). The research investigates both thermal treatment and solidification/stabilisation using geopolymerisation.
- Machine learning has found a niche opportunity within the areas of material science and civil engineering. This has enabled scientists to develop innovative models those were not possible to develop using theoretical modelling techniques. The example of such models are: model to predict the compressive strength of High Performace Concrete (HPC) (Asteris et al., 2016, Jin et al., 2018a, Van Damme, 2018), model to predict the transition temperature of glass and steel (Nazari et al., 2011, Cassar et al., 2018, Chen et al., 2008, Liu and Cao, 2009), to predict the behavior of glass (its solubility) based on its composition (Brauer et al., 2007). The research will investigate the use of machine learning techniques to develop a model to predict the compressive strength of the APC residues based material and also classify different types of ashes.

1.6 Structure of the thesis

INTRODUCTION

Chapter 1 Introduction: This chapter identifies the potential of this research by defining the aim, objectives and structure of this thesis.

LITERATURE REVIEW

Chapter 2 Literature Review: This chapter provides a review of Municipal Solid Waste Incineration (MSWI) process, thermal treatment, cold bonding and machine learning.

PART 1 – EXPERIMENTAL TECHNIQUES

Chapter 3 Characterisation of Air Pollution Control (APC) residues: This chapter characterises Air Pollution Control (APC) residue using Inductively Coupled Plasma Optical Emission Spectroscopy (ICP-OES), X-Ray diffraction (XRD) spectroscopy, X-Ray fluorescence (XRF) spectroscopy and ion chromatography. It also looks at the leaching behaviour of APC residue.

Chapter 4 Thermal Treatment of APC residues: This chapter investigates sintering, pan pelletisation process and induction heating system.

Chapter 5 Solidification of Air Pollution Control (APC) residue using geopolymerisation: This chapter develops APC residues based geopolymer material using different solid to liquid ratios and sodium silicate to sodium hydroxide ratios.

PART 2 – MACHINE LEARNING

Chapter 6 Machine learning to predict the compressive strength of the geopolymer-based material: This chapter uses the results from chapter 5 to develop a model to predict the compressive strength of the geopolymer based material. The results from this model were then used to reformulate the geopolymer based material to re-evaluate the machine learning model.

Chapter 7 Identification of ash using Artificial Neural Network (ANN): The chapter develops and evaluates Artificial Neural Network (ANN) model to classify different types of ashes.

CONCLUSION

Chapter 8 Conclusion and recommendation for further research: The chapter provides an overall conclusion of the research and provides recommendations for further work.

2 Literature Review

This chapter will first review the ashes from Municipal Solid Waste Incineration (MSWI) process, heat treatment techniques, heating technologies and cold bonding techniques. Lastly, the chapter will introduce Artificial Intelligence (AI), machine learning, programming languages and its libraries.

2.1 Review of ashes from Municipal Solid Waste Incineration (MSWI)

There are many different definitions and terms used to identify ashes from Municipal Solid Waste Incineration (MSWI) process in research papers. According to a review paper by Dou et al. (2017) in one of the highest impact factor journals in the subject area - Renewable & Sustainable Energy Reviews (IF = 9.184) - incineration of Municipal Solid Waste (MSW) produces bottom ash and Incineration fly ash (IFA). However, according to the book by Chandler et al. (1997), part of The International Ash Working Group (IAWG), MSWI mainly produces bottom ash, grate siftings, heat recovery ash, fly ash and air pollution control residues. Many peer-review papers have used this naming scheme with few changes (Chimenos et al., 1999, Thomson, 2009, Abramov et al., 2018, Caprai et al., 2018). The definition of these ashes provided by Sabbas et al. (2003) and Reddy (2016) are as follows:

- Bottom ash is unburned organic and non-combustible coarse material collected from the combustion chamber in a cooling tank.
- Grate siftings is a fine powder collected at the bottom of the combustion chamber. This makes it very difficult to collect it separately from bottom ash; therefore, bottom ash contains grate siftings.
- Heat recovery ash or boiler and economiser ash: These are coarse particles collected from the heat recovery system.
- Fly ash is collected from flue gases before treatment.
- Air Pollution Control (APC) residues are fine particles collected after the treatment of flue gases.

The problem with a simplistic definition used by many review papers on the subject - stating that MSWI produces bottom ash and fly ash (Lam et al., 2010, Zhang and Hu, 2012, Jiao et al., 2016, Sun et al., 2016, Dou et al., 2017), is that it causes confusion because the flue gases produced by the MSWI require treatment before they can be released into the atmosphere. In literature, the effect of this unclear definition can be seen where researchers are trying to define or identify these ashes incorrectly by using many different names. For example: del Valle-Zermeño et al. (2013) states that MSWI produces bottom ash and APC residues which is a mixture of fly ash, organic pollutants and salts, but the paper uses words such as: APC fly ash, APC ash and APC residue interchangeably. Keppert et al. (2015) used the word MSWI fly ash to describe it as a combination of fly ash and APC residues, similar transposable words were also used by Colangelo et al. (2012) and Ferone et al. (2013). Ginés et al. (2009) used Air Pollution Control fly ash (APCFA). Examples of other peer-review papers are as follows:

Margallo et al. (2015) identified that MSWI produces three types of ashes: bottom ash, fly ash and APC residues. Whereas Rendek et al. (2006) specify that MSWI generates: solid residues, bottom ash and fly ash.

Funari et al. (2017) used the word untreated raw fly ash (FA-RAW) to distinguish from treated MSW fly ash. Some of the other instances of where MSWI fly ash or fly ash is used to refer to treated ash can be seen in the following peer-review papers: You and Ahn (2012), Ye et al. (2016), Tian et al. (2018) and Wang et al. (2016).

It can be seen that some researchers have used a very broad definition, but there are papers where further explanation is provided to better understand the origin of different types of ashes. For example, Allegrini et al. (2014) provides more information related to the types of ashes produced by the MSWI. This paper identifies that in the case of an energy recovery system the plant would produce boiler ash and bottom ash. Otherwise, it would just produce bottom ash. It also identifies fly ash and APC residues as ashes collected from the flue gas treatment system. The paper by Purgar et al. (2016) investigated four different incineration plants and was able to identify different streams of ashes produced, identifying the

following outputs: filter cakes, fly ash, slag, filter ash and boiler ash. It can be seen that the identification of ash is an issue in many peer-review papers, hence making it very difficult for future researchers to identify literature in the right subject area.

2.1.1 Flue gas treatment process

The chemical composition of MSWI APC residues mainly depends on the type of process that is used to treat the flue gases (dry, semi-dry, semi-wet or wet) and it also depends on the type of waste that is being incinerated - making the mineralogical composition of APC residues very complex and variable. The variation in the chemical composition of different types of ashes produced by MSWI can be seen in Table 2.1; therefore, it is important to understand the flue gas treatment process and ash collection system used in MSWI plants.

Element	Bottom ash (mg/kg)	Fly ash (mg/kg)	Dry-semi-dry APC residues (mg/kg)	Wet APC residues (mg/kg)
Al	22,000–73,000	49,000–90,000	12,000–83,000	21,000–39,000
As	0.1–190	37–320	18–530	41–210
Ba	400–3000	330–3100	51–14,000	55–1600
Ca	370–123,000	74,000–130,000	110,000–350,000	87,000–200,000
Cd	0.3–70	50–450	140–300	150–1400
Cl	800–4200	29,000–210,000	62,000–380,000	17,000–51,000
Cr	23–3,200	140–1100	73–570	80–560
Cu	190–8200	600–3200	16–1700	440–2400
Fe	4,100–150,000	12,000–44,000	2600–71,000	20,000–97,000
Hg	0.02–8	0.7–30	0.1–51	2.2–2300
K	750–16,000	22,000–62,000	5900–40,000	810–8600
Mg	400–26,000	11,000–19,000	5100–14,000	19,000–170,000
Mn	80–2400	800–1900	200–900	5000–12,000
Mo	2–280	15–150	9–29	2–44

Element	Bottom ash (mg/kg)	Fly ash (mg/kg)	Dry-semi-dry APC residues (mg/kg)	Wet APC residues (mg/kg)
Na	2800–42,000	15,000–57,000	7600–29,000	720–3400
Ni	7–4200	60–260	19–710	20–310
Pb	100–13,700	5300–26,000	2500–10,000	3300–22,000
S	1000–5,000	11,000–45,000	1400–25,000	2700–6000
Sb	10–430	260–1100	300–1,100	80–200
Si	91,000–308,000	95,000–210,000	36,000–120,000	78,000
V	20–120	29–150	8–62	25–86
Zn	610–7800	9000–70,000	7000–20,000	8100–53,000

Table 2.1: Chemical composition range of different types of ashes (Sabbas et al., 2003, Chandler et al., 1997)

2.1.1.1 Dry scrubbers

Flue gases enter directly into the reactor from the incinerator without being dedusted. These acidic gases are allowed to react with reagents such as lime (calcium hydroxide) or bicarbonate, to neutralise them. The reagents are pneumatically injected into the reactor in powdered form (Santoleri et al., 2000). The illustration of the process can be seen in Figure 2.1. The heavy metals and organic compounds are then adsorbed by activated carbon (Williams, 2005). This has a very low implementation and operational cost (Rogoff and Screve, 2011) but the neutralisation reactions are slow and require large amounts of reagents (Reddy, 2016).

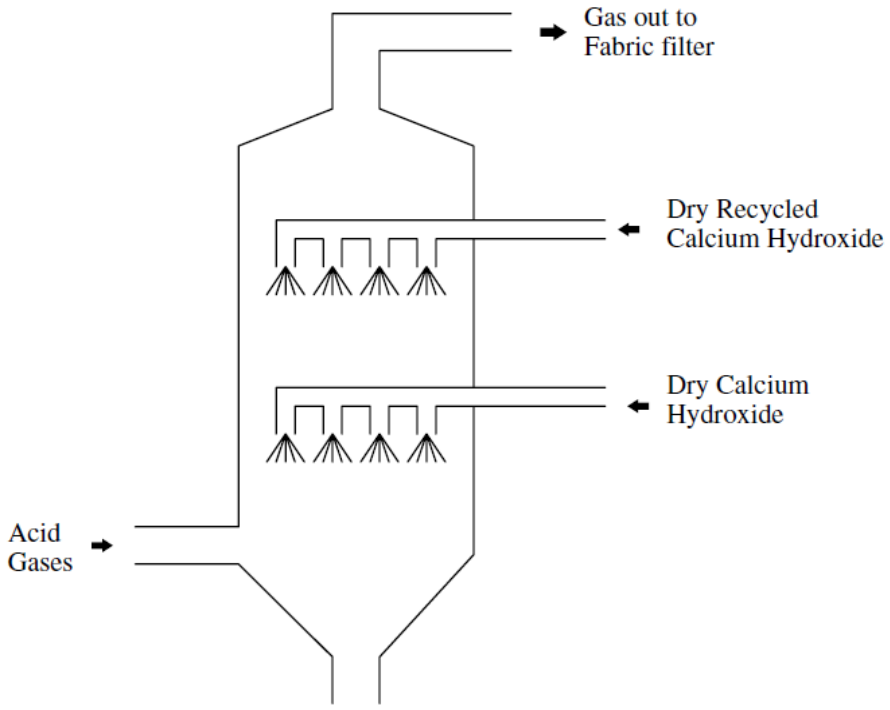

Figure 2.1: Shows the dry scrubber process (Williams, 2005)

2.1.1.2 Semi-dry scrubbers

Semi-dry scrubbers are very similar to dry scrubbers, but the main difference is that the flue gasses are treated by injecting droplets of calcium hydroxide (Williams, 2005). This process uses less reagent (by volume) than dry scrubber (Liu and Lipták, 1999) but the disadvantage of this process is that agglomeration of particles can occur leading to clogging of pipes and filtration units (Rogoff and Screve, 2011). The illustration of the process can be seen in Figure 2.2. After this, activated carbon is injected into the system and solid particles are removed from flue gases by a dust collector (ESP or baghouse) (Wang et al., 2004).

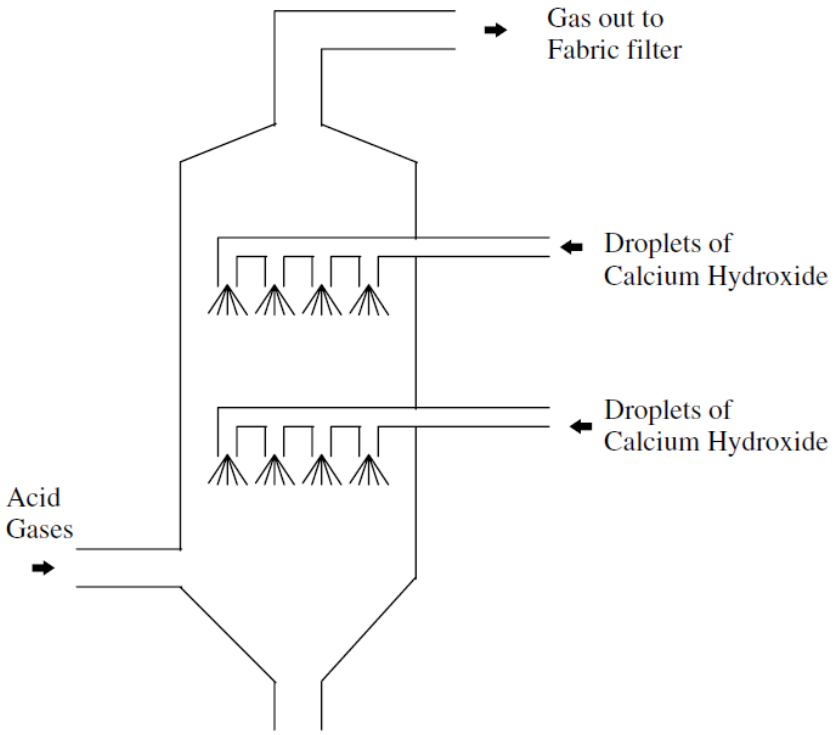

Figure 2.2: Shows the semi-dry scrubber (Williams, 2005)

2.1.1.3 Wet scrubbers

Flue gases are cooled down to about 60^{o}C, below their dew point and are then sprayed with water to condense the acidic gases into liquid. This causes hydrogen fluoride and hydrogen chloride gases to form hydrofluoric acid and hydrochloric acid (Williams, 2005). After this alkaline solution is used to neutralise it. This method can be very effective at removing heavy metals such as cadmium, mercury and lead (Liu and Lipták, 1999, Williams, 2005). This process is very expensive to install, and it uses a lot of water (Reddy, 2016) but has very high efficiency (Williams, 2005, Rogoff and Screve, 2011). The illustration of the process can be seen in Figure 2.3.

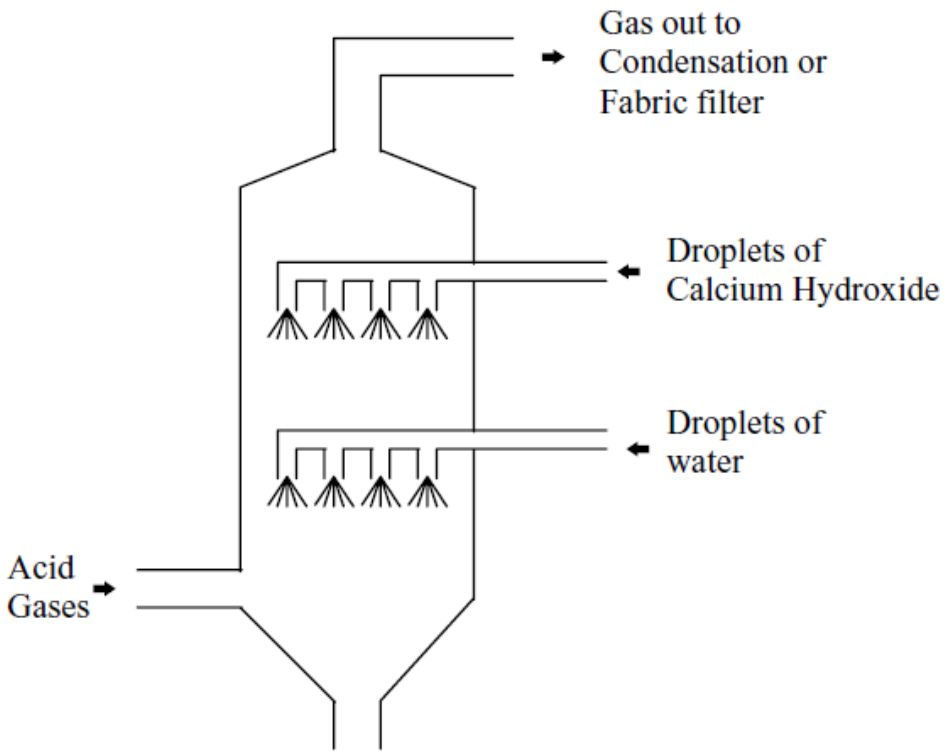

Figure 2.3: Shows the wet scrubber (Williams, 2005)

2.1.2 Ash collection system

The fine ash particles are collected using mainly cyclone filtration system, bag filter or electrostatic precipitator. The description of these systems are as follows:

2.1.2.1 Cyclone filtration system

The cyclone filtration system collects the particles by using centrifugal forces. The flue gases enter the system and are allowed to move in a circular motion, which forces the particles towards the walls and allowing them to be easily collected. The clean flue gases are allowed to escape up and out from the centre (Williams, 2005). This system is most effective at collecting particles larger than 15μm, but they are not very effective at particle size smaller then 15μm therefore, they are often used in conjunction with electrostatic precipitators or bag filtration system to allow greater control over emissions (Williams, 2005).

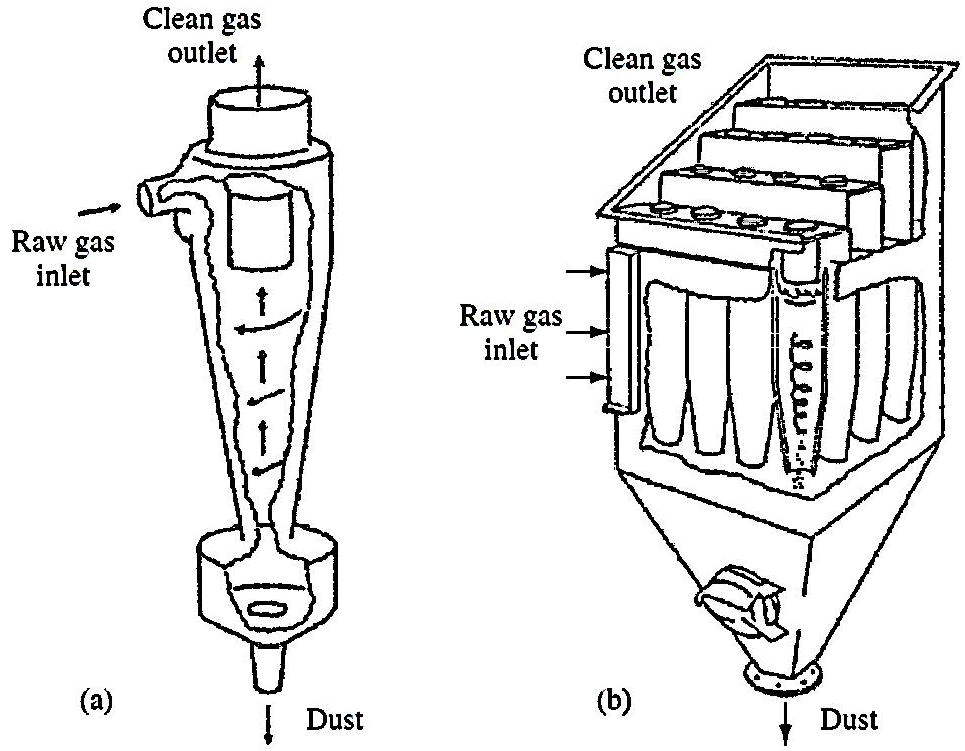

Figure 2.4: cyclone system (Williams, 2005)

2.1.2.2 Fabric filtration system

Fabric filters are the most common type of filtration system used to recover ash particles from the flue gases. They can be used on their own or with an electrostatic precipitator for greater control over the emission of fine particles (Williams, 2005). These filters consist of a porous material such as textiles, paper or ceramics (Heidenreich, 2013). These materials act like a macroscopic sieve through which flue gases are passed through to extract any ash particles, which are collected on the surfaces of these filters. The quality of the separation of ash particles depends on the macroscopic distance or porosity of the filtration material (Heidenreich, 2013). These filters can also be coated with catalyst or absorption agent to remove organic compounds such as furans and dioxins (Williams, 2005, Heidenreich, 2013). The particles are removed from the filters by compressed air. Typical fabric filtration system used in incinerators can be seen in Figure 2.5.

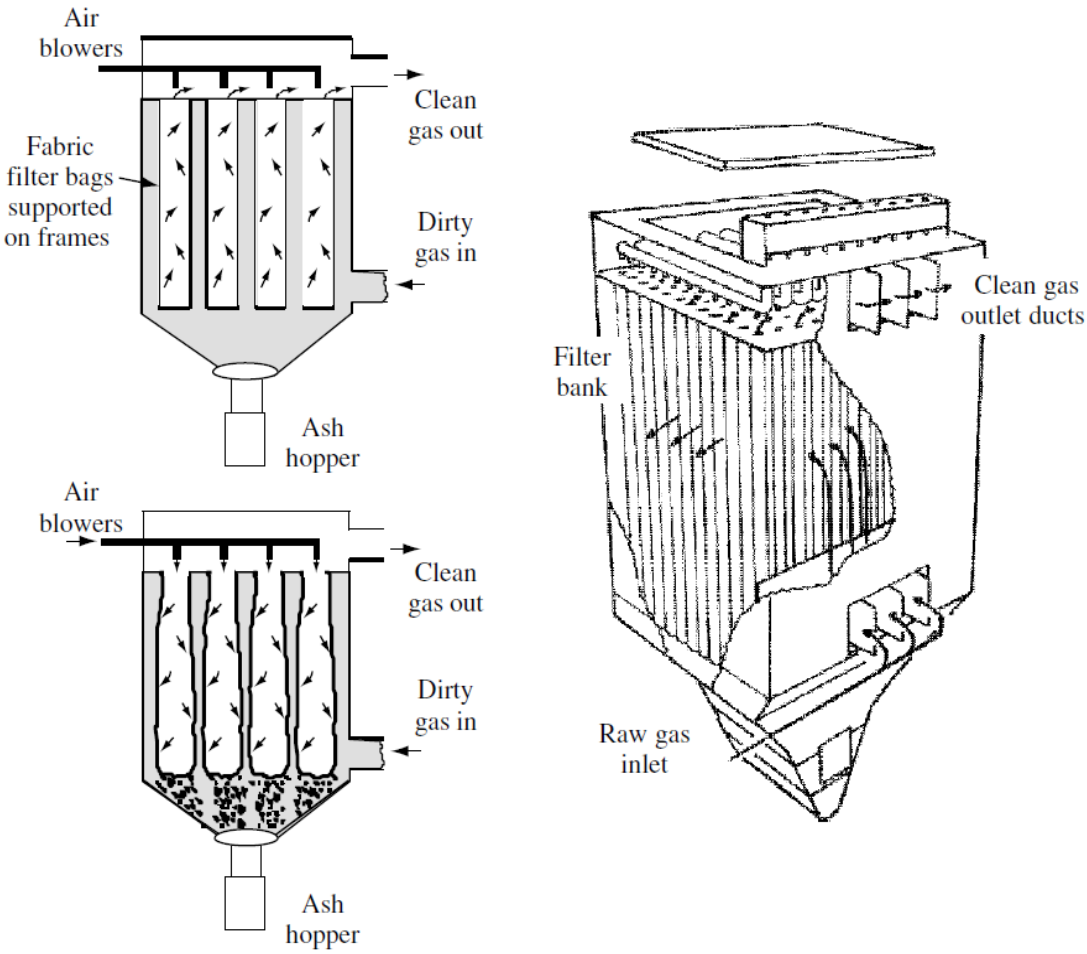

Figure 2.5: Typical fabric filtration system used in incinerators (Williams, 2005)

2.1.2.3 Electrostatic precipitators

They can operate from 35ºC to 850ºC (Intra et al., 2014). The primary function of electrostatic precipitators is to capture ash particles present in the flue gases, and they can capture particles up to submicron level, better than any other system defined above as can be seen in Figure 2.6. During this process particles are charged negatively by a cathode and then these negatively charged particles are passed through an array of positively charged plates (anode), causing these particles to be attracted by the anode as can be seen in Figure 2.7 and Figure 2.8. The particles are removed from the surface of the anode, mechanically by shaking these plates with hammers (Worrell et al., 2012). Electrostatic precipitators have

high voltage electrodes composed of a cathode and an anode, arranged in straight or profiled blades with a potential difference between them. They are arranged in this configuration to increase the surface area and mechanical strength of these electrode blades, which are typically charged at 50 kV (Williams, 2005). This system has a high removal efficiency of 97% to 99.5% (Williams, 2005, Intra et al., 2014).

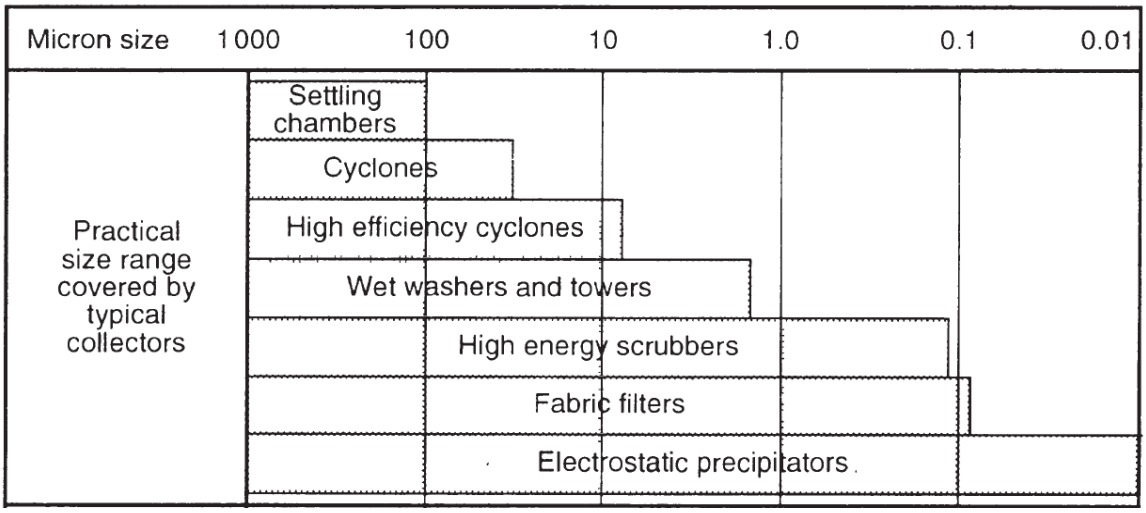

Figure 2.6: Effectiveness of a particle collection system in terms of particle size (Parker, 1997)

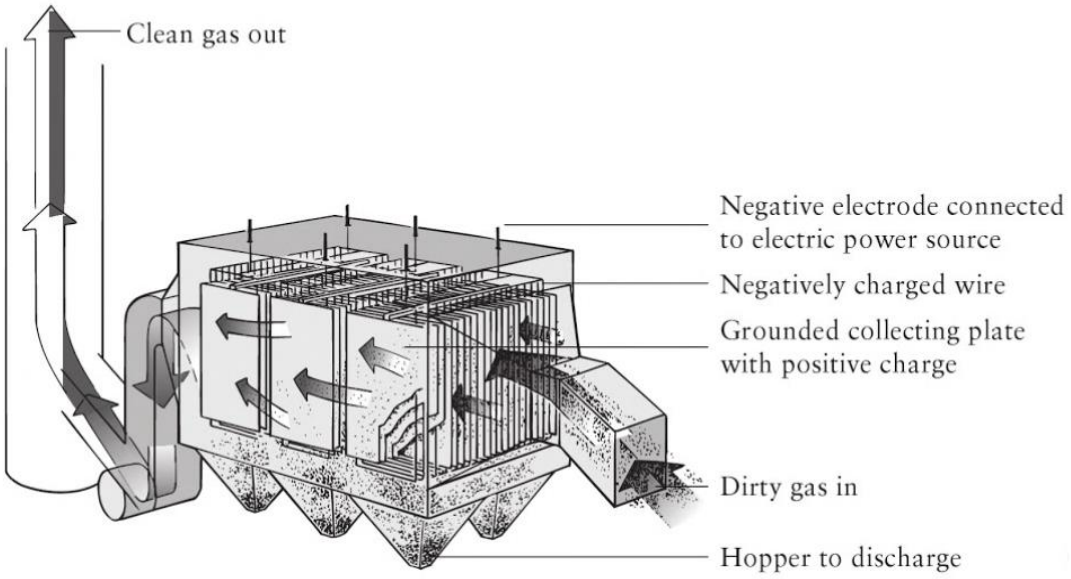

Figure 2.7: Electrostatic precipitator (Worrell et al., 2012)

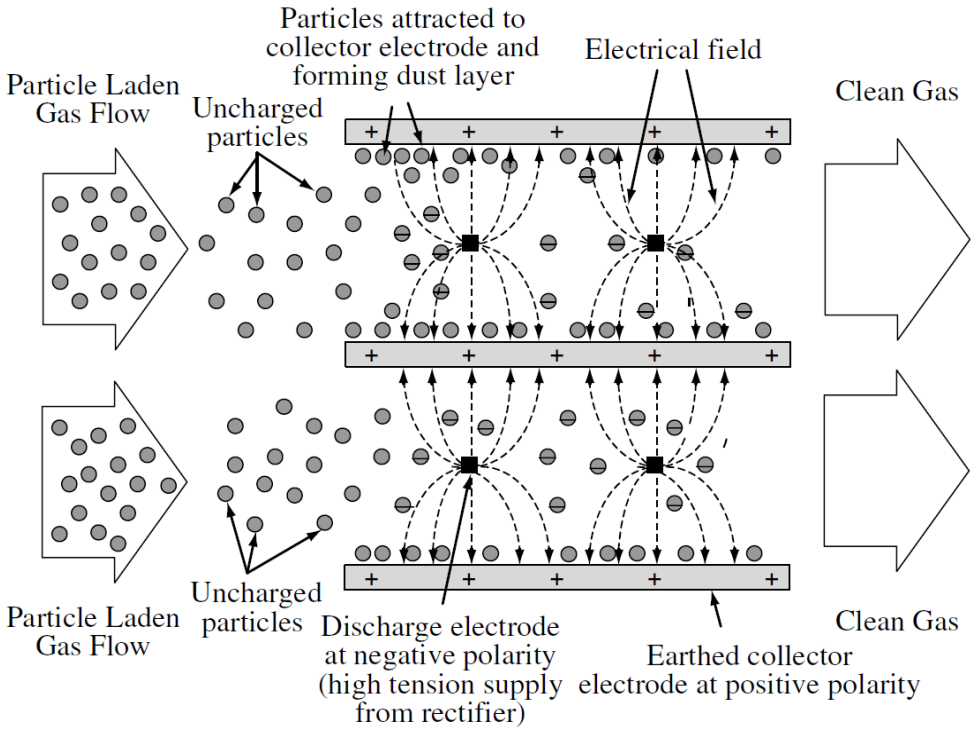

Figure 2.8: Operation of an electrostatic precipitator (Williams, 2005)

2.2 Review of thermal treatment of APC residues

Air Pollution Control (APC) residues can be thermally treated to improve its mechanical properties and resistance to leaching by densifying it into a more stable matrix. The use of high temperatures is also very effective at destroying dioxins and furans. According to the review paper by Lindberg et al. (2015) there are four different types of thermal treatment processes, and they are vitrification, melting, sintering and vaporisation/condensation. Vitrification is a process to produce glass which is amorphous in structure whereas melting is a process described by Lindberg et al. (2015) as being very similar to vitrification, but the outcome of the process is a solid that has an amorphous and crystalline structure and is produced without the addition of any additives. The temperature range for both these thermal treatment processes are very similar (ranging from 1200^{o}C to 1600^{o}C). During the sintering process, APC residues are heated just below their melting point to produce densified material, and lastly, Vaporization/condensation technique is used to extract volatile metals from the waste ash (Lindberg et al., 2015). In the

literature, there is another class of thermally treated materials, and those are called glass-ceramics. These class of materials are developed by heat treating the vitrified glass to change some of its amorphous glass structure into crystals; this improves its physical and chemical properties (Roether et al., 2010, Riello et al., 2001, Park and Heo, 2002, Han et al., 2018).

2.2.1 Vitrification

Vitrification is a process to produce glass. This process can be used to develop inert, stable ash based materials (Han et al., 2018) by integrating ash and glass forming agent (such as silica) to their melting points, around 1100^{o}C to 1500^{o}C. After this the material is rapidly cooled from a liquid to solid phase, resulting in a glassy product (Lindberg et al., 2015). This process encapsulates contaminants in a matrix and is therefore widely used as a thermal technique to stabilise hazardous wastes (Fei and Liu, 2016). The most commonly used glass forming agents are borosilicate and phosphate glass (Ojovan and Lee, 2005) but researchers have also investigated the use of other glass forming agents – like silica and alumina (Amutha Rani et al., 2008b). APC residues can be treated in this way, by using DC plasma arc technology to develop a glassy material using silica and alumina as additives at 1600^{o}C (Amutha Rani et al., 2008b). The process produces an inert material, but high energy requirement makes it unfeasible (Bingham and Hand, 2006). El-Alaily et al. (2018) recommends using glass cullet rich in silica to produce a stable material and discourages the addition of borax, indicating that the presence of sodium ions can interact with the leaching solution and can cause corrosion of the material. The paper also indicates that the presence of aluminium, calcium, iron, phosphorus and silicon ions in MSWI ashes can help in blocking the diffusion of corroding elements.

Furthermore, Guzmán-Carrillo et al. (2018) developed a glass by melting 58.5% coal fly ash, 31.5% metallurgical slag and 10.0% sodium oxide at 1450^{o}C in an electric furnace. Even though sodium oxide was used as an additive, it still managed to produce a non-hazardous glass. Wang et al. (2017) used a pilot-scale plant to produce vitrified material using MSW fly ash from bag filters. The plant

used a swirling melting furnace to vitrify the ash at 1400^{o}C and produced a non-hazardous dark amorphous material that can be used as a fill material in construction.

Although vitrification is a very effective technique to thermally treat waste materials. However, it is considered to be a very expensive processing technique due it being extremely energy intensive, and it also produces secondary ash. Despite being effective at transforming waste to non-hazardous in classification, the resultant material often has few applications (Wang et al., 2017, Astrup et al., 2016, Gomez et al., 2009, El-Alaily et al., 2018). It is possible to improve the properties of the vitrified material by further heat treating it to produce a glass-ceramic material (Yang et al., 2009, Amutha Rani et al., 2008b).

2.2.2 Glass-Ceramics

Glass-ceramics have better mechanical and chemical properties than standard base glass material. These types of materials have crystalline and glass (amorphous) phases (Marghussian, 2015) and are most commonly produced by using oxide-containing powdered glass, heating it to its transition temperature (temperatures just below its melting point) (Riello et al., 2001). This causes nucleation and at this stage devitrification of glass can be controlled to allow the formation of crystalline phases or both crystalline and amorphous phases (Cormier, 2014). The rate of cooling and the nucleation temperature controls the amount of crystallisation of the final glass-ceramic material (Cormier, 2014). It can occur homogeneously throughout the material or heterogeneously around the nucleating centre or on the surface of the material (Sen and Mukerji, 1999, Cormier, 2014). Different nucleating agents can also be added to control crystallisation - such as titanium dioxide, phosphorus pentoxide, zirconium dioxide and calcium fluoride (Zhu et al., 2018, Han et al., 2018); but titanium dioxide tends to be the most popular choice (Park and Heo, 2002, Yang et al., 2009).

El-Alaily et al. (2018) produced a glass using MSW ash and glass cullet, by heating it for 5 hours at 700^{o}C to burn off all the volatile compounds and organic residues. After this, the ash was heated to 1300^{o}C in a platinum crucible within an electric furnace for 2 hours. During this process, melted material is swirled in the crucible every 30 minutes to ensure the mixture is homogeneous and free of any air bubbles. Once ready, the glass is poured into a mould and annealed for 2 hours at 500^{o}C. Lastly, the material is allowed to cool overnight inside the furnace before being safely removed. The paper recommends using 30% glass cullet and 70% MSWI ash to produce the most stable material. Roether et al. (2010) produced a glassy material using DC plasma arc technology, APC residues, silica and alumina. The produced material was crushed and milled to produce a powder which was later pressed and sintered at different temperatures ranging from 750^{o}C to 1150^{o}C, producing a glass-ceramic. The research found that the best results (mechanical strength of 81MPa) were achieved at 950^{o}C. Devaraj et al. (2010) also used DC plasma technology to produce an inert glass and later used it to produce glass-ceramic tiles by pressing and sintering it to produce tiles with a very high flexural strength of 60MPa and a bulk density of 2.4g/cm^{3}.

Cheng et al. (2002a) used thermal plasma technology to vitrify MSW incinerated ash with subsequent heat treatments at 850^{o}C, 950^{o}C, 1050^{o}C and 1150^{o}C. The paper noticed that lower temperatures (850^{o}C and 950^{o}C) help produce better glass-ceramic material than higher temperatures. In a follow-on paper, Cheng et al. (2002b) vitrified MSW ash using an induction heating system in a graphite crucible for 20 minutes at 1400^{o}C followed by rapid cooling in water to produce glass. This was later sintered at many different temperatures (850^{o}C, 900^{o}C, 950^{o}C, 1000^{o}C and 1050^{o}C) for 2 hours to produce a glass-ceramic. The best compressive strength was achieved at 900^{o}C of 56.29MPa followed by 53.96MPa at 950^{o}C.

Yang et al. (2009) produced a glass-ceramic material using MSWI fly ash. The addition of iron slag and silica sand powder lowered the melting temperatures from 1500^{o}C to 1200^{o}C. The material was heated to 1200^{o}C for 2 hours and then was heated treated for 1 to 2 hours at 800^{o}C to 900^{o}C to produce a glass-ceramic material. Borax and sodium carbonate were used as a fluxing agent and titanium

dioxide as a nucleating agent. Even though Yang et al. (2009) were able to lower the melting point of the glass, the production cost of the produced glass-ceramics is still very high –therefore it is important to investigate sintering as it is a single stage process (thus more economical) to produce a densified material.

2.2.3 Sintering

Sintering is a thermal process during which the material is heated, below its melting point for several hours and then it is allowed to cool slowly. The synthesis cycle must be long enough to allow enough time for crystals to multiply and grow (Lindberg et al., 2015). This reconfigures the chemical structure of the sintered material to densify it. Sintering causes the formation of a crystalline structure composed of one or more mineral phases with different crystal sizes. The properties of the sintered material depend on the initial composition, temperature and the type of bonds formed during the heating process. The temperature range typically used for sintering APC residues is between 700^{o}C to 1200^{o}C (Lindberg et al., 2015). The sintering process can be used to produce ceramic tiles, glass ceramic or lightweight aggregates (Quina et al., 2008, Lindberg et al., 2015). Ceramic materials are dielectric - those do not allow electricity to flow through them, as electrons are trapped in the ceramic structure – hence making them very good insulators. They are also very resistant to extreme temperature variations; unlike glass that can break/crack with sudden changes in temperature. The properties of ceramics can be improved by applying pressure. This densifies the material, reduces the porosity and improves the compressive strength of the material (Devaraj et al., 2010).

2.3 Review of heating technologies

The material such as APC residues can be melted, sintered or vitrified in a furnace. There are mainly two classes of furnaces and they are fuel burning-based furnaces and electric furnaces. These two classes can be further expanded depending on the type of technology employed by the furnaces. The electrical furnace technologies are summarised below but for the purpose of this research electrical resistance furnace (muffle furnace) technology and induction heating system will be explored further (Sakai and Hiraoka, 2000, Ecke et al., 2001, Colombo et al., 2003, Gomez et al., 2009, Lindberg et al., 2015):

- Electrical resistance furnace: This furnace provides indirect heating by radiation and convection to heat the material, and an example of such a furnace is a muffle furnace.
- Electric arc furnace: These types of furnaces generate heat by producing an electric arc between two electrodes to heat the material.
- Plasma heating furnace: This technology can achieve very high temperatures of up to 20,000^{o}C - much higher than any other type of furnaces. The plasma in the furnaces can be generated by using RF inductively coupled discharge technology; DC transferred arc plasma torches or DC non-transferred arc plasma torches.
- Cold Crucible Induction Melter (CCIM): This technology uses electromagnetic waves to induce heat in the material directly or can be configured to heat material indirectly. It has been used to develop metal alloys and has been very effective in producing them using reactive metals such as tantalum (Morita et al., 2000, Sugilal et al., 2016). It has successfully been used to stabilise nuclear waste and is considered to be very effective because it can heat the waste directly to produce a glass ceramic (Crum et al., 2014, Vernaz and Bruezière, 2014). Therefore, an induction heating system was developed to investigate its effectiveness to solidify/stabilise APC residues.

2.3.1 Introduction to induction

Materials can be either heated indirectly by the source or be influenced to heat directly (Chindris and Sumper, 2012). In an indirect method of heating, a sample is placed in proximity to the source of heat energy; whereas direct method allows for the material to be influenced or subjected to generate heat directly, making this method of heating more efficient as it eliminates losses generated by indirect transmission of heat from the heat source to the sample (Chindris and Sumper, 2012).

One of the methods to generate direct and indirect heat is by using a process called induction. Induction is used in large applications to melt metals in furnaces as it allows the user to heat the material directly, and in small applications induction is used to make induction cooking hobs relying on an indirect method of heating. Induction heating is widely used in the food industry to seal tin lids as well as being used for melting and welding metals (Rudnev et al., 2017). Michael Faraday laid the foundation of electromagnetic induction, whereby heating is a direct application of two physical laws, Lenz's law and the Joule effect. Lenz’s law states that the rate of change of flux induces electromotive force and the Joule effect causes the material to heat up when an electrical current is passed through the conductor due to the resistance of the conducting material (Serway and Vuille, 2011). The induction heating process is different from conventional resistive heaters because the heat energy is not transferred to the material through a thermal gradient, but is directly generated in the material by using the alternating magnetic field (Haimbaugh, 2015). Induction only works on conductive materials those are inserted in an alternating magnetic field that is generated by passing a current through a coil producing electromagnetic waves in the vicinity of the coil (Prytz, 2015). These electromagnetic waves influence the conductive material to heat by causing resistance to the magnetic oscillations, causing molecules to rub against each other and thereby creating heat (Serway and Vuille, 2011). The heat generated by the induction heating system depends on the eddy current and losses due to the hysteresis effect.

2.3.2 Hysteresis losses

Losses due to the hysteresis effect are dependent on the hysteresis loop for each material. Strong magnetic materials have broad hysteresis loops, and soft magnetic materials have a narrow hysteresis loop as can be seen in Figure 2.9. The broader the hysteresis loop, the higher the loss (Hurley and Wölfle, 2013). The loss of energy per cycle per volume (P_h) can be calculated using Steinmetz's equation shown in Equation 2.1. This shows that magnetic materials help generate more heat when warmed using an induction heating system.

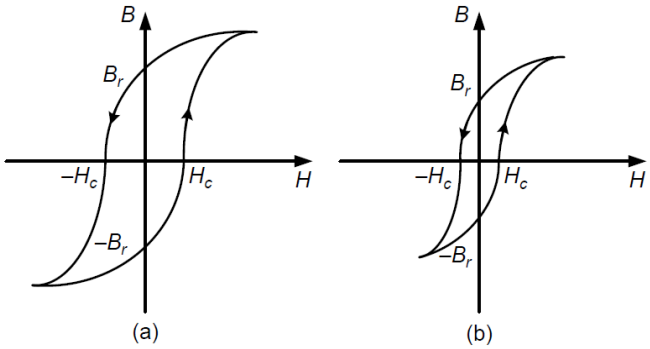

Figure 2.9: Hysteresis loop of hard magnetic material (a) and soft magnetic material (b) (Hurley and Wölfle, 2013)

$$P_h = K_c f^{\alpha} B_{max}^{\beta}$$

$K_c =$ Core loss coefficient

$\alpha =$ Frequency constant

$B =$ Peak magnetic flux density

$\beta =$ Magnetic flux density constant

Equation 2.1: Steinmetz equation (Hurley and Wölfle, 2013)

2.3.3 Eddy current

The alternating magnetic field causes conductive materials to release free electrons, making the field to move in a circular motion (Haimbaugh, 2015). This motion is called eddy current, and it causes loss of energy hence causing the

conductive material to heat up. The eddy current is a big issue in electrical transformers. Therefore, the core of the transformer is divided into several parts to isolate one from the other restricting the space for electrons to move (Lopez-Fernandez et al., 2012). As electrons cannot move in a circular motion over a large area. This reduces the Eddy current, but in an inductive heating application, it is important to increase the Eddy current to help heat the conductive material to high temperatures. The power dissipation (P_e) due to Eddy current can be calculated using Equation 2.2.

$$P_e = kB_{max}^2 f^2 t^2 V$$

$f = \text{Frequency}$

$k = \text{ Eddy current constant}$

$t = \text{ Thickness of the material}$

$V = \text{ Volume of the material}$

Equation 2.2: Power loss due to eddy current (Saxena, 2010)

2.3.4 Benefits of induction heating

The main advantage of induction heating is that it can heat the material directly as everything else around the material is cooler hence reducing the loss of heat dissipation through transmission making it very energy efficient (Tsai et al., 2009). It can instantaneously heat the material to very temperatures and can be designed to heat a specific area of the material without affecting the surrounding areas (Rudnev et al., 2017). The depth of penetration of heat and its intensity can also be controlled (Blazynski, 1993). It is also possible to control chemical reactions on the surface of the material by developing an inert atmosphere around the material, reducing material degradation (Tsai et al., 2009).

2.4 Review of Cold bonding techniques

Cold bonding is the term used to describe a material that can set/cure at temperatures ranging from 10ºC to 100ºC (van der Wegen and Bijen, 1985, Matthys, 1990, Wesche, 2004) to form a matrix that has the ability to hold itself together into a desired shape and size (Matthys, 1990, Wesche, 2004). Some researchers have specified higher temperature ranges; with the formation of the material occurring at temperatures ranging from room temperature to 250ºC (Pels and Sarabèr, 2011). However, it is most commonly accepted that the temperature range from 100ºC to 200ºC is called hydrothermal and cold bonding temperature range is as stated, between 10ºC to 100ºC (Matthys, 1990, Wesche, 2004). Temperature range greater than 900ºC is considered as sintering.

2.4.1 Solidification/Stabilisation

Treatment through solidification/stabilisation is one of the most popular methods used in the industry, and it is considered as non-destructive method of treatment – as it does not reduce or eliminate the number of hazardous compounds present in the waste, instead the technique encapsulates, absorbs or changes the physicochemical makeup of the hazardous waste by chemically binding it into the matrix. This stabilisation makes it less soluble to the environment; as it changes the surface area, volume, porosity and permeability of the material through which hazardous compounds can leach out hence limiting the solubility and mobility of the hazardous compounds (Van Jaarsveld et al., 1997, Colangelo et al., 2015, Kim, 2015, Silva et al., 2017). The concentrations of pollutants in the treated waste are also often lower than the untreated waste because this process tends to dilute the compounds with the additional reagents, such as hydraulic binders (the most common being cement or lime) (Nochaiya et al., 2010, Yoon et al., 2010, Singh and Pant, 2006). Resistance to leaching of the final output product depends on the number of contaminants present, as well as the type of binder used to stabilise it (Gesoğlu et al., 2007, Colangelo et al., 2015, Tang and Brouwers, 2017).

Cold bonding is regarded as an ideal technique to achieve Solidification/Stabilisation of hazardous waste materials (Colangelo et al., 2015) as the method uses additives or binders to physically and/or chemically immobilise hazardous compounds present in the waste (Van Jaarsveld et al., 1997). Air Pollution Control (APC) residue waste could, therefore, be an ideal candidate for cold bonding treatment. Due to the presence of high levels of toxic compounds, those are thermodynamically unstable under ambient conditions due to it being produced under high-temperature conditions (Wächter and Ionel, 2013). This means that it changes its mineralogical and physicochemical properties to reach thermodynamic equilibrium with its surrounding environment (Wächter and Ionel, 2013). Therefore, it is essential to treat APC residues waste before depositing it to landfill. Up to now, this has been widely achieved by using hydraulic binders, such as cement (Chen et al., 2009), which does not completely stabilises the material but reduces the leaching of heavy metals by forming a solid matrix of very low permeability (Chen et al., 2009). However, the solids obtained retain their polluting potential, making this technique far from optimal, but it is used because it is among the least expensive and most simple to implement. Methods such as sintering and vitrification use high temperatures, hence making them expensive to implement (Chen et al., 2009, Guo et al., 2017) and thus not environmentally or economically sustainable. Therefore, if cold bonding could be successfully implemented on APC residue wastes, not only would it be energy efficient, but the resulting product would also be very cost-effective to produce.

2.4.2 Solidification/Stabilisation using Ordinary Portland Cement (OPC)

Ordinary Portland Cement (OPC) mainly consists of the compounds, di-calcium silicate and tri-calcium silicate, which help it to develop strength (Bye, 1999). The chemical formula for di-calcium silicate is $(CaO)_2 \cdot SiO_2$, but in cement, chemistry notation is simplified to C_2S. The symbolic notation commonly used in cement chemistry is shown in Table 2.2.

Oxide	CaO	SiO_2	Al_2O_3	Fe_2O_3	H_2O	Na_2O	K_2O	SO_3	MgO	CO_2
Chemistry notations	C	S	A	F	H	N	K	$\bar{S}$	M	$\bar{C}$

Note: These notations will be used interchangeably with a chemical notation in this chapter when referring to cement and geopolymer chemistry.

Table 2.2: Symbols used in cement chemistry (Bye, 1999)

OPC reacts with water to hydrate the cement and form a paste that cures by absorbing carbon dioxide. It is possible to add additives to OPC to help it achieve higher or lower compressive strength, depending on the type and percentage of additive used in the formulation. For example, to make concrete - sand and crushed stones are typically added. It is also possible to add any additional materials containing CaO and/or SiO_2 - such as fly ash, Ground Granulated Blast-furnace Slag (GGBS), silica fume or calcined clay (Siddique and Khan, 2011). Mixing cement with other materials (such as those mentioned above) can significantly improve/enhance the mechanical properties of the cement.

The incorporation of cement into APC residues can be an effective solution to immobilisation heavy metals as it can react with calcium oxide and alkali metal hydroxide when mixed to form a curing paste (Guo et al., 2017). The heat generated by the hydration of OPC is an important factor in the initiation of the reaction. During the curing stage, APC residues particles fill the spaces between the cement particles; this effect reduces the permeability which influences the strength of the cement - as low permeability means high durability. The permeability of concrete is influenced by many factors; such as the amount of

cementitious material, water content, particle size, consolidation and curing conditions (Chen et al., 2009).

The effect of APC residues on the relative strength of the cement can be predicted by determining the quantity of calcium hydroxide and silicate present. High amounts of calcium hydroxide can have adverse effects on the strength of the cement composite because calcium hydroxide forms a fragile crystalline structure leading to weak concrete. Whereas high silicate contents can have a positive impact on the compressive strength because it can increase interfacial bond strength to help produce concrete with good mechanical properties (Wong et al., 1999). Pan et al. (2008) developed a cement using MSWI ashes and OPC that met the requirement of Chinese National Standard (CNS) of Type II OPC; but the cement setting times were longer. The paper suggested that this was due to the issues with salt contents in MSWI fly ash and bottom ash when they are used as cement additives, but that this can be remedied by washing the ash with water or acid prior to use. Despite this, the paper only recommends the addition of 1.75% MSWI fly ash (APC residues) and 3.5% of bottom ash for the best results. Most recently, Yang et al. (2018a) investigated the use of washed MSWI fly ash and bottom ash as a supplementary cementitious material. The results of the research indicated that they could be used successfully in cement, at 20wt% to 40wt% replacement volumes, with economic and environmental benefits. Although MSWI ash does have cementitious properties but it was noticed that the compressive strength of the cement composite decreases as the percentage of MSWI ash increases, as can be seen in Figure 2.10. The researchers also observed that washed MSWI ashes had adverse effects on the compressive strength of the cement composite as compared to unwashed additions. According to Yang et al. (2018b), the compressive strength of cement composite prepared using 30wt% MSWI fly ash decreased the compressive strength by lowing the proportion of formation of the CSH phase.

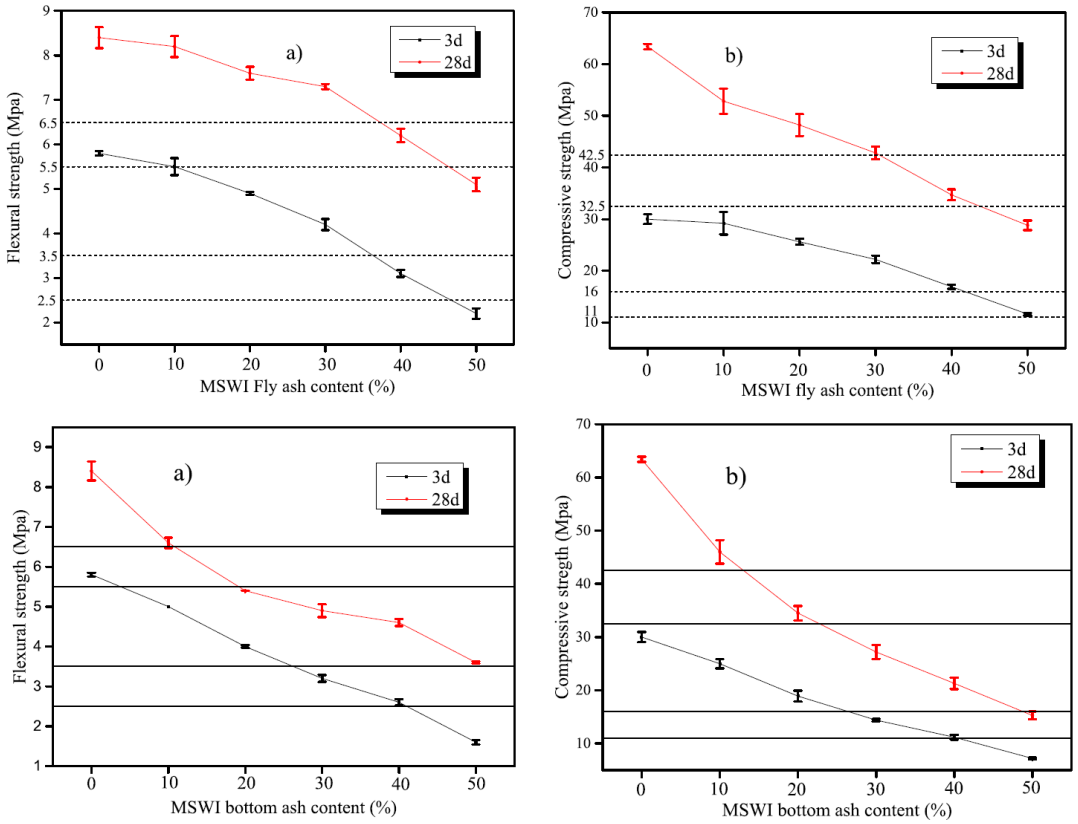

Figure 2.10: Compressive strength of MSWI fly ash and MSWI bottom ash, used as an additive in cement – from Yang et al. (2018a)

Although APC residues can be used in the production of concrete, it does have some potentially serious disadvantages, such as low resistance to climate change with toxic heavy metal compounds that can leach out, causing a risk to the environment (Formosa et al., 2017). According to Lederer et al. (2017), the addition of MSWI into cement increases the leaching of lead and cadmium by 170% and 310% respectively, and he suggests that a 22% addition of MSWI should be considered as too high for cement production. In terms of sustainability and environmental problems, cement itself is an issue as it uses a lot of energy in the production of lime (CaO) from calcium carbonate ($CaCO_3$), hence contributing to the production of carbon dioxide (Mellado et al., 2014). Therefore, this research will investigate the cold bonding of APC residues using a geopolymerisation process, as it can reduce the production of carbon dioxide (as can be seen in Figure 2.11).

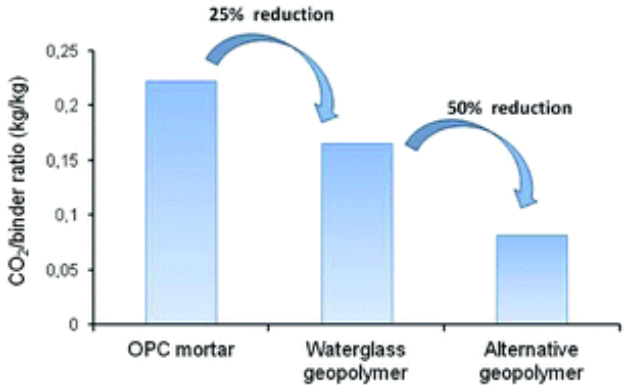

Note: The alternative geopolymer mentioned uses rice husk ash as an alternative to waterglass (Sodium Silicate)

Figure 2.11: Comparison of carbon dioxide produced by OPC mortar and geopolymerisation process from Mellado et al. (2014)

2.4.3 Geopolymers

The word geopolymer was first used by Davidovits in 1979 to describe alkali silicate activated material developed using metakaolin (calcined kaolin clay) (Davidovits, 2008). Since then many different types of geopolymer based materials have been developed using silica and alumina rich powdered material such as: fly ash from coal, red mud, slag and bottom ash (Duxson et al., 2007, Davidovits, 2008, Onori et al., 2011, Toniolo et al., 2018). Geopolymers are formed by the addition of strong alkaline agent into silica and alumina rich material causing the formation of aluminosilicate gel, which cures to form a three-dimensional tetrahedral structure of silicates and aluminates those are insoluble in water (Wagh, 2005, Provis and Van Deventer, 2009). They are inorganic polymers those exhibit cement-like properties and can replace Ordinary Portland Cement (OPC) in a number of different applications (Zheng et al., 2011). These materials are considered to be more sustainable as compared to OPC because the production of OPC releases high levels of carbon dioxide to produce calcium oxide from calcium carbonate (Heath et al., 2013, Mellado et al., 2014, Toniolo and Boccaccini, 2017). The presence of calcium oxide is vital for cement as it forms the CSH gel during curing which creates a hard cement matrix. Whereas geopolymers do not require CSH gel to cure and harden instead they rely on aluminosilicate gel to cure, which can be formed using alkaline activators, such as sodium hydroxide and sodium silicate (Mellado et al., 2014, Toniolo and Boccaccini, 2017).

There are many recent publications related to the geopolymerisation of fly ash from coal and sewage sludge (Zacco et al., 2014, Chakraborty et al., 2017, Chen and Poon, 2017, Chen et al., 2018) but these ashes have large amounts of amorphous alumina and silica which can be the source of aluminosilicate to help produce geopolymer-based material by using alkaline activators (Toniolo and Boccaccini, 2017, Chen et al., 2018). A review paper on bottom ash from MSWI by Silva et al. (2017) indicates that it is possible to achieve high strength using this waste ash because it contains high levels of silica and alumina (as compared to APC residues). Similarly, Gao et al. (2017) developed a geopolymer using granite powder, slag, sand and MSWI bottom ash and achieved a compressive strength ranging from 20 MPa to 70 MPa. The alkaline activator used in this study was a mixture of sodium silicate and sodium hydroxide. According to this research, bottom ash negatively affected the strength of the geopolymer whereas granite powder acted as a filler. However, there are very few papers on the geopolymerisation of Municipal Solid Waste incineration (MSWI) APC residue.

2.4.3.1 Benefits of geopolymers

Geopolymer based materials are usually manufactured at room temperature - hence making them economically favourable. They also have good resistance to high temperatures and are also highly durable (Davidovits, 2008). Some of the other benefits of geopolymer-based materials are that they can withstand aggressive conditions for several months much better than OPC – in terms of its physical and chemical properties. These materials are very resistant to chemical attack and have great potential to immobilise toxic heavy metals in their matrix, as they form a very insoluble material that is able to encapsulate heavy metals. Luna Galiano et al. (2011) investigated MSWI fly ash and found that the developed geopolymer based material was very effective at immobilising heavy metals. The study investigated different combinations of alkaline activators (sodium silicate, sodium hydroxide, potassium silicate and potassium hydroxide) and five different materials (coal fly ash, MSWI fly ash, kaolin, metakaolin and GBFS) at different percentages to form a matrix to encapsulate the heavy metals. The compressive strength achieved was between 1 MPa to 9 MPa, and the samples were tested

after 7 and 28 days respectively. According to Li et al. (2014) leaching of zinc, lead and cadmium present in MSWI fly ash can be reduced significantly by the addition of 20% silica fume that can be added as a source of silicate in MSWI fly ash. Silica fume mainly contains amorphous silicon dioxide and provides a large surface area, making it an effective pozzolanic material. Pozzolanic materials are silica and/or alumina based material those may exhibit cementitious properties in the presence of calcium hydroxide and water (Ramezanianpour, 2013). It is effective because during hydration it can be converted into more stable compounds. The reaction between pozzolanic materials (such as silica fume) converts heavy metals into insoluble hydroxides and complex silicates as they are encapsulated in the CSH matrix. Nikolić et al. (2018) also investigated leaching by adding 4% lead nitrate to coal fly ash based geopolymer and conducting leaching tests in accordance with the European standard EN 12457-2 followed by a compressive test. The alkaline activators used in this research were a mixture of sodium silicate and sodium hydroxide. It was noticed that leaching of lead reduces as the compressive strength of the geopolymer increases and geopolymer matrix was successfully able to immobilise 4% addition of lead, after being cured for 28 days at room temperature in a humid chamber (with humidity greater than 90%).

Another paper by Lancellotti et al. (2010) developed a geopolymer using Metakaolin that had a SiO_2 to Al_2O_3 ratio of 1.5 by weight. Metakaolin was made by the calcination of kaolinite for 4 hours at 700^oC. Metakaolin was mixed with 20% fly ash (FA) extracted from an electric filter and an ash fabric filter. Sodium silicate in the experiment was prepared by mixing SiO_2 and Na_2O with a molar ratio of 3:1. The complete formulations used in the paper is shown in Figure 2.12. This paper only investigated the leaching behaviour of the geopolymer, and it concluded that leaching of the heavy metals could be reduced by using a geopolymer to immobilise heavy metals.

	Metakaolin MK (g)	Fly Ash FA (g)	Sodium hydroxide (g)	Silicate (g)	H_2O (g)	Si/Al	Na/Al	H_2O/Na
GP[a]	51	0	7	52.7	7	1.9	0.99	11.1
GPEF20[b]	51	10.2	6.5	52.7	7	1.8	0.98	11.5
GPFF20[c]	51	19.2	4	46.5	10	1.8	1	14.9

[a] GP: 100% metakaolin geopolymer.

[b] GPEF20: metakaolin geopolymer with 20 wt% of electro filter ash.

[c] GPFF20: Metakaolin geopolymer with 20 wt% of fabric filter ash.

Figure 2.12: Shows the geopolymer formation using metakaolin with FA and an alkaline activator (Lancellotti et al., 2010)

2.4.3.2 Geopolymerisation and heat

It is possible to use low heating temperatures to cure a geopolymer-based material, but the use of higher temperatures would allow the crystallisation of the material. Therefore, the developed material can no longer be classified as geopolymer-based – because geopolymers are amorphous to semi-crystalline in nature (Davidovits, 2008, Khale and Chaudhary, 2007). The material due to the crystalline structure would be classified as zeolite-based material. Both these materials are very similar as they both are aluminosilicate based. The main difference between the two is that zeolite has a crystalline structure whereas geopolymer is amorphous to semi-crystalline (Davidovits, 2008, Khale and Chaudhary, 2007). The crystalline structure of the zeolite can be achieved by heating the material above 100^{o}C. The temperature range can be seen in Figure 2.13. According to Provis and Van Deventer (2009), zeolites and geopolymers are very similar at the atomic scale as they both have structural orders less than 1nm. However, lower Si/Al ratios, higher water contents and higher synthesis temperatures that can allow the formation of crystals within the geopolymer gel (Provis et al., 2005).

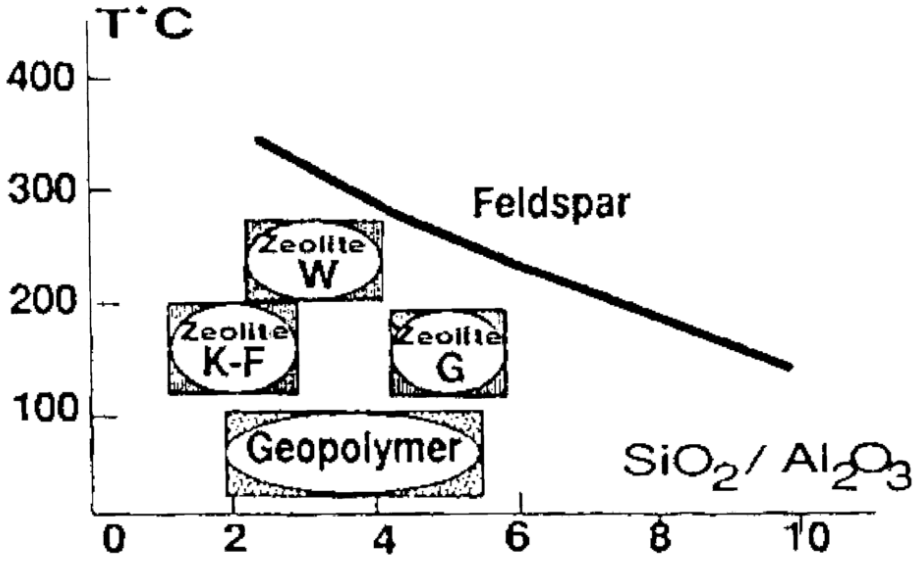

Figure 2.13: Geopolymer and zeolite temperatures ranges from (Khale and Chaudhary, 2007)

Erdoğan (2015) developed an alkali-activated material using perlite and tested curing at both room temperature and at elevated temperatures (heat treatment). The compressive strength achieved at room temperature was higher than that from the heat-treated materials of the same composition. The paper investigated sodium hydroxide of three different concentrations namely: 4M, 8M and 16M, and mixed with perlite in a 1:2 (sodium hydroxide: perlite) ratio by mass. The mixer was covered and cured at 100^{o}C for 3 to 24 hours. The cured material strength was reported to have a compressive strength of 4MPa, 12MPa and 40MPa respectively according to the concentration of sodium hydroxide. Thus, higher sodium hydroxide concentrations produced higher strength in the product. The material was then heated at 300^{o}C and 500^{o}C for 1 hour to investigate the pore size of the material. Higher temperature (500^{o}C) produced higher porosity whereas lower temperature (300^{o}C) produced lower porosity. The increase in volume was up to 225% due to bloating. The compressive strength of the material was between 3MPa to 7MPa. The result from this paper indicated that heat treatment reduced the compressive strength of this perlite-based geopolymer.

Suksiripattanapong et al. (2015b) also came to a similar conclusion but used lower temperatures of around 85^{o}C. They also found that heat treatment resulted in a weaker geopolymer; due to the material developing micro-cracks, caused by loss of moisture and hence reducing the overall compressive strength of the geopolymer. Due to these results, heat treatment of the geopolymer will not be investigated in this research. This research will aim to investigate geopolymerisation without the application of any external energy (heat), therefore, curing at room temperature will be explored in chapter 5.

2.4.3.3 Alkaline activators

Researchers have investigated many different types of alkaline activators such as sodium hydroxide, lithium hydroxide, calcium hydroxide and potassium hydroxide (Guo and Shi, 2015, Phoo-Ngernkham et al., 2015, Suksiripattanapong et al., 2015b, Król et al., 2018, Luukkonen et al., 2018). These activators are used with sodium silicate to provide a silicate source for geopolymerisation (Maghsoodloorad et al., 2014). The hydroxide (OH^{-}) ions act as a catalyst for the reaction, and a metal cation is used to balance the negative charge. Król et al. (2018) investigated the addition of different types of alkaline activators to produce coal fly ash based geopolymer material (50.58% silica and 34.94% alumina by weight) but did not investigate the resulting compressive strength. The paper compared sodium hydroxide, potassium hydroxide and lithium hydroxide addition to formulate a geopolymer-based material and suggests that sodium hydroxide and potassium hydroxide activation process is very similar, but that lithium hydroxide is much slower (in the geopolymerisation process) to form aluminosilicate. The study also indicated that it is difficult to obtain lithium-based geopolymers because lithium hydroxide is less soluble in water compared to sodium hydroxide and potassium hydroxide. The paper used an alkaline solution of 8M concentration with, liquid to solid ratio by mass of 0.4. Similarly, Toniolo et al. (2018) developed a geopolymer-based material using red mud, waste glass cullet and sodium hydroxide with 6M concentration. The study was able to formulate a material with a very high compressive strength of 45 MPa.

2.5 Review of Artificial Intelligence (AI) and machine learning

The word Artificial Intelligence (AI) was coined by John McCarthy in 1955 (Maglogiannis, 2007). He, along with Marvin Minsky, co-founded the field (Sawyer, 2006). They established the Artificial Intelligence (AI) lab at MIT in 1959 to promote the research in the field and in 1965 John McCarthy founded Stanford Artificial Intelligence Laboratory (SAIL) and became its founding director. The laboratory researched graphical interactive computing, machine intelligence and autonomous vehicles (Henderson, 2007, Nilsson, 2010). Arthur Samuel first used the term machine learning in 1959 (Bell, 2015). At that time, AI research heavily relied on logic and knowledge-based methods to develop expert systems whereas machine learning research relied heavily on statistics to provide the computers with an ability to learn from data without directly programming the behaviour (Flasiński, 2016). This meant that computers were not hard-coded with rules to make decisions, the input data, statistics and probability theory were used to develop models that made decisions or predictions; with complex algorithms which were designed to recognise patterns and make predictions based on these specific patterns (Bishop, 2006, Bonaccorso, 2017).

AI is a study to develop a machine that can sense the environment and learn from it, to achieve a given goal successfully. It is the study to mimic or simulate human intelligence that can solve problems by learning (Poole and Mackworth, 2010). AI is a field that takes its knowledge from many different fields such as mathematics, psychology, philosophy and computer science. There has been a lot of development in this area due to the continuous increase in computing power and the availability of large amounts of data (Sutton and Barto, 1998). It is regarded as a science with a broader concept; whereas machine learning is a study to develop algorithms to make machines intelligent, therefore it is seen as an application of AI; or it can be said that machine learning is a subfield of AI (Sutton and Barto, 1998).

2.5.1 Types of learning

There are many different types of machine learning algorithms but some of the common classes of algorithms are decision trees, Support Vector Machines (SVM), linear regression, clustering, Bayesian networks, reinforcement learning algorithms, genetic algorithms and Artificial Neural Networks (ANN) (Shalev-Shwartz and Ben-David, 2014, Goodfellow et al., 2016). These algorithms can learn from data using many different types of learning techniques based on their design. The different types of learning techniques are as follows:

Supervised learning: The algorithm is provided with a training dataset of inputs and outputs, and it uses this data to develop a model to make future predictions (Goodfellow et al., 2016).

Unsupervised learning: The algorithm is provided with data that is not labelled, hence the algorithm tries to recognise patterns and structure in the data (Dangeti, 2017).

Semi-supervised learning: Uses a combination of labelled and unlabeled training datasets to help produce a model. It is considered to be in between supervised and unsupervised learning (Abney, 2008).

Active learning: The model is initially developed using a small training dataset but is programmed to optimise itself as the labelled data becomes available (Hady and Schwenker, 2013).

Reinforcement learning: For this kind of learning, the data is provided in the form of reward and punishment. For example, a model can be developed to play a game where every time the opponent kills the modelled agent; it negatively impacts the learning algorithm. This provides information to the model to improve, and if the modelled agent kills the opponent, it positively impacts the model. In this type of learning, the model is able to continuously learn and evolve (Buduma and Locascio, 2017, Sutton and Barto, 1998).

2.5.2 Classification and regression modelling problems

In supervised machine learning, there are mainly two types of modelling problems classification and regression. Classification modelling techniques are used to make discrete predictions, whereas regression modelling techniques are used to make predictions on continuous quantities (Bonaccorso, 2017). For a classification modelling problem, it is important to define the number of discrete quantities that the model is likely to classify. It can be two or more discrete classes; for example, a model can be developed to classify a set of images to identify numerical digits from 0 to 9. In this case, there will be ten discrete classes (Ciregan et al., 2012). Some of the other examples are to develop a model to identify traffic signs or to classify if an image contains a dog, zebra or a cat (Ciregan et al., 2012, Sarkar et al., 2018). An example of a regression problem can be to use it to predict housing prices, based on one or more input features - such as the number of rooms in a house, number of floors and plot area (Sarkar et al., 2018). The example of a regression model can be linear regression, and for classification, it can be logistic regression, but Artificial Neural networks (ANN) provides the researchers with the flexibility to develop both types of models (Gulli and Pal, 2017). Some of the other machine learning modelling problems can be anomaly detection, structured annotation, translation, clustering and transcription (Sarkar et al., 2018).

2.5.3 Application of machine learning

The use of machine learning in a civil engineering application at present is limited; whereas it is gaining a lot of popularity in electrical engineering, mechanical engineering, computer science, medical diagnostics and many other fields. It provides researchers with an ability to develop sophisticated models based on data, by establishing the relationships between the input and output variables. It also provides researchers with layers of abstraction to help them develop machine learning models where it may not be possible to develop a theoretical model; this may be due to the requirement of complex variables required to model the concept or where full theoretical understanding has not been established. In 2008, researchers from Google published a paper “Detecting influenza epidemics using

search engine query data” in the journal Nature (Ginsberg et al., 2008). They were able to accurately predict influenza cases in the United States by region, based solely on google search enquiries. This is a good example of where the level of abstraction that machine learning models can provide to assist researchers in developing complex predictive models.

2.5.4 Introduction to Artificial Neural Networks (ANN)

The increase in computing power is allowing humans to develop and implement computationally complex models, as computers can perform calculations reliably and more efficiently than people. Due to this there is a lot of research in the areas of machine learning and Artificial intelligence (AI), but it is not yet possible for computers to be truly intelligent; however, progress is being made. Artificial Neural Networks (ANN) are the main areas currently being researched by the big companies such as Google, Microsoft, IBM and many others– as it is regarded as one of the newly emerging fields in computer science (Mohammed et al., 2016). ANN tries to mimic the human brain to achieve intelligence but is struggling to be robust (Khan, 2018). To achieve intelligence, labelled training datasets are required. However, the real human brain can self-process and handle much more complex information. Brains have very high parallelism and are also very compact in relation to their processing power; furthermore, they have the ability to adapt to the changing environments easily, whereas ANN has not yet reached this level of maturity. ANN can handle probability and noisy information but suffers from low power efficiency (Khan, 2018).

Biological neural networks consist of 100 billion neurons connected to each other in a very complex network (Khan, 2018). Each neuron consists of an axon, dendrites and a cell body which has a nucleus which is regarded as the central processing unit (CPU) of the neuron. The information from the nucleus is transmitted to other neurons by the axon and is received by the dendrites. The connection between the axon and dendrite is called a synapse, which transmits information in the form of electrical impulses that helps propagate information from one neuron to another (Khan, 2018). The ANN is modelled on the Biological neural

networks template, with the first mathematical model developed in 1943 by McCulloch and Pitts (1943). They proposed that neural networks can be presented in the form of a net and these nets can compute propositional logic to produce an output by computing the weighted sum of input features. This system produced a binary output, of either ones or zeros. This ANN was an extremely simplified version of the biological neural network, but over the year's researchers have developed more complex models those can compute much more complex functions. Each neuron in an ANN has an activation function that provides it with the ability to model functions, and some of the examples of these are: sigmoid function, hyperbolic tangent function, rectified linear unit (ReLU) amongst others (Raschka and Mirajalili, 2017). However, there are many other types of functions developed to help produce different types of ANN models, but it is important for the activation function to be a nonlinear function to take full advantage of ANN. The activation functions are calculated in a neuron. In literature, a neuron is also called a node or a unit. These neurons in a neural network are processing units each responsible for computation and transmission of information from one unit to another (Mohammed et al., 2016).

Artificial Neural Network (ANN) is a non-deterministic algorithm (Holzinger, 2014). This means that it does not execute all the steps in the same way each time, unlike deterministic algorithms, which systematically execute all the steps, in the same way every time they are executed. The ANN is non-deterministic because weights are assigned randomly to each neuron to help it produce an output based on a set of inputs features (Holzinger, 2014). These weights try to map the input to the output, and they are changed iteratively by comparing the output of the model to the actual value. The comparison is achieved by computing error and is used by the algorithm to minimise this error to produce a good fit to the model – as predictions made by the model depend on the weights of the neurons.

Later in this research, Artificial Neural Networks (ANN) with supervised machine learning will be used to predict the compressive strength of geopolymer-based material and also to identify different types of ash. It is supervised learning

because the training dataset to develop a model is labelled. The term ‘label’ means that the input data supplied to the model is mapped to the known output.

2.5.4.1 Type of Artificial Neural Networks (ANN)

In 1958, Rosenblatt (1958) first developed a Single Layer Perceptron (SLP) ANN model, However, since then many different types of ANN models have been developed. The most commonly used ones are as follows: Multilayer Perceptron (MLP) – can be used to solve a regression problem or classification problem; Recurrent Neural Networks (RNN) – which are used to develop sequence prediction models; Convolutional Neural Networks (CNN) – which are most commonly used to develop models involving images and hybrid neural networks – are a combination of two or more types of ANN (Goodfellow et al., 2016, Aghdam and Heravi, 2017).

In this research, MLP ANN models are of interest because they are very flexible and can be used to develop classification or regression models with tabular data or images. MLP comprises of an input layer, one or more hidden layers and an output layer. The number of hidden layers and nodes/neurons within these are known as hyperparameters and are two of the most important elements of the ANN. The hyperparameters help define the configuration of the ANN, as the total number of hidden layers and the number of neurons in each hidden layer directly impact the performance of the model. Therefore, they should be configured carefully by testing different models systematically to help produce the best model possible.

2.5.4.2 Defining and representing the configuration of Artificial Neural Networks (ANN)

Some of the most important terms used to define ANN is its architecture, size, depth and width. Architecture is the configuration of neurons in a neural network; size is the total number of neurons, depth is defined as the number of hidden layers (including the output layer), and width is the number of neurons in a hidden layer (Silva et al., 2016). The MLP with one hidden layer is called two-layer MLP because it takes into account the output layer and a hidden layer. Each node in a

neural network is called perceptron or neuron, and these all have a specific weight assigned to them. A group of neurons or perceptron connected to each other to produce a network with the configuration of the ANN written as: *Number of input features - Number of nodes in the hidden layer - Number of nodes in the output layer*. For example, six input feature neural networks with ten nodes in the hidden layer and two nodes in the output layer is written as follows: 6-10-2. This kind of notation will be used throughout this research to identify the configuration of the MLP.

2.5.4.3 Features and complexities of Machine Learning

The most powerful feature of the machine learning algorithms is called generalisation. This basically means that machine learning algorithms have the ability to make predictions on unseen data (Kodratoff and Michalski, 1990); but these predictions can have uncertainty in some cases, and this can be presented with the help of probability. They can have issues of under-fitting or over-fitting the training dataset, which can reduce the ability of the algorithm to make useful predictions. Therefore, it is important for the hypothesis function to be as complex as the training data that the researcher is trying to model. As simple hypothesis function will result in underfitting of the data and use of very complex function would result in overfitting; therefore, it is important for the designer of the model to understand the hypothesis functions to fit the training dataset correctly (Izenman, 2008). A graphical representation of these issues can be seen in Figure 2.14.

a b c

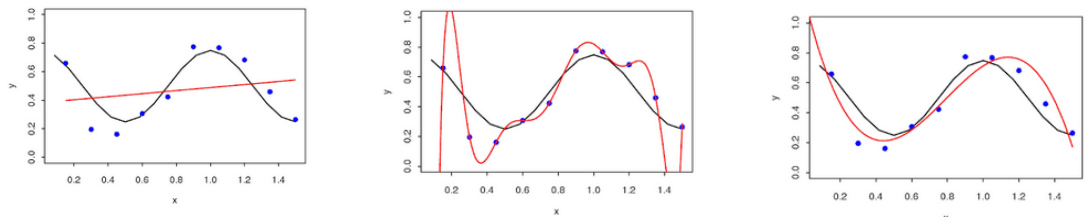

Figure 2.14: (a) red line shows under-fitting of the hypothesis function (b) red line shows over-fitting of the hypothesis function (c) red line shows good fitting of the hypothesis function (Izenman, 2008)

2.5.5 Optimisation in machine learning

Machine learning applies knowledge developed in the field of mathematical optimisation to iteratively find the maximum or the minimum value of the given function (Clarke et al., 2009). The use of optimisation in machine learning is limited to the minimisation of the cost function (or error function) by using the gradient descent algorithm. However, the broader subject area of optimisation looks at many different types of optimisation problems in the fields of engineering, economics and finance, computer science and mathematics (Craven and Islam, 2005, Clarke et al., 2009, Geem, 2011).

2.5.5.1 Gradient descent

Gradient descent is one of the most important algorithms in machine learning. It is used, both in regression and in ANN to minimise the error of the model to best fit the training dataset (Raschka and Mirajalili, 2017). It iteratively updates weights of the model in order to optimise or minimise the error by comparing the training dataset to the expected output. The algorithm systematically continues to update the weights until the error is minimised or the algorithm reaches a defined number of steps (Goodfellow et al., 2016). The error is determined by an error function or cost function, which measures the performance of the model.

The three common types of gradient descent algorithms are: batch gradient descent, mini-batch gradient descent and Stochastic Gradient Descent (SGD) (Buduma and Locascio, 2017). All these algorithms have hyperparameters to tweak the performance to produce an output that improves with every iteration. However, the success of this is dependent on factors such as the hypothesis function. The important hyperparameters are epochs and batch size. Epoch is an integer number defined to specify the number of times the algorithm will iterate through the training dataset. For example, if the batch gradient descent is defined as one, this will mean the algorithm will iterate through the entire training dataset just once. Batch size is also an integer number used to specify the number of iterations through the training data before updating the internal weights of the model. For example, if the hyperparameter batch size is defined as 10 and epochs

as 500, then the gradient descent will update the weights of the model after every 10 samples and iterate through the whole training dataset 500 times. The batch size is the main difference between the three types of algorithm. A stochastic gradient descent (SGD) uses a batch size of one, a mini-batch gradient descent uses batch sizes larger than one but smaller than the entire training dataset, and finally, a batch gradient descent uses the whole training dataset (Zheng et al., 2011).

The gradient descent algorithm is shown in Equation 2.3. The subject of the equation is the parameter that needs to be optimised; in this case, it is the weight of the model. The requirement of this algorithm is to define a performance measure such as a cost function or an error function. Many different types of cost functions can be used but in the example below a cost function for a regression model has been employed (it is often used to fit regression models). The other requirement of this model is to define the partial derivative of the cost function that is given by Equation 2.5. The algorithm updates the value of all W from $\mathrm{j} = 0, \ldots, \mathrm{n}$ simultaneously using $\mathrm{J(W)}$ and $\frac{\partial}{\partial \mathrm{W_j}} \mathrm{J(W)}$ (Gluck and Myers, 2001).

For multiple training examples, it is possible to use a batch gradient decent given by Equation 2.6 and a stochastic gradient descent given by Equation 2.7. The stochastic gradient descent has many advantages over a batch gradient descent as it convergences much faster by updating after going through a single training dataset, and it is also more efficient than batch gradient descent (Cichosz, 2015). However, batch gradient descent convergences to the solution much better than Stochastic gradient as it is noisy in nature (Goodfellow et al., 2016, Géron, 2017). A graphical presentation of all three algorithms converging to the solution can be seen in Figure 2.15.

$$W_j := W_j - \alpha \frac{\partial}{\partial W_j} J(W)$$

$W_j =$ Weight of feature *j*

$\alpha =$ The learning rate

$J(W) =$ Cost of the function for the regression problem

Equation 2.3: Gradient descent (Gurney, 1997, Skansi, 2018, Raschka and Mirajalili, 2017)

$$J(W) = \frac{1}{2} \sum_{i=1}^{m} \left(y^i - h_W(x^i) \right)^2$$

$J(W) =$ Cost of the function for the regression problem

$m =$ Number of training examples

$h_W =$ Hypothesis function of weight *w*

$y^i =$ Output value in row i

$x^i =$ Input features in row i

Equation 2.4: Cost function for a regression problem (Raschka, 2015, Raschka and Mirajalili, 2017)

$$\frac{\partial}{\partial W_j} J(W) = \frac{\partial}{\partial W_j} \frac{1}{2} \sum_{i=1}^{m} \left(y^i - h_W(x^i) \right)^2$$

$$= \frac{1}{2} \sum_{i=1}^{m} 2 \left(y^i - h_W(x^i) \right) . \frac{\partial}{\partial W_j} \left(y^i - h_W(x^i) \right)$$

$$= \sum_{i=1}^{m} \left(y^i - h_W(x^i) \right) . \frac{\partial}{\partial W_j} \left(y^i - \sum_{i=1}^{m} w_j^i x_j^i \right)$$

$$= - \sum_{i}^{m} (y^i - h_W(x^i)) x_j^i$$

Equation 2.5: Partial derivative of the cost function for a regression problem (Raschka, 2015)

$$W_j := W_j - \alpha \left(h_W(x^i) - y^i \right) x_j^i$$

Repeat until convergence {

$$W_j := W_j - \alpha \sum_{i=1}^{m} \left(y^i - h_W(x^i) \right) x_j^i \quad \text{(updated for every j)} \quad \}$$

Equation 2.6: Batch gradient descent algorithm for a regression problem (Raschka, 2015)

Loop { for i = 1 to m, {

$$W_j := W_j - \alpha \left(y^i - h_W(x^i) \right) x_j^i \quad \text{(updated for every j)} \quad \} \}$$

Equation 2.7: Stochastic gradient descent algorithm for a regression problem (Raschka, 2015)

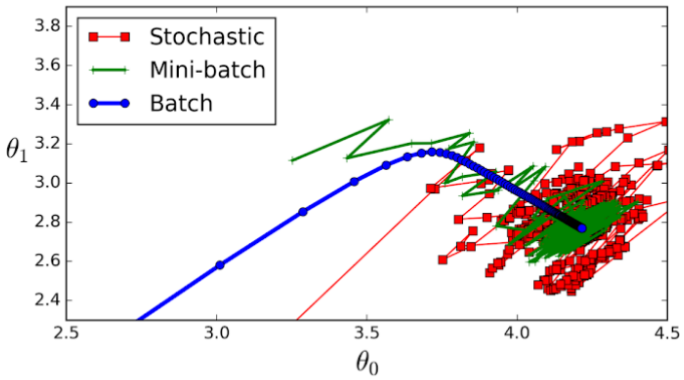

Note: θ_0 and θ_1 are two different weights/parameters of the model.

Figure 2.15: Convergence of different gradient descent algorithms (Géron, 2017)

2.5.6 Programming language and its libraries to develop ANN models

GNU Octave, Python programming language and its libraries were used in the research to develop a multivariate regression model and ANN models. The justification for its use is explained below with a brief review: -

- **Python programming language:** Is a general-purpose dynamic high-level programming language developed by Guido van Rossum and was released in 1991. The motivation to create this language was to provide the programmer with something that is easy to read and simple to program – even for complex software development (Desai, 2015). The language is dynamic because it provides an instant output when an operation is typed in the command line and it also automatically manages the memory. It is a general programming language that supports many different types of programming paradigms such as: functional, imperative, object-oriented and procedural. It is an open source programming language that functions on many different operating systems; therefore it is incredibly versatile and popular (Lutz, 2006). Python also provides a large number of programming libraries such as TensorFlow.
- **TensorFlow:** Is a programming library, developed by the Google brain team, specifically for researchers and engineers. It is an open source library for high-performance numerical computation. The library allows programmers to take advantage of Central Processing Units (CPUs),

Graphics Processing Units (GPUs) and Tensor processing units (TPUs) to perform numerical computation efficiently; and is also used by Google to develop machine learning and deep learning models. Tensor processing units (TPUs) are a distinct piece of hardware developed by Google, specifically to run machine learning models (Gulli and Kapoor, 2017). Google released it in 2015 under Apache 2.0 open source license. The project started in 2011 initially by the name of DistBelief and was improved in terms of its performance and features and then was released as TensorFlow (Karim, 2017). It supports multiple operating systems such as Windows, macOS, Linux, iOS and Android. It also supports various programming languages such as Python, C, C++, Java, JavaScript, Java, Go, Swift among others (Karim, 2017). In this research, Artificial Neural Network (ANN) models were developed mainly using TensorFlow in the Python programming environment.

- **NumPy:** Is another programming library for the Python programming language. It is highly optimised to handle large multi-dimensional matrices and arrays - providing the programmers with an ability to perform large number of high-level mathematical operations. Functions can also be implemented on large multi-dimensional matrices and arrays (Bressert, 2012); thus it is a library used to arrange and manage multi-dimensional data in this research.
- **GNU Octave:** Is a free numerical computation software that uses high-level programming language, very similar to MATLAB (Hansen, 2011). It is used by students, the scientific community and by the industry to perform numerical calculations to develop and solve, linear and nonlinear problems. It is regarded as the best free alternative to MATLAB with a lot of code cross-compatibility, meaning it can run on MATLAB and vice-versa. The software program is written in C++ and provides the programmer with Graphical User Interface (GUI) and Command Line Interface (CLI). Octave scripting language also provides the programmer with many features to perform operations on high-dimensional matrices and is also compatible with windows, macOS and Linux operating systems (Hansen, 2011).

3 Characterisation of Air Pollution Control (APC) residues

The Air Pollution Control (APC) residue investigated in this research is from MSWI. The flue gases from the MSWI are treated by spraying lime slurry to neutralise the acidic nature of these gases. After this activated carbon is used to remove the dioxins and heavy metals. Lastly, the baghouse filtration system is used to collect Air Pollution Control (APC) residues. In this chapter, analytical technics to examine the chemical and physical properties of APC residues will be discussed.

3.1 Total metal composition using Inductively Coupled Plasma Optical Emission Spectroscopy (ICP-OES)

ICP-OES can detect all the major elements present in a sample simultaneously (Craigie, 2018). The sample is injected into the nebuliser by a peristaltic pump, and from another inlet argon gas is injected, this causes the sample to form very fine droplets, which are passed through the nebulisation chamber where only droplets of the size less than 10μm are passed to be ionised by high-temperature plasma generated by inductive coupling (De Silva and Gregoire, 1998). This causes the emission of spectral lines or beams of light because of the property of atoms to move from a higher energy level to a lower energy level by emitting a light beam at a specific wavelength, to get back to a stable state. These are separated into different wavelengths, and a photomultiplier is used to measure the intensity of light. The relationship between the amount of energy and the wavelength is expressed by the Planck's equation as shown in Equation 3.1. This relationship between photons and wavelength help ICP-OES to detect different elements present in the sample. The presence of heavy metals in APC residues was analysed using ICP-OES (Perkin Elmer ICP-OES Optima 8300). As the sample is

in solid form, therefore it is prepared by dissolving the sample in concentrated nitric acid and hydrochloric acid in 1:3 volumetric ratio. This technique is called aqua regia digestion technique specified in BS EN 13657 (2002) to characterise waste.

$$E = h\frac{c}{\lambda}$$

h = Planck's constant (6.62607004 × 10^{-34} Js)

λ = Wavelength

c = Speed of light (3.00 × 10^{8} m/s)

E = energy of the photon

Equation 3.1: Planck's equation (Skoog et al., 2007)

The chemical composition of APC residues analysed using ICP-OES is shown in Table 3.1. It can be seen that it contains a very high concentration of heavy metals, especially zinc and lead. These compounds can be very hazardous to humans and the environment; therefore, it is important to analyse their stability by conducting a leaching test to better understand the behaviour of these heavy metals. The leaching behaviour of APC residues will be discussed in section 3.3.

Elements	mg/kg
Sb	428
As	39.1
Ba	730
Cd	127
Cr	121
Cu	510
Pb	1390
Hg	<0.945
Mo	12.1
Ni	127
Se	<1.72
Zn	9270
pH	12.67

Table 3.1: Chemical analysis of APC residues used in this research

3.2 Ion Chromatography (IC) to characterise anions

Ion Chromatography (IC) system was used to analyse the concentration of anions present in a sample. The IC system consists of an eluate delivery system, a sample injection system, a guard column, separator column, suppresser column and a detector. The sample is loaded into the IC system for analysis by using the sample injection system. After this high-pressure pump is used to push the sample and eluent through the guard column that consists of polymeric resins to help remove the contaminants from the sample. The sample ions are separated as it (a mixture of eluent and sample) passes through the separator column. This stage is called ion exchange. The rate of migration of ions present in a sample propagates through the column at a different rate depending on the ion type. After this, the suppressor selectively suppresses the conductivity of the eluent and helps enhance the detection of the sample ions. Lastly, these sample ions are detected by measuring the electrical conductance of the sample ions. This is then used by the software to detect the concentration of anions present in the sample. The illustration of the IC process can be seen in Figure 3.1.

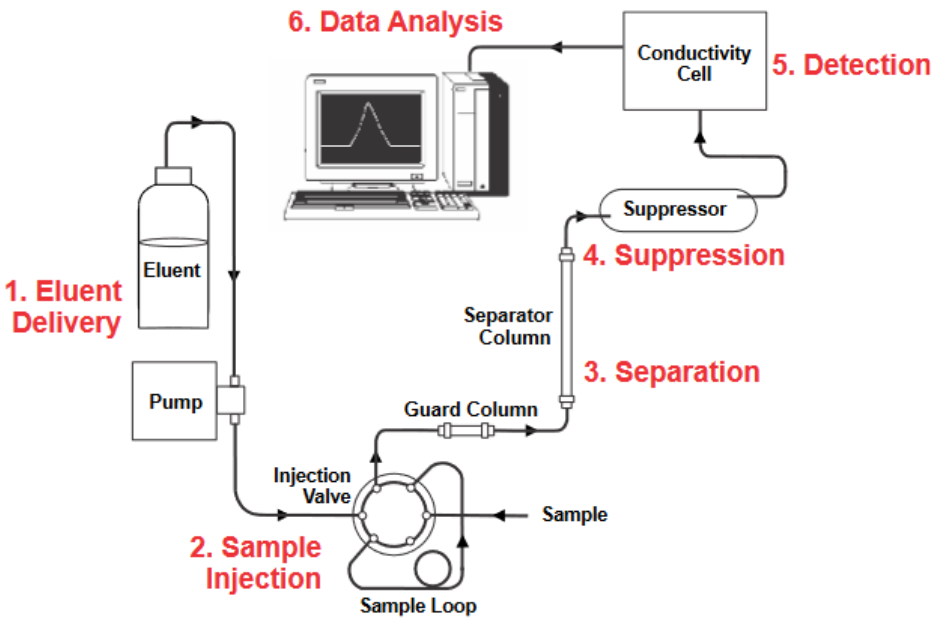

Figure 3.1: Ion chromatography (IC) analysis process (Thermo Fisher Scientific, 2016)

The leachate from APC residue was analysed using IC to detect the concentration of chloride, sulphate and fluoride in accordance with BS 6068-2.46 (1995). Sodium carbonate solution was used as a liquid eluent. The process of analysis starts by running deionised water as a first sample. After this, three working calibration standards and one Analytical Quality Control (AQC) standard are analysed. The three calibration standards had the following concentration of chloride, fluoride and sulphate concentrations: Sample A (Cl = 5 mg/l, F = 2 mg/l, SO4 = 2 mg/l), Sample B (Cl = 50 mg/l, F = 20 mg/l, SO4 = 20 mg/l), Sample C (Cl = 500 mg/l, F = 200 mg/l, SO4 = 200 mg/l). The AQC standard had the following concentration (Cl = 50 mg/l, F = 20 mg/l, SO4 = 20 mg/l). After analysing all the standards and a blank sample (deionised water) is analysed after which APC residue leachate is filtered using a 0.45μm filter before loading it into the IC for analysis. After this IC system is cleaned by analysing a blank sample. All the data is processed by the IC software to provide the concentration of ions present in the leachate.

3.3 Leaching test

The leaching tests were performed according to BS EN 12457-2 (2002). The sample in this case APC residue was first sieved using 4mm sieve to ensure at least 95% of the particles were below 4mm. The APC residue is mixed with deionised water at liquid to solid ratio of 10 l/kg in a bottle. The bottle is sealed by using a cap and is then placed in an end-over-end tumbler for 24 hours. After this, the mixture is filtered using vacuum filtration system with a 0.45μm filter paper. The filtrate is collected and is analysed to determine the concentration of heavy metal composition using an ICP-OES and concentration of anions such as chloride, fluoride and sulphate were analysed using ion chromatography.

It can be seen from Table 3.2 that APC residues exceed the hazardous waste landfill limit for lead and chloride; therefore, it cannot be landfilled in the UK according to UK waste acceptance criteria. Therefore, it requires treatment before it can be disposed into a hazardous landfill site.

Leachable Elements	Leaching of APC residue (mg/kg)	Inert waste limit (mg/kg)	Non-hazardous waste limit (mg/kg)	Hazardous waste limit (mg/kg)
As	DL	0.5	2	25
Ba	27.95	20	100	300
Cd	DL	0.04	1	5
Cr	0.2	0.5	10	70
Cu	DL	2	50	100
Hg	DL	0.01	0.2	2
Mo	2.49	0.5	10	30
Ni	0.13	0.4	10	40
Pb	279.9	0.5	10	50
Sb	DL	0.06	0.7	5
Se	DL	0.1	0.5	7
Zn	53.14	4	50	200
Cl	154659.7	800	15,000	25,000
F	37.4	10	150	500
SO_4	21383.8	1,000	20,000	50,000

DL: Detection Limit

Table 3.2: Elemental leaching of MSWI APC residue and leaching limits for the classification of granular waste according to 2003/33/EC

3.4 X-Ray Diffraction (XRD) spectroscopy

The X-ray diffraction (XRD) spectroscopy is a non-destructive method to identify molecular structure and nature of crystals present in a sample. This technique transmits x-rays of a fixed wavelength at the sample and then detects the intensity of x-rays diffracted (Suryanarayana and Norton, 1998). These diffracted x-rays are then analysed as a function of the angle formed by the incident rays and the diffracted rays. On the resulting diffraction pattern, the peak position is used to determine the crystal lattice of the solid using Bragg's law, while the intensities of the peaks provide information on the average positions of the atoms in the lattice. Bragg's law also allows the XRD to determine the distances between two successive crystallographic planes of that family on the plane also called interplanar spacing (Waseda et al., 2011). Each angle at which a peak is observed corresponds to a family of lattice planes that are indicated by Miller indices. The diffraction pattern or peaks are then compared to experimental databases that allow the user to identify various peaks hence characterising crystalline compounds (Suryanarayana and Norton, 1998).

XRD analysis was conducted on APC residues, and the results can be seen in Table 3.3. The ash is 45.8% amorphous and has small percentage of silicate, quartz, aluminate, iron, zincite and hydroxide chloride. The presence of these compound can vary as it mainly depends on the type of waste incinerated, location, technical specification of the furnace, flue gas treatment process and ash collection technology employed by the plant (Tang and Steenari, 2016).

Compounds / % w/w	APC residue
Calcium Hydroxide Chloride (Ca(OH)Cl)	0.6
Sylvite (KCl)	3.6
Halite (NaCl)	4.9
Anhydrite ($CaSO_4$)	4
Calcite ($CaCO_3$)	16.3
Quartz (SiO_2)	3.3
Szomolnokite ($MSO_4.H_2O$ M = Mg, Mn, Fe, Cu and Zn)	0.4
Marialite ($(Ca, Na)_4[(Al, Si)_{12}O_{24}]$ Cl)	0.7
Tri-Calcium Silicate (Ca_3SiO_5)	1.7
Di-Calcium Silicate (Ca_2SiO_4)	7.4
Tri-Calcium Aluminate (Ca_3Al2O_6)	1
Perovskite ($CaTiO_3$)	0.7
Periclase (MgO)	0.5
Apatite ($Ca_5(PO_4)_3(O, OH, F)$)	1.8
Iron (Fe)	0.4
Aluminum (Al)	0.6
Zincite (ZnO)	0.1
Spinel (M_3O_4 M = Mg, Al and Transition metal)	0.1
Pyroxene ($(Ca, Mg, Fe)_2Si2O_6$)	0.5
Gehlenite ($Ca_2Al_2SiO_7$)	0.2
Alkali Feldspar ($(Na, K) AlSi_3O_8$)	0.7
Amorphous	45.8
Nickelalumite ($(Ni, Cu) Al_4(SO_4)(OH)_{12}.3H_2O$)	1
Polyhalite ($K_2Ca_2Mg(SO_4)_4.2H2O$)	1.8
Pentahydrite (MgSO4.5H2O)	1.2
Nosean ($Na_8[Al_6Si_6O_{24}](SO_4)$)	0.3
Cristobalite (SiO_2)	0.5

Table 3.3: XRD results of MSWI APC residue

3.5 X-ray fluorescence (XRF) spectroscopy

X-ray fluorescence (XRF) spectrometer emits high energy X-ray to detect the element present in a sample (Margui and Van Grieken, 2013). The sample is targeted by an x-ray causing it to scatter and absorb this energy. The x-ray beam that is not absorbed by the atom is scattered, and this scattering is elastic scattering as no energy is lost by the x-ray photon during the collision with electrons. This type of scattering is called Rayleigh scatter or coherent scatter. The other type of scattering is called Compton scatter or incoherent scatter, during this photon loss some of its energy after the collision with the electrons.

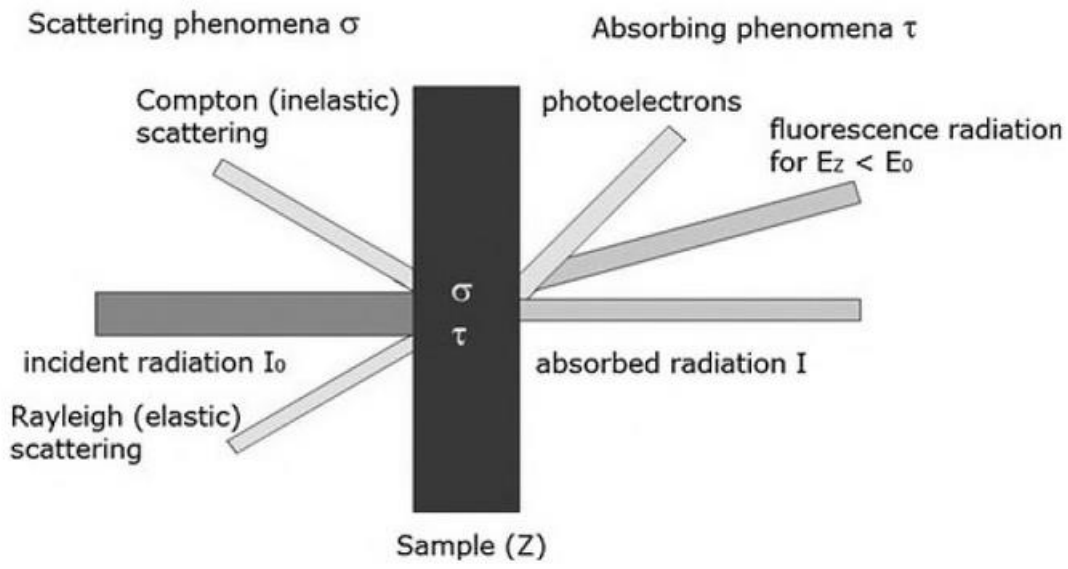

Figure 3.2: Shows the interaction of x-ray with a sample (Haschke, 2014)

The X-ray beam that is absorbed by the XRF causes the atom to ionise. This ionisation is due to the absorption of x-ray photon by an atom causing it to release an electron from its inner shell. This process is called photoelectric absorption (Als-Nielsen and McMorrow, 2011). The release of an electron makes the atom unstable and it regains stability by rearranging an electron from an outer shell to an inner shell. This is called the Auger effect and graphical representation of this can be seen in Figure 3.3. The other process by which it gains stability is by transfer of

electrons from the outer shell to the inner shell by releasing a fluorescent X-ray, and this is used to identify the element as it is unique to each element; therefore, it is called characteristic X-ray. The transfer of electrons is unique due to the configuration of electrons in the orbits or shells of an atom (Harrison, 2007). These orbits are identified by letters such as K is used to identify the innermost orbit of an atom and the letter is incremented as the number of orbits in an atom increases depending on the element (Van der Heide, 2012). It can be seen in Figure 3.3 that this illustration uses an atom with three orbits, those are identified by K, L and M (where M is the outer most orbit). The transfer of electrons from these orbits can be identified by Siegbahn notation to define the origin of characteristic photon for example: transfer of elements from M to L is denoted as L_α (L-alpha), from L to K is K_α (K-alpha) and from M to K is K_β (K-beta) (Podgorsak, 2016). The transfer of an electron from these shells release specific characteristic energy which is detected by the XRF to detect the element in a sample (Vutchkov et al., 2013).

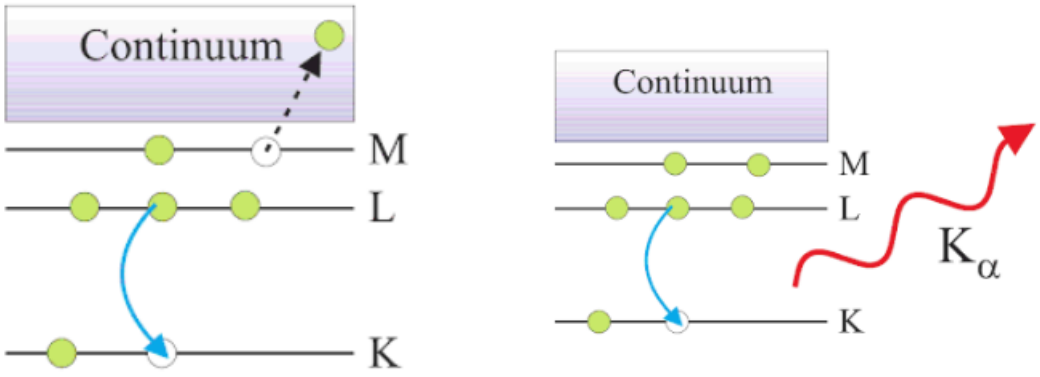

Figure 3.3: a) Auger effect b) characteristic x-ray (Als-Nielsen and McMorrow, 2011)

The chemical composition of APC residue was identified using XRF spectrometer by first using a hydraulic press to pelletise the powdered material into a disc. This disc was then placed into the XRF spectrometer for analysis. The results from the test will be discussed in chapter 5.

3.6 Scanning Electron Microscopy (SEM)

The microstructure and morphology of the samples can be studied by using Scanning Electron Microscopy (SEM) (Goldstein et al., 2003). It is a microscopy technique that emits a beam of electrons at the surface of the sample that is to be analysed. A tungsten filament generates the beam of electrons. The electron beam is focused on the surface of the sample in the form of a spot, and then the beam is moved linearly in the form of a rectangular scanning pattern. The beam penetrates and diffuses into the sample in a pear shape as illustrated in Figure 3.5. The volume of this pear shape depends on the average atomic number of the sample and the incident electron energy (Goldstein et al., 2003). The penetration of electron beam causes the atoms in the sample to emit electrons, and these electrons are detected by the detector to produce a very detailed image of the surface of the sample — the detector on an SEM typically uses secondary electron and backscattered electrons to generate an image (Reimer, 1998). SEM can provide partial resolution of 1 nm to allow the user to analysis features those are up to 1 nm apart (Ul-Hamid, 2018).

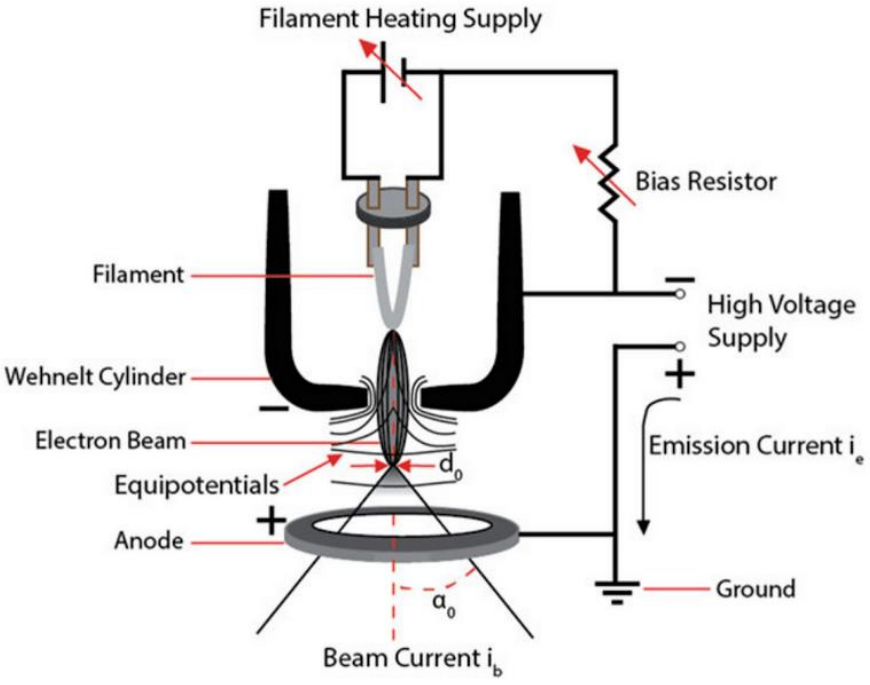

Figure 3.4: Design of a thermionic emission electron gun (Ul-Hamid, 2018)

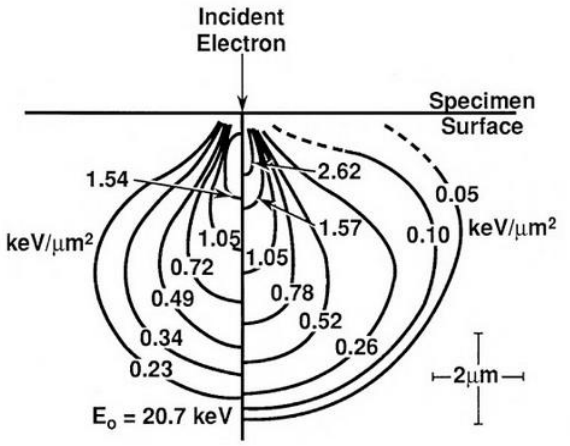

Figure 3.5: Electron beam penetration into the sample (Goldstein et al., 2003)

The backscattered electrons are primary electrons emitted as a resulting of elastic interaction of the primary electron beam with the atomic nuclei of the sample. They are representative of the atomic number of the atoms in a sample (Goldstein et al., 2018a). The spatial distribution of backscattered electrons depends on the angle between the normal to the surface of the beam. The backscattered electrons have high energy therefore they can be emitted from the sample at a greater depth than that of the secondary electrons, but due to this, they have much lower topographic sensitivity but high sensitivity to the density of the mineral phases present in the sample (Goldstein et al., 2018a) whereas secondary electrons have low energy; therefore, they can provide high spatial resolution, allowing the user to analyse the topography of the sample (Echlin, 2009, Goldstein et al., 2018b).

SEM was used to analyse the microstructure of the APC residues based geopolymer material (chapter 5). The surface of the sample was fractured and coated with an ultra-fine layer of gold/palladium (conductive material) using a sputter coater. It is important to coat the material (those exhibit low conductivity) to prevent the build-up of static charge as this can increase the detection of secondary electrons by the SEM hence increasing the noise in the image (Goldstein et al., 2003, Echlin, 2009). The conductive layer also reduces the penetration of the electron beam hence allowing sharper feature resolution (Echlin, 2009, Ul-Hamid, 2018).

4 Thermal Treatment of APC residues

This chapter will investigate sintering, pan pelletisation process to produce granules and induction heating system. The pan pelletisation process is investigated to help produce green granules, which can then be thermally treated to produce aggregate.

4.1 Sintering of clay and APC residues-based Light Weight Aggregate (LWA) in a muffle furnace

Lightweight Aggregates (LWA) can be manufactured using many different types of materials such as expanded clay, vermiculite, industrial ashes, perlite and expanded glass (Arioz et al., 2008, Silva et al., 2010). However, expanded clay LWA are very widely researched and are also available commercially as Lightweight Expanded Clay Aggregate (LECA) (Merikallio et al., 1996, Bogas et al., 2014, Boarder et al., 2016). Therefore, this research will use clay as a base material to produce LWA and will use a similar approach to the one used by Quina et al. (2014). This paper produced LWA by using clay as a base material with different percentages of APC residues, 1% oil and 20% water. The mixture was then homogenised and rolled into a spherical shape by hand and then dried for 2 hours at 200^{o}C before being fired in a chamber oven at 1170 °C for 8 minutes over calcium carbonate. The paper investigated as-received APC residues and washed APC residues to produce LWA. APC residues were washed for 10 minutes at liquid to solid ratio of 10:1. After this, the material was filtered and dried at 105 °C overnight to remove soluble compounds. It can be seen from Figure 4.1 that the compressive strength of LWA increases as the percentage of APC residues increases. The paper only tested 5%, and 10% washed APC residues incorporation with clay, but it can be seen that washed granules managed to achieve higher compressive strength as compared as-received APC residues. The

methodology in this chapter will build on the results produced by this paper but will also investigate a higher percentage addition of APC residues without the addition of oil and the produced pellets will not be fired over calcium carbonate.

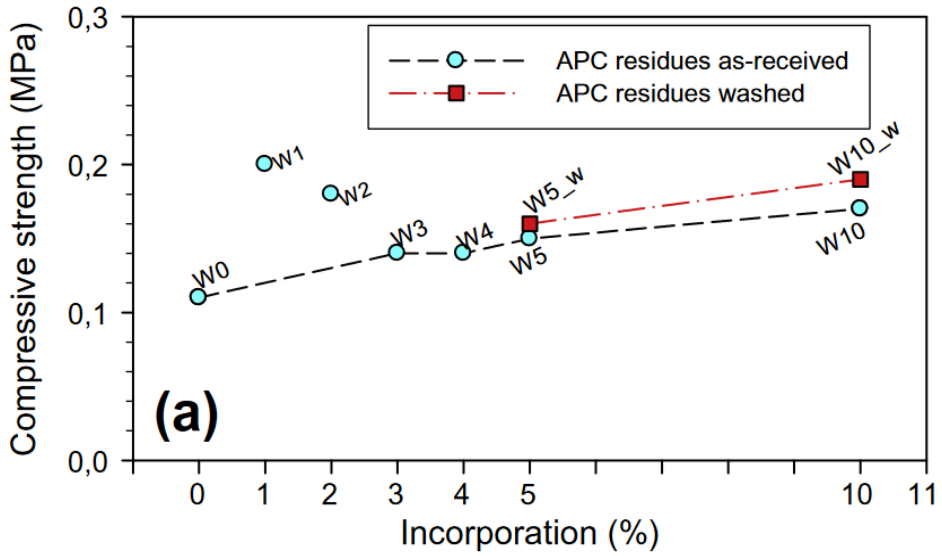

Figure 4.1: Shows the compressive of the LWA (Quina et al., 2014)

4.1.1 Methodology to produce APC residues-based granules for sintering

The APC residues-based granules were sintered using muffle furnace to achieve solidification/stabilisation. The granules were developed using clay and APC residues with 25% water. The granule formation is summarised in Table 4.1. The clay and APC residues were passed through a 600μm sieve and then were homogenised to produce granules each 2.4g in weight. In total 20 granules were made for each formulation. The granules were then dried for 24 hours at 100^{o}C. After this, the granules were heated in a muffle furnace, and it was programmed to reach the temperature of 1170^{o}C at 13^{o}C per minute, and once the furnace reached 1170^{o}C, it maintained that temperature for 20 minutes. After this, the granules were left in the furnace to slowly cool down for 12 hours. After this, the LWA were tested for their strength and leaching characteristics.

Sample name	S0	S2	S5	S20
Clay (g)	100	98	95	80
APC residue (g)	0	2	5	20

Table 4.1: Clay and APC residues-based granule formulations

4.1.2 Testing and discussion of clay and APC residues-based LWA

The LWA were tested for their strength by placing each granule between two plates - the distance between the plates reduces to apply force until the point of fracture. The testing equipment provides the user with the peak force at the point of fracture. This peak force is used to calculate strength. In literature, the widely used formula to calculate strength is shown in Equation 4.1 – but there seems to be a lot of confusion in the literature regarding the precise definition of it, with González-Corrochano et al. (2009) referring to it as compressive strength and others describing it as maximum tensile stress or tensile strength (Tanaka et al., 2006, Li et al., 2000).

$$S = \frac{2.8P}{\pi d^2}$$

Where:

$S = \ Fracture\ strength$

$P = \ Fracture\ force$ or critical load

$d = \ Distance\ between\ the\ loading\ points$

Equation 4.1: Fracture strength of an aggregate

Kourti and Cheeseman (2010) and Shinohara et al. (2002) in their paper describes it as an equation to calculate tensile strength but then later discuss and report the output of the results as compressive strength. In another paper by Cheeseman and Virdi (2005) they describe it as a formula to calculate compressive strength. All these papers refer back to papers by Hiramatsu et al. (1965), Hiramatsu and Oka (1966) or Yashima et al. (1987). However, the paper by Yashima et al. (1987) refers back to Hiramatsu et al. (1965). Therefore, the source of this equation can

be traced back to a paper written in Japanese by Hiramatsu et al. (1965) and it refers to it as tensile strength. The paper published in English Hiramatsu and Oka (1966) also identifies it as an equation to calculate tensile strength. The confusion seems to arise because the granules are compressed during the test between two plates. The compressive forces applied to circular granules creates high compressive stress at the point of contact between the plate and the granule which causes the sample to fail under tension, vertically, along the compression axis (in other words they fracture under compression due to tension) (Li et al., 2000, Pejchal et al., 2017, Heard et al., 2018, Žagar et al., 2018). The equation was originally developed to calculate the tensile strength of irregular rocks. However, the formula is only valid if the contact compressive force angle is less than 5^{o}. However, Oka and Majima (1970) has identified, that the equation is valid for contact compressive force angle of 10^{o} to 20^{o} and it assumes that the fracture occurs due to tensile stress reaching the tensile strength (Oka and Majima, 1970). These assumptions can be argued as contact point between the granule and the contact plates applying the force can vary and as these granules are not perfect spheres, therefore, fracture due to compression or due to stresses on the surface can occur as these sintered granules have air voids in them, therefore, it is difficult to assess stress distribution in the granules. Therefore, in the case of sintered granules, it is better to refer to it as *fracture strength*.

The production of LWA using APC residues and clay has been very effective at achieving high fracture strength and was also able stabilise APC residue. It can be seen from Figure 4.2 that the fracture strength of the LWA increases as the percentage of APC residues in clay increases. At 20% inclusion, LWA achieved the fracture strength of 5.78 MPa, and it can be seen that LWA produced just using clay only managed to achieve the fracture strength of 1.48 MPa. However, this increase in strength was due to the densification of LWA caused by the inclusion of APC residues - increasing the bulk density of LWA as can be seen in Figure 4.3. The LWA produced with 20% APC residues had a bulk density of 1044 kg/m^3 whereas LWA produced using clay had a bulk density of 606 kg/m^3. These were determined using Equation 4.2. The use of clay matrix to produce LWA has also

proven to be very effective in stabilising APC residue as it can be seen from Table 4.2. The produced material can be classified as inert even at very high percentage (20%) of APC residue inclusion in clay. The leaching test was conducted according to BS EN 12457-2 (2002). This test helps to identify long term behaviour of hazardous compounds present in the formulated material. In this case, clay and APC residue-based granules by quantifying the immobilisation of different heavy metals ions leaching out of the material. The methodology to conduct leaching has been explained in section 3.3. It can be seen that all the heavy metals were below the detection limit and leaching of chloride and sulphate were well below the inert waste limit for the landfills in the UK.

In section 4.3, a novel induction heating system will be investigated to help sinter the material as the use of muffle furnace has proven to be very effective to produce an inert material.

$$\rho_{bulk} = \frac{6M}{\pi D^3}$$

$M = Mass\ of\ the\ aggregate$

$D = Diameter\ of\ the\ aggregate$

Equation 4.2: Formula to calculate the bulk density of aggregates

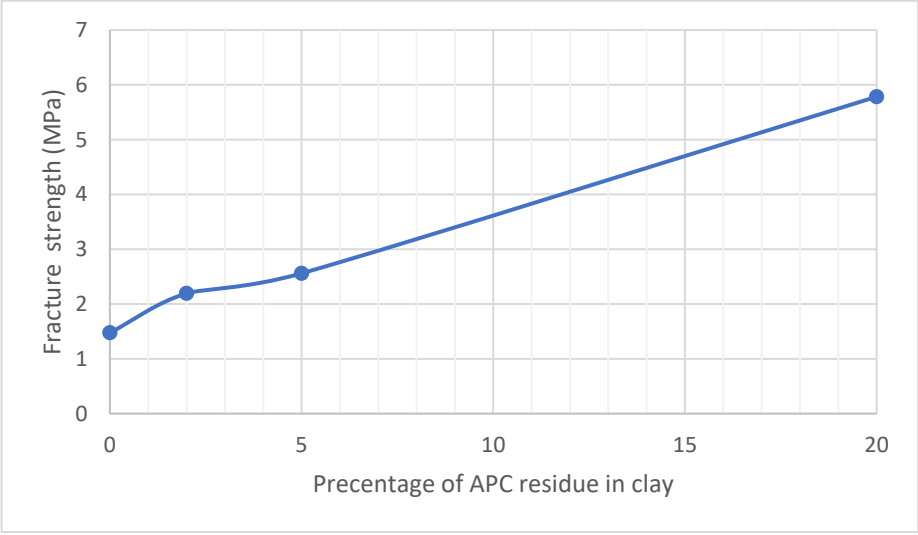

Figure 4.2: Fracture strength of APC residues-based granules

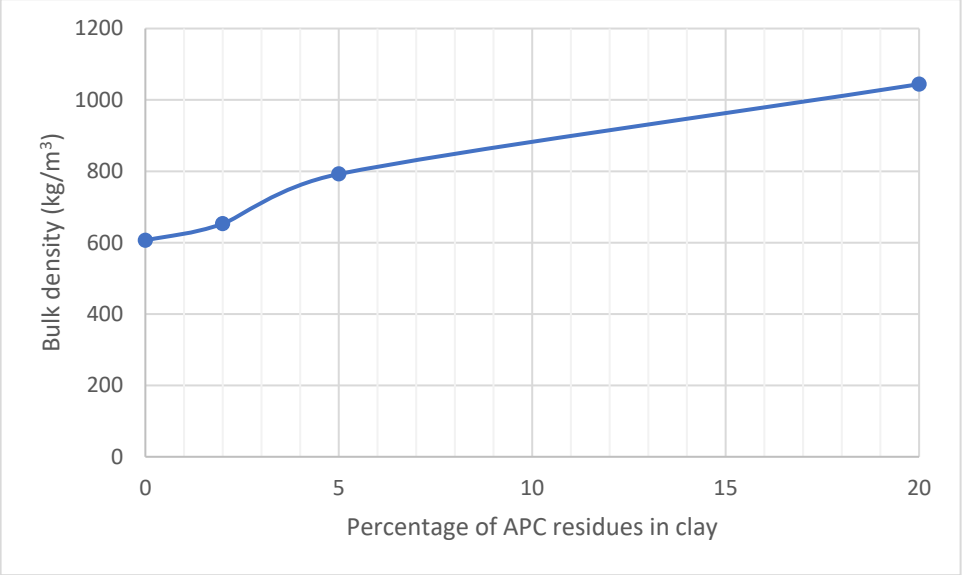

Figure 4.3: Bulk density of LWA

	S2 (mg/kg)	S5 (mg/kg)	S20 (mg/kg)	Inert waste limit (mg/kg)
As (arsenic)	<DL	<DL	<DL	0.5
Ba (barium)	<DL	<DL	<DL	20
Cd (cadmium)	<DL	<DL	<DL	0.04
Cr (chromium (total))	<DL	<DL	<DL	0.5
Cu (copper)	<DL	<DL	<DL	2
Hg (mercury)	<DL	<DL	<DL	0.01
Mo (molybdenum)	<DL	<DL	<DL	0.5
Ni (nickel)	<DL	<DL	<DL	0.4
Pb (lead)	<DL	<DL	<DL	0.5
Sb (antimony)	<DL	<DL	<DL	0.06
Se (selenium)	<DL	<DL	<DL	0.1
Zn (zinc)	<DL	<DL	<DL	4
Cl (chloride)	67	82	234	800
SO_4 (sulphate)	321	225	442	1,000

Note: DL is detection limit

Table 4.2: Leaching test results of APC residues-based clay granules

4.2 Investigation of the pan pelletisation process

The pan pelletiser relies on tumble/growth agglomeration process to produce green granules/pellets by using powdered materials and these can then be used as aggregates in civil engineering applications, such as inclusion into concrete (Videla and Martinez, 2002). Agglomeration is a mechanical process that influences the particles to stick to each other to form a circular object (Pietsch, 2008). These types of pelletisers are widely used in the food industry to make food granules and in the mining industry to make granules of metal ores (Couper, 2010). A typical pan pelletiser can be seen in Figure 4.4. It has a shallow pan or disk connected to a motor in the centre that helps it to rotate/spin. The pan pelletiser allows the user to change the tilt and revolution per minute of the pan to control the agglomeration process. The centripetal force plays a vital role in this process, as the size and compressive strength of the granules are influenced by the tilt and revolution per minute of the disc pelletiser (Abdoli et al., 2018). In practice, the dry powdered material is sprayed with a solution (liquid) while the pan spins. This coats the material with droplets of liquid causing other dry or wet particles to stick together (Abdoli et al., 2018). The powdered material starts to agglomerate to form granules/pellets, as illustrated in Figure 4.5. The discharge of the granules from the pan pelletiser can be controlled by the operator by managing the tilt and revolution per minute of the pan (Pietsch, 2008).

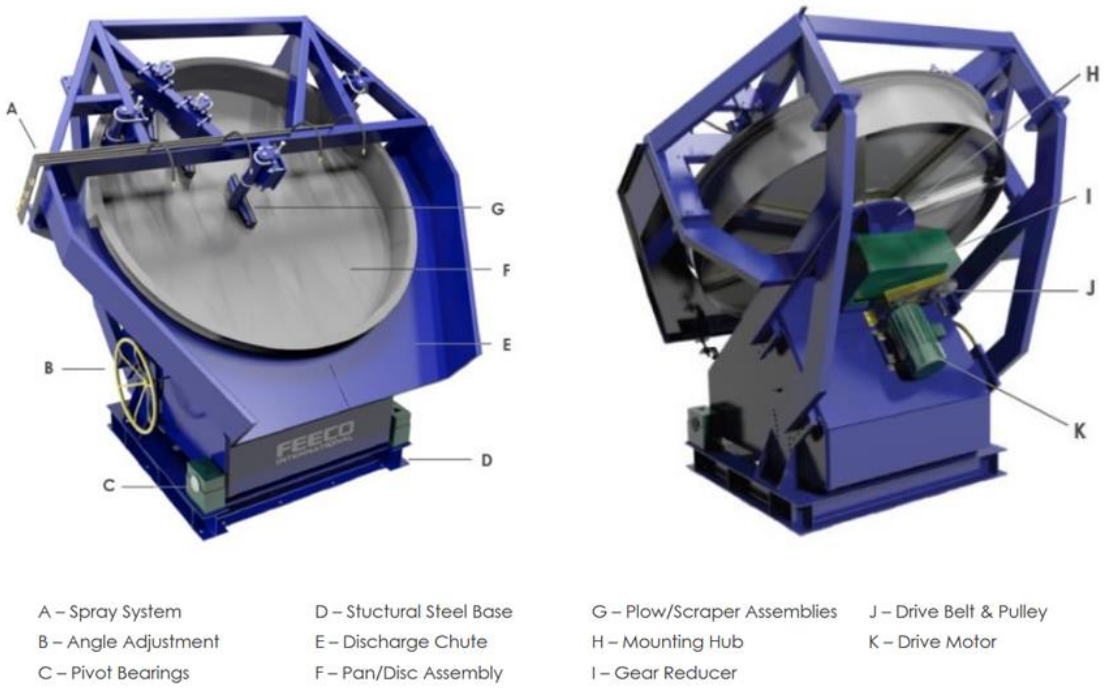

Figure 4.4: Pan pelletiser (Feeco International, 2017)

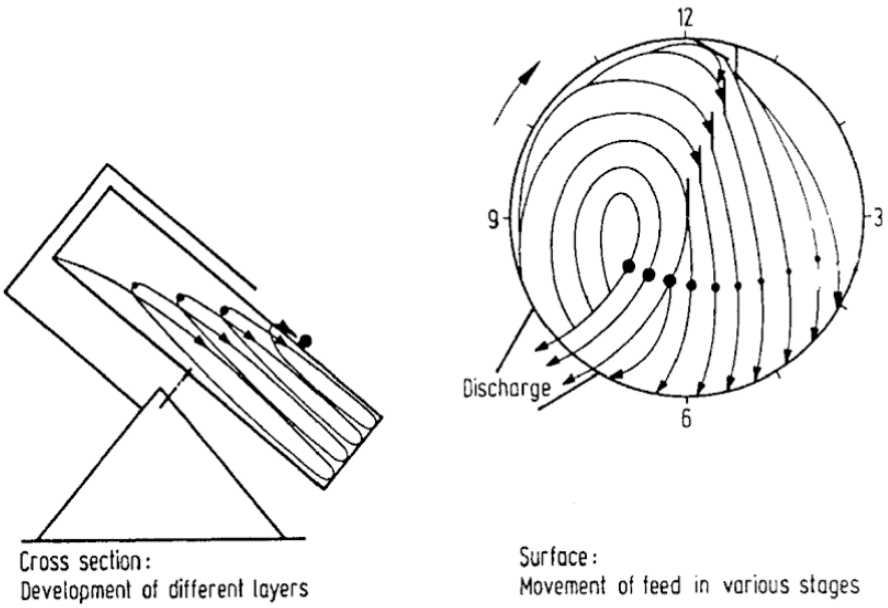

Figure 4.5: Motion and formation of granules in the pan pelletiser (Pietsch, 2008)

The pan pelletisation process has been used by many peer-review papers to produce ‘green’ (unfired) granules/pellets for the production of Light Weight Aggregates (LWA) (Verma et al., 1998, Sear, 2002, Gesoğlu et al., 2012, Colangelo and Cioffi, 2013, Colangelo et al., 2015, Tang et al., 2017, Huber et al., 2018). Lura et al. (2014) produced lightweight aggregate (LWA) using sugar cane bagasse fly ash and sodium bentonite. The dry mix was placed in a pan pelletiser and was sprayed with water to produce granules. These granules were then sintered at 1100 °C to produce LWA. Xu et al. (2015) produced porous ceramic aggregates using electrical insulator waste, fly ash and sawdust using the pan pelletisation process. Once formed, granules were dried for 24 hours at 110 °C and then sintered in three batches for 3 hours at 1100°C, 1200°C and 1300°C respectively. The highest strength of 35.3N was achieved at 1200°C.

The use of pan pelletisation process was investigated in this research to produce granules. A typical pan pelletisation system is installed with a motor control system to control the revolution per minute of the pan but is not usually installed with an automated pan-tilt adjustment system. Similarly, the pan pelletiser in the laboratory did not allow the user to measure the tilt of the pan; therefore tilt control system was designed to measure and control the tilt of the pan precisely to help better understand the pan pelletisation process.

4.2.1 Mechanical design to measure and control the tilt of the pan

The pan pelletiser used in this research can be seen in Figure 4.6. The mechanical design requirement to measure and control the tilt of the pan requires, firstly to design a mechanical mechanism to mount a sensor onto the pan pelletiser to measure the tilt and secondly, it requires mechanical design to mount the motor onto the pan pelletiser to allow the user to control the tilt accurately. A potentiometer was used as a sensor to measure the tilt. Other options included Micro-Electro-Mechanical Systems (MEMS), such as accelerometers or gyroscopes to measure the tilt, but MEMS are very sensitive to vibration and under high vibration (caused by the rotational speed of the pelletiser) they can completely lose their ability to sense. Potentiometers, on the other hand, are much more

robust under these conditions (Huang et al., 2017). [The electronic design and operation of the potentiometer will be explained later in this chapter]. The installation of the potentiometer requires two types of connections to measure rotation. The body of the potentiometer should be fixed to the stationary frame of the pan pelletiser so that it can measure the tilt relative to the stationary point and the control knob of the potentiometer should be mounted to the tilting pan to allow the knob to rotate. This rotation can be measured by the digital system to measure the tilt of the pan. The body of the potentiometer was placed at the centre of rotation (of the tilt) of the pan, as can be seen in Figure 4.6 and Figure 4.7. It was not possible to directly connect the knob of the potentiometer to the pan; therefore, a special lever arm mechanism was designed as can be seen in Figure 4.8.

The second step was to mount the motor onto the valve that is connected to the large tilt control screw. The technical issue is that the screw moves as the pan tilts, due to this it required coupling to be installed on two pin joints (Figure 4.7). These two pin joints manage the axis of rotation of the screw; thus a large coupling was required on the lower pin joint that goes up to the top of the valve to provide a suitable place to mount the motor without affecting the pan's normal movement. The coupling was then able to move in parallel to the screw, hence providing the motor with constant contact with the valve. A special coupling was also designed to connect the valve and the motor. To achieve this, a deep hex socket was attached to the valve, while its posterior was connected to a brass rod and was joined to the motor (Figure 4.9).

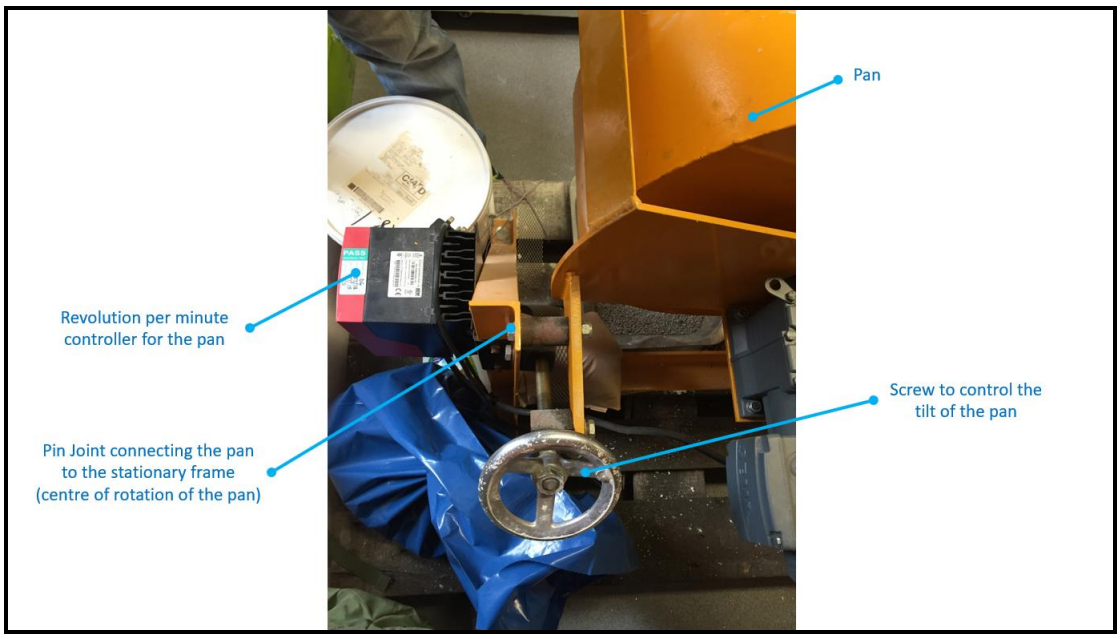

Figure 4.6: Different components of the pan pelletiser

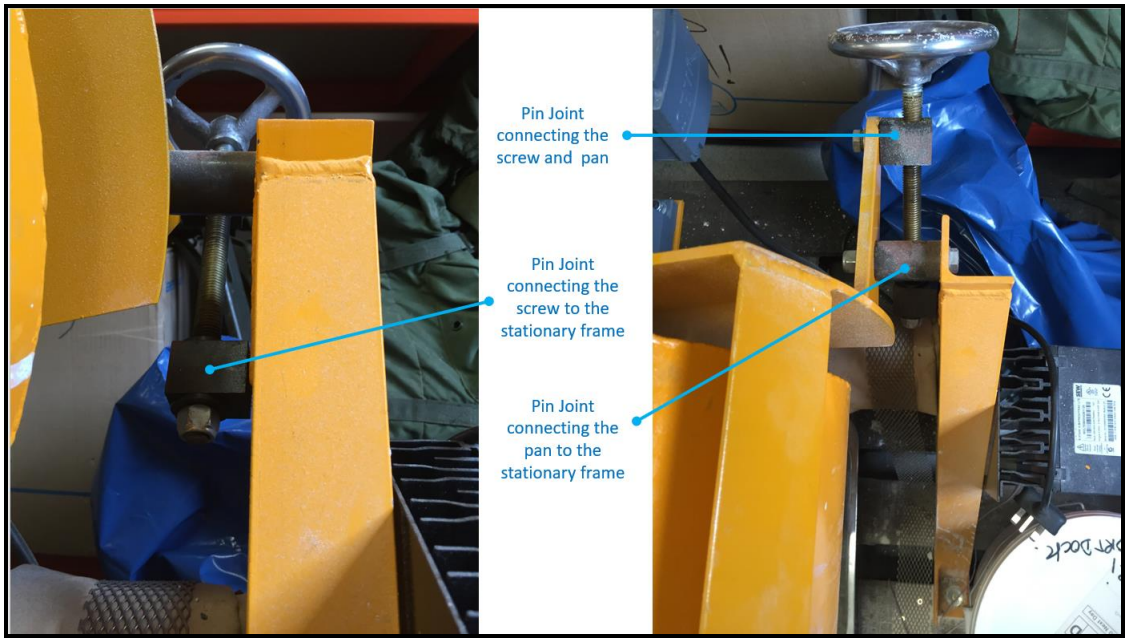

Figure 4.7: Pin joint connection of the screw on the pan pelletiser to manage the tilt

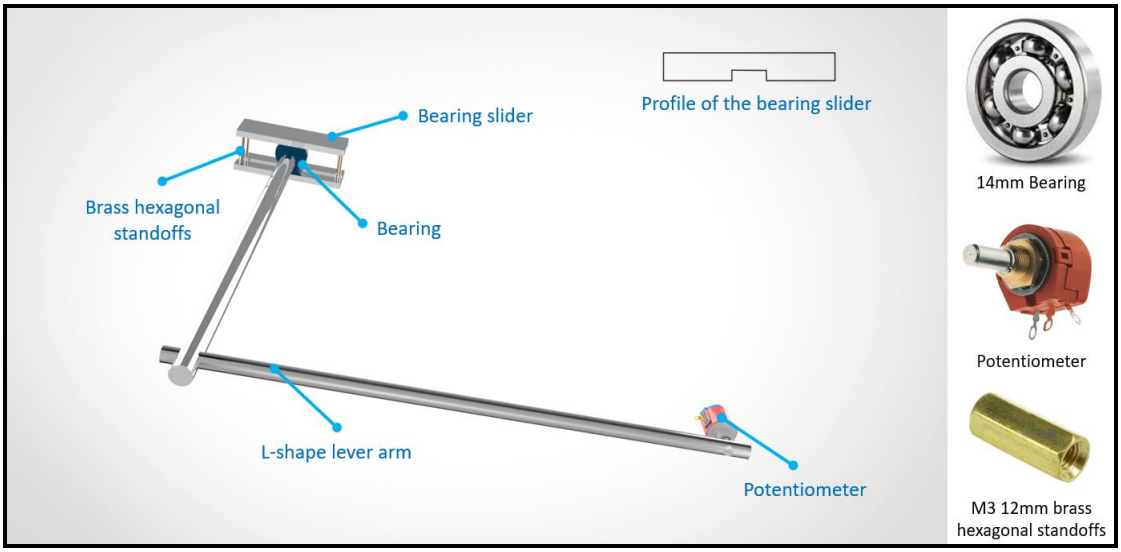

Figure 4.8: The design of the lever arm mechanism to measure the tilt of the pan

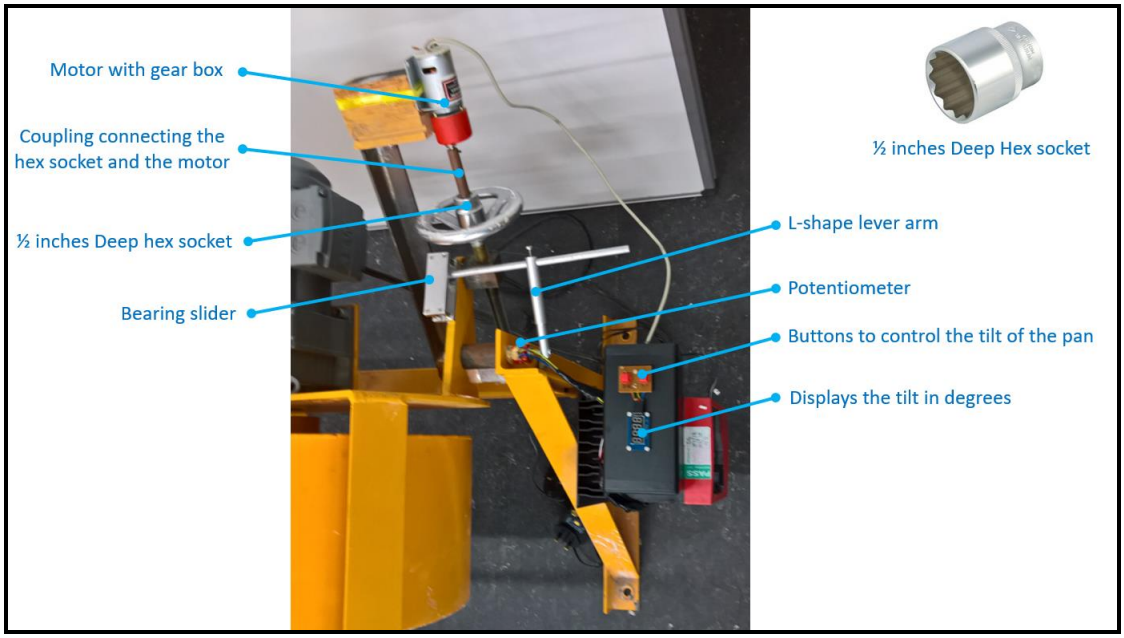

Figure 4.9: The complete mechanical design to measure and control the tilt of the pan

4.2.2 Electronic design to measure and control the tilt of the pan

After completing the mechanical design, it was important to design the electronic circuit that allows the user to specify the angle of tilt. This input from the user can be used to control the motion of the motor, based on the reading provided by the sensor (in this case a potentiometer). The complete design of the circuit can be seen in Figure 4.11. The circuit uses an Arduino Leonardo microcontroller to help control all the inputs and outputs. This microcontroller uses a 10-bit Analog to Digital converter (ADC), which means it can read the input from the potentiometer and convert it into a digital reading. The potentiometer used in this design can measure a rotation maximum up to 265° with an uncertainty of ±5° (this can be mitigated by calibration). The output of the potentiometer changes linearly as the knob of the potentiometer is rotated. The maximum resistance of the potentiometer used in this experiment was 100Ω, but the potentiometer of any resistance can be used in this experiment because of the design configuration of the circuit. It is configured to be used as a potential divider; therefore, the output voltage read by the microcontroller is unaffected by the maximum resistance of the potentiometer as theoretically it is a ratio of two resistors (graphically shown in Figure 4.10). This can be mathematically represented as an equation shown in Equation 4.3.

In this design, a 10-bit ADC microcontroller was used to read the angle of tilt with a precision of 0.259^{o}, as shown in Equation 4.4. The individual components used in this design are shown in Table 4.3, and the complete electronic design can be seen in Figure 4.9. The electronic circuit was first implemented on a large breadboard and tested. Once this was proved viable, it was replicated onto a smaller breadboard which was later fixed inside a plastic casing to prevent the circuit from being exposed to outside elements (Figure 4.12). The completed pan pelletiser can be seen in Figure 4.9.

(a) (b)

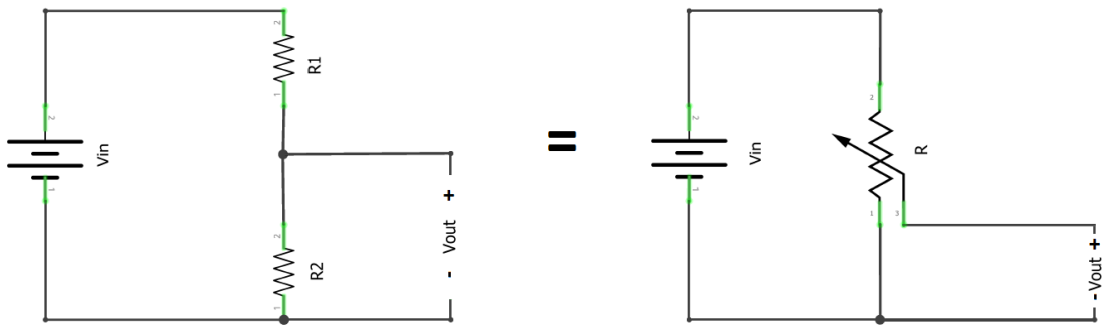

Figure 4.10: (a) shows the output produced by the potential divider and (b) shows the output produced by a potentiometer

$$V_{out} = \frac{R_2}{R_2 + R_1} \times V_{in}$$

Equation 4.3: Calculate the output voltage from the potential divider (Platt, 2014)

$$Angle\ measuring\ resolution = \frac{maxium\ rotation\ a\ potentiometer\ can\ measure}{2^{Resolution\ of\ ADC} - 1}$$

$$Example: Angle\ measuring\ resolution = \frac{265}{2^{10} - 1} \approx 0.259^{o}$$

Equation 4.4: Calculate the angle measuring the precision of the potentiometer connected to the microcontroller

Part type	Model No:	Image
Potentiometer	TW1101KA	
LED display	TM1637 (7 segments, 4-digits LED display)	
Microcontroller	Arduino Leonardo	
Motor driver	L298N motor driver module	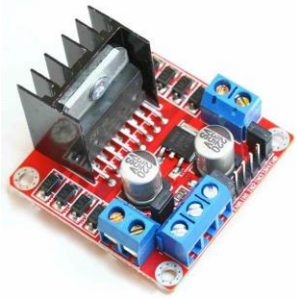
Motor with gearbox	MFA Gearbox and Motor 3000:1	

Table 4.3: List of major components used in the design of the circuit to control and measure the tilt of the pan pelletiser

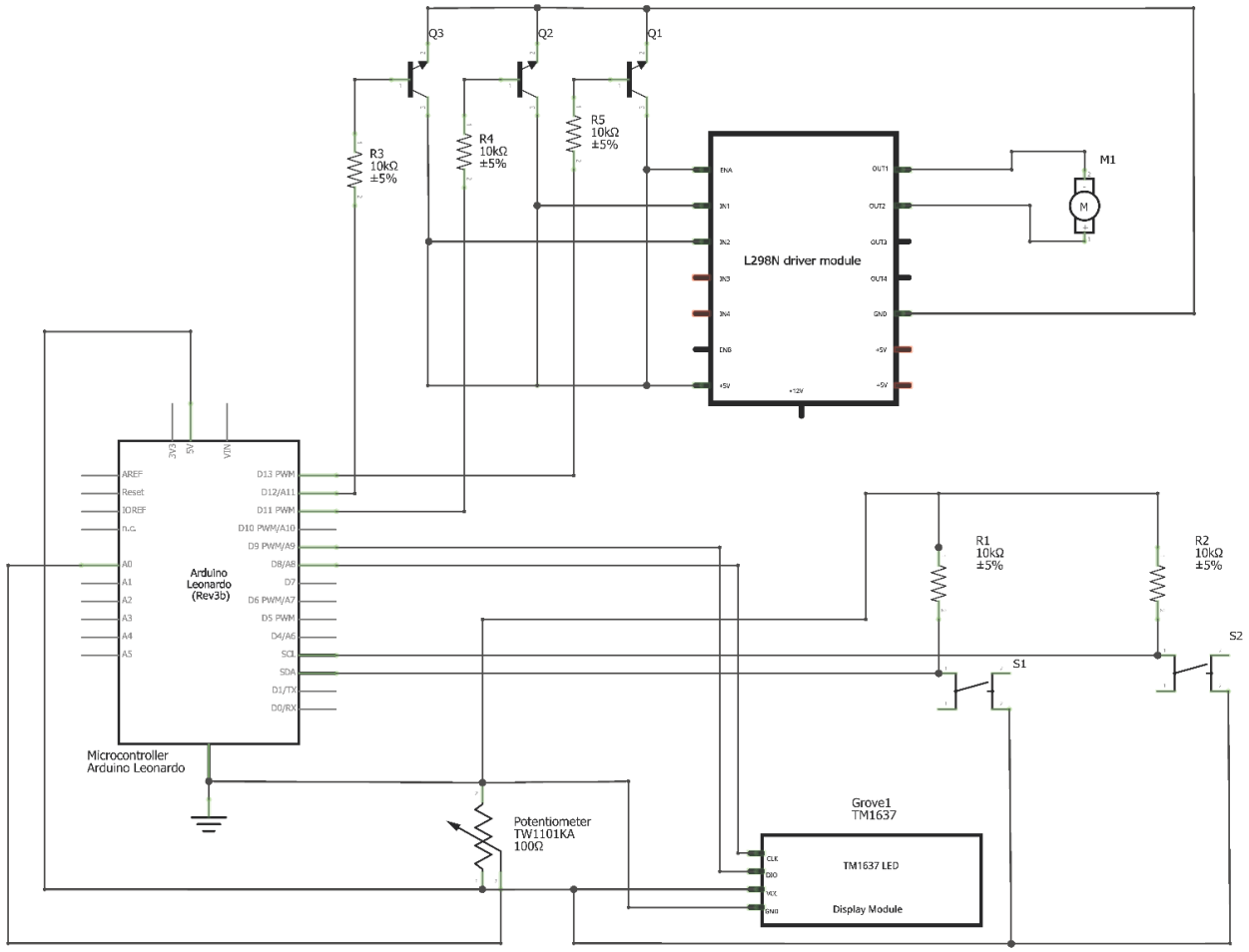

Figure 4.11: Complete circuit design to control and measure the tilt of the pan pelletiser

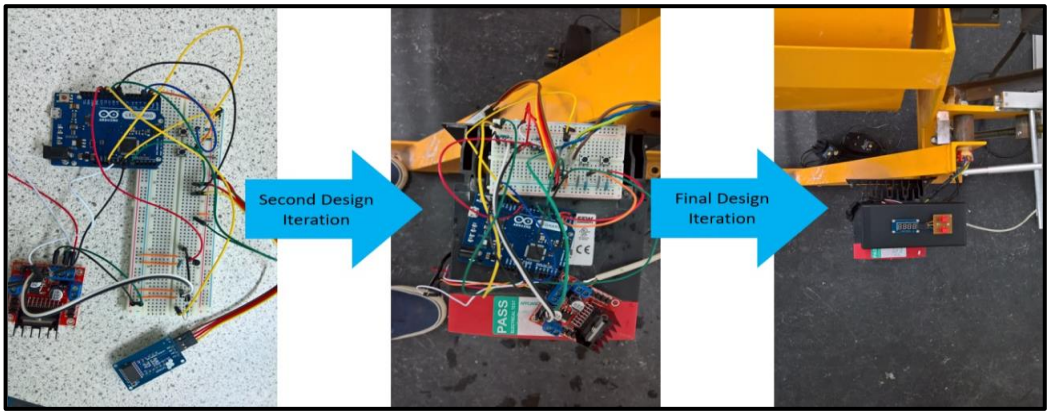

Figure 4.12: Shows some of the design iteration of the electronic circuit to measure and control the tilt of the pan on the pan pelletiser

4.2.3 Testing of pan pelletisation process

The pan pelletisation process was tested using 200g of APC residue and 1000g of dried clay; both were passed through a 600µm sieve before pelletisation. The pan was loaded with 1.2kg of material to ensure the material did not tumble/roll out of the pan during testing. The mixture was placed in the pan of the pan pelletiser, and different revolution per minute (rpm) and the angle of tilt of the pan were tested ranging from 20 degrees to 50 degrees. It was noticed that angle of tilt and rpm were critical, as very high rpm resulted in granules exiting the pan even at a low angle of tilt and very low rpm resulted in very slow agglomeration of granules. It was very difficult to conclude the most suitable angle of inclination and rpm therefore for the purpose of testing the process - the angle of tilt was set to 40 degrees, and rpm was set to 35. The material was sprayed with deionised water instead of normal water to establish a sound control for hydration and to control leaching characteristics of the produced material; as normal water contains minerals which can affect these variables. The volume and rate of flow of water were both very critical to the pan pelletisation process as high volume causes oversaturation of granules and low volume of water results in the formation of smaller granules because the volume of liquid is essential to allow the particles (powder material) to tumble/grow and agglomerate. The example of oversaturation can be seen in Figure 4.13, resulting in large agglomerated material stuck to the surface of the pan pelletiser. The other observation that was made during the

experimentation was that high rate of flow of water for a fixed volume of water produced granules with considerable variation in granule size whereas the low rate of flow produced granules with less variation in size (as compared to a high rate of flow).

Figure 4.13: High volume of water causing oversaturation

The main issue with the pan pelletisation process identified during the testing was that it is not possible to accurately produce one size granules. The large size distribution (Figure 4.14) would produce high standard deviations (in terms of compressive strength). It is possible to achieve an acceptable level of homogenisation in the end product, but still, there are some other issues with the process such as changing the composition of the powdered material would change the volume of water/liquid that is required to produce an optimal batch of granules. Similar problems were also reported by Kleynhans et al. (2012), Neizel et al. (2013) and Quina et al. (2014) indicating that varying size, shape and weight of the granules would make it very difficult to replicate the results in the laboratory. After considering all these issues, it was decided that the pan pelletisation process is not an effective process to test the formulation of different material compositions in a laboratory setting, but it can be a very effective process to help produce granules in a commercial setting because known formulations can be optimised (for amount of material, rate of hydration, size of the pan, angle of tilt and rpm) to produce high volume of granules of varying size. The size distribution of granules can be beneficial if the produced granules are used as aggregates in concrete (Meddah et al., 2010).

Figure 4.14: Pan pelletisation of clay and APC residue granules

4.3 Development of an induction heating system

Induction heating system induces heat by using the electromagnetic field. Therefore it is important to generate a high electromagnetic field for fast and efficient induction heating, which can be achieved by applying high current to the coil (Haimbaugh, 2015). It can be generated by using one or more coils through which an alternating current is passed. This alternating current induces heat in the conductive material placed inside the field. The created field oscillates at the same frequency as the current (Rapoport and Pleshivtseva, 2006), and its intensity is in the form of a loop. However it is flowing in the opposite direction, and this produces heat, with a power that is proportional to the square of the induced current (Rapoport and Pleshivtseva, 2006). The shape and form of the coil can also be modified to change the frequency and electromagnetic field generated by the system. In this thesis cylindrical coil was designed to induce heat in the material. The rate at which heat can be inducted in a material depends on the electrical and magnetic properties of the material as induction heating generates heat due to eddy current and hysteresis losses (Haimbaugh, 2015). It is vital to properly develop and configure the induction heating system to heat the granules efficiently by taking into consideration these elements:

- Frequency of the induction heating system, penetration depth and the characteristics of skin effect induced by the distribution of current in the material.
- The relative arrangement of the coil and the material to be heated.
- The size and shape of the coil.
- Temperature dependent characteristics of the material to be heated, such as magnetic properties, electrical resistivity and thermal conductivity.

4.3.1 Penetration depth

Penetration depth can be defined as the distance from the surface of the material towards its centre/core over which current density is reduced by a factor of one, as compared to the value that it has on the surface (Totten, 2006). In an electromagnetic field current is concentrated in layers near the surface of the conductive material, and this is because current density decreases exponentially from the surface of the material to the centre due to skin effect; therefore current density is highest on the surface of the material and lowest in the centre in a cylindrical coil configuration (Hashmi, 2014). This type of configuration is of significance because in this research it is used to investigate the sintering of APC residue-based granules.

The penetration depth (δ) can be calculated using Equation 4.5 and it can be seen from this equation that the penetration depth depends on the material's properties and the frequency of the induction heating system. It is not always possible to change the properties of the material, but it is possible to change the operating frequency of the induction heating system to control the heating. It can be seen in Figure 4.15 that penetration depth decreases with increasing frequency due to skin effect; Therefore, the penetration depth is greater at lower frequencies. The efficiency of the induction heating system also depends on the ratio between the depth of penetration and the thickness of the material. This means that higher ratios would result in increased efficiency (Niknejad and Meyer, 2000). The penetration depth also depends on the magnetic permeability and resistivity, which

are both temperature dependent. For non-magnetic materials (such as copper or aluminium) magnetic permeability is 1, whereas for ferromagnetic material (such as iron and steel) it is much higher (Totten, 2006). Higher coefficient of magnetic permeability means lower the penetration depth. The coefficient of magnetic permeability strongly depends on the type of the material, and the conditions materials are subjected to, such as temperature, magnetic field intensity and saturation. The coefficient of magnetic permeability drops to 1 at Curie temperature which also causes a rapid increase in penetration depth of a magnetic material (Liu et al., 2005).

$$\delta = \sqrt{\frac{2}{\omega\mu\sigma}} = \sqrt{\frac{2}{2\pi f\mu\sigma}}$$

Where: $\omega = 2\pi f$

$f =$ Frequency of the magnetic field

$\mu =$ Magnetic permeability of the material

$\sigma =$ The specific electrical conductivity of the material

Equation 4.5: Penetration depth in meters (Fawzi et al., 1985)

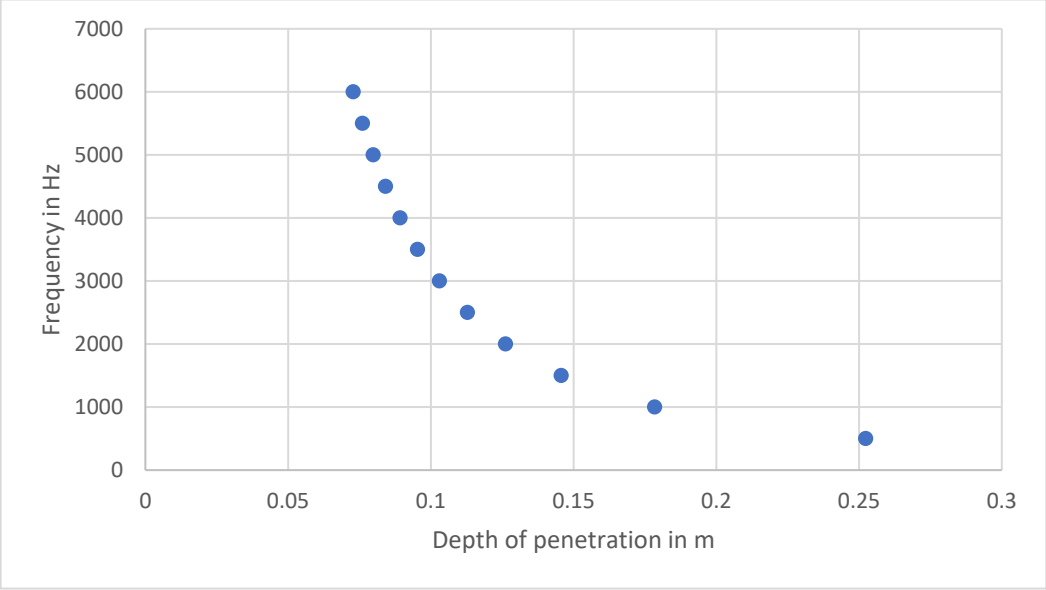

Figure 4.15: Penetration depth (δ) with respect to frequency (f)

4.3.1.1 Effect of frequency on induction heating

It is possible to control the frequency of the induction heating system to change the penetration depth. The induction heating system can be classified by using its operating frequencies. It can be divided into three frequency ranges: low frequency from 1 Hz to 10 kHz, medium frequency from 10 kHz to 70 kHz and high frequency is greater than 70kHz (Hashmi, 2014). Low frequency is used for fusion and wrought; medium frequency is used for superficial tempering, forging, annealing or brazing and high frequency is used for tube welding and heat sealing (Rudnev et al., 2017).

It is very important to understand the principles and effects of these three frequency ranges to better identify the most suitable frequency that can be used in this research to sinter the granules. High frequency induces current close to the surface of the material whereas low frequency induces current deep inside the material (Hashmi, 2014). This is mainly due to eddy current and hysteresis effect, as higher frequencies lead to higher power loss. Therefore, it is important to identify an optimal frequency to increase the efficiency of the induction heating system based on the application. The use of low-frequency range is recommended to heat thick materials as it can penetrate deep into the material, whereas higher frequencies are recommended for surface heating or to heat small areas. However, the advantage of using higher frequency is that it produces greater heat, but this higher heat on the surface of the material also means that more energy is dissipated to the surrounding environment (Rapoport and Pleshivtseva, 2006). In this research, an induction heating system operating at around 100 kHz was developed to ensure the granulated APC residues-based material is heated from inside out.

4.3.2 Design of the coil for induction heating

The electric current flowing through the coil generates magnetic field, and this induces current in the conductive material placed inside it. The ratio between the number of turns of the coil and properties of the material help identify the amount of current induced in the material (Carretero et al., 2011). For the purpose of this research, a cylindrical coil was designed to heat the granules. When a current is passed through the coil, it generates a hollow cylindrical electromagnetic field, and this field is concentrated towards the centre of the coil (Haimbaugh, 2015). The field induces a current in the conductive material and causes the formation of eddy currents and hysteresis effect which creates heat as discussed in sections (2.3.2 and 2.3.3).

The cylindrical coil was designed using 0.6cm copper pipe which was turned 6 times into a coil with a radius of 2.7cm and overall length of 7cm. The inductance of the coil is an important parameter in the design of the induction heating system, and it is possible to estimate by using Wheeler's approximation formula as given by Equation 4.6. This formula can approximate the inductance of the coil within 1% of its original value (Wheeler, 1928, Mukerjee and Thakur, 2011). This formula uses all the dimensions of the coil in inches and outputs the inductance of the coil in microhenry. The formula is only valid for coils those satisfy the condition, that the length of the coil should be greater than 0.8 times the radius of the coil. It can be seen from Equation 4.6 that the designed coil satisfies this condition. The inductance of the designed coil is $1.096\ \mu H$.

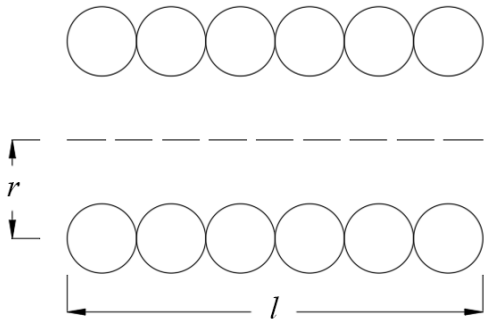

$$L_{coil} = \frac{r^2 n^2}{9r + 10l}$$

$$l > 0.8r$$

$$2.756 > 0.85$$

$$L_{coil} = \frac{1.063^2 \times 6^2}{(9 \times 1.063) + (10 \times 2.756)} = 1.096\ \mu H$$

$r = Radius\ of\ the\ coil\ (Inches)$

$l\ =\ Length\ of\ the\ coil\ (Inches)$

$n =\ number\ of\ turns$

$L_{coil}\ =\ Inductance\ of\ the\ the\ coil\ (\mu H)$

Equation 4.6: Wheeler's approximation formula for single layer coil (Wheeler, 1928, Mukerjee and Thakur, 2011)

4.3.3 Induction heating system circuit design

The main components of the induction heating system circuit design are Metal-Oxide-Semiconductor Field-Effect Transistors (MOSFETs), capacitors, inductors and a coil. These circuit components help produce an oscillating circuit that helps induce heat. It can be seen from Figure 4.17 that there are two MOSFET in this circuit. These MOSFETs open and close when a voltage is applied to their gates, hence allowing the current to flow through the source and the drain. This

configuration of the MOSFET ensures charging and discharging of the capacitors connected in parallel, this process help produce an alternating current that is supplied to the coil, and this generates the electromagnetic field. The operating frequency of the oscillating circuit can be changed by changing the total capacitance and inductance of the circuit. It can be seen from Figure 4.17 that all the capacitors in the circuit are connected in parallel and it is possible to easily change the frequency of the circuit by adding or removing the capacitors connected in parallel. The circuit uses Mazzilli's driver circuit, and its design is based on Zero-Voltage Switching (ZVS) power resonating circuit and Royer oscillating circuit (Costanzo et al., 2013, Hapidin et al., 2017).

The operating frequency of the circuit can be calculated by using Equation 4.7. This equation uses inductance of the coil and total capacitance of the circuit to determine the working frequency of the circuit. The designed circuit operates at 108.039kHz. It is important to understand that high current passing through the coil and heat generated by the material that the coil is inducting heat into can make the coil to heat up through convection and radiation (Runde et al., 2011). This heating can change the inductance of the coil; therefore, it is important to cool the coil to maintain a stable frequency. This can be achieved by circulating cooling liquid through the coil and by using an insulating material between the coil and the material (that is being heated).

$$f = \frac{1}{2\pi\sqrt{L \times C}}$$

$$f = \frac{1}{2\pi\sqrt{(1.096 \times 10^{-6}) \times (1.98 \times 10^{-6})}} = 108.039kHz$$

Equation 4.7: Formula to calculate the frequency of the system (Forest et al., 2000)

The circuit (Figure 4.17) was designed and simulated in NI Multisim software, with the circuit producing a Root Mean Square (RMS) current of 147A and RMS voltage of 76V. These value can be used to calculate the magnetic field generated by the coil using Equation 4.8 where N is number of turns of the coil, L is the length of the coil, I is the current in the coil and μ_0 is absolute magnetic permeability of free space which is $4\pi \times 10^{-7}$ (H/m) (Singh, 2011). For this equation to be valid, it is assumed that the magnetic field is concentrated within the coil and it is also constant.

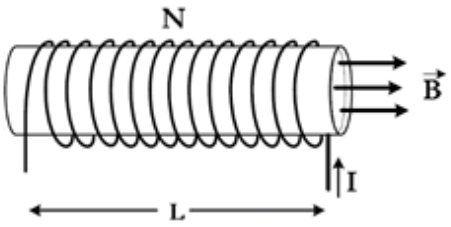

$$B = \mu_0 \frac{NI}{L}$$

$$B = 4\pi \times 10^{-7} \times \frac{6 \times 147}{7 \times 10^{-2}} = 15.834mT$$

Equation 4.8: Formula to calculate magnetic field (Singh, 2011)

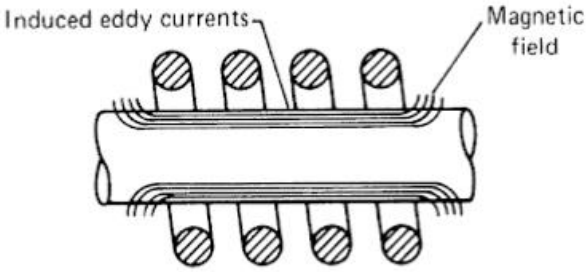

Figure 4.16: Magnetic field produced by the multiturn induction coil (Haimbaugh, 2015)

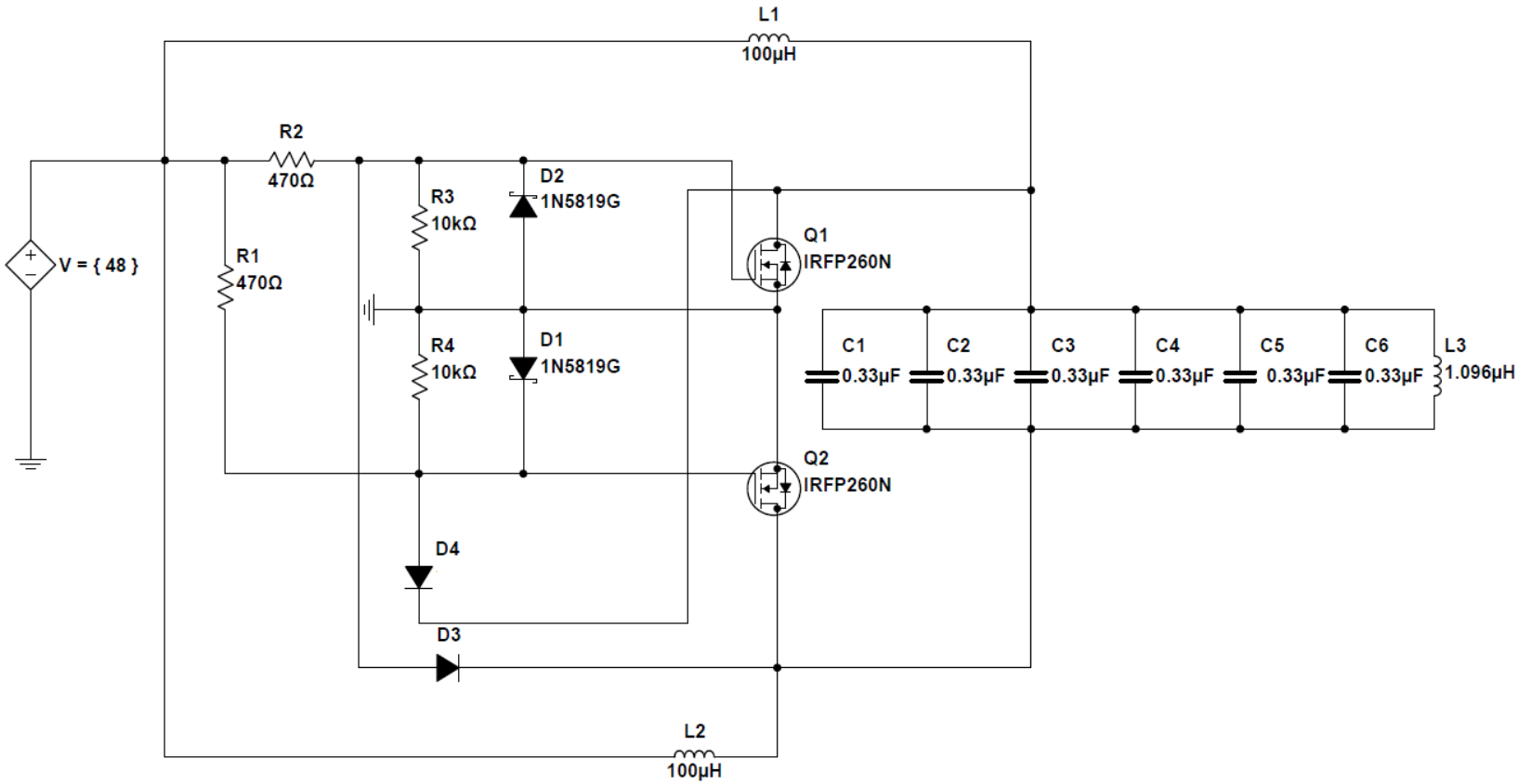

Figure 4.17: Induction heating circuit diagram

4.3.4 Induction experiment and discussion

The requirement of the induction heating system is that the material should be conductive therefore APC residues and powdered clay was homogenised with magnetic materials. All these materials were sieved through a 600μm sieve. The granules were doped with magnetic materials to allow them to have conductive and magnetic properties. The three magnetic materials those were used are iron filings (ferrimagnetic), magnetite (ferrimagnetic) and graphite (diamagnetic). The formulations for these granules are summarised in Table 4.4. These formulations were homogenised with 25% water to form into granules of 2.4g each. These were then dried for 24 hours at 100^{o}C.

Sample Name	G25,70 (g)	G35,60 (g)	I25,70 (g)	I35,60 (g)	M25,70 (g)	M35,60 (g)
APC residues	5	5	5	5	5	5
Clay	70	60	70	60	70	60
Graphite	25	35	0	0	0	0
Iron filings	0	0	25	35	0	0
Magnetite	0	0	0	0	25	35

Table 4.4: Formulation of the granules for induction experiment

The produced granules were placed inside the coil of an induction heating system, and it was noticed that within few seconds of being in the magnetic field these granules were shattering and this behaviour was noticed for all the granules. This was due to the rapid heating of the magnetic material homogenised in a clay matrix causing a temperature gradient within the material. This rapid heating causes localised thermal stresses to be induced within the granules due to electromagnetic field leading to rapid expansion of clay. This expansion causes the granules to shatter. In this case, the use of induction heating system was not effective, but this technology has a lot potential for further investigation to develop a special material that can behave like an electrolyte when placed inside the electromagnetic field and when it cures/solidifies it losses its conductance and magnetic properties. For example, Sugilal (2008) melted sodium borosilicate glass in an induction heating system by first melting a small amount (45g) of glass using graphite heating rings and then once the glass was hot enough to conduct electricity, additional glass was added into the induction heating system for melting.

The induction heating system was not investigated further because of the time constraint and cost implication of this project as it required a lot of additional development work to implement it successfully, and it was beyond the scope of this research to develop a special material that can be cured using an induction heating system. However, this project will be carried forward as post-doctoral research. The implementation and development of this type of technology can be very beneficial for the future as this can open new possibilities with novel applications to investigate a whole new class of materials for induction heating system - allowing the material to be heated without coming in direct contact with the heating source. The application of such a material with high compressive strength can be used for 3D printing of houses and buildings.

4.4 Conclusions

Thermal treatment of APC residues can be a very effective technique to achieve solidification/stabilising. It was possible to achieve inert material by sintering clay with APC residues at 1170^{o}C for 20 minutes, and the granules achieved the highest fracture strength of 5.78MPa with 20% APC residue and 80% clay. The chapter also investigated the use of an induction heating system to heat the granules, but it was not able to sinter the granules because of the heat stresses generated within the granules causing it to shatter. However, further development of this type of system can be very beneficial for the future as it can reach high temperatures very rapidly and can be used to solidify materials to achieve very high compressive strength. The application of this kind of system can be to 3D print houses, buildings and other civil engineering infrastructure. It was shown that it is possible to successfully treat APC residues using high temperatures, but the process is not environmentally friendly as it has very high energy demands. In the next chapter (Chapter 5) geopolymerisation will be investigated to achieve solidification/stabilisation. There is evidence suggesting that cold bonding technique such as geopolymerisation can be very effective as Kourti et al. (2010) developed a geopolymer based material using APC residues by using alkaline activators to produce a material with very high compressive strength of about 130 MPa but the paper used DC plasma technology to first produce a glass rich in calcium aluminosilicate using APC residues hence making the process very energy inefficient but it is possible to achieve geopolymerisation using APC residues without utilising heat.

5 Solidification of Air Pollution Control (APC) residue using geopolymerisation

There has been an increase in peer-review papers on Cold Bonded Light Weight Aggregates (CBLA) produced using fly ash (Bui et al., 2012, Yliniemi et al., 2017, Patel et al., 2018, Tajra et al., 2018, Tang and Brouwers, 2018) but utilisation of MSWI APC residues to produce CBLA will not be explored. The MSWI based geopolymer developed in this chapter can be used as CBLA but the investigation of various different sodium silicate to sodium hydroxide ratios and solid to liquid ratios led to the production of material that could only be cured in a mould – as it was not possible to hand produce the pellets. The word solid in this chapter will be used to refer to APC residue and liquid refers to an alkaline activator (solution of sodium hydroxide and sodium silicate). The effect of various different ratios, especially sodium silicate to sodium hydroxide was investigated to understand the importance of sodium silicate because according to Rashidian-Dezfouli et al. (2018), the addition of sodium silicate was not as important as the amount of sodium hydroxide to produce the geopolymer based material whereas in literature (Duxson et al., 2007, Khale and Chaudhary, 2007, Toniolo and Boccaccini, 2017, Vafaei and Allahverdi, 2017) it was evident that the presence of silica is one of the most factors in the production of a geopolymer based material.

5.1.1 Methodology to develop MSWI APC residue based geopolymer

The experiment will investigate the effect of washed and unwashed APC residues. The washed APC residues were prepared by mixing deionised water with APC residues, at a ratio of 3:1 for 5 minutes as recommended by Yang et al. (2017). After this, the mixture was filtered and dried at 105^{o}C for 24 hours. Lastly the dried, washed APC residues were balled milled for 2 hours, and the particles were allowed to pass through a 600-micron sieve. [Note: Different papers have

recommended different washing procedures such as Zheng et al. (2011) washed MSWI fly ash using deionised water at 1:1 ratio (ash (g) to water (ml)). The mixture was left to stand for 40 minutes before being filtered, and the ash was washed twice. After this, the ash was dried for 24 hours at 80ºC. The APC residues in this research were washed using the technique recommended by Yang et al. (2017) because this paper has investigated the effect of different washing procedures and their effects on the leaching behaviour of APC residues].

The sodium hydroxide solution of 10M concentration was used in the experiment and this was prepared using sodium hydroxide pearls (99.99%). The calculation used to prepare the solution is shown in Equation 5.1, whereby 400 g of sodium hydroxide pearls were mixed with 1L of distilled water, and the mixture was stirred after every 10 minutes for 1 hour to allow all the pearls to dissolve completely. The sodium silicate used in this research had a molar ratio of 3.2:1 (SiO_2:Na_2O), sourced from Avonchem, UK. Additional water was not added into the geopolymer mixture as it changes the concentration of the alkaline activator; higher water to solid ratio leads to weaker geopolymer and can interfere with the geopolymerisation process and hence weakens it (Khale and Chaudhary, 2007). The other reason is that higher concentration of sodium hydroxide led to higher compressive strength hence the addition of water into the geopolymer mixture reduces the concentration and leads to the formation of weak geopolymer (Boca Santa et al., 2016).

$$\text{Moles per litre (Molar)} = \frac{\text{Grams of Sodium hydroxide}}{\text{Water (l)} \times \text{Molecular weight of Sodium hydroxide}}$$

$$\text{Moles per litre (Molar)} = \frac{400}{1 \times 39.997}$$

$$\text{Moles per litre (Molar)} = 10.00075\ \text{M}$$

Equation 5.1: Sodium Hydroxide solution preparation

APC residues-based geopolymer material was cured in a 25 mm cube mould. This size mould was chosen because it has been used by many researchers to investigate geopolymerisation (Wang and Cheng, 2003, Tippayasam et al., 2011,

Khater, 2012, Hassaan et al., 2015, Ogundiran and Kumar, 2015, Tome et al., 2018). APC residues were passed through a 600micron sieve and particles larger than 600 microns were passed through the sieve with the help of the pestle (Figure 5.1). This is important because small particle sizes optimise the geopolymerisation process to help achieve a more homogenous matrix. The geopolymer cubes were prepared by first mixing sodium hydroxide with sodium silicate to produce a homogenous solution of alkaline activator. The alkaline activator solution was then mixed with APC residues using a hand mixer for 1 minute. The mixture was created quickly as it solidifies in a very short period of time. It was then quickly poured into cubical moulds and was allowed to cure for 24 hours before being removed and allowed to continue curing at room temperature (22^{o}C ± 2^{o}C) for testing after 7, 14 and 28 days respectively. The flowchart of the methodology can be seen in Figure 5.2. A summary of different formulations for the experiment can be seen in Table 5.1 and Table 5.2. For each formulation, 12 samples were prepared for compressive strength testing. The experiment used both washed and unwashed APC residues therefore in total, 864 samples were produced and tested.

Figure 5.1: Sieving of APC residues using the pestle to produce a fine powder suitable for mixing

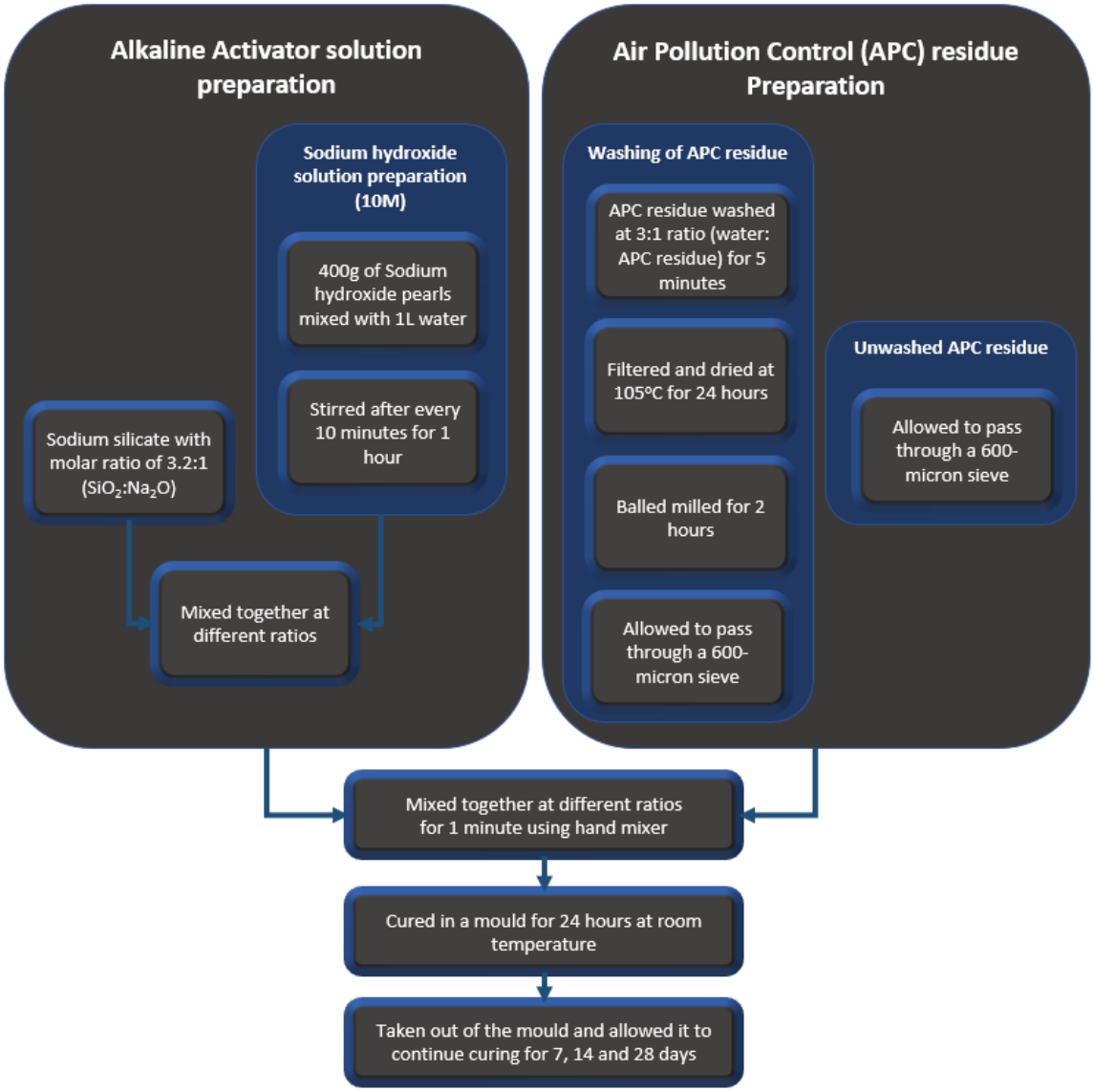

Figure 5.2: Flowchart of the methodology to prepare APC residue based geopolymer material

The descriptors used for different experimental compositions are systemically designed to ease the identification of the compositional ratio used to prepare the material. The first letter of the descriptor indicates the type of APC residues being used; where W denotes washed APC residues, and U denotes for unwashed APC residues. The number after this letter indicates the solid to liquid ratio (APC residue to alkaline activator ratio) and the number at the end of the descriptor identifies sodium silicate to sodium hydroxide ratio as a single number that is obtained by dividing one from another respectively, as can be seen in Figure 5.3.

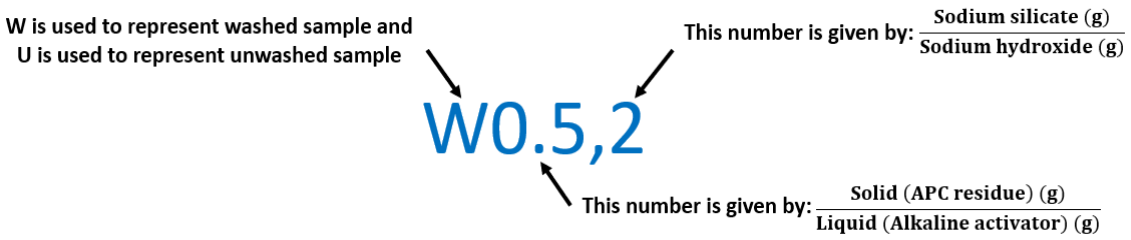

Figure 5.3: Definition of the label descriptor used in this experiment

Descriptors	Solid to liquid ratio	Sodium silicate to sodium hydroxide ratio	APC residues (g)	Solution needed (g)	Sodium silicate (g)	Sodium hydroxide (g)
U0.5,4	1:2	4:1	240	480	384	96
U0.5,3	1:2	3:1	240	480	360	120
U0.5,2	1:2	2:1	240	480	320	160
U0.5.1.5	1:2	3:2	240	480	288	192
U0.5,1	1:2	1:1	240	480	240	240
U0.5,0.5	1:2	1:2	240	480	160	320
U0.33,4	1:3	4:1	200	600	480	120
U0.33,3	1:3	3:1	200	600	450	150
U0.33,2	1:3	2:1	200	600	400	200
U0.33,1.5	1:3	3:2	200	600	360	240
U0.33,1	1:3	1:1	200	600	300	300
U0.33,0.5	1:3	1:2	200	600	200	400

Table 5.1: Summary of the geopolymer samples prepared using unwashed APC residues

Descriptors	Solid to liquid ratio	Sodium silicate to sodium hydroxide ratio	APC residues (g)	Solution needed (g)	Sodium silicate (g)	Sodium hydroxide (g)
W0.5,4	1:2	4:1	240	480	384	96
W0.5,3	1:2	3:1	240	480	360	120
W0.5,2	1:2	2:1	240	480	320	160
W0.5.1.5	1:2	3:2	240	480	288	192
W0.5,1	1:2	1:1	240	480	240	240
W0.5,0.5	1:2	1:2	240	480	160	320
W0.33,4	1:3	4:1	200	600	480	120
W0.33,3	1:3	3:1	200	600	450	150
W0.33,2	1:3	2:1	200	600	400	200
W0.33,1.5	1:3	3:2	200	600	360	240
W0.33,1	1:3	1:1	200	600	300	300
W0.33,0.5	1:3	1:2	200	600	200	400

Table 5.2: Summary of the geopolymer samples prepared using washed APC residues

5.1.2 Results and discussion

The experimental results obtained suggest that, as the number of days increases, so does the compressive strength of the material as can be seen in Figure 5.4 and Figure 5.5. The highest compressive strength achieved by the unwashed APC residues based geopolymer material was 984 kPa after 28 days for sample U0.5,2. The second highest compressive strength of 874 kPa was achieved by sample U0.5,3 (after 28 days). The washed samples achieved the highest compressive strength of 2348 kPa for sample W0.5,1.5 followed by sample U0.5,2 with a compressive strength of 2185 kPa. Overall, the best performing solid to liquid ratio was 1:2 for both washed and unwashed APC residues. However, the best performing sodium silicate to sodium hydroxide ratio for unwashed APC residues based geopolymer material was 3:2 followed by 2:1 whereas for unwashed APC residues it was 2:1 followed by 3:1 as can be seen in Figure 5.4 and Figure 5.5. The unwashed APC residues were not able to achieve higher compressive strength because of the presence of higher levels of salts. The effect of inorganic salts was investigated by Zheng et al. (2011) and Lee and van Deventer (2002). According to Zheng et al. (2011) presence of calcium chloride, magnesium chloride and potassium chloride is decremental to geopolymerisation whereas the presence of potassium carbonate and calcium carbonate help improve the strength of the geopolymer and also indicates that water washing of MSWI fly ash help produces geopolymer with higher strength. The study by Lee and van Deventer (2002) concluded that the presence of chloride salts maybe causing the crystallisation of aluminosilicate gel and this may be causing the weakening of the geopolymer based material. The other reason washed APC residues produced stronger material was because after washing the percentage of silica and alumina increased as soluble compounds were removed by washing. The chemical composition of washed and unwashed APC residues can be seen in Table 5.3. To better understand the effect of silica and alumina, it is important to first understand the stages of the geopolymerisation reaction and these will be discussed in the next section.

Major chemical compounds	Unwashed (%)	Washed (%)
SiO_2	11.2	20.6
Al_2O_3	7.9	10.4
Fe_2O_3	2.7	4.4
CaO	31.5	35.2
MgO	3.4	4.4
Na_2O	6.7	1.3
Cl	12.3	1.4
K_2O	3.2	1.1
SO_3	9.8	10.4

Table 5.3: Unwashed and washed MSW APC residues chemical composition

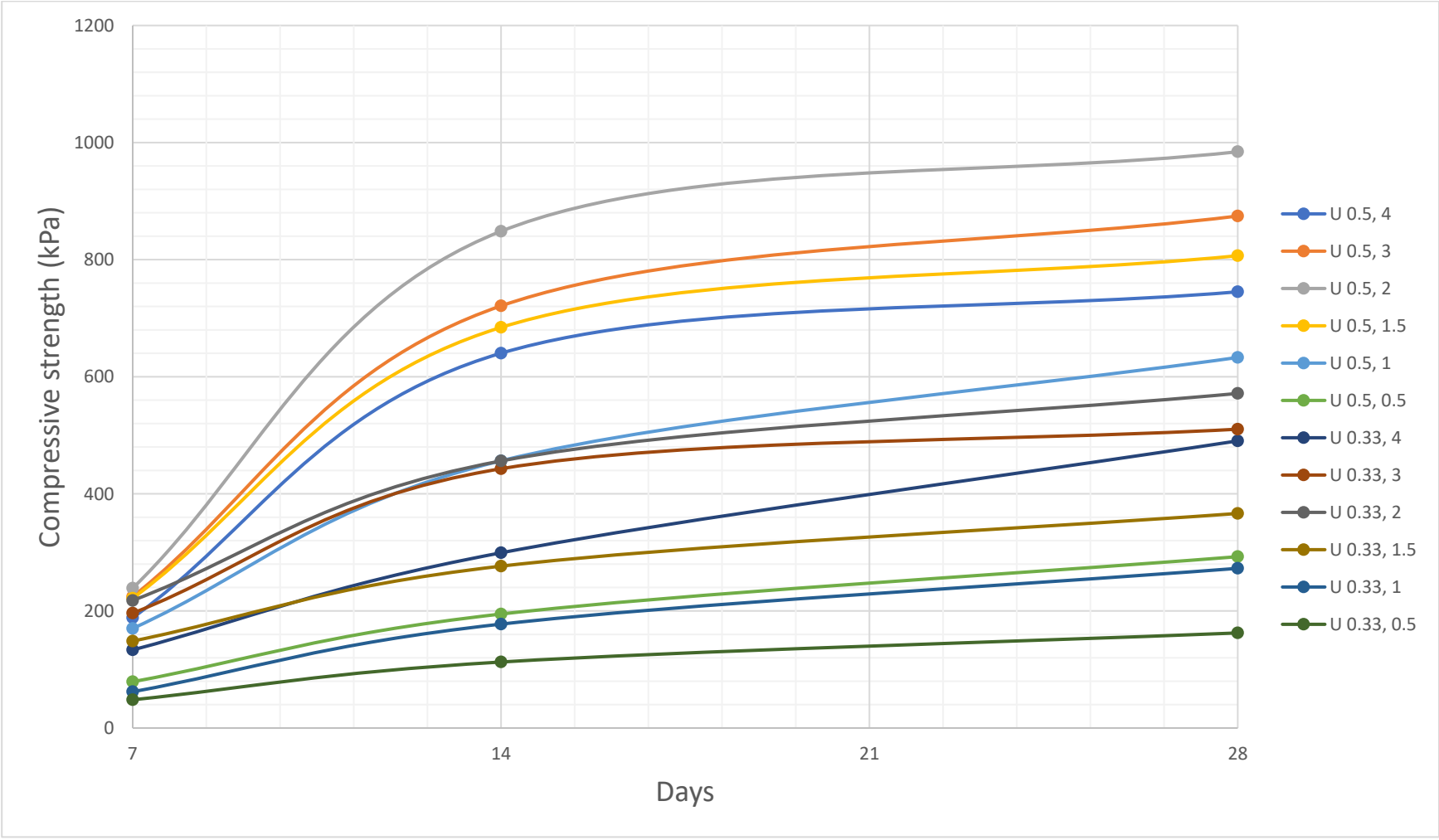

Figure 5.4: Compressive strength of unwashed APC residues based geopolymer material after 7, 14 and 28 days

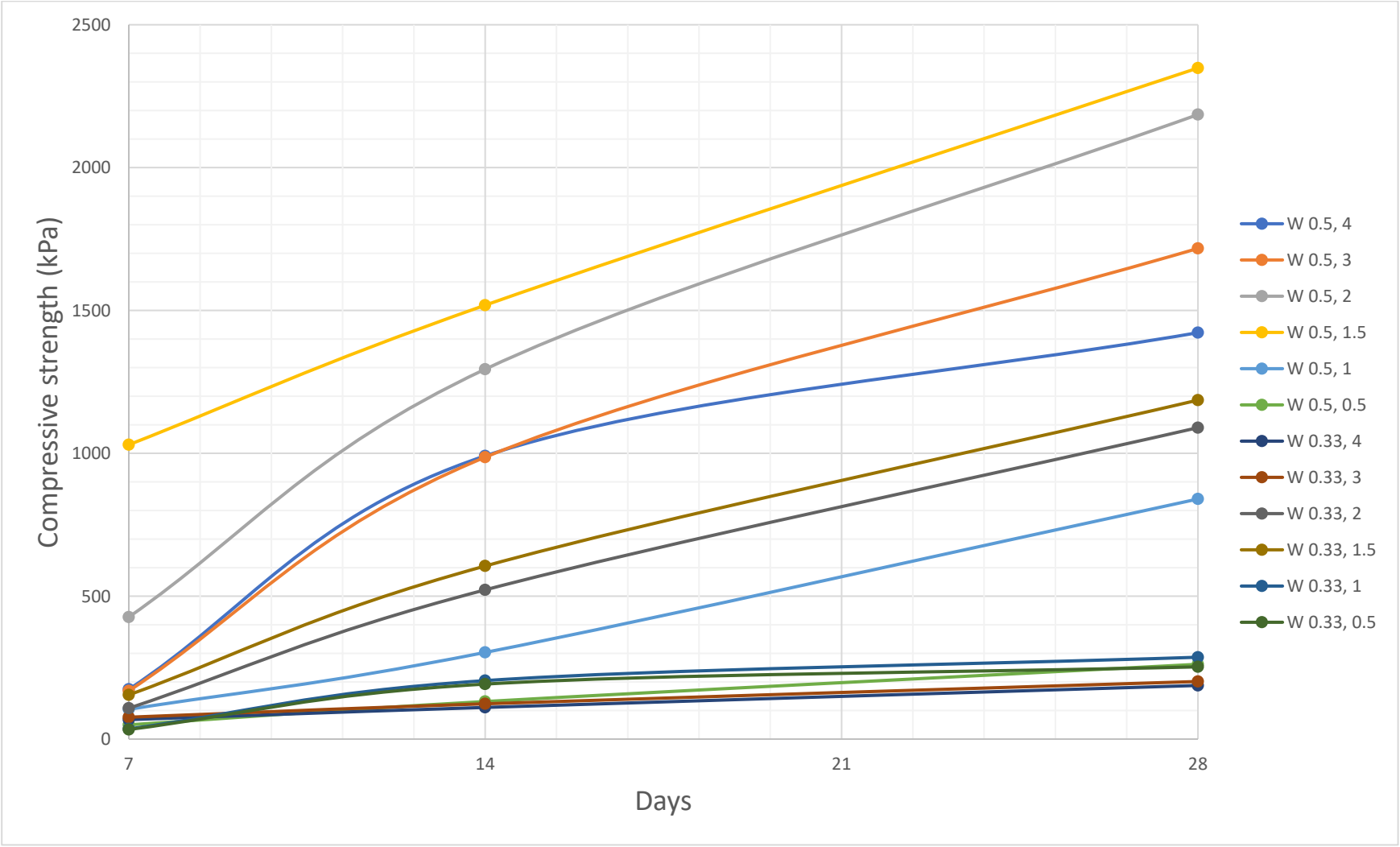

Figure 5.5: Compressive strength of washed APC residues based geopolymer material after 7, 14 and 28 days

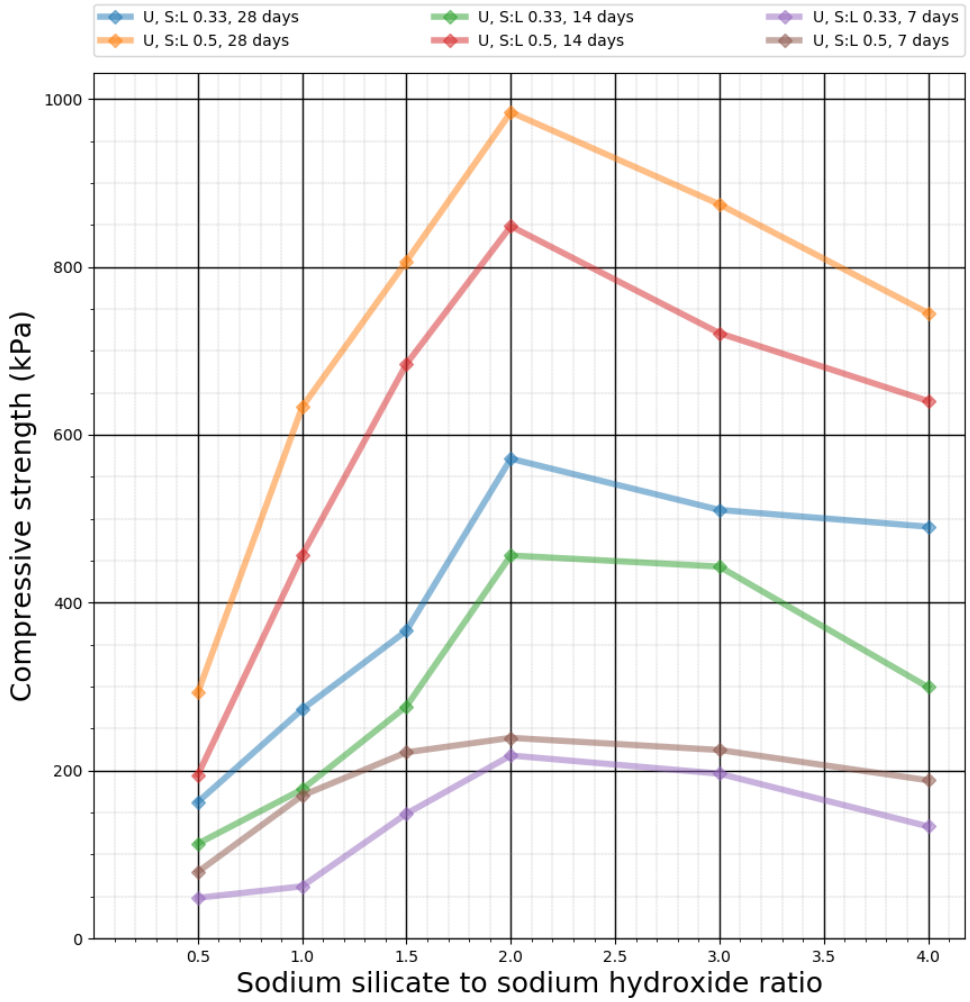

Note: S:L is Solid to liquid ratio

Figure 5.6: Compressive of unwashed APC residues based geopolymer material after 7, 14 and 28 days against sodium silicate to sodium hydroxide ratio

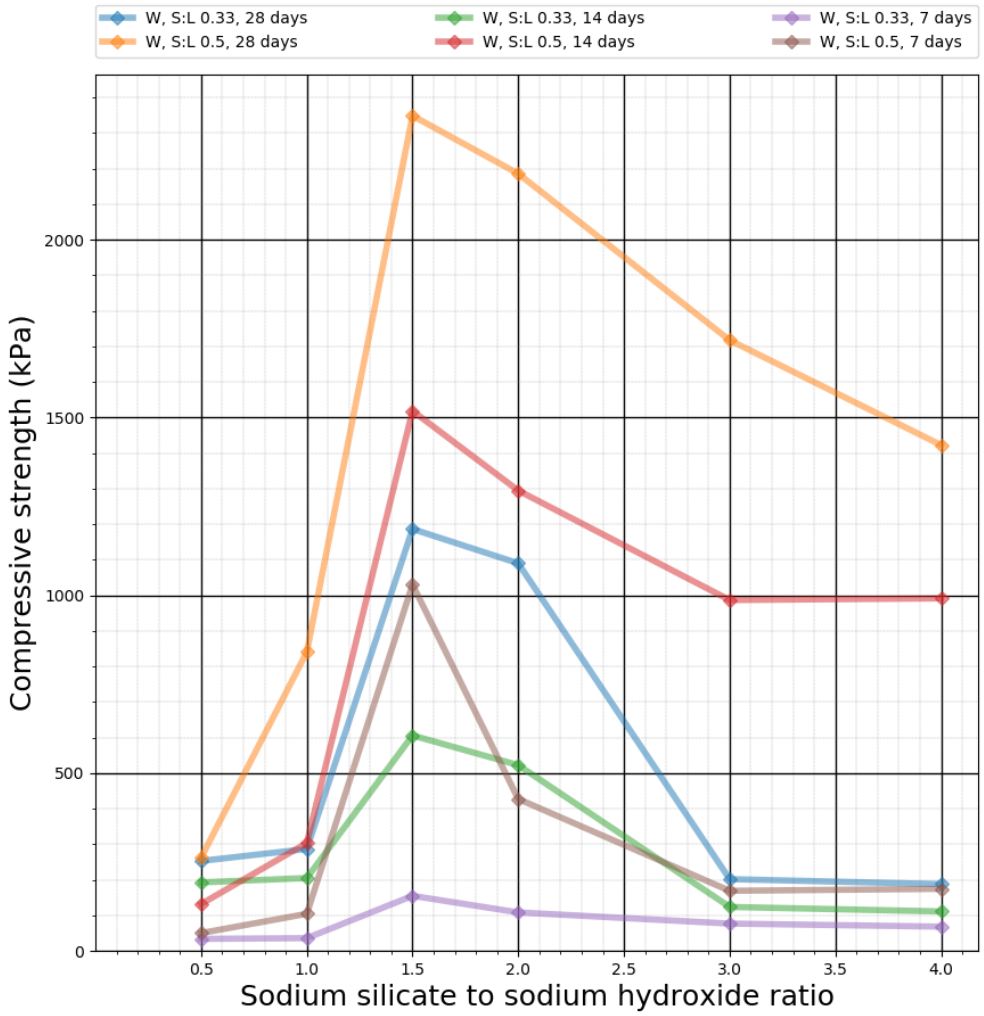

Note: S:L is Solid to liquid ratio

Figure 5.7: Compressive of washed APC residues based geopolymer material after 7, 14 and 28 days against sodium silicate to sodium hydroxide ratio

5.1.2.1 Geopolymerisation process and effect of silica and alumina

The geopolymerisation process takes place in three stages, and these are as follows:

(i) **Dissolution:** Highly alkaline liquid attacks the MSW APC residues and hydrolysis. This causes disruption of Si-O-Si and Si-O-Al compounds present in the material, and as this material is very high in calcium content, it will also cause disruption of Si-O-Ca bonds. These disrupted compounds are used as a reactive precursor to form Si $(OH)_4$ and Al $(OH)_4$ in the solution mixture. These precursors condense and yield to precipitation. The process causes the formation of gases, and these gases get trapped and cause the formation of voids. This process partially opens the internal porosity, and the alkaline solution penetrates further inside the material. The mixture carries a negative charge, and this electronic imbalance is compensated by an alkali metal cation (Na^+, K^+, Ca^{2+}) (Davidovits, 1991).

(ii) **Reordering and creation of monomers:** After dissolution, ionic precursors Al and Si move to a highly alkaline environment. They react with water and alkali causes the formation of monomer units. These units form a metastable gel around the material (Duxson et al., 2007).

(iii) **Polymerisation/Polycondensation:** In the third and the final stage, polymerisation or also called polycondensation occurs and at this stage monomer units becomes large and forms a gel. The gel creates a barrier around the powdered material and prevents the penetration of the alkaline solution. At this time soluble silicate is incorporated in the gel (Davidovits, 2008). During this stage certain amount of water is released by evaporation. After this, a three-dimensional polymer chain and a ring structure composed of Si-O-Al-O is formed (an amorphous structure), but according to Somna et al. (2011) some crystalline phases may be present in the material, and these are more evident particularly in low silica-based material. Moreover, it can be seen that the silica content of MSW APC residues is very low hence, therefore, the MSW APC

residues based geopolymer would have crystalline and amorphous phases.

It can be seen that the main elements of geopolymerisation are silica and alumina; therefore, the low presence of these two compounds is contributing to a weak material. Many papers have indicated that properties of geopolymers very much depend on the Si/Al ratio (Onori et al., 2011, Lancellotti et al., 2010, Duxson et al., 2005, Somna et al., 2011, Pimraksa et al., 2011, Noor ul et al., 2017, Wan et al., 2017, Glid et al., 2017). According to Mohseni (2018), higher Si/Al ratio leads to higher strength, and it is one of the most important factors in the encapsulation of toxic compounds (Giro-Paloma et al., 2017a). Lancellotti et al. (2010) indicated that Si/Al ratio should be between 1.5 to 2.5 and Na/Al ratio should be between 1 to 1.29 to achieve the best physical properties for a geopolymer, but it is important to examine the overall percentage of these elements instead of just these ratios as these ratios can be maintained even if the overall percentage of these elements are very low.

5.1.2.2 Effect of Calcium

It can be seen from Table 5.3 that APC residue contains high percentage of calcium and its presence has been investigated by many researchers. Tzanakos et al. (2014) used bottom ash and fly ash from the incineration of medical waste, calcium carbonate and kaolinite to produce a geopolymer by using sodium hydroxide and sodium silicate as the alkaline activator. The paper determined that the strength of the geopolymer could be significantly increased by the addition (7 – 16%) of calcium carbonate, with medical waste ash and kaolinite. The ratios of medical waste ash to kaolinite that were investigated were; 10:100, 30:100 and 50:100. It can be seen from Figure 5.8 that addition of calcium carbonate increased the compressive of the geopolymer. This may suggest that high levels of calcium present in the APC residues can be beneficial in the process to allow the formation of a strong material. Normally, the addition of sodium silicate with sodium hydroxide would help the formation of sodium aluminosilicate hydrate (NASH); but in the presence of the high calcium content, calcium aluminosilicate hydrate (CASH) and calcium silicate hydrate (CSH) can be produced (Phoo-Ngernkham et

al., 2015). It is also possible to get calcium silicate hydrate (CSH) gel forming along with NASH gel and calcium aluminosilicate hydrate (CASH) gel. Calcium-rich material also forms ettringite ($Ca_6Al_2[SO_4]_3[OH]_{12}\cdot 26H_2O$) when a reaction occurs between anhydrite ($CaSO_4$) and aluminosilicate. The formation of ettringite can cause microcracks during the curing of the geopolymer - resulting in a weak geopolymer matrix (Garcia-Lodeiro et al., 2011). However, Li et al. (2014) indicated that the production of CSH matrix consequently reduced the pore size to increase the strength and also accelerated the hardening process of the geopolymer. Vafaei and Allahverdi (2017) added calcium aluminate as a source of alumina to develop a geopolymer using waste glass powder that had a low alumina content. The sodium silicate and sodium hydroxide were used as an alkaline activator. The addition of calcium aluminate cement helped increase the strength of the geopolymer, as it improved the microstructure. Furthermore, Kourti et al. (2011) used the DC plasma treatment of APC residues to produce APC residues glass that is rich in calcium aluminosilicate. The resulting geopolymer was able to achieve a high compressive strength of 110MPa after 28 days, with additions of sodium hydroxide and sodium silicate. From these studies, it appears that high calcium content present in the APC residues would aid in the strengthening of the geopolymer. So, it can be concluded that presence of high calcium can benefit the geopolymer based material to achieve higher strength, but the high presence of salt, heavy metals and low presence of silica and alumina has led to the formation of a weak material.

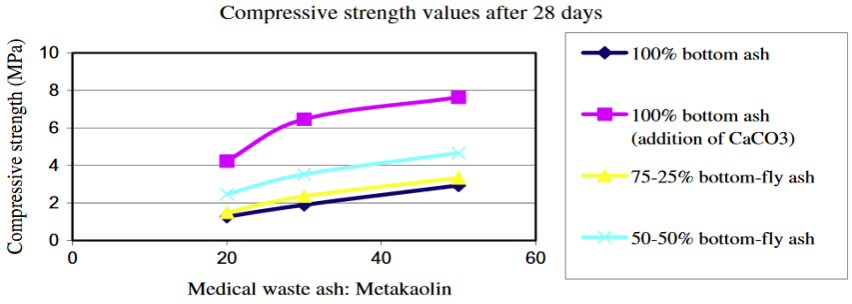

Figure 5.8: The compressive strength of medical waste ash based geopolymer material (Tzanakos et al., 2014)

5.1.3 Scanning Electron Microscope (SEM) images and leaching characteristics of APC residues based geopolymer material

The highest compressive strength of APC residues based geopolymer material were achieved by the sample with solid to liquid ratio of 1:2 and sodium silicate to sodium hydroxide ratio of 2:1 for unwashed sample and for washed sample it was achieved by solid to liquid ratio of 1:2 and sodium silicate to sodium hydroxide ratio of 3:2. The compressive strength achieved by the washed sample was 2.35 MPa whereas the unwashed sample was only able to achieve 0.98 MPa. The reason identified above for a weak material produced by the unwashed APC residues was due to the presence of high levels of soluble salts and heavy metals negatively influencing the alkali activation reactions in the material. This was validated by observing the structure of both washed and unwashed APC residues-based geopolymer material using a Scanning Electron Microscope (SEM). It can be seen from Figure 5.9 and Figure 5.10 that there are no visible cracks for washed sample, whereas for unwashed sample there are visible microcracks at 500 magnification. These observations were made on three different samples for a particular formulation (W0.5,1.5 and U0.5,2) to confirm the finding. This indicates that unwashed APC resides causes disruption in chemical reactions, hence causing the formation of microcracks. The leaching characteristic of the unwashed and washed sample also confirm this as leaching of lead, zinc, chloride and sulphate is very high as compared to the washed sample. The unwashed sample even after treatment exceeds the hazardous waste landfill limit whereas washed sample was able to stabilise APC residues to below non-hazardous waste limit as can be seen Table 5.4.

Leachable Elements	Sample U0.5, 2 (mg/kg)	Sample W0.5, 1.5 (mg/kg)	Inert waste limit (mg/kg)	Non-hazardous waste limit (mg/kg)	Hazardous waste limit (mg/kg)
As	<DL	<DL	0.50	2.00	25.00
Ba	<DL	<DL	20.00	100.00	300.00
Cd	<DL	<DL	0.04	1.00	5.00
Cr	<DL	<DL	0.50	10.00	70.00
Cu	<DL	<DL	2.00	50.00	100.00
Hg	<DL	<DL	0.01	0.20	2.00
Mo	<DL	<DL	0.50	10.00	30.00
Ni	<DL	<DL	0.40	10.00	40.00
Pb	91.72	4.43	0.50	10.00	50.00
Sb	<DL	<DL	0.06	0.70	5.00
Se	<DL	<DL	0.10	0.50	7.00
Zn	34.94	2.42	4.00	50.00	200.00
Cl	46,345.23	7,052.32	800.00	15,000.00	25,000.00
SO_4	9,452.40	783.24	1,000.00	20,000.00	50,000.00

DL: Detection Limit

Table 5.4: Leaching test of the best performing APC residues based geopolymer material

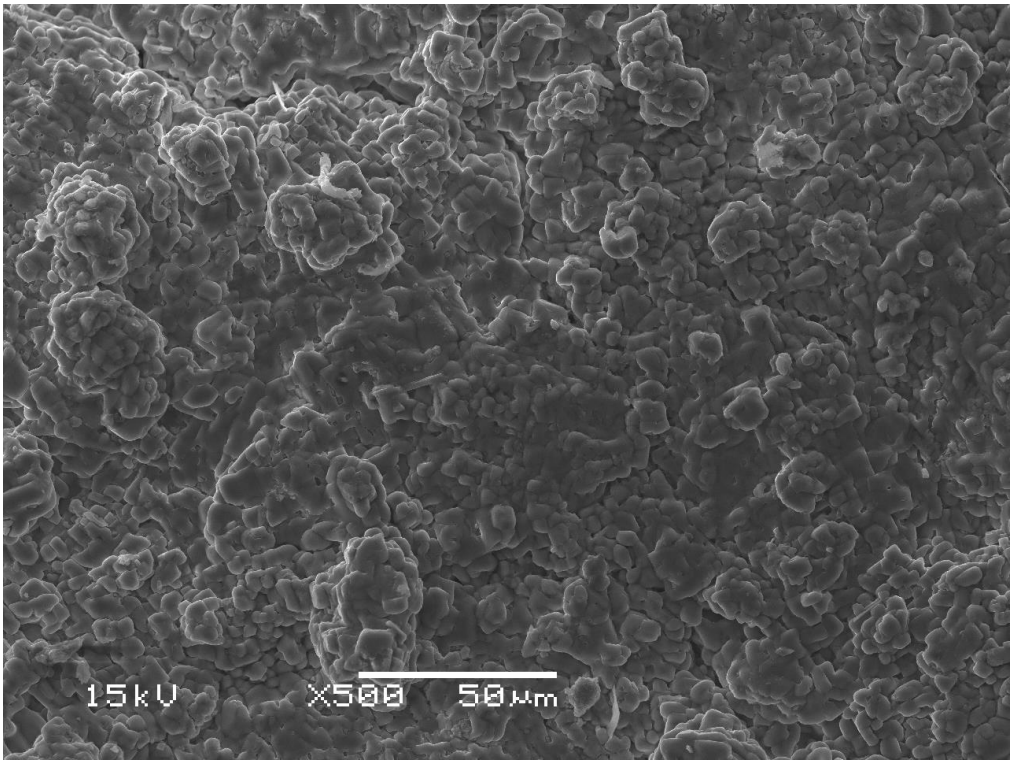

Figure 5.9: Sample W0.5,1.5 after 28 days

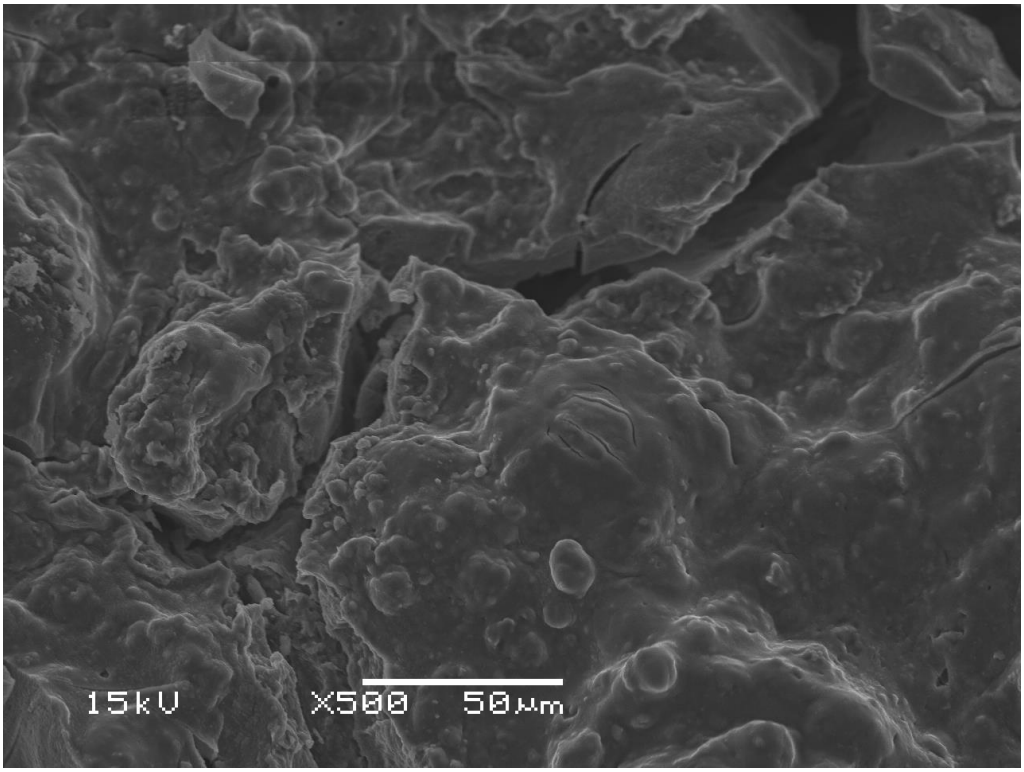

Figure 5.10: Sample U0.5,2 after 28 days

5.2 Conclusion

The treatment through cold bonding was achieved by developing, APC residues-based geopolymer material. This method of treatment was adequate to achieve solidification/stabilisation. The research investigated different solid to liquid ratios and sodium hydroxide to sodium silicate ratios to identify the relationship of these ratios to the physical and chemical characteristics of the material. The most suitable solid to liquid ratio identified in this research was 1:2, and for sodium hydroxide to sodium silicate, it was 2:1 and 3:2. These ratios managed to produce a material with the compressive strength of 2.35 MPa for washed APC residues. The use of unwashed APC residues was also investigated, but it was concluded that unwashed APC residues produce material with undesirable properties. Regarding the leaching behaviour, its performance was not as good as of the sintered material, but in terms of classification, it can be classified as non-hazardous material according to UK landfill Directive 2008/98/EC. Therefore, this technique can be used to achieve solidification/stabilisation of APC residues, as untreated APC residues exceed the hazardous waste limit for landfills in the UK for lead and chloride. The data from this experiment will be used in chapter 6 to develop a machine learning model to predict the compressive strength of the material.

6 Machine learning to predict the compressive strength of the geopolymer-based material

The novelty of this chapter is to develop a machine learning model using key input experimental parameters to help predict the compressive strength of the APC residue-based geopolymer material. Machine learning algorithms provide researchers with a layer of abstraction to help them model complex behaviours, whereas developing a similar theoretical model would require a very high-level understanding of the phenomena itself. For this research, key experimental parameters from APC residues-based geopolymer material are used as an input to the machine learning model to predict the compressive strength of the material. These types of models have an advantage over theoretical models because the prerequisites for the development are the known parameters whereas development using theoretical modelling techniques would require a complete understanding of key chemical reactions and bond formations. In the case of APC residues, it has a very complex chemical makeup; therefore the development of a theoretical model to predict the compressive strength of the geopolymer-based material is just not suitable. ANN is a very effective technique to model problems those are very difficult to model (Asteris et al., 2016).

Machine learning techniques such as ANN and multivariate regression models have been used by researchers to predict the compressive strength of concrete (Sarıdemir, 2009, Bilgehan and Turgut, 2010, Dantas et al., 2013, Asteris et al., 2016, Chithra et al., 2016, Eskandari-Naddaf and Kazemi, 2017). The behaviour of concrete is comparatively easy to model according to Van Damme (2018) therefore linear and non-linear multivariate regression modelling techniques can be used to model their behaviour but for high-performance concrete use of non-linear multivariate regression models are not suitable because of the complexity of the material. However, researchers have used non-linear multivariate regression

modelling techniques to model high-performance concrete behaviour such as Jin et al. (2018b) used it to produce a model to predict the compressive strength with an accuracy of 99% for Fibre reinforced polymer (FRP) recycled aggregate concrete. In another paper by Jin et al. (2018a) developed a nonlinear multivariate regression model to predict the compressive strength of sustainable concrete with an R^2 value of 0.955. Yoon et al. (2014) developed a multivariate regression model to predict the mechanical properties (Compressive strength and Young's modulus) of coal fly ash-based concrete with a Mean Square Error (MSE) of 12.1 for compressive strength and 4.1 for Young's modulus. It can be seen from these that it is possible to produce a good model using non-linear multivariate regression, but the performance of ANN cannot be matched. Chithra et al. (2016) investigated the performance of ANN and a multivariate regression model to predict the compressive strength of the High-performance concrete containing Nano silica and copper slag, and it was concluded that ANN model produces a better fit to training dataset then multivariate regression. ANN are powerful because they have the ability to combine many different statistical techniques to produce a model that provides them with an ability to produce models in many different disciplines such as engineering. Therefore they are used for autonomous driving vehicles, image recognition and many other applications (Van Damme, 2018). However, it is considered to be a black-box because it is very difficult to reason the outputs and also require large training dataset to be efficient (Chopra et al., 2018). Chopra et al. (2018) also compared some of the other machine learning techniques (decision tree modelling technique, random forest modelling technique and ANN) to develop a model to predict the compressive strength of the concrete after 28, 56 and 91 days and concluded that ANN produces the best results. It has been seen that ANN models are very effective at predicting the compressive strength of the concrete, but it has also been effective at modelling the steel transition temperature to predict the material transition from ductile phase to brittle phase (Nazari et al., 2011).

6.1 Implementation of a Multivariate Regression Model

The most commonly used machine learning model is a regression model. In this section, the multivariate regression model was developed to predict the compressive strength of the APC residues-based geopolymer material. It is straightforward to develop a regression model using two variables/parameters (one input variable and one output variable) in Microsoft Excel, but it is difficult to implement a multivariate regression model as it requires the user to program it in Visual Basic (VB). In this chapter, the multivariate regression model was programmed in Octave programming environment. The model was developed using key experimental variables such as solid to liquid ratios, sodium silicate to sodium hydroxide ratios and days as key inputs to the model.

The hypothesis function $h_\beta(x)$ for a multivariate regression model can be written as shown in Equation 6.1. This hypothesis function $h_\beta(x)$, predicts Y, given input features, X. This can be mathematically written as $h: X \rightarrow Y$. It is essential to fully understand the hypothesis function to help predict the compressive strength of the geopolymer-based material, and it is also vital to arrange all the variables into matrices and vectors in order to conclusively determine model parameters.

$$h_\beta(x) = \beta_0 x_0 + \beta_1 x_1 \dots\dots\dots + \beta_n x_n$$

n = number of input features

β = Parameters

Equation 6.1: Hypothesis function for multivariate regression model (Raschka et al., 2016)

6.1.1 The arrangement of data

In machine learning, it is essential to arrange data in the form of matrices and vectors, as programming languages are optimised to perform computations on them which reduces the development time. The hypothesis function $h_\beta(x)$ for multivariate regression requires input features x. These input features can be arranged into a matrix, where each feature within it can be identified by x_j^i, where j is the feature number and i is its index. The input features are mapped to the output y^i. The input feature x_j^i can be arranged into a matrix, X and output feature y^i into a vector Y as shown in Equation 6.2. The input matrix, X, of x_j^i training examples and output vector, Y, of y^i training examples are sets of real numbers, and they can be represented mathematically as $X = \mathbb{R}^{m \times n}$ and $Y = \mathbb{R}^m$. The dimensions of the real numbers $\mathbb{R}$ in matrix X and vector Y directly depends on the total number of training examples m and the total number of features n.

$$X = \begin{bmatrix} x_1^1 & \cdots & x_n^i \\ \vdots & \ddots & \vdots \\ x_1^m & \cdots & x_n^m \end{bmatrix}$$

$$Y = \begin{bmatrix} y^1 \\ \vdots \\ y^m \end{bmatrix}$$

$m = \text{total number of training examples}$

$n = \text{total number of features}$

Equation 6.2: Matrix arrangement of the input feature X and vector arrangement of the output feature Y

6.1.2 Examination of input features to model non-linearity

The hypothesis function defined in Equation 6.1 with all three input features (sodium silicate to sodium hydroxide ratio, solid to liquid ratio and days) would produce a linear model/regression model; but (as can be seen from Figure 6.1 and Figure 6.2) the data from the experiments do not behave linearly. Therefore, it is important to modify the hypothesis function (Equation 6.1) to produce a non-linear model by defining non-linear functions. Figure 6.1 and Figure 6.2 show that sodium silicate to sodium hydroxide ratio and compressive strength for both unwashed and washed samples can be modelled by using a polynomial function. It is very difficult to match all the data points, but it is possible to use a polynomial function with the power of two (quadratic function) to model both the sodium silicate to sodium hydroxide ratio and the solid to liquid ratio. The relationship between compressive strength and number of days can be modelled by using a natural logarithm function because as the material cures, its strength increases rapidly for the first few days but after a certain time period the material reaches its maturity, and the rate of strength increase reduces. All these non-linear features are included in the hypothesis function and the modified version is given by Equation 6.3. This function would have six input features because feature number zero, is a biased unit (has a value of one) and therefore the size of input matrix X is m by 6-dimensions ($\mathbb{R}^{\mathrm{m}\times 6}$). After defining all the input features, the next most crucial step is to determine β for all the corresponding set of input features in order to best fit the training dataset and accurately predict the compressive strength.

$$h_\beta(x) = \beta_0 x_0 + \beta_1 x_1 + \beta_2 x_2 + \beta_3 {x_1}^2 + \beta_4 {x_2}^2 + \beta_5 \ln(x_3)$$

$x_0 = 1$ (is a biased unit)

$x_1 = \text{Solid: Liquid ratio}$

$x_2 = \text{Sodium Silicate: Sodium hydroxide ratio}$

$x_3 = \text{Days}$

Equation 6.3: Multi-variable regression to predict the compressive strength

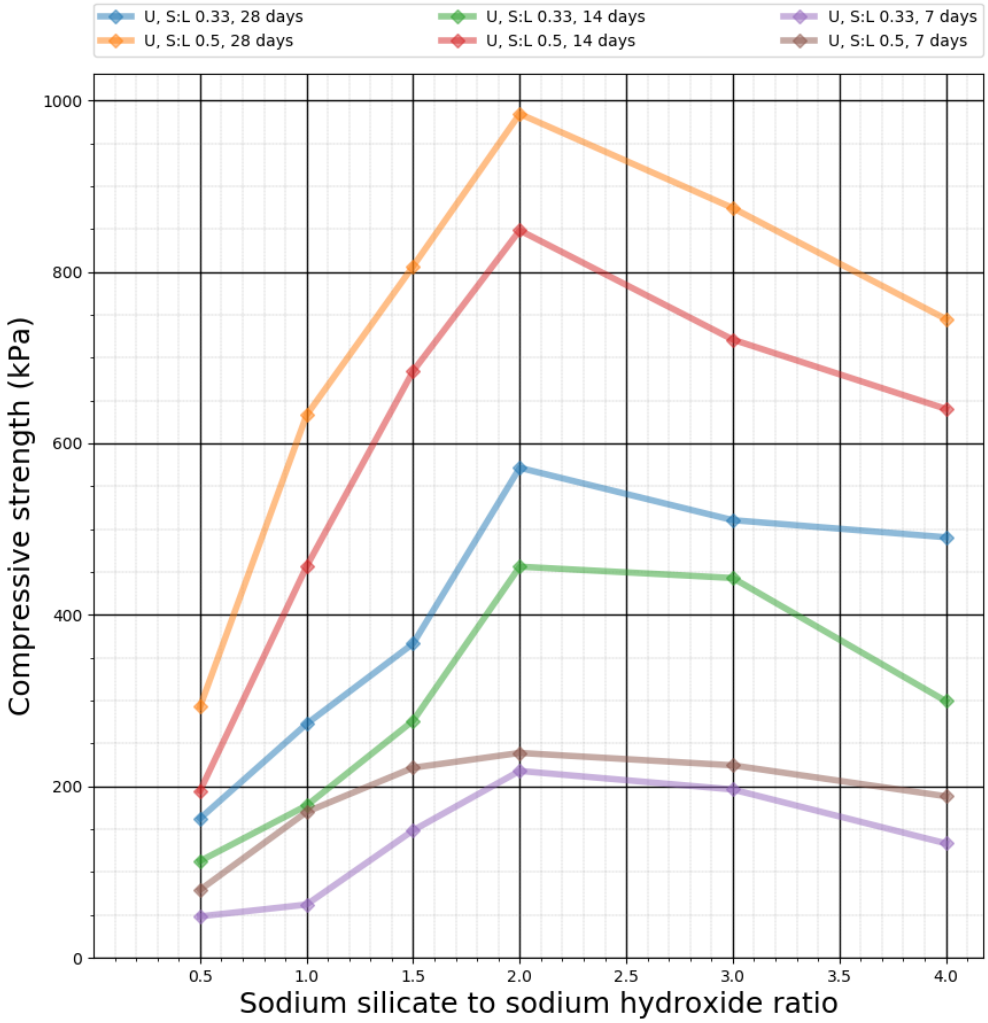

Figure 6.1: Shows the relationship between sodium silicate to sodium hydroxide ratio and compressive strength for unwashed samples

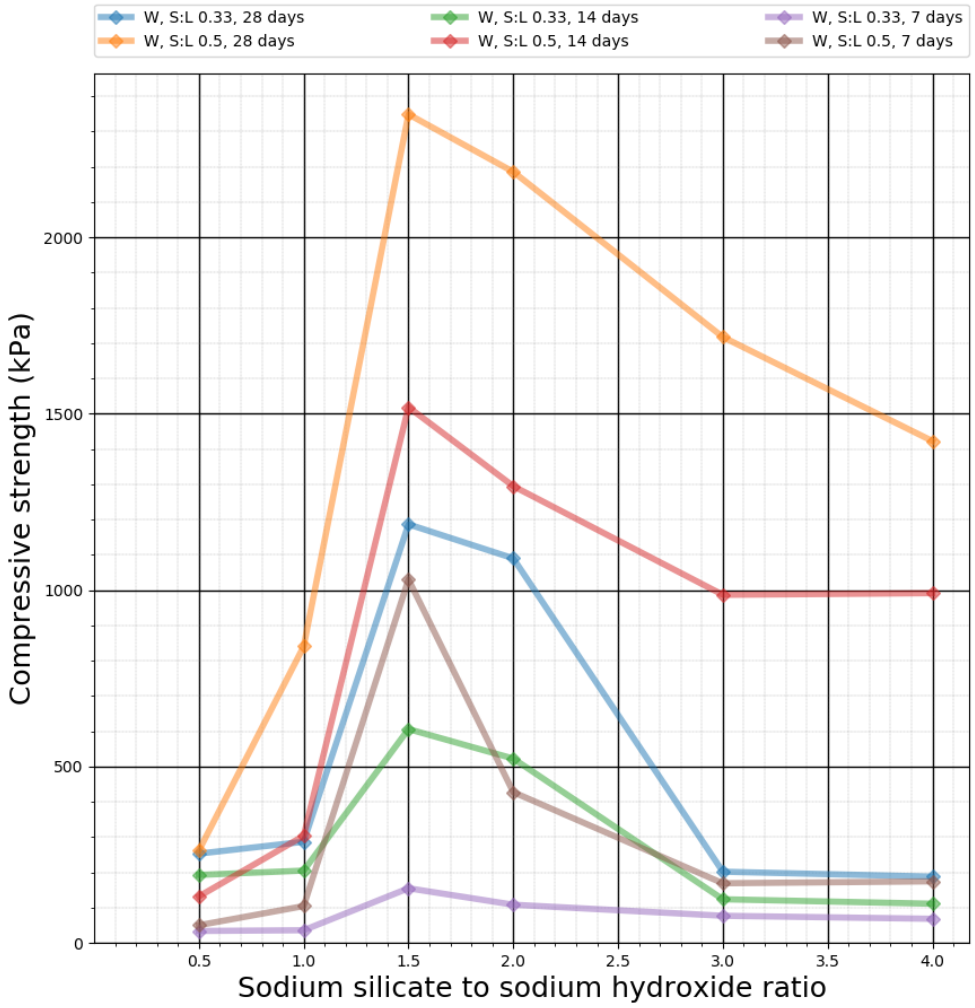

Figure 6.2: Shows the relationship between sodium silicate to sodium hydroxide ratio and compressive strength for washed samples

6.1.3 Determination of parameters for the multivariate regression model

After defining the hypothesis function $h_\beta(x)$, the next step is to find all the values of β to best fit the training dataset that maps X to Y. There are mainly two methods of finding all values of β; by either using a gradient descent algorithm (that was defined in section 2.5.5.1) or by using a normal equation. The requirement of both these methods is to define the cost or error function to measure the performance of the model to the actual values. This cost function is then minimised by both the methods to determine the values of β. The cost function for a regression model is given by an Ordinary Least Squares (OLS) equation (Equation 6.4). In this section, a normal equation method will be used, to minimise the cost function for all β. The normal equation can be derived by finding the partial derivative of the OLS equation and then setting the derivative to zero to find the values of β. This equation provides a direct solution to the hypothesis function whereas gradient descent uses iteration to find it. The partial derivative of the OLS equation can be found by using a vector identity. It specifies that: the sum of square vectors can be rewritten as vector transpose multiplied by the vector itself, as shown in Equation 6.5. Therefore, the OLS equation can be rewritten as in Equation 6.6. The partial derivative of the OLS equation, $\nabla_\beta J(\beta)$ with respect to β, is given by Equation 6.7. This is then set to zero and rearranged to find all the values of β that minimises the cost function (Equation 6.8). The normal equation was implemented in the Octave programming environment to determine β.

$$J(\beta) = \frac{1}{2}\sum_{i=1}^{m}\left(h_\beta(x^i) - y^i\right)^2$$

$J(\beta) = \text{Cost of the function}$

$m = \text{Number of training examples}$

Equation 6.4: The cost of the function using Ordinary Least Squares (OLS) (Raschka et al., 2016)

$$\sum_{i} v_i^2 = v^T v$$

$v = \text{Vector}$

$T = \text{Vector transpose}$

Equation 6.5: Shows the vector identity for the sum of square vectors

$$\frac{1}{2}(X\beta - \vec{y})^T(\beta - \vec{y}) = \frac{1}{2}\sum_{i=1}^{m}\left(h_\beta\left(x^i\right) - y^i\right)^2$$

Equation 6.6: Cost function is rewritten using the sum of square vectors identity

$$\nabla_\beta J(\beta) = \nabla_\beta \frac{1}{2}(X\beta - \vec{y})^T(\beta - \vec{y})$$

$$\nabla_\beta J(\beta) = \frac{1}{2}(X^T X\beta + X^T X\beta - 2X^T\vec{y})$$

$$\nabla_\beta J(\beta) = X^T X\beta - X^T\vec{y}$$

(note: some of the derivation steps have not been shown)

Equation 6.7: Matrix derivative of the cost function with respect to β (Allen, 2007)

$$X^T X\beta - X^T\vec{y} = 0$$

$$\beta = (X^T X)^{-1}X^T\vec{y}$$

Equation 6.8: Normal equation to find the parameter β of the multivariate regression model (Allen, 2007)

6.1.4 Results from the multivariate regression model

After implementing the above equations in the programming environment, two separate multivariate regression models were developed using experimental data from washed and unwashed APC residues-based geopolymer experiments. The values of β for unwashed material is given by Equation 6.11, and for washed material Equation 6.12 was employed. The models were compared and evaluated

by using predicted compressive strength values produced by the model against the actual compressive strength achieved from the laboratory experiments. It is possible to evaluate the model by using many different model evaluation mathematical techniques; such as using R-square, Mean Absolute Error (MAE) or Root Mean Square Error (RMSE). However, according to (Kvålseth, 1985, Spiess and Neumeyer, 2010), R-square is not recommended for the evaluation of a non-linear model, but it is a useful metric for assessing linear models. Thus, RMSE and MAE will be used to assess the model as they are the most appropriate (and commonly used) for assessing nonlinear models (Mohseni et al., 1998, Sousa et al., 2007). The formula to calculate RMSE and MAE is given by Equation 6.9 and Equation 6.10.

It can be seen from Table 6.1 that both multivariate regression models produced very high RMSE and MAE values, indicating that the multivariate model was not able to produce a good fit to the training dataset. It is considered to be a good practice to plot the predicted values and actual values against the sample number to visually compare the results. On the x-axis, the sample number is used because it is not possible to represent all the input features on a single graph with their respective compressive strength values. The set of input features with their corresponding sample number can be seen fully in Appendix B and Appendix C. Similar conclusions can be drawn from Figure 6.3 and Figure 6.4, where multivariate regression models were not able to predict the compressive strength for a given set of input features for washed and unwashed samples. It may be possible to define a different set of input features to produce a model that may provide better results, but it is very challenging to determine and test all the different functions conceivable. Therefore, in the next section, a more advanced machine learning technique (Artificial Neural Network (ANN)) will be used to produce the model to predict the compressive strength of the geopolymer based material.

$$Root\ mean\ squared\ error\ (RMSE) = \sqrt{\frac{\sum(y - \bar{y})^2}{m}}$$

$\bar{y} = predicted\ value$

$y = actual\ value$

$m = total\ number\ of\ training\ examples$

Equation 6.9: Root mean squared error (RMSE), (Sammut and Webb, 2010)

$$Mean\ Absolute\ Error\ (MAE) = \frac{\sum|y - \bar{y}|}{m}$$

Equation 6.10: Mean Absolute Error (MAE), (Sammut and Webb, 2010)

$$h_\beta(x) = -1266.1186 + 798.4148x_1 + 444.8909x_2 + 665.3457{x_1}^2 - 82.6195{x_2}^2 + 287.4296\ln(x_3)$$

Equation 6.11: Multi-variable regression model equation for unwashed APC residues

$$h_\beta(x) = -2965.8766 + 2068.5113x_1 + 1008.7120x_2 + 1723.7594{x_1}^2 - 211.4338{x_2}^2 + 574.040\ln(x_3)$$

Equation 6.12: Multivariable regression model equation for washed sample

	MAE	**RMSE**
Unwashed APC residues	82.62	105.44
Washed APC residues	301.78	371.13

Table 6.1: Shows the performance of the multivariable regression model

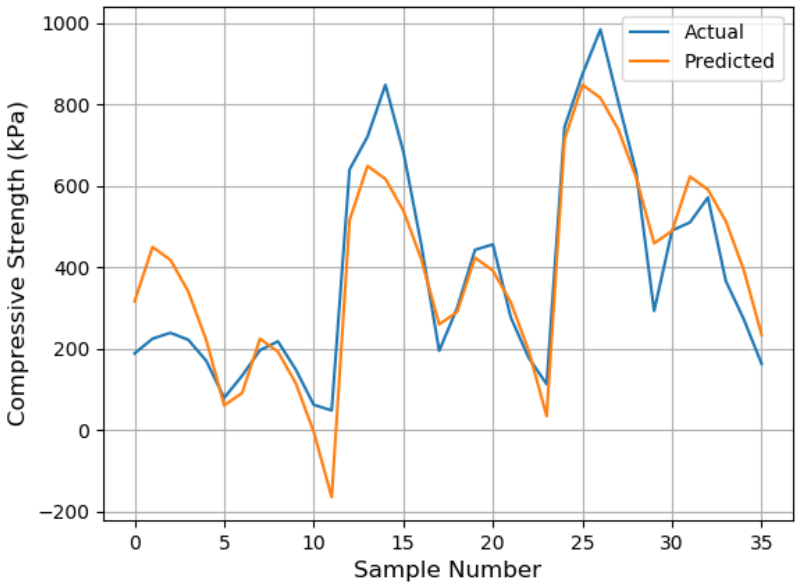

Figure 6.3: Regression model predictions for the unwashed sample as compared to the actual experimental results

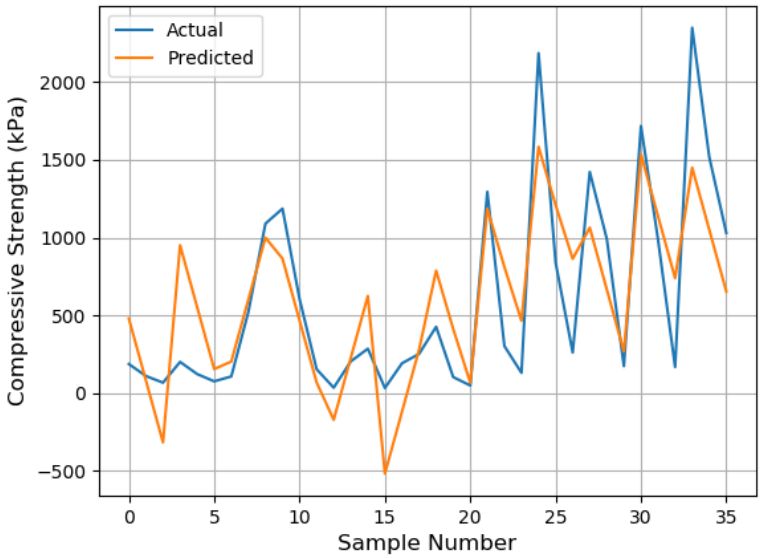

Figure 6.4: Regression model predictions for washed APC residues as compared to the actual experimental results

6.2 Artificial Neural Network (ANN) to produce a regression model

The multivariate regression modelling technique is a very popular and simple modelling technique. However, it was not able to produce a good fit to the experimental data from APC residues-based geopolymer material; therefore, a more powerful technique, like the Artificial Neural Network (ANN), can be used to model material behaviour more effectively. ANN is able to learn very complex nonlinear functions from the set of input features (Gurney, 1997), which is a major advantage to this method. It eliminates the need for the model designer to identify the mathematical functions in order to model the data (Rojas, 1996, Aggarwal, 2018). ANNs can improve and learn as the new data becomes available, hence improving the predictive power of the model over time. However, there are some disadvantages to these types of models; computationally they are very expensive to train (Shalev-Shwartz and Ben-David, 2014) and they also have issues with making predictions outside the training dataset range, hence reducing their accuracy (Wang, 2006, Dobrzański et al., 2014).

6.2.1 Shallow ANN and Deep Neural Network (DNN)

Deep Neural Networks (DNN), or deep learning, is gaining a lot of popularity because of their ability to learn better than shallow ANN (Goodfellow et al., 2016). In principle, DNN is an ANN with additional hidden layers, and according to Goodfellow et al. (2016) and Hwang and Chen (2017), there is no defined set number of hidden layers, to classify the model as DNN. According to Bengio (2009), an ANN with up to three hidden layers is considered to be shallow. An ANN with a lot of hidden layers (DNN) is very complicated to train because the magnitude of weights reduces as the depth of the neural network increases (if trained using a backpropagation algorithm). This reduces the influence of the first few layers of the model, therefore, in DNN a principle known as a greedy layer-wise training algorithm is used to train the model. This algorithm trains one hidden layer at a time to help produce a more optimised DNN model (Bengio, 2009). In this chapter, the ANN model with up to three hidden layers will be developed and

tested as the training dataset is too small to use DNN effectively. According to Hwang and Chen (2017) and Aggarwal (2018), DNN can learn very complex features using large training datasets very effectively, but on small training datasets, they can cause over-fitting.

6.3 Modelling of experimental results using ANN

The key element to designing an ANN model is to choose the activation function that will be used in each neuron/unit. There are many different types of activation functions to help solve a given problem. Some of the most popular activation functions are: sigmoid functions, hyperbolic tangent (Tanh) functions and Rectified Linear Units (ReLU) (Buduma and Locascio, 2017). However, other functions also used include, Leaky Rectified Linear Units (LReLU), Exponential Linear Units (ELU) and Scaled Exponential Linear Unit (SELU). All have different properties and allow the ANN model to be fully customisable for the given application (Pedamonti, 2018). The properties of these different activation functions can be seen in Figure 6.5. The sigmoid function has an output range of zero to one, and it is usually used to solve the classification problem. The other ideal function for this is the Tanh function, with output ranges from negative one to positive one. ReLU and LReLU can be suitably used for regression problems. The output of the ReLU function can go to infinity for values of input above zero, making it a very useful function in modelling the experimental results from the geopolymerisation experiment (as the value of compressive strength cannot go below zero). However, ReLU function can only be used in the hidden layers of ANNs and because of this, the output layer will be a linear function. It is essential to use nonlinear activation functions (defined in Figure 6.5) in the hidden layer to take the full advantage of ANN. The use of the linear functions in these layers would produce the same output as linear regression. This can be mathematically proven with the sum of two or more weights (W^1, W^2… W^n) with a linear function (W^1x, W^2x… W^nx), which can be written as a function of a single weight $\bar{W}x$ (Somani and P. Rostykus, 1991). Therefore, it is counterintuitive to develop a complex ANN model using multiple linear functions in the hidden layer.

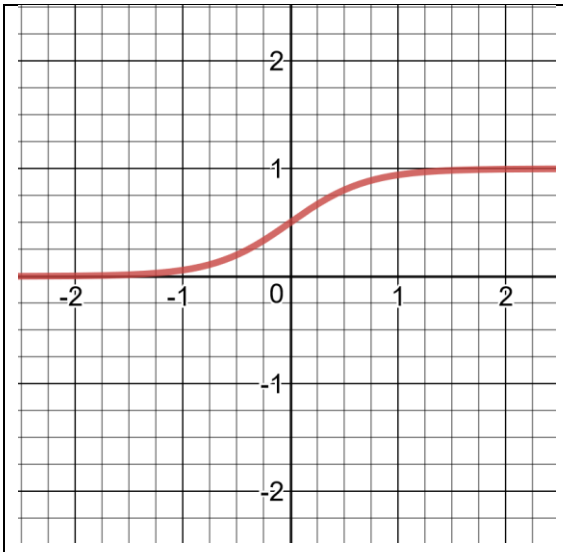	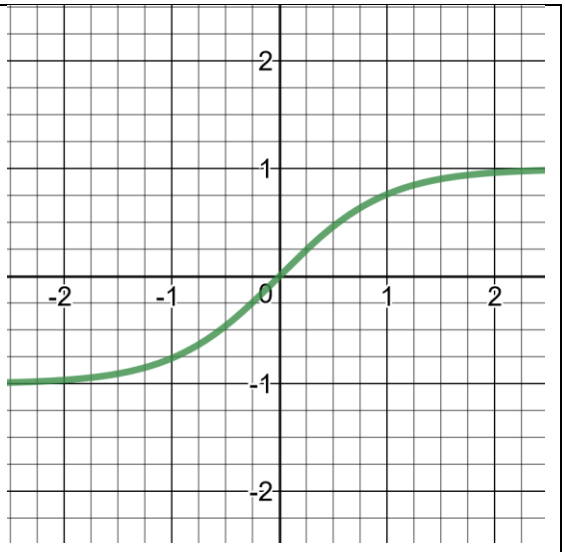
Sigmoid function: $$f(z)\frac{1}{1+e^{-z}}$$	Hyperbolic tangent (Tanh) function: $$f(z)=\frac{e^{z}-e^{-z}}{e^{z}+e^{-z}}$$
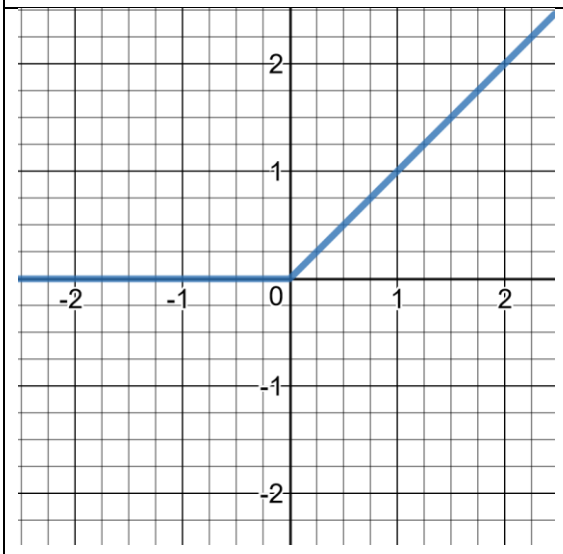	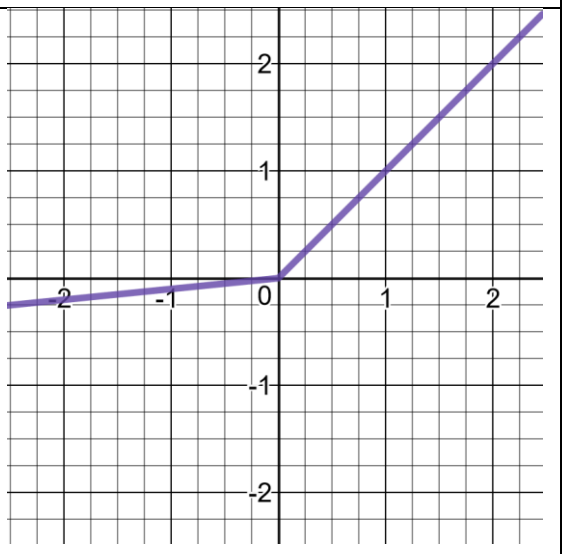
Rectified Linear Units (ReLU): $$f(z)=\begin{cases}0, & if\ z\leq 0\\ z, & if\ z>0\end{cases}$$ Alternatively, written as: $$f(z)=\max(0,z)$$	Leaky Rectified Linear Units (LReLU): $$f(z)=\begin{cases}\alpha z, & if\ z\leq 0\\ z, & if\ z>0\end{cases}$$ Alternatively, written as: $$f(z)=\max(\alpha z,z)$$

Figure 6.5: ANN activation functions (Buduma and Locascio, 2017, Pedamonti, 2018)

6.3.1 Input features and activation functions of an ANN model

The most critical element of an ANN model is its configuration, which is also the most difficult one to determine as finding the most suitable configuration requires many different arrangments to be tested through trial and error. In this chapter, various configurations (with two and three hidden layers) were tested to identify the most suitable model to predict the compressive strength of the geopolymer-based material. The input features used in the model development are described in Equation 6.13. The first input feature was ash type ("1" for washed and "2" for unwashed). The second feature is days, followed by solid to liquid ratio and lastly sodium silicate to sodium hydroxide ratio.

$$X = \begin{matrix} \vdots & \vdots & \vdots & \vdots \\ x_m^1 & x_m^2 & x_m^3 & x_m^4 \\ \vdots & \vdots & \vdots & \vdots \end{matrix}$$

$x^1 =$ Ash type (washed or unwashed)

$x^2 =$ Days

$x^3 =$ Solid to liquid ratio

$x^4 =$ Sodium Silicate to sodium hydroxide ratio

Equation 6.13: Input feature for the ANN model

The ANN model was configured to use the ReLU activation function in all its hidden layers. The activation function is identified by a_j^l, where letter l refers to layer number and j refers to the neuron in the layer l of the neural network. The first hidden layer with the activation function is indexed using number "1", as the input features are indexed at 0 ($x_1 = a_1^0$). In an ANN model, all activation values are saved in a matrix or a vector depending on the configuration and setup of the model. The activation values of the first hidden layer are shown in Equation 6.14. As each neuron or unit in a hidden layer uses a ReLU function, the computation will be performed as shown in Equation 6.15.

$$a^1 = \begin{bmatrix} a_1^1 \\ \vdots \\ a_j^1 \end{bmatrix}$$

Equation 6.14: Activation function values of the first hidden layer

$$a^1 = g(z)$$

$$g(z) = \max(z, 0)$$

$$\text{Where } z = W^T X + b$$

Equation 6.15: ReLU as an activation function

6.3.2 Feedforward Multi-Layer Perceptron (MLP)

After defining the input features and identifying the activation function, the next step is to implement a feedforward Multi-Layer Perceptron (MLP) model. This model will be fully connected, meaning that all the inputs are connected to all the neurons in the next layer, very similar to the one shown in Figure 6.6. In this methodology, an ANN model with two and three hidden layers will be tested to predict the compressive strength of the washed and unwashed APC residues-based geopolymer material. For the purpose of demonstration in this section, a model with three hidden layers will be implemented with their respective equations.

The first, second and third hidden layers will be using ReLU activation function and the sum of all these layers will produce the final output of the model. The weights, W, are all assigned using a random number generator in the Python programming language and all the activation functions are implemented using TensorFlow library. The weights (W) are initialised randomly in feedforward propagation to break the symmetry. If all the weights were the same, then their contribution influencing the loss or error produced by an MLP would make each neuron equally responsible for the output; hence making each neuron learn exactly the same function, causing the algorithm to fail. This process of randomly initialising the weights in an ANN is referred to as 'breaking the symmetry' (Kirk, 2017, Zafar et al., 2018). The complete implementation of the feedforward MLP model can be seen in Equation 7.3. These equations are adapted from Rojas (1996) and Rumelhart et al. (1986).

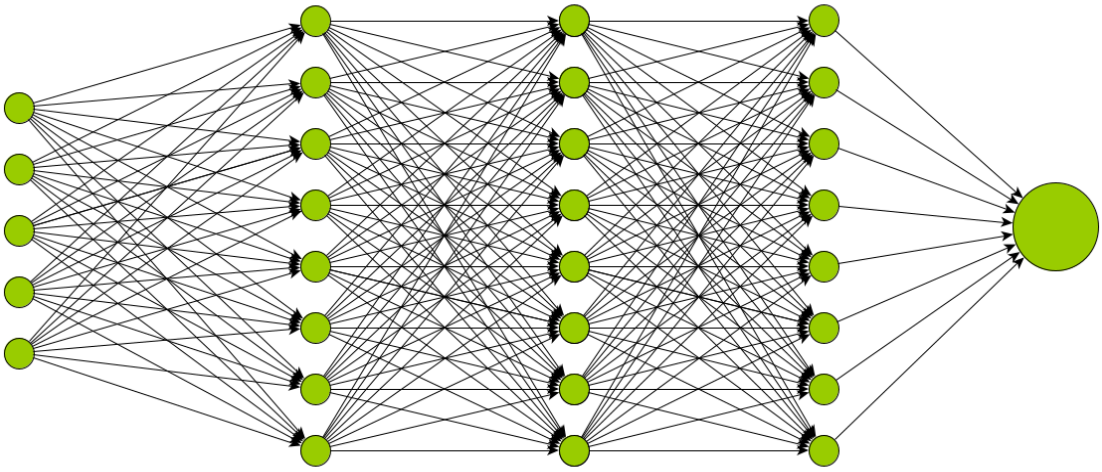

Figure 6.6: Four-layer MLP ANN model illustration

$$a^{(1)} = X$$

$$z^{(2)} = W^{(1)} a^{(1)}$$

$$a^{(2)} = g\left(z^{(2)}\right) \quad \text{add after computation } a_0^2 \ (biased\ unit)$$

$$z^{(3)} = W^{(2)} a^{(2)}$$

$$a^{(3)} = g\left(z^{(3)}\right) \quad \text{add after computation } a_0^3 \ (biased\ unit)$$

$$z^{(4)} = W^{(3)} a^{(3)}$$

$$a^{(4)} = g\left(z^{(4)}\right) \quad \text{add after computation } a_0^4 \ (biased\ unit)$$

$$a^{(5)} = W^{(4)} a^{(4)}$$

Equation 6.16: The activation functions for each layer in an ANN model

6.3.3 Backpropagation

The next step after implementing the feed-forward MLP is to implement backpropagation. This algorithm systemically changes the weights of each neuron to help reduce error and produce a good fit to the training dataset. The algorithm first compares the output of the model generated by the feed-forward MLP and compares this with the actual value by subtracting one from the other to calculate the error. Similarly, the errors for each layer are computed starting from the output layer, back to the first hidden layer as graphically illustrated in Figure 6.7. The term Δ for all the layers are computed, and following this, all the weights of the neurons are updated, as shown in Equation 7.6. The gradient descent algorithm is used to minimise the error. The minimisation of error in each layer helps to reduce the overall error produced by the model and consequently produces a good fit to the training dataset. The implementation of the backpropagation has been adapted from Rojas (1996) and Rumelhart et al. (1986).

$$\delta_j^{(5)} = a_j^{(5)} - y_j$$

$$\delta_j^{(4)} = (W^{(4)})^T \delta^{(5)} . \times g'(z^{(4)})$$

$$\delta_j^{(3)} = (W^{(3)})^T \delta^{(4)} . \times g'(z^{(3)})$$

$$\delta_j^{(2)} = (W^{(2)})^T \delta^{(3)} . \times g'(z^{(2)})$$

$\delta_j^{(l)} = \text{Error term}$

$l = \text{Layer}$

$j = \text{Unit} - \text{Neuron}$

Equation 6.17: Computing the error term for backpropagation

$$\Delta^4 := \Delta^4 + \delta^5 (a^4)^T$$

$$\Delta^3 := \Delta^3 + \delta^4 (a^3)^T$$

$$\Delta^2 := \Delta^2 + \delta^3 (a^2)^T$$

$$\Delta^1 := \Delta^1 + \delta^2 (a^1)^T$$

$$W^4 := \frac{1}{m} \Delta^4$$

$$W^3 := \frac{1}{m} \Delta^3$$

$$W^2 := \frac{1}{m} \Delta^2$$

$$W^1 := \frac{1}{m} \Delta^1$$

Equation 6.18: Updating backpropagation

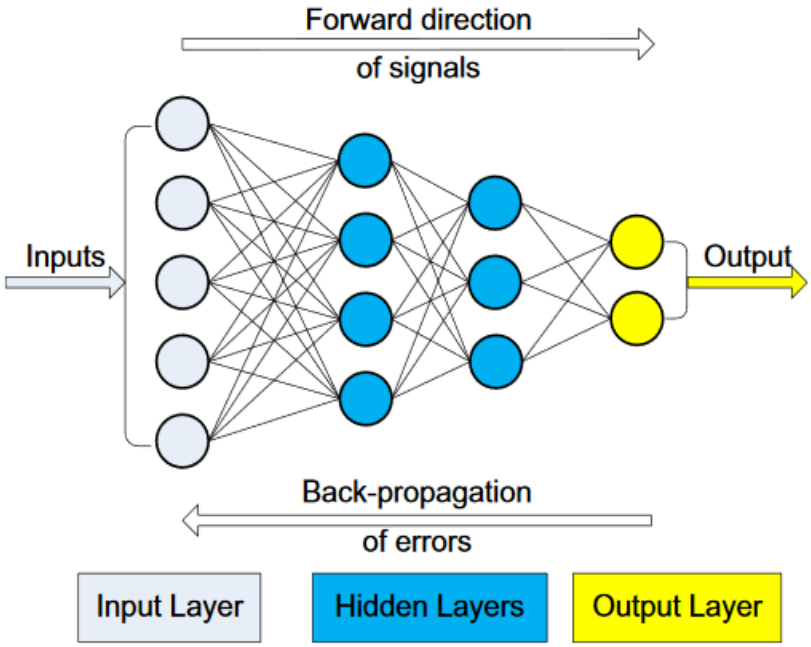

Figure 6.7: Graphical representation of backpropagation, (Asteris et al., 2016)

6.3.4 Results from different ANN models

Many different configurations of ANN models were tested and the results of the model with their Mean Absolute Error (MAE) are shown in Table 6.2. Usually, ANN models are evaluated by dividing the existing dataset into two different datasets. The first dataset is used to train the model and the second training set is used to assess it. In this chapter, the model was trained using all the training dataset produced in chapter 5 to build the model, with MAE calculated based on the prediction made by the model on the seen training dataset. This methodology was followed to identify the best model (based on this data) to help identify and produce geopolymer-based material using different sets of formulations.

The model that best matched the training dataset was the one with two hidden layers, each with fifty neurons. This model produced MAE of 2.3 kPa, and it can also be seen from Figure 6.8 that this model very closely matches the training dataset. Therefore, this model was used to predict the compressive strength of the geopolymer-based material on an unseen dataset. This in turn was used to help identify different formulations which would reproduce the successful geopolymer-based material. The output of the model at different solid to liquid ratios (0.33, 0.4, 0.5, 0.6 and 0.7) and sodium silicate to sodium hydroxide ratios (0.5, 1, 1.5, 2, 3 and 4) can be seen in Figure 6.9. This figure shows actual data plotted in solid lines and predictions made by the model using “dash” lines. The solid to liquid ratios of 0.4, 0.6 and 0.7 only contain the predicted values as these were used in section 6.3.5 to reformulate the geopolymer-based material in the laboratory (using the same methodology developed in chapter 5) and also to re-evaluate the performance of the model on unseen dataset.

Model type	Mean Absolute Error (MAE)	Root Mean Squared Error (RMSE)
4-50-50-1	2.3299	3.4442
4-40-40-40-1	3.9244	6.4697
4-50-50-50-1	6.0043	7.6647
4-35-35-35-1	11.0959	17.0963
4-40-40-1	20.5833	31.1605
4-20-20-1	33.2969	47.7755
4-20-20-20-1	37.3515	67.4092
4-35-35-1	42.3152	56.6683

Table 6.2: Neural network model comparison to predict the compressive strength of washed and unwashed APC residues

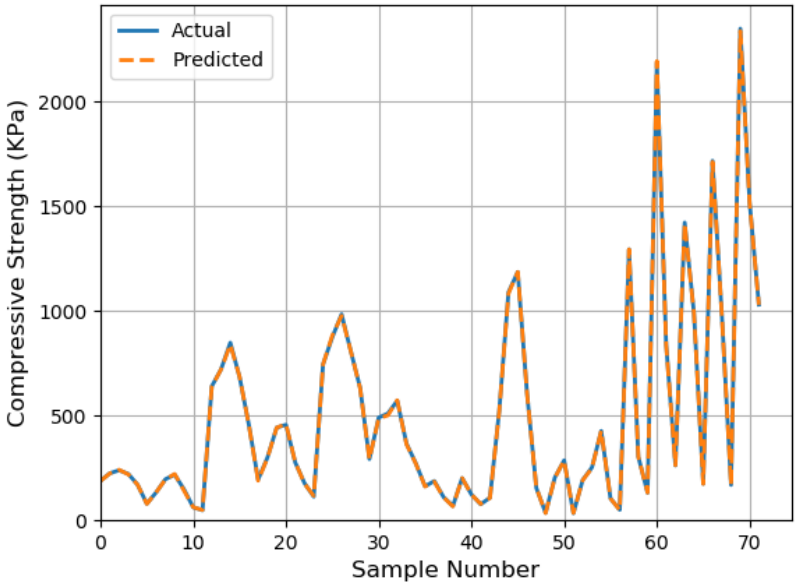

Figure 6.8: Shows the performance of the ANN model with 4-50-50-1 configuration

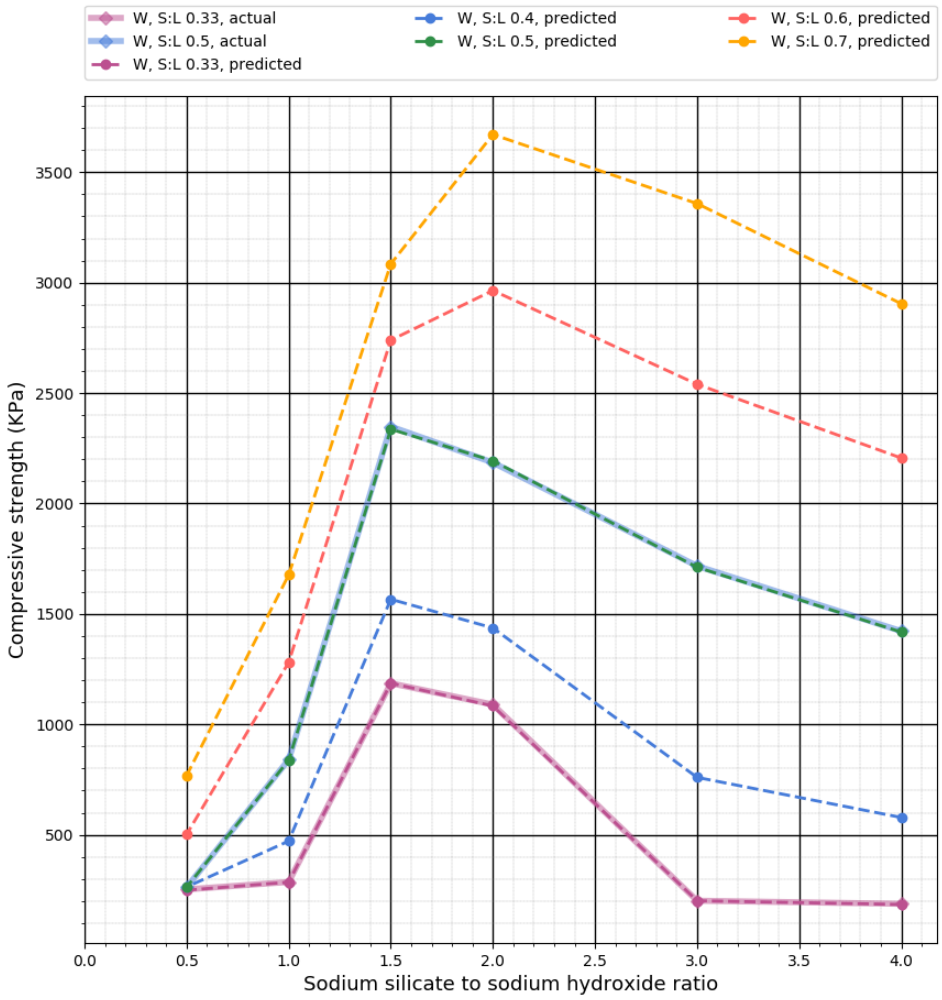

Note: S:L is Solid to liquid ratio

Figure 6.9: Shows the comparison between actual values from the geopolymer experiment and predicted values from the ANN model with 4-50-50-1 configuration (28th days compressive strength of washed APC residues)

6.3.5 Reformulation of APC residues-based geopolymer

After reviewing the machine learning model, APC residues-based geopolymers were reformulated using three different solid to liquid ratios (0.7,0.6 and 0.4). The ANN model predicted that the highest compressive strength could be obtained with a solid to liquid ratio of 7:10, but practically it was noticed that at this ratio there is not enough liquid to hydrate the solid (APC residues). This highlights the criticality of defining the boundary conditions of the model to allow relationships to be established within known physical constraints.

The reformulation of the APC residues-based geopolymer material allowed the models to be re-evaluated on unseen dataset and also to better understand the relationship between compressive strength, solid to liquid ratios and sodium silicate to sodium hydroxide ratios. It can be seen from Figure 6.10 that the best performing sodium silicate to sodium hydroxide ratio is 3:2 (1.5) and solid to liquid ratio of 1:2 (0.50). The other observation that can be made from Figure 6.10 is that higher solid to liquid ratio will not necessarily produce higher compressive strength as there is decrease in strength for solid to liquid ratio of 3:5 (0.6). This again highlights the significance of identifying and using optimum amount of liquid (alkaline activator) to allow the solid (APC residue) to fully hydrate. As this would allow the formation of a stronger APC residue-based geopolymer material.

It is important to re-evaluate the model because the seen dataset was used to train and provide a general indication of the performance of the model which helped tune the model configuration. Therefore, MAE error for the seen dataset is lower than unseen datasets for a given model, as can be seen in Table 6.3. The other significant observation is that the model with a configuration of 4-50-50-1 performed better than any other models tested on the seen dataset. However, the performance of this model was not the best on the unseen dataset as compared to other models. The model configuration of the best performing model on the unseen dataset was 4-35-35-35-1 with MAE of 479.5 kPa. The MAE produced by 4-50-50-1 was higher (492.8 kPa). Therefore, it is important to understand that small training datasets can lead to the problem of overfitting, as indicated in the literature (Deco and Obradovic, 1996, Ciaburro and Venkateswaran, 2017, Ghotra and Dua,

2017, Capelo, 2018, Hodnett and Wiley, 2018). However, it is possible to mitigate this problem by testing the performance of the model on unseen dataset. The graphical comparison of both the models can be seen in Figure 6.11, Figure 6.12 and Figure 6.13 for seen and unseen dataset as these figures provide a visual indication of the predictions made by model against the actual value. It can be seen that in general, both the models were not able to make reasonable predictions above solid to liquid ratio of 1:2 (0.5) as this was the highest ratio used to train the model. However, the predictions made by the model on solid to liquid ratios of 2:5 (0.4) are much better; mainly due to these set of values lying in between 1:3 (0.33) and 1:2 (0.5), which were the set of values used to train the model.

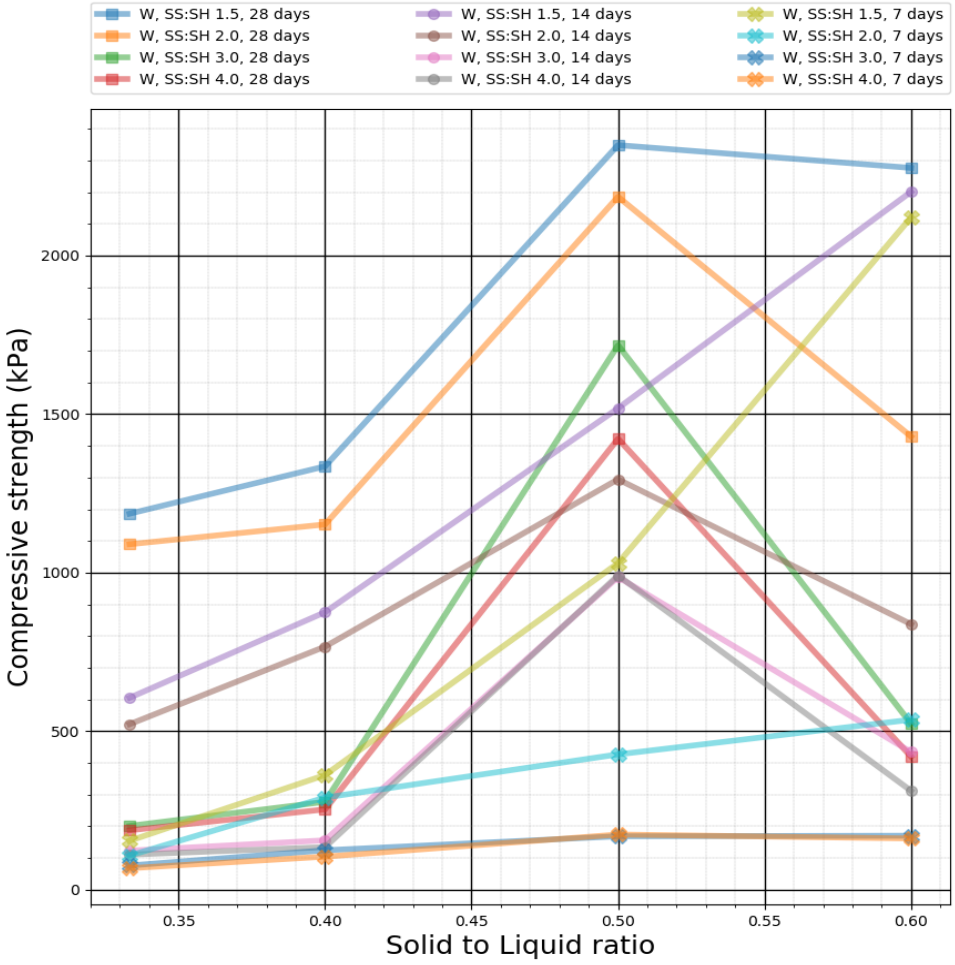

Note: SS:SH is Sodium Silicate to Sodium Hydroxide ratio (SS:SH)

Figure 6.10: Shows the relationship between solid to liquid ratio and compressive strength for washed samples

Model type	Seen dataset (MAE)	Unseen dataset (MAE)
4-35-35-35-1	11.0959	479.4956
4-40-40-40-1	3.9244	479.6948
4-20-20-20-1	37.3515	481.3576
4-50-50-1	2.3299	492.8206
4-20-20-1	33.2969	505.3727
4-35-35-1	42.3152	541.2309
4-40-40-1	20.5833	546.3542
4-50-50-50-1	6.0043	559.0546

Table 6.3: Comparison using MAE on the seen training dataset and unseen training dataset

Model type: 4-35-35-35-1	Model type: 4-50-50-1
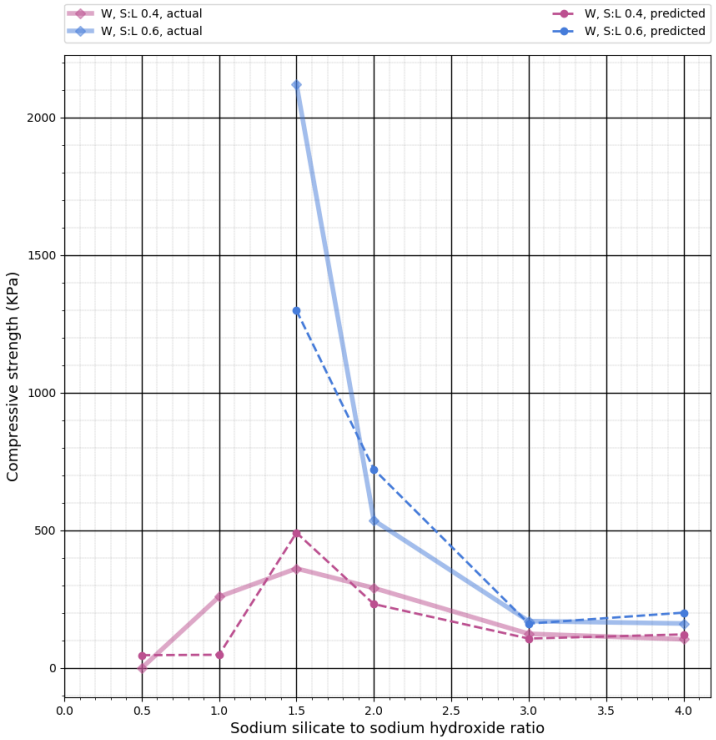	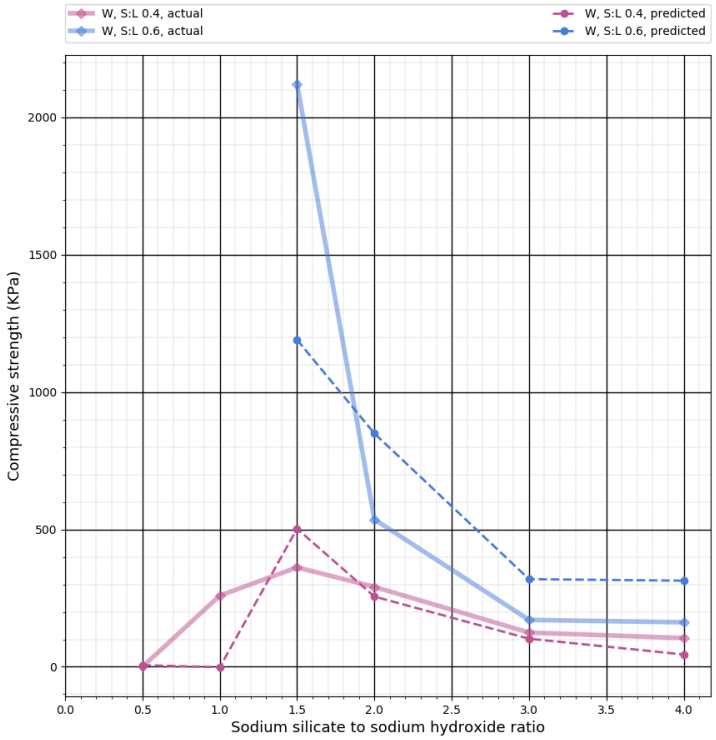

Figure 6.11: Shows the comparison between the actual values from the geopolymer experiment and predicted values from the ANN model (7th days compressive strength of washed APC residues)

Model type: 4-35-35-35-1	Model type: 4-50-50-1
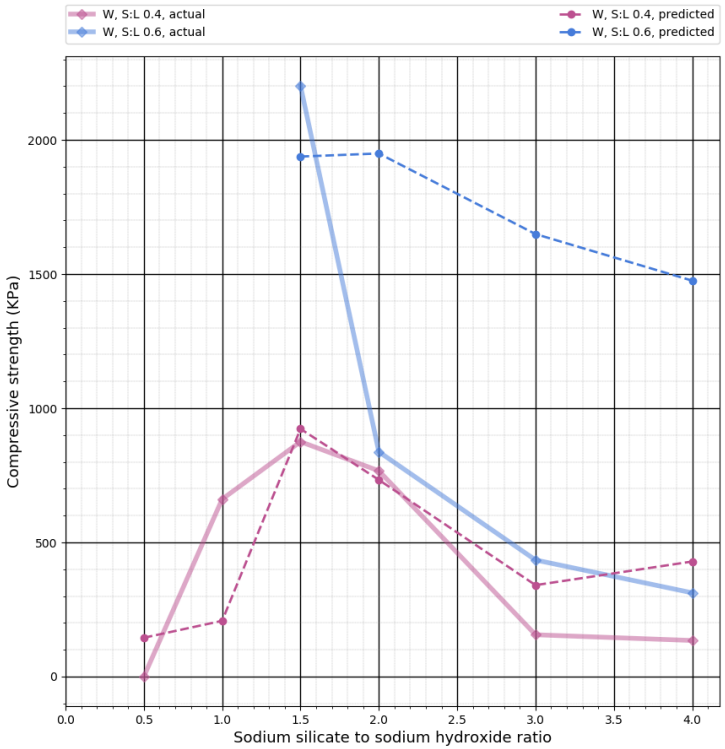	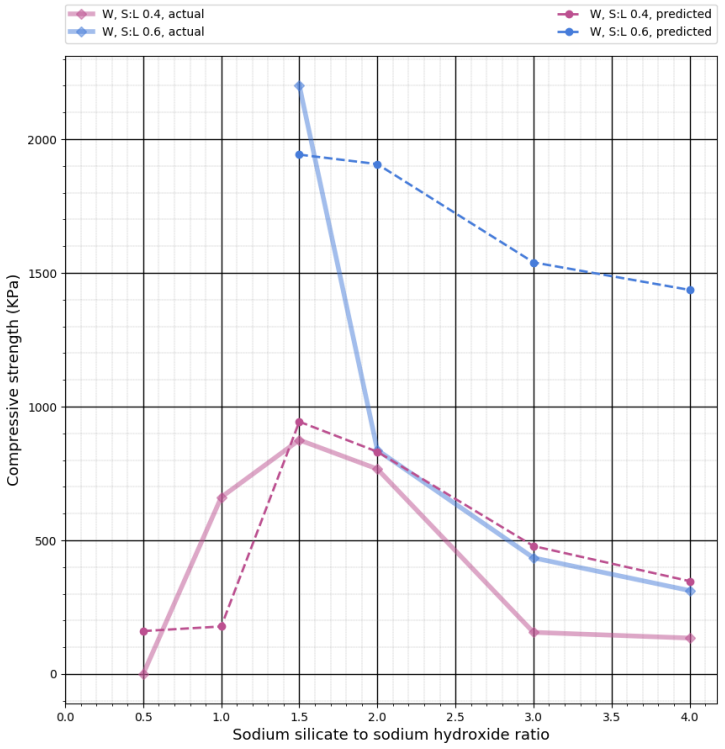

Figure 6.12: Shows the comparison between the actual values from the geopolymer experiment and predicted values from the ANN model (14th days compressive strength of washed APC residues)

Model type: 4-35-35-35-1	Model type: 4-50-50-1
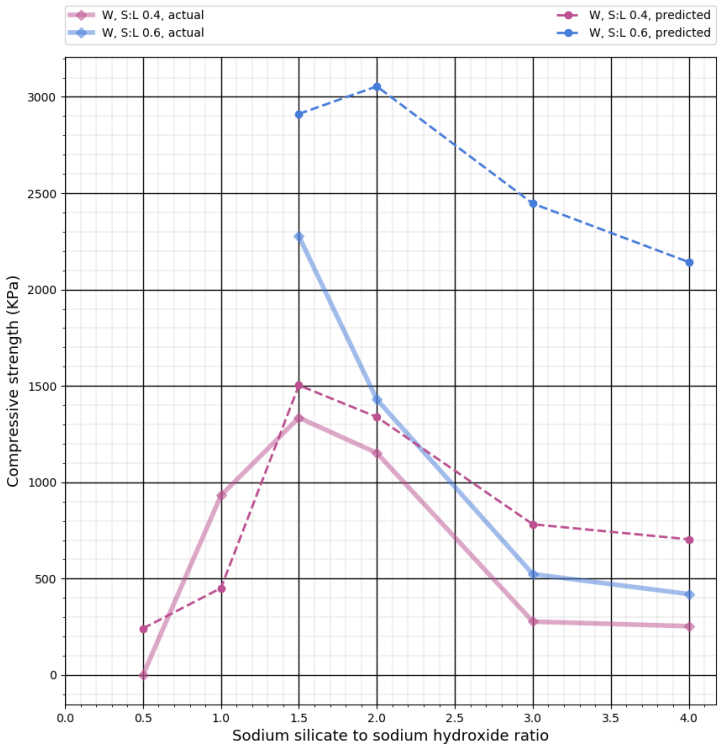	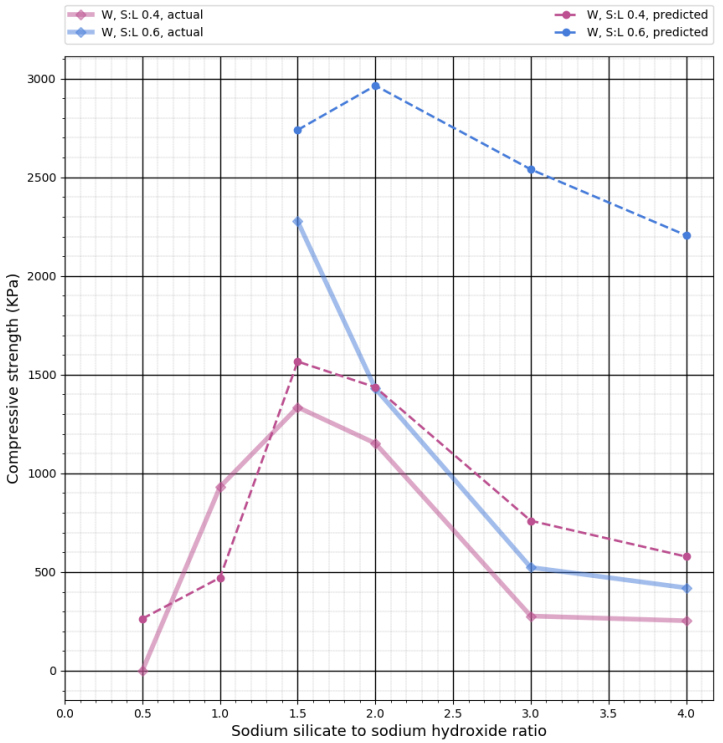

Figure 6.13: Shows the comparison between the actual values from the geopolymer experiment and predicted values from the ANN model (28th days compressive strength of washed APC residues)

6.4 Conclusion and further recommendations

It can be seen from this chapter, that the development of ANN models can be extremely useful in identifying and modelling the behaviour of APC residues-based material. Results indicated that a single ANN model was able to correctly predict the compressive strength of both washed and unwashed APC residues-based geopolymer material. This is encouraging considering they have different percentages of elemental compositions and also very different compressive strengths when using the same ratios of geopolymerisation agents. The research developed a multivariate nonlinear regression model to predict the compressive strength of the material, but this technique was not able to produce a good model, as Mean Absolute Error (MAE) was 301.8 kPa for unwashed and 82.6 kPa for washed APC residues-based geopolymer material. The use of Artificial Neural Network (ANN) was investigated, and this machine learning technique was able to produce a model with a MAE of 2.3 kPa. The effectiveness of this ANN model was tested by reformulating the geopolymer based material and testing it against unseen dataset. The model was able to identify a general trend in data but was not able to accurately predict the compressive strength of the material. Therefore, it was concluded that ANN model could be very effective at predicting the compressive strength of the material for seen data (data that is used to train the model), but it cannot make a good prediction on unseen data as MAE for unseen data was 479.5 kPa. However, the accuracy of the model can be improved by using larger training dataset as the use of small training dataset can lead to the problem of overfitting.

7 Identification of ash using Artificial Neural Network (ANN)

The main problem, identified by Lam et al. (2010) and Lindberg et al. (2015) in their review papers on ashes produced by the MSWI, is that it is challenging to produce ash-based products in large quantities due to variations in physical and chemical compositions of these ashes. These variations make it very difficult to predict the properties of the ash-based product, and thus high-value products are impossible to manufacture at a commercial scale. The issues surrounding the identification and composition of APC residues are due to the various types of waste incinerated by the plant and its configuration, which includes: the specific flue gas treatment process and the ash collection system that is installed in the plant (Quina et al., 2008). The other problem is that APC residues are not classified standardly in the literature; with various terms applied to cover the broad differences in ashes (such as fly ash, APC fly ash or MSW fly ash). According to Zacco et al. (2014) and Toniolo and Boccaccini (2017), fly ash can be from MSW, biomass or coal; therefore, it is important to explicitly mention the source of the fly ash to provide the reader with a better understanding of the type of ash being researched. There are many examples of peer-reviewed papers (Gesoğlu et al., 2012, Gomathi and Sivakumar, 2014, Nikolić et al., 2018, Rożek et al., 2018) those do not explicitly mention the source of the fly ash in their title, making it difficult to ascertain precisely the source of the ash. After meticulous examination, it was noticed that usually, a paper with no reference to the source of the fly ash is referring to coal fly ash, but there are also other issues related to the use of the term “fly ash” itself as identified in the literature review in section 2.1.

7.1 Novelty

The novelty of this chapter is to develop an Artificial Neural Network (ANN) model to help identify different types of ashes using XRF data extracted from many different published peer-reviewed papers. The model will identify different types of ashes from many different sources not just limited to MSWI-based ashes as there is not enough data available to develop a model to distinguish between different types of MSWI based ashes. However, the model will be able to distinguish between MSWI bottom ash, MSWI APC residues, coal fly ash and sewage sludge fly ash. This model can be used as a proof of concept to further develop a model that can identify many other types of ashes.

7.2 Identification and arrangement of input data

The training data that was used to develop and validate the MLP model can be seen in Table 7.1, Table 7.2, Table 7.3, Table 7.4 and Table 7.5. The training dataset size is relatively small (18 training examples), but this chapter aims to prove the concept of using machine learning to deal with the problem of identifying ashes. The input matrix for the MLP model is denoted by letter X as can be seen in Equation 7.1. The model uses seven input features to train the model.

$$X = \begin{bmatrix} \vdots & \vdots & \vdots & \vdots & \vdots & \vdots & \vdots \\ x_m^1 & x_m^2 & x_m^3 & x_m^4 & x_m^5 & x_m^6 & x_m^7 \\ \vdots & \vdots & \vdots & \vdots & \vdots & \vdots & \vdots \end{bmatrix}$$

$m =$ number of training examples (in this case it is 18)

$X^1 = Al_2O_3\ composition\ in\ percentage$

$X^2 = CaO\ composition\ in\ percentage$

$X^3 = K_2O\ composition\ in\ percentage$

$X^4 = MgO\ composition\ in\ percentage$

$X^5 = Na_2O\ composition\ in\ percentage$

$X^6 = SiO_2\ composition\ in\ percentage$

$X^7 = (100 - (X^1 + X^2 + X^3 + X^4 + X^5))$

Equation 7.1: Input feature matrix to model the classification of ashes

Coal Fly ash	Test and train dataset	Major elements (wt%) XRF reference		
Compounds	(Phoo-Ngernkham et al., 2015)	(Król et al., 2018)	(Rożek et al., 2018)	(Luna Galiano et al., 2011)
Al_2O_3	27.04	34.94	36.4	21.5
CaO	3.32	1.65	1.4	3.94
Fe_2O_3	6.85	3.93	3.9	5.86
K_2O	1.29	3.02	2	1.67
MgO	1.23	1.26	1.2	1.84
Na_2O	1.15	0.91	1	0.68
SiO_2	52.31	50.58	50.7	63.9
TiO_2		1.21		

Table 7.1: XRF results collected from different research papers for coal fly ash

MSW bottom ash	Major elements (wt%) XRF reference				Test dataset
Compounds	(Pan et al., 2008)	(Yang et al., 2018a)	(Giro-Paloma et al., 2017a)	(Gao et al., 2017)	(Giro-Paloma et al., 2017b)
Al_2O_3	1.26	8.7	5.8	12.037	6.58
Br	0.06				
CaO	50.39	14.3	16.9	43.115	14.69
Cl	3.24		0.14	0.166	
Cr_2O_3	0.18			0.15	
CuO	1.51		0.23	0.872	1.26
Fe_2O_3	8.84		14.1	9.313	8.38

MSW bottom ash	Major elements (wt%) XRF reference				Test dataset
Compounds	(Pan et al., 2008)	(Yang et al., 2018a)	(Giro-Paloma et al., 2017a)	(Gao et al., 2017)	(Giro-Paloma et al., 2017b)
K_2O	1.78	1.1	1.11	0.848	1.41
MgO	2.26	1.9	2.22	2.116	2.32
Na_2O	12.66	11.7	7.58	2.359	7.78
NiO	0.16			0.042	
P_2O_5	3.19	1.7	1.97	2.625	
PbO	2.11			0.317	
SiO_2	13.44	53.8	44.3	19.122	49.38
SO_3	1.79	0.3	0.65	2.393	0.57
TiO_2	2.36		0.35	2.48	
ZnO	2.6		0.18	1.287	0.38
Ag_2O				0.158	
BaO				0.239	
MnO				0.196	
SrO				0.132	
ZrO_2				0.035	

Table 7.2: XRF results collected from different research papers for MSWI bottom ash

Sewage sludge fly ash	Major elements (wt%) XRF reference	
Compounds	(Suksiripattanapong et al., 2015b)	(Suksiripattanapong et al., 2015a)
AL_2O_3	12.96	13.14
CaO	5.79	30.24
Fe_2O_3	15.64	6.66
K_2O	2.83	1.63
MgO	2.94	
Na_2O	2.83	0.41
SiO_2	49.32	47.51
SO_3	7.29	

Table 7.3: XRF results collected from different research papers for sewage sludge fly ash

	Major elements (wt%) XRF reference								Test Dataset	
Compounds	(Zheng et al., 2011)	(Yang et al., 2018b)	(Yang et al., 2018a)	(Pan et al., 2008)	(Li et al., 2014)	(Lancellotti et al., 2010)		(Formosa et al., 2017)	(Gong et al., 2017)	(Wan et al., 2006)
Al_2O_3	7.2	1.4	1.2	0.92	4.7	5.88	1.11	4.02	1	8.18
CaO	28.8	47.8	41.8	45.42	31.5	26.28	7.46	48.35	53	22.78
Fe_2O_3	3.6			3.83	5.9	2.06	0.72	0.79	1.9	4.83
K_2O	4.3		4.2	3.85		2.24	1.16	4.33		5.6
MgO	2.2	1.9	1.7	3.16		1.87	0.43	1.73	3.8	2.64
Na_2O	6.5		7.3	4.16		6.42	22.08	4.28	7.7	5.28
P_2O_5		0.5	0.4	1.72				1.36	0.3	2.49
SiO_2	15.4	3.5	3.1	13.6	16.4	8.7	2.63	6.64	3.9	23.64
SO_3	8.7	4.8	4.2	6.27	6.3			6.24	5.9	13.99
TiO_2		0.5		3.12				0.86	0.5	1.36
ZnO		0.6		2.32				0.72		0.93
Br				0.35						
Cl				9.73	14.5	10.16	26.4	8.85	19.9	6.4
Cr_2O_3				0.19						0.15
CuO				0.25						0.14
PbO				0.57				0.12		0.55
MnO										0.27

Table 7.4: XRF results collected from different research papers for MSW fly ash

	Major elements (wt%) XRF reference		
Compounds	(Nikolić et al., 2018)	(Rashidian-Dezfouli et al., 2018)	(Patel et al., 2018)
SiO_2	55.23	50.7	59.63
Al_2O_3	21.43	25.1	29.53
Fe_2O_3	7.42	12.5	4.62
CaO	7.94	3.3	0.97
MgO	2.61	1.1	0.65
SO_3	0.81		0.21
Na_2O	0.64	0.51	0.22
K_2O	1.35	2.27	1.32
MnO			0.05

Table 7.5: XRF results of fly ash collected from different research papers used for testing the model (Test dataset)

7.3 Feedforward MLP

The MLP with a single hidden layer was tested in this chapter. The single hidden layer can model any continuous function, given that the model is of finite width (Cybenko (1989). The first step in developing an MLP is to implement forward propagation; this means that it transmits numerical information in the forward direction or in the direction of the output as was implemented in chapter 6. However, this model uses a different type of activation function (sigmoid function as shown in Equation 7.2 and Equation 7.3).

$$g(z) = \frac{1}{1 + e^{-z}}$$

Equation 7.2: Sigmoid function (Ketkar, 2017)

$$g(W^T x) = \frac{1}{1 + e^{-W^T x}}$$

$$g(z) = \frac{1}{1 + e^{-z}}$$

$$a^{(1)} = X$$

$$z^{(2)} = W^{(1)} a^{(1)}$$

$$a^{(2)} = g\left(z^{(2)}\right) \text{ add after computation } a_0^2$$

$$z^{(3)} = W^{(2)} a^{(2)}$$

$$a^{(3)} = g\left(z^{(3)}\right)$$

Equation 7.3: Computation of MLP with the sigmoid activation function

7.4 Backpropagation

After computing the forward propagation, the next step is to compute or perform backpropagation. During backpropagation, the algorithm begins computing the error by subtracting the output of the final layer with the actual values before it is able to move back through each layer to compute the error. The error for all the layers using backpropagation is determined using computation steps, as shown in Equation 7.5. This equation requires the derivative of a sigmoid function, which is given by Equation 7.4. The error term is then used to compute Δ for all the layers, and after this, all the weights of neurons are updated using Equation 7.6. The cost of the sigmoid function is calculated using Equation 7.7.

$$g(z) = \frac{1}{1 + e^{-z}}$$

$$\frac{d}{dz} g(z) = \frac{d}{dz} \frac{1}{1 + e^{-z}}$$

$$= \frac{1}{(1 + e^{-z})^2} (e^{-z})$$

$$= \frac{1}{(1 + e^{-z})} \cdot \left(1 - \frac{1}{1 + e^{-z}}\right)$$

$$\frac{d}{dz} g(z) = g(z) (1 - g(z))$$

Equation 7.4: Derivative of sigmoid function (Witten et al., 2011, Rojas, 1996)

$$\delta_j^3 = a_j^3 - y_j$$

$$\delta_j^{(2)} = (W^{(2)})^T \delta^{(3)} . g'(z^{(2)})$$

$\delta_j^{(l)}$ is the error term

l is the layer

j is the node

Equation 7.5: Computing the error term for backpropagation

$$\Delta^2 := \Delta^2 + \delta^3 (a^2)^T$$

$$\Delta^1 := \Delta^1 + \delta^2 (a^1)^T$$

$$W^2 := \frac{1}{m} \Delta^2$$

$$W^1 := \frac{1}{m} \Delta^1$$

Equation 7.6: Updating back propagation

$$J(W) = -\frac{1}{m}\left[\sum_{i=1}^{m}\sum_{k=1}^{K} y_k^i \log\left(h_w(x^i)\right)_k + \left(1 - y_k^i\right)\log\left(1 - \left(h_w(x^i)\right)_k\right)\right]$$

Equation 7.7: Multi-class negative log-likelihood function (MacKay, 2004, Patterson and Gibson, 2017)

7.5 Results and discussion of the MLP model to classify ashes

Many different configurations of ANN were tested, as can be seen in Figure 7.1. The final model was able to achieve an accuracy of 100% in classifying ashes. The final model had 530 neurons in the hidden layer [the weights matrix of the final model is given in Appendix I]. The weights matrix is 530 by 8 for the first layer and 4 by 531 for the output layer. These weight matrices can be used by other researchers to test and validate the model. The model was able to predict the source of all the fly ashes, shown in Table 7.5, to be from coal fly ash. These ashes were not explicitly identified in the paper; therefore, each paper was carefully investigated to confirm the output of the model. Nikolić et al. (2018) stated that their fly ash was from Morava power plant, which is a power plant that uses coal to produce electricity. Likewise, Rashidian-Dezfouli et al. (2018) only identified the ash as a locally sourced class F fly ash and Patel et al. (2018), identified theirs as a Class F ash from a thermal power plant in India. Therefore, it was very difficult to identify the actual origin of both these fly ashes, but the model was able to predict the source of these ashes to be from coal.

The model developed in this chapter is very limited because it uses a very small training dataset. However, the performance of the model can be improved by using larger dataset when these become accessible. This would allow the model to be rigorously tested and improved. It is possible to develop a pdf crawler to extract data from published research papers, to develop a very comprehensive database, although this was not within the scope of this work. The future use of these types of models can help identify papers that have similar ash characteristics to those of interest. This would help researchers identify solutions to the problem and help them develop and mitigate problems associated with the type of ash they are investigating.

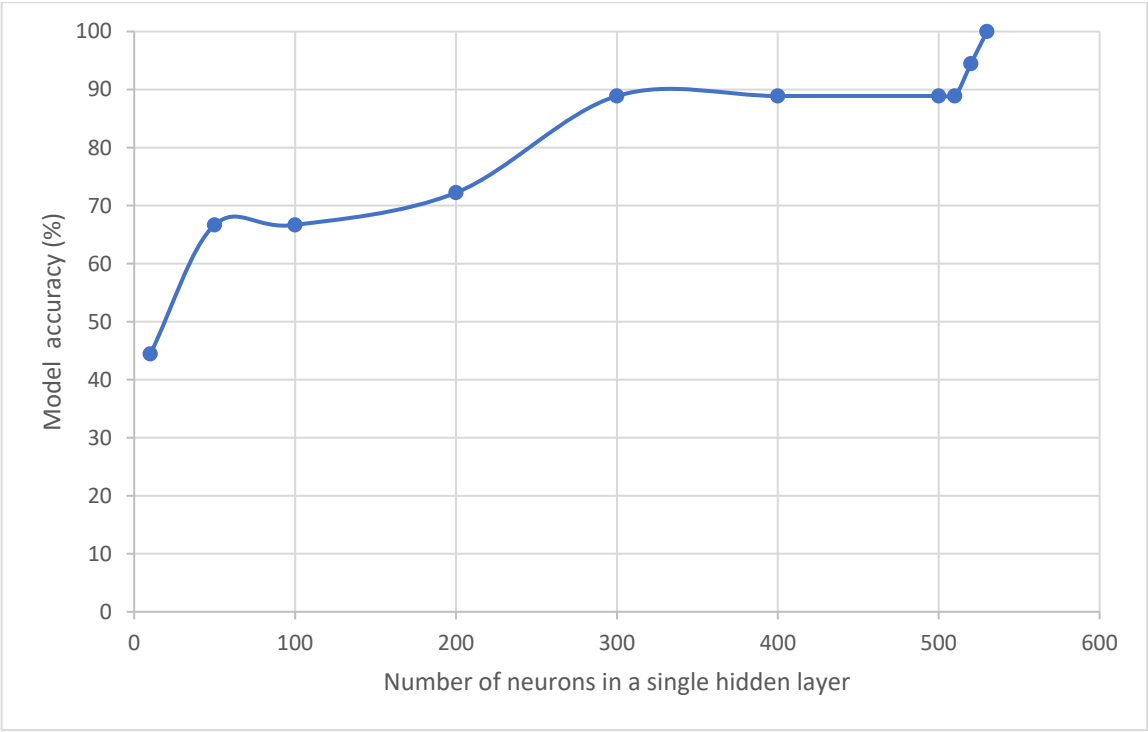

Figure 7.1: Shows the influence of neuron numbers (in a single hidden layer) on the accuracy of an ANN model

7.6 Conclusion and future of machine learning in ash-based research

Even though the initial objective of the research was to develop a model to investigate the physical behaviour (compressive strength) of the APC residue-based material but during the research, it was noticed that the bigger issue was - identification of ashes and its changing composition leading to difficulty in reproducing results. This was an issue because in literature researchers have identified APC residues by many different names, hence making it very difficult to identify research papers. The other issue was related to the variation in ash composition caused by the type of waste incinerated by the plant (MSW incinerator), type of flue gas treatment process and type of ash collection system used by the plant. This research was only able to demonstrate the use of novel ANN technique to classify different types of ashes based on their chemical composition identified using X-ray Fluorescence (XRF) spectroscopy. The developed model was able to achieve 100% accuracy in classifying waste ashes from the literature, albeit on a limited dataset. However, the robustness of the model can be improved by using larger training dataset. Therefore, the potential for research in this area is promising for the future as this can be the first step towards developing a comprehensive set of techniques those can be used in the future to develop a robust database of ash-based experiments.

8 Conclusion and recommendation for further research

8.1 The overall conclusion of the research

The research investigated various heat treatment techniques and cold bonding of APC residues. The heat treatment through sintering in a muffle furnace and induction heating system was explored for its potential to produce Light Weight Aggregates (LWA). Treatment through cold bonding was investigated by developing APC residues-based geopolymer material. The results from this experiment were used to develop a machine learning model to help predict the compressive strength of the produced material. Lastly, an Artificial Neural Network (ANN) model was developed to identify different types of ashes. It can be concluded from this research that further development and investigation to develop a model using machine learning techniques can be of paramount importance as the main issue is due to variation in the composition of ash. As current literature is only applicable to the ashes with a similar chemical composition (which is very difficult to find, given the variation in ash composition). The other solution can be to utilise these types of ash in small quantities in a stable base material such as cement, concrete or clay, as the properties of the final material will not be significantly influenced by the change in the chemical composition of these types of ashes. The main conclusion that can be drawn from this research are as follows:

1. From our research, the addition of APC residue to clay increased the strength of LWA. The highest fracture strength of 5.79MPa was achieved by the LWA, developed using 20% APC residues with 80% clay, sintered at 1170^{o}C in a muffle furnace. In addition, the sintered LWA also had very good chemical properties determined through leaching test conducted according to BS EN 12457-2 (2002).
2. The use of an induction heating system to sinter green pellets/granules to produce LWAs was not successful. However, it was observed that green pellets doped with magnetic/conductive powdered material caused shattering of the pellets due to a rapid increase in localised heat within the pellets.
3. The treatment through cold bonding was adequate to achieve solidification/stabilisation. The research investigated different solid to liquid ratios and sodium hydroxide to sodium silicate ratios to identify the relationship of these ratios and their effects on the physical and chemical characteristics of the material. The most suitable solid to liquid ratio identified in this research was 3:5, and for sodium silicate to sodium hydroxide, it was 3:2. These ratios managed to produce a material with the compressive strength of 2.35 MPa for washed APC residues. The use of unwashed APC residues was also investigated, but it was concluded that unwashed APC residues produce material with chemically/physically undesirable properties. With reference to the leaching behaviour, its performance was not as good as of the sintered material, but in terms of waste classification, it can be classified as non-hazardous material according to UK landfill Directive 2008/98/EC Hence, this technique can be used to achieve solidification/stabilisation of APC residues as untreated APC residues exceed the hazardous waste limit for landfills in the UK for lead and chloride; therefore, it requires treatment before disposal.
4. The machine learning techniques were applied to model APC residues-based geopolymer material. The research developed a Multivariate Nonlinear Regression model to predict the compressive strength of the material, but this technique was not able to produce a good model, as the

Mean Absolute Error (MAE) was 301.8 KPa. The use of Artificial Neural Network (ANN) was investigated, and this machine learning technique was able to produce a model with a MAE of 2.3 KPa. The effectiveness of this ANN model was tested by reformulating the geopolymer based material to test the model on unseen dataset. The model was able to identify a general trend in data but was not able to accurately predict the compressive strength of the material. Therefore, it was concluded that ANN model could be very effective at predicting the compressive strength of the material for seen data (data that is used to train the model), but it cannot make a good prediction on unseen data as MAE for unseen data was 479.5 KPa. However, the accuracy of the model can be improved by using a larger training dataset as the use of small training datasets can lead to the problem of overfitting.

5. This research was able to demonstrate the use of a novel ANN model to classify different types of ash based on their chemical composition, identified by using X-ray Fluorescence (XRF) spectroscopy. The model was able to identify different types of ash, with an accuracy of 100%.

8.2 Novelty and contribution to knowledge

The major novelty and contribution to the knowledge of the research is the identification and utilisation of machine learning techniques, whereas the development of materials using APC residues has added value to existing knowledge. These can be summarised as follows:

1. The novelty in the research with reference to the heat treatment of APC residues was investigation using an induction heating system. However, the use of this system was not successful in achieving sintering of the green pellets/granules doped with a magnetic/conductive material, but further development and investigation of such system can be beneficial academically and commercially (will be discussed in section 8.4).
2. The research was able to identify the use of incorrect terminologies in existing literature such as: use of term fly ash to identify APC residues and confusion related to an equation to calculate fracture strength, which is widely used by different peer-review papers, referring to it as equation to calculate compressive strength, tensile strength and tensile stress.
3. The investigation of different solid to liquid ratios and sodium hydroxide to sodium silicate ratios to produce APC residues based geopolymer material to help identify and understand the influence of different ratios on the compressive strength of the material.
4. Development of a novel machine learning (ANN) model to predict the compressive strength of the APC residues based geopolymer material.
5. This research also produced another novel ANN model to help identify different types of ashes based on their chemical composition. The development of two different types of ANN model in this research demonstrated the effectiveness of ANN to solve regression problem (prediction of compressive strength) and classification problem (identification of ash).

8.3 Limitations of the research

This research has two limitations, the changing chemical composition of the MSWI APC residue and the use of a small training dataset to train the machine learning model, but despite this, the research has established an understanding to help tackle the limitations for future researchers. The problem related to the changing chemical composition of MSWI ashes has also been identified by Lam et al. (2010) and Lindberg et al. (2015) in their review papers. Therefore, the experimental results produced in this research and the results from the current published literature relating to the subject area should be utilised to establish a general understanding of the effectiveness of different treatment techniques and that it is not always possible to fully reproduce the results. In terms of this research, the results from thermal treatment of APC residues indicate that the addition of APC residue generally increases the fracture strength of the clay aggregates. Similarly, the results from the geopolymerisation experiment can be used to establish an understanding of the effect of solid to liquid ratio (MSWI APC residue to alkaline activator ratio) and sodium silicate to sodium hydroxide ratio.

The machine learning models developed in chapter 6 and 7 both suffer from the use of small training dataset to train the model. The use of a larger training dataset can help improve the accuracy of the model and can also help mitigate the problem of overfitting of the training dataset. Therefore, the results from these chapters should be used as proof of concept to help identify the benefits of using machine learning techniques to aid in the identification of different types of ashes based on their chemical composition and also to develop a more standardised approach to help produce predictable experimental results.

8.4 Recommendation for further research

The ability of the induction heating system to rapidly and directly induce heat within the material opens new possibilities in materials processing development; these materials have clear opportunities for the 3D printing of large structures such as houses and buildings. Therefore, this technology has great future potential and could be researched further as a post-doctoral opportunity to investigate the development of special materials and implementation of this technology. The other potential for further research can be to conduct Cost-Benefit Analysis (CBA) and Multi-Criteria Analysis (MCA) to determine the benefits of heat treatment of APC residues and cold bonding techniques.

The other recommendation for further research can be to produce or to collect large amounts of data from existing literature to help develop better machine learning models. The development of a repository of data can be of paramount importance in the advancement of ash-based materials research, as this can allow accumulation of a large amount of data to help develop a comprehensive machine learning model. These models can help standardise procedures to tackle the problem of reproducibility of results based on variation in ash composition and can also help in the identification of ashes. The development of data repositories has proven to be very beneficial in other areas of research as it has allowed data access to more people for experimentation. Examples of large machine learning repositories are Kaggle and UCI Machine Learning repository.

9 References

2003/33/EC: Council Decision of 19 December 2002 establishing criteria and procedures for the acceptance of waste at landfills pursuant to Article 16 of and Annex II to Directive 1999/31/EC.

Abdoli, M. A., Golzary, A., Hosseini, A. and Sadeghi, P. (2018) *Wood Pellet as a Renewable Source of Energy: From Production to Consumption.* New York, NY: Springer Berlin Heidelberg.

Abney, S. P. (2008) *Semisupervised learning for computational linguistics.* Boca Raton; London: Chapman & Hall/CRC.

Abramov, S., He, J., Wimmer, D., Lemloh, M.-L., Muehe, E. M., Gann, B., Roehm, E., Kirchhof, R., Babechuk, M. G., Schoenberg, R., Thorwarth, H., Helle, T. and Kappler, A. (2018) 'Heavy metal mobility and valuable contents of processed municipal solid waste incineration residues from Southwestern Germany', *Waste Management,* 79, pp. 735-743.

Aggarwal, C. C. (2018) *Neural Networks and Deep Learning: A Textbook.* Cham, Switzerland: Springer International Publishing.

Aghdam, H. and Heravi, E. J. (2017) *Guide to convolutional neural networks : a practical application to traffic-sign detection and classification* Cham, Switzerland: Springer.

Ahamed, M. and Siddiqui, M. K. J. (2007) 'Low level lead exposure and oxidative stress: Current opinions', *Clinica Chimica Acta,* 383(1), pp. 57-64.

Allegrini, E., Boldrin, A., Jansson, S., Lundtorp, K. and Fruergaard Astrup, T. (2014) 'Quality and generation rate of solid residues in the boiler of a waste-to-energy plant', *Journal of Hazardous Materials,* 270, pp. 127-136.

Allen, M. P. (2007) *Understanding Regression Analysis.* New York: Springer US.

Allsopp, M., Costner, P. and Johnston, P. (2001) 'Incineration and human health', *Environmental Science and Pollution Research,* 8(2), pp. 141-145.

Als-Nielsen, J. and McMorrow, D. (2011) *Elements of modern X-ray physics.* 2nd edn. Hoboken: Wiley.

Amutha Rani, D., Boccaccini, A. R., Deegan, D. and Cheeseman, C. R. (2008a) 'Air pollution control residues from waste incineration: Current UK situation and assessment of alternative technologies', *Waste Management,* 28(11), pp. 2279-2292.

Amutha Rani, D., Gomez, E., Boccaccini, A. R., Hao, L., Deegan, D. and Cheeseman, C. R. (2008b) 'Plasma treatment of air pollution control residues', *Waste Management,* 28(7), pp. 1254-1262.

Arioz, O., Kilinç, K., Karasu, B., Kaya, G., Arslan, G., Tuncan, M., Tuncan, A., Korkut, M. and Kivrak, S. (2008) 'A Preliminary Research On The Properties of Lightweight Expanded Clay Aggregate', *Journal of the Australiasian Ceramic Society,* 44(1), pp. 23-30.

Asteris, P. G., Kolovos, K. G., Douvika, M. G. and Roinos, K. (2016) 'Prediction of self-compacting concrete strength using artificial neural networks', *European Journal of Environmental and Civil Engineering,* 20(sup1), pp. s102-s122.

Astrup, T., Muntoni, A., Polettini, A., Pomi, R., Van Gerven, T. and Van Zomeren, A. (2016) 'Chapter 24 - Treatment and Reuse of Incineration Bottom Ash', in Prasad, M.N.V. & Shih, K. (eds.) *Environmental Materials and Waste*: Academic Press, pp. 607-645.

Aydın Ahmet, A. and Aydın, A. (2016) 'Heavy Metals', *Handbook of Combustion*.

Bell, J. a. (2015) *Machine learning : hands-on for developers and technical professionals.* Indianapolis, USA: John Wiley & Sons.

Bengio, Y. (2009) 'Learning Deep Architectures for AI', *Foundations and Trends in Machine Learning,* 2(1), pp. 1-127.

Beyene, H. D., Werkneh, A. A. and Ambaye, T. G. (2018) 'Current updates on waste to energy (WtE) technologies: a review', *Renewable Energy Focus,* 24, pp. 1-11.

Bilgehan, M. and Turgut, P. (2010) 'Artificial Neural Network Approach to Predict Compressive Strength of Concrete through Ultrasonic Pulse Velocity', *Research in Nondestructive Evaluation,* 21(1), pp. 1-17.

Bingham, P. A. and Hand, R. J. (2006) 'Vitrification of toxic wastes: a brief review', *Advances in Applied Ceramics,* 105(1), pp. 21-31.

Bishop, C. M. (2006) *Pattern recognition and machine learning.* New York: Springer.

Blazynski, T. Z. (1993) '4 - Metal Forming', in Koshal, D. (ed.) *Manufacturing Engineer's Reference Book*. Oxford: Butterworth-Heinemann, pp. 4/1-4/130.

Boarder, R. F. W., Owens, P. L. and Khatib, J. M. (2016) '10 - The sustainability of lightweight aggregates manufactured from clay wastes for reducing the carbon footprint of structural and foundation concrete', in Khatib, J.M. (ed.) *Sustainability of Construction Materials (Second Edition)*: Woodhead Publishing, pp. 209-244.

Boca Santa, R. A. A., Soares, C. and Riella, H. G. (2016) 'Geopolymers with a high percentage of bottom ash for solidification/immobilization of different toxic metals', *Journal of Hazardous Materials,* 318, pp. 145-153.

Bogas, J. A., Nogueira, R. and Almeida, N. G. (2014) 'Influence of mineral additions and different compositional parameters on the shrinkage of structural expanded clay lightweight concrete', *Materials & Design (1980-2015),* 56, pp. 1039-1048.

Bonaccorso, G. (2017) *Machine learning algorithms: reference guide for popular algorithms for data science and machine learning.* Birmingham, UK: Packt Publishing.

Brauer, D. S., Rüssel, C. and Kraft, J. (2007) 'Solubility of glasses in the system P2O5–CaO–MgO–Na2O–TiO2: Experimental and modeling using artificial neural networks', *Journal of Non-Crystalline Solids,* 353(3), pp. 263-270.

Bressert, E. (2012) *SciPy and NumPy.* Sebastopol, CA: O'Reilly.

BS 6068-2.46 (1995) 'Water quality. Determination of dissolved anions by liquid chromatography of ions. Determination of fluoride, chloride, nitrite, orthophosphate, bromide, nitrate and sulfate ions. Method for water with low contamination'.

BS EN 12457-2 (2002) 'Characterisation of waste. Leaching. Compliance test for leaching of granular waste materials and sludges. One stage batch test at a liquid to solid ratio of 10 l/kg for materials with particle size below 4 mm (without or with size reduction)'.

BS EN 13657 (2002) 'Characterization of waste. Digestion for subsequent determination of aqua regia soluble portion of elements'.

Buduma, N. and Locascio, N. (2017) *Fundamentals of deep learning: designing next-generation machine intelligence algorithms.* Sebastopol, CA: O'Reilly Media.

Bui, L. A.-t., Hwang, C.-l., Chen, C.-t., Lin, K.-l. and Hsieh, M.-y. (2012) 'Manufacture and performance of cold bonded lightweight aggregate using alkaline activators for high performance concrete', *Construction and Building Materials,* 35, pp. 1056-1062.

Bye, G. C. (1999) *Portland cement : composition, production and properties.* 2nd edn. London: Thomas Telford.

Capelo, L. (2018) *Beginning Application Development with TensorFlow and Keras: Learn to design, develop, train, and deploy TensorFlow and Keras models as real-world applications.* Birmingham, UK: Packt Publishing.

Caprai, V., Florea, M. V. A. and Brouwers, H. J. H. (2018) 'Evaluation of the influence of mechanical activation on physical and chemical properties of municipal solid waste incineration sludge', *Journal of Environmental Management,* 216, pp. 133-144.

Carretero, C., Lucía, O., Acero, J., Alonso, R. and Burdío, J. M. (2011) 'An application of the impedance boundary condition for the design of coils used in domestic induction heating systems', *COMPEL-The International Journal for Computation and Mathematics in Electrical Engineering,* 30, pp. 1616-1625.

Cassar, D. R., de Carvalho, A. C. P. L. F. and Zanotto, E. D. (2018) 'Predicting glass transition temperatures using neural networks', *Acta Materialia,* 159, pp. 249-256.

Celenza, G. (2000) *Industrial Waste Treatment Processes Engineering: Specialized Treatment Systems.* Pennsylvania: Taylor & Francis.

Chakraborty, S., Jo, B. W., Jo, J. H. and Baloch, Z. (2017) 'Effectiveness of sewage sludge ash combined with waste pozzolanic minerals in developing sustainable construction material: An alternative approach for waste management', *Journal of Cleaner Production,* 153, pp. 253-263.

Chandler, A. J., Eighmy, T. T., Hjelmar, O., Kosson, D. S., Sawell, S. E., Vehlow, J., van der Sloot, H. A. and Hartlén, J. (1997) *Municipal Solid Waste Incinerator Residues. Studies in Environmental Science* Amsterdam: Elsevier Science.

Cheeseman, C. R. and Virdi, G. S. (2005) 'Properties and microstructure of lightweight aggregate produced from sintered sewage sludge ash', *Resources, Conservation and Recycling,* 45(1), pp. 18-30.

Chen, Q. Y., Tyrer, M., Hills, C. D., Yang, X. M. and Carey, P. (2009) 'Immobilisation of heavy metal in cement-based solidification/stabilisation: A review', *Waste Management,* 29(1), pp. 390-403.

Chen, X., Sztandera, L. and Cartwright, H. M. (2008) 'A neural network approach to prediction of glass transition temperature of polymers', *International Journal of Intelligent Systems,* 23(1), pp. 22-32.

Chen, Y.-C. (2016) 'Potential for energy recovery and greenhouse gas mitigation from municipal solid waste using a waste-to-material approach', *Waste Management,* 58, pp. 408-414.

Chen, Z., Li, J.-S., Zhan, B.-J., Sharma, U. and Poon, C. S. (2018) 'Compressive strength and microstructural properties of dry-mixed geopolymer pastes synthesized from GGBS and sewage sludge ash', *Construction and Building Materials,* 182, pp. 597-607.

Chen, Z. and Poon, C. S. (2017) 'Comparative studies on the effects of sewage sludge ash and fly ash on cement hydration and properties of cement mortars', *Construction and Building Materials,* 154, pp. 791-803.

Cheng, H. and Hu, Y. (2010) 'Municipal solid waste (MSW) as a renewable source of energy: Current and future practices in China', *Bioresource Technology,* 101(11), pp. 3816-3824.

Cheng, T. W., Chu, J. P., Tzeng, C. C. and Chen, Y. S. (2002a) 'Treatment and recycling of incinerated ash using thermal plasma technology', *Waste Management,* 22(5), pp. 485-490.

Cheng, T. W., Ueng, T. H., Chen, Y. S. and Chiu, J. P. (2002b) 'Production of glass-ceramic from incinerator fly ash', *Ceramics International,* 28(7), pp. 779-783.

Chimenos, J. M., Segarra, M., Fernández, M. A. and Espiell, F. (1999) 'Characterization of the bottom ash in municipal solid waste incinerator', *Journal of Hazardous Materials,* 64(3), pp. 211-222.

Chindris, M. and Sumper, A. (2012) 'Industrial Heating Processes', *Electrical Energy Efficiency*. Chichester, UK: John Wiley & Sons, Ltd, pp. 295-334.

Chithra, S., Kumar, S. R. R. S., Chinnaraju, K. and Alfin Ashmita, F. (2016) 'A comparative study on the compressive strength prediction models for High Performance Concrete containing nano silica and copper slag using regression analysis and Artificial Neural Networks', *Construction and Building Materials,* 114, pp. 528-535.

Chopra, P., Sharma, R. K., Kumar, M. and Chopra, T. (2018) 'Comparison of Machine Learning Techniques for the Prediction of Compressive Strength of Concrete', *Advances in Civil Engineering,* 2018, pp. 9.

Ciaburro, G. and Venkateswaran, B. (2017) *Neural Networks with R: Smart models using CNN, RNN, deep learning, and artificial intelligence principles.* Birmingham, UK: Packt Publishing.

Cichosz, P. (2015) *Data Mining Algorithms: Explained Using R.* Chichester, West Sussex; Malden, MA: Wiley.

Ciregan, D., Meier, U. and Schmidhuber, J. 'Multi-column deep neural networks for image classification'. *2012 IEEE Conference on Computer Vision and Pattern Recognition*, 16-21 June 2012, 3642-3649.

Clarke, B. S., Fokoue, E. and Zhang, H. H. (2009) *Principles and theory for data mining and machine learning.* Dordrecht; London: Springer.

Colangelo, F. and Cioffi, R. (2013) 'Use of Cement Kiln Dust, Blast Furnace Slag and Marble Sludge in the Manufacture of Sustainable Artificial Aggregates by Means of Cold Bonding Pelletization', *Materials,* 6(8).

Colangelo, F., Cioffi, R., Montagnaro, F. and Santoro, L. (2012) 'Soluble salt removal from MSWI fly ash and its stabilization for safer disposal and recovery as road basement material', *Waste Management,* 32(6), pp. 1179-1185.

Colangelo, F., Messina, F. and Cioffi, R. (2015) 'Recycling of MSWI fly ash by means of cementitious double step cold bonding pelletization: Technological assessment for the production of lightweight artificial aggregates', *Journal of Hazardous Materials,* 299, pp. 181-191.

Colombo, P., Brusatin, G., Bernardo, E. and Scarinci, G. (2003) 'Inertization and reuse of waste materials by vitrification and fabrication of glass-based products', *Current Opinion in Solid State and Materials Science,* 7(3), pp. 225-239.

Cormier, L. (2014) 'Nucleation in Glasses – New Experimental Findings and Recent Theories', *Procedia Materials Science,* 7, pp. 60-71.

Costanzo, A., Dionigi, M., Mastri, F. and Mongiardo, M. 'Rigorous modeling of mid-range wireless power transfer systems based on royer oscillators'. *2013 IEEE Wireless Power Transfer (WPT)*, 15-16 May 2013, 69-72.

Couper, J. R. (2010) *Chemical process equipment: selection and design.* 2nd edn. Amsterdam; Boston: Elsevier.

Craigie, N. S. (2018) *Principles of elemental chemostratigraphy: a practical user guide. Advances in oil and gas exploration & production* Cham, Switzerland: Springer.

Craven, B. D. and Islam, S. M. N. (2005) *Optimization in economics and finance: some advances in non-linear, dynamic, multi-criteria and stochastic models.* Dordrecht: Springer.

Crum, J., Maio, V., McCloy, J., Scott, C., Riley, B., Benefiel, B., Vienna, J., Archibald, K., Rodriguez, C., Rutledge, V., Zhu, Z., Ryan, J. and Olszta, M. (2014) 'Cold crucible induction melter studies for making glass ceramic waste forms: A feasibility assessment', *Journal of Nuclear Materials,* 444(1), pp. 481-492.

Cybenko, G. (1989) 'Approximation by superpositions of a sigmoidal function', *Mathematics of Control, Signals and Systems,* 2(4), pp. 303-314.

Dangeti, P. (2017) *Statistics for Machine Learning: Techniques for exploring supervised, unsupervised, and reinforcement learning models with Python and R.* Birmingham, UK: Packt Publishing.

Dantas, A. T. A., Batista Leite, M. and de Jesus Nagahama, K. (2013) 'Prediction of compressive strength of concrete containing construction and demolition waste using artificial neural networks', *Construction and Building Materials,* 38, pp. 717-722.

Davidovits, J. (1991) 'Geopolymers: inorganic polymeric new materials', *Journal of Thermal Analysis,* 37(8), pp. 1633-1656.

Davidovits, J. (2008) *Geopolymer chemistry and applications.* Saint-Quentin: Geopolymer Institute.

De Silva, N. and Gregoire, D. C. (1998) 'Inductively coupled plasma optical emission and mass spectrometry', in Alfassi, Z.B. (ed.) *Instrumental Multi-Element Chemical Analysis*. Dordrecht: Springer Netherlands, pp. 151-200.

Deco, G. and Obradovic, D. (1996) *An information-theoretic approach to neural computing. Perspectives in neural computing* New York: Springer.

DEFRA (2011) *Local authority collected waste – definition of terms* Available at: https://www.gov.uk/guidance/local-authority-collected-waste-definition-of-terms (Accessed: 12/08/2016).

DEFRA (2013) *Mechanical heat treatment of municipal solid waste*: Department for Environment, Food & Rural Affairs. Available at: https://assets.publishing.service.gov.uk/government/uploads/system/uploads/attachment_data/file/221040/pb13891-heat-treatment-waste.pdf (Accessed: 21/04/2017).

DEFRA (2018a) *Digest of waste and resource statistics, 2018 edition*: Department for Environment, Food & Rural Affairs. Available at: https://assets.publishing.service.gov.uk/government/uploads/system/uploads/attachment_data/file/710124/Digest_of_Waste_and_Resource_Statistics_2018.pdf (Accessed: 12/04/2018).

DEFRA (2018b) *UK Statistics on Waste*: Department for Environment, Food & Rural Affairs.

del Valle-Zermeño, R., Formosa, J., Chimenos, J. M., Martínez, M. and Fernández, A. I. (2013) 'Aggregate material formulated with MSWI bottom ash and APC fly ash for use as secondary building material', *Waste Management,* 33(3), pp. 621-627.

Desai, P. (2015) *Python Programming for Arduino.* Birmingham, UK: Packt Publishing.

Devaraj, A. R., Cheeseman, C. R., Boccaccini, A. R. and Deegan, D. (2010) 'Glass-ceramic tiles prepared by pressing and sintering DC plasma-vitrified air pollution control residues', *International Journal of Applied Ceramic Technology,* 7(6), pp. 925-934.

Directive 2008/98/EC *Directive 2008/98/EC of the European Parliament and of the Council of 19 November 2008 on waste and repealing certain Directives*.

Dobrzański, L. A., Trzaska, J. and Dobrzańska-Danikiewicz, A. D. (2014) '2.09 - Use of Neural Networks and Artificial Intelligence Tools for Modeling, Characterization, and Forecasting in Material Engineering', in Hashmi, S., Batalha, G.F., Van Tyne, C.J. & Yilbas, B. (eds.) *Comprehensive Materials Processing*. Oxford: Elsevier, pp. 161-198.

Dou, X., Ren, F., Nguyen, M. Q., Ahamed, A., Yin, K., Chan, W. P. and Chang, V. W.-C. (2017) 'Review of MSWI bottom ash utilization from perspectives of collective characterization, treatment and existing application', *Renewable and Sustainable Energy Reviews,* 79, pp. 24-38.

Duxson, P., Fernández-Jiménez, A., Provis, J. L., Lukey, G. C., Palomo, A. and van Deventer, J. S. J. (2007) 'Geopolymer technology: the current state of the art', *Journal of Materials Science,* 42(9), pp. 2917-2933.

Duxson, P., Provis, J. L., Lukey, G. C., Mallicoat, S. W., Kriven, W. M. and van Deventer, J. S. J. (2005) 'Understanding the relationship between geopolymer composition, microstructure and mechanical properties', *Colloids and Surfaces A: Physicochemical and Engineering Aspects,* 269(1), pp. 47-58.

Echlin, P. (2009) *Handbook of Sample Preparation for Scanning Electron Microscopy and X-Ray Microanalysis.* Boston, MA: Springer US.

Ecke, H., Sakanakura, H., Matsuto, T., Tanaka, N. and Lagerkvist, A. (2000) 'State-of-the-art treatment processes for municipal solid waste incineration residues in Japan', *Waste Management and Research,* 18(1), pp. 41-51.

Ecke, H., Sakanakura, H., Matsuto, T., Tanaka, N. and Lagerkvist, A. (2001) 'Effect of Electric Arc Vitrification of Bottom Ash on the Mobility and Fate of Metals', *Environmental Science & Technology,* 35(7), pp. 1531-1536.

El-Alaily, N. A., Abou Hussein, E. M. and Ezz ElDin, F. M. (2018) 'Chemical and Optical Degradation of Some Glass Formulated from Common Municipal Solid Waste; Decorated Glass', *Silicon,* 10(5), pp. 2031-2042.

Erdoğan, S. T. (2015) 'Inexpensive intumescent alkali-activated natural pozzolan pastes', *Journal of the European Ceramic Society,* 35(9), pp. 2663-2670.

Eskandari-Naddaf, H. and Kazemi, R. (2017) 'ANN prediction of cement mortar compressive strength, influence of cement strength class', *Construction and Building Materials,* 138, pp. 1-11.

Directive 2010/75/EU of the European Parliament and of the Council of 24 November 2010 on industrial emissions (integrated pollution prevention and control) Text with EEA relevance.

Fawzi, T., Ahmed, M. and Burke, P. (1985) 'On the use of the impedance boundary conditions in eddy current problems', *IEEE Transactions on Magnetics,* 21, pp. 1835-1840.

Feeco International (2017) *FEECO Disc Pelletizers*. Available at: https://feeco.com/disc-pelletizers/ (Accessed: 11/04/17).

Fei, Y. and Liu, C. (2016) 'Chapter 12 - Detoxification and Resource Recovery of Chromium-Containing Wastes', in Prasad, M.N.V. & Shih, K. (eds.) *Environmental Materials and Waste*: Academic Press, pp. 265-284.

Ferone, C., Colangelo, F., Messina, F., Santoro, L. and Cioffi, R. (2013) 'Recycling of Pre-Washed Municipal Solid Waste Incinerator Fly Ash in the Manufacturing of Low Temperature Setting Geopolymer Materials', *Materials,* 6(8).

Flasiński, M. (2016) *Introduction to artificial intelligence.* New York, NY: Springer Berlin Heidelberg.

Forest, F., Laboure, E., Costa, F. and Gaspard, J. Y. (2000) 'Principle of a multi-load/single converter system for low power induction heating', *IEEE Transactions on Power Electronics,* 15, pp. 223-230.

Formosa, J., Giro-Paloma, J., Maldonado-Alameda, A., Huete-Hernández, S. and Chimenos, J. M. (2017) 'APC fly ashes stabilized with Portland cement for further development of road sub-base aggregates', *IOP Conference Series: Materials Science and Engineering,* 251(1), pp. 012124.

Funari, V., Mäkinen, J., Salminen, J., Braga, R., Dinelli, E. and Revitzer, H. (2017) 'Metal removal from Municipal Solid Waste Incineration fly ash: A comparison between chemical leaching and bioleaching', *Waste Management,* 60, pp. 397-406.

Gao, X., Yuan, B., Yu, Q. L. and Brouwers, H. J. H. (2017) 'Characterization and application of municipal solid waste incineration (MSWI) bottom ash and waste granite powder in alkali activated slag', *Journal of Cleaner Production,* 164, pp. 410-419.

Garcia-Lodeiro, I., Palomo, A., Fernández-Jiménez, A. and Macphee, D. E. (2011) 'Compatibility studies between N-A-S-H and C-A-S-H gels. Study in the ternary diagram Na2O–CaO–Al2O3–SiO2–H2O', *Cement and Concrete Research,* 41(9), pp. 923-931.

Geem, Z. W. (2011) *Optimization in civil & environmental engineering.* Philadelphia: Old city publishing.

Géron, A. (2017) *Hands-on machine learning with Scikit-Learn and TensorFlow: concepts, tools, and techniques to build intelligent systems* Sebastopol, CA: O'Reilly Media.

Gesoğlu, M., Güneyisi, E. and Öz, H. Ö. (2012) 'Properties of lightweight aggregates produced with cold-bonding pelletization of fly ash and ground granulated blast furnace slag', *Materials and Structures,* 45(10), pp. 1535-1546.

Gesoğlu, M., Özturan, T. and Güneyisi, E. (2007) 'Effects of fly ash properties on characteristics of cold-bonded fly ash lightweight aggregates', *Construction and Building Materials,* 21(9), pp. 1869-1878.

Gharfalkar, M., Court, R., Campbell, C., Ali, Z. and Hillier, G. (2015) 'Analysis of waste hierarchy in the European waste directive 2008/98/EC', *Waste Management,* 39, pp. 305-313.

Ghotra, M. S. and Dua, R. (2017) *Neural Network Programming with TensorFlow: Unleash the power of TensorFlow to train efficient neural networks.* Birmingham, UK: Packt Publishing.

Ginés, O., Chimenos, J. M., Vizcarro, A., Formosa, J. and Rosell, J. R. (2009) 'Combined use of MSWI bottom ash and fly ash as aggregate in concrete formulation: Environmental and mechanical considerations', *Journal of Hazardous Materials,* 169(1), pp. 643-650.

Ginsberg, J., Mohebbi, M. H., Patel, R. S., Brammer, L., Smolinski, M. S. and Brilliant, L. (2008) 'Detecting influenza epidemics using search engine query data', *Nature,* 457, pp. 1012.

Giro-Paloma, J., Maldonado-Alameda, A., Formosa, J., Barbieri, L., Chimenos, J. M. and Lancellotti, I. (2017a) 'Geopolymers based on the valorization of Municipal Solid Waste Incineration residues', *IOP Conference Series: Materials Science and Engineering,* 251(1), pp. 012125.

Giro-Paloma, J., Ribas-Manero, V., Maldonado-Alameda, A., Formosa, J. and Chimenos, J. M. (2017b) 'Use of municipal solid waste incineration bottom ash and crop by-product for producing lightweight aggregate', *IOP Conference Series: Materials Science and Engineering,* 251.

Giusti, L. (2009) 'A review of waste management practices and their impact on human health', *Waste Management,* 29(8), pp. 2227-2239.

Glid, M., Sobrados, I., Rhaiem, H. B., Sanz, J. and Amara, A. B. H. (2017) 'Alkaline activation of metakaolinite-silica mixtures: Role of dissolved silica concentration on the formation of geopolymers', *Ceramics International,* 43(15), pp. 12641-12650.

Gluck, M. A. and Myers, C. E. (2001) *Gateway to Memory: An Introduction to Neural Network Modeling of the Hippocampus and Learning.* Cambridge, Mass.: MIT Press.

Goldstein, J., Newbury, D. E., Joy, D. C., Lyman, C. E., Echlin, P., Lifshin, E., Sawyer, L. and Michael, J. R. (2003) *Scanning Electron Microscopy and X-Ray Microanalysis.* 3rd edn. Boston, MA: Springer US.

Goldstein, J. I., Newbury, D. E., Michael, J. R., Ritchie, N. W. M., Scott, J. H. J. and Joy, D. C. (2018a) 'Backscattered Electrons', in Goldstein, J.I., Newbury, D.E., Michael, J.R., Ritchie, N.W.M., Scott, J.H.J. & Joy, D.C. (eds.) *Scanning Electron Microscopy and X-Ray Microanalysis*. New York, NY: Springer New York, pp. 15-28.

Goldstein, J. I., Newbury, D. E., Michael, J. R., Ritchie, N. W. M., Scott, J. H. J. and Joy, D. C. (2018b) 'Secondary Electrons', in Goldstein, J.I., Newbury, D.E., Michael, J.R., Ritchie, N.W.M., Scott, J.H.J. & Joy, D.C. (eds.) *Scanning Electron Microscopy and X-Ray Microanalysis*. New York, NY: Springer New York, pp. 29-37.

Gomathi, P. and Sivakumar, A. (2014) 'Cold bonded fly ash lightweight aggregate containing different binders', *Research Journal of Applied Sciences, Engineering and Technology,* 7(6), pp. 915-920.

Gomez, E., Rani, D. A., Cheeseman, C. R., Deegan, D., Wise, M. and Boccaccini, A. R. (2009) 'Thermal plasma technology for the treatment of wastes: A critical review', *Journal of Hazardous Materials,* 161(2), pp. 614-626.

Gong, B., Deng, Y., Yang, Y., Tan, S. N., Liu, Q. and Yang, W. (2017) 'Solidification and Biotoxicity Assessment of Thermally Treated Municipal Solid Waste Incineration (MSWI) Fly Ash', *International journal of environmental research and public health,* 14(6), pp. 626.

González-Corrochano, B., Alonso-Azcárate, J. and Rodas, M. (2009) 'Production of lightweight aggregates from mining and industrial wastes', *Journal of Environmental Management,* 90(8), pp. 2801-2812.

Goodfellow, I., Bengio, Y. and Courville, A. (2016) *Deep learning. Adaptive computation and machine learning* Cambridge, Massachusetts: The MIT Press.

Greim, H. and Snyder, R. (2008) *Toxicology and risk assessment: a comprehensive introduction.* Chichester: John Wiley.

Gulli, A. and Kapoor, A. (2017) *TensorFlow 1.x Deep Learning Cookbook: Over 90 unique recipes to solve artificial-intelligence driven problems with Python.* Packt Publishing.

Gulli, A. and Pal, S. (2017) *Deep learning with Keras: implement neural networks with Keras on Theano and TensorFlow.* Birmingham, UK: Packt Publishing Ltd.

Guo, B., Liu, B., Yang, J. and Zhang, S. (2017) 'The mechanisms of heavy metal immobilization by cementitious material treatments and thermal treatments: A review', *Journal of Environmental Management,* 193, pp. 410-422.

Guo, X. and Shi, H. (2015) 'Metakaolin-, fly ash- and calcium hydroxide-based geopolymers: effects of calcium on performance', *Advances in Cement Research,* 27(10), pp. 559-566.

Gurney, K. (1997) *An introduction to neural networks.* London: UCL Press.

Guzmán-Carrillo, H. R., Pérez, J. M., Aguilar Reyes, E. A. and Romero, M. (2018) 'Coal fly ash and steel slag valorisation throughout a vitrification process', *International Journal of Environmental Science and Technology,* 15(8), pp. 1757-1766.

Hady, M. F. A. and Schwenker, F. (2013) 'Semi-supervised Learning', in Bianchini, M., Maggini, M. & Jain, L.C. (eds.) *Handbook on Neural Information Processing*. Berlin, Heidelberg: Springer Berlin Heidelberg, pp. 215-239.

Haimbaugh, R. E. (2015) *Practical Induction Heat Treating.* 2nd edn. Materials Park, Ohio: ASM International.

Han, L., Song, J., Lin, C., Liu, J., Liu, T., Zhang, Q., Luo, Z. and Lu, A. (2018) 'Crystallization, structure and properties of MgO-Al2O3-SiO2 highly crystalline transparent glass-ceramics nucleated by multiple nucleating agents', *Journal of the European Ceramic Society,* 38(13), pp. 4533-4542.

Hansen, J. S. (2011) *GNU Octave: Beginner's Guide: Become a Proficient Octave User by Learning this High-level Scientific Numerical Tool from the Ground Up.* Packt Publishing.

Hapidin, D. A., Saleh, I., Munir, M. M. and Khairurrijal (2017) 'Design and Development of a Series-configuration Mazzilli Zero Voltage Switching Flyback Converter as a High-voltage Power Supply for Needleless Electrospinning', *Procedia Engineering,* 170, pp. 509-515.

Harrison, R. M. (2007) *Principles of environmental chemistry.* Cambridge: Royal Society of Chemistry.

Haschke, M. (2014) *Laboratory micro-x-ray fluorescence spectroscopy: instrumentation and applications. Springer series in surface sciences volume 55* Cham: Springer.

Hashmi, S. (2014) *Comprehensive Materials Processing.* Elsevier Science.

Hassaan, M. M., Khater, H. M., El-Mahllawy, M. S. and El Nagar, A. M. (2015) 'Production of geopolymer composites enhanced by nano-kaolin material', *Journal of Advanced Ceramics,* 4(4), pp. 245-252.

Heard, W., Song, B., Williams, B., Martin, B., Sparks, P. and Nie, X. (2018) 'Dynamic Tensile Experimental Techniques for Geomaterials: A Comprehensive Review', *Journal of Dynamic Behavior of Materials,* 4(1), pp. 74-94.

Heath, A., Paine, K., Goodhew, S., Ramage, M. and Lawrence, M. (2013) 'The potential for using geopolymer concrete in the UK', *Proceedings of the Institution of Civil Engineers - Construction Materials,* 166(4), pp. 195-203.

Heidenreich, S. (2013) 'Hot gas filtration – A review', *Fuel,* 104, pp. 83-94.

Henderson, H. (2007) *Artificial intelligence: mirrors for the mind. Milestones in discovery and invention* New York, N.Y.: Chelsea House.

Hiramatsu, Y. and Oka, Y. (1966) 'Determination of the tensile strength of rock by a compression test of an irregular test piece', *International Journal of Rock Mechanics and Mining Sciences & Geomechanics Abstracts,* 3(2), pp. 89-90.

Hiramatsu, Y., Oka, Y. and Kiyama, H. (1965) 'Rapid Determination of the Tensile Strength of Rocks with Irregular Test Pieces', *Journal of the Mining and Metallurgical Institute of Japan,* 81(932), pp. 1024-1030.

Hodnett, M. and Wiley, J. F. (2018) *R Deep Learning Essentials: A step-by-step guide to building deep learning models using TensorFlow, Keras, and MXNet, 2nd Edition.* Packt Publishing.

Holzinger, A. (2014) *Biomedical informatics: discovering knowledge in big data* Cham: Springer.

Huang, C.-M., Vasan, A. S. S., Huang, Y., Doraiswami, R., Osterman, M. and Pecht, M. (2017) 'MEMS Reliability', *MEMS Packaging: Vol. Volume 5 WSPC Series in Advanced Integration and Packaging*: WORLD SCIENTIFIC, pp. 279-343.

Huber, F., Herzel, H., Adam, C., Mallow, O., Blasenbauer, D. and Fellner, J. (2018) 'Combined disc pelletisation and thermal treatment of MSWI fly ash', *Waste Management,* 73, pp. 381-391.

Hurley, W. G. and Wölfle, W. H. (2013) *Transformers and Inductors for Power Electronics: Theory, Design and Applications.* Wiley.

Hwang, K. and Chen, M. (2017) *Big-Data Analytics for Cloud, IoT and Cognitive Computing.* Wiley.

Intra, P., Yawootti, A. and Tippayawong, N. (2014) 'Demonstration of a modular electrostatic precipitator to control particulate emissions from a small municipal

waste incinerator', *Journal of Electrical Engineering and Technology,* 9(1), pp. 239-246.

Izenman, A. J. (2008) *Modern Multivariate Statistical Techniques: Regression, Classification, and Manifold Learning.* Springer Publishing.

Jiao, F., Zhang, L., Dong, Z., Namioka, T., Yamada, N. and Ninomiya, Y. (2016) 'Study on the species of heavy metals in MSW incineration fly ash and their leaching behavior', *Fuel Processing Technology,* 152, pp. 108-115.

Jin, R., Chen, Q. and Soboyejo, A. B. O. (2018a) 'Non-linear and mixed regression models in predicting sustainable concrete strength', *Construction and Building Materials,* 170, pp. 142-152.

Jin, R., Yan, L., Soboyejo, A. B. O., Huang, L. and Kasal, B. (2018b) 'Multivariate regression models in estimating the behavior of FRP tube encased recycled aggregate concrete', *Construction and Building Materials,* 191, pp. 216-227.

Karim, M. R. (2017) *Predictive Analytics with TensorFlow: Implement deep learning principles to predict valuable insights using TensorFlow.* Packt Publishing.

Kathirvale, S., Muhd Yunus, M. N., Sopian, K. and Samsuddin, A. H. (2004) 'Energy potential from municipal solid waste in Malaysia', *Renewable Energy,* 29(4), pp. 559-567.

Keppert, M., Siddique, J. A., Pavlík, Z. and Černý, R. (2015) 'Wet-Treated MSWI Fly Ash Used as Supplementary Cementitious Material', *Advances in Materials Science and Engineering,* 2015.

Ketkar, N. (2017) *Deep learning with Python: a hands-on introduction.* United States: Apress.

Khale, D. and Chaudhary, R. (2007) 'Mechanism of geopolymerization and factors influencing its development: a review', *Journal of Materials Science,* 42(3), pp. 729-746.

Khan, G. M. (2018) *Evolution of artificial neural development in search of learning genes. Studies in computational intelligence* Cham: Springer.

Khater, H. M. (2012) 'Effect of Calcium on Geopolymerization of Aluminosilicate Wastes', *Journal of Materials in Civil Engineering,* 24(1), pp. 92-101.

Kim, H.-K. (2015) 'Utilization of sieved and ground coal bottom ash powders as a coarse binder in high-strength mortar to improve workability', *Construction and Building Materials,* 91, pp. 57-64.

Kirk, M. (2017) *Thoughtful machine learning with Python: a test-driven approach.* First edn. Beijing; Boston: O'Reilly.

Kleynhans, E. L. J., Beukes, J. P., Van Zyl, P. G., Kestens, P. H. I. and Langa, J. M. (2012) 'Unique challenges of clay binders in a pelletised chromite pre-reduction process', *Minerals Engineering,* 34, pp. 55-62.

Kodratoff, Y. E. and Michalski, R. S. E. (1990) *Machine learning: an artificial intelligence approach: International meeting on advances in learning.* San Mateo, Ca: Morgan Kaufman.

Komilis, D., Evangelou, A., Giannakis, G. and Lymperis, C. (2012) 'Revisiting the elemental composition and the calorific value of the organic fraction of municipal solid wastes', *Waste Management,* 32(3), pp. 372-381.

Kourti, I. and Cheeseman, C. R. (2010) 'Properties and microstructure of lightweight aggregate produced from lignite coal fly ash and recycled glass', *Resources, Conservation and Recycling,* 54(11), pp. 769-775.

Kourti, I., Devaraj, A. R., Guerrero Bustos, A., Deegan, D., Boccaccini, A. R. and Cheeseman, C. R. (2011) 'Geopolymers prepared from DC plasma treated air pollution control (APC) residues glass: Properties and characterisation of the binder phase', *Journal of Hazardous Materials,* 196, pp. 86-92.

Kourti, I., Rani, D. A., Deegan, D., Boccaccini, A. R. and Cheeseman, C. R. (2010) 'Production of geopolymers using glass produced from DC plasma treatment of air pollution control (APC) residues', *Journal of Hazardous Materials,* 176(1), pp. 704-709.

Król, M., Rożek, P., Chlebda, D. and Mozgawa, W. (2018) 'Influence of alkali metal cations/type of activator on the structure of alkali-activated fly ash – ATR-FTIR studies', *Spectrochimica Acta - Part A: Molecular and Biomolecular Spectroscopy,* 198, pp. 33-37.

Kumar, A. and Samadder, S. R. (2017) 'A review on technological options of waste to energy for effective management of municipal solid waste', *Waste Management,* 69, pp. 407-422.

Kvålseth, T. O. (1985) 'Cautionary Note about R 2', *The American Statistician,* 39(4), pp. 279-285.

Lam, C. H. K., Ip, A. W. M., Barford, J. P. and McKay, G. (2010) 'Use of incineration MSW ash: A review', *Sustainability,* 2(7), pp. 1943-1968.

Lampris, C., Stegemann, J. A. and Cheeseman, C. R. (2009) 'Solidification/stabilisation of air pollution control residues using Portland cement: Physical properties and chloride leaching', *Waste Management,* 29(3), pp. 1067-1075.

Lancellotti, I., Kamseu, E., Michelazzi, M., Barbieri, L., Corradi, A. and Leonelli, C. (2010) 'Chemical stability of geopolymers containing municipal solid waste incinerator fly ash', *Waste Management,* 30(4), pp. 673-679.

Lederer, J., Trinkel, V. and Fellner, J. (2017) 'Wide-scale utilization of MSWI fly ashes in cement production and its impact on average heavy metal contents in cements: The case of Austria', *Waste Management,* 60, pp. 247-258.

Lee, W. K. W. and van Deventer, J. S. J. (2002) 'Effects of Anions on the Formation of Aluminosilicate Gel in Geopolymers', *Industrial & Engineering Chemistry Research,* 41(18), pp. 4550-4558.

Li, X., Chen, Q., Zhou, Y., Tyrer, M. and Yu, Y. (2014) 'Stabilization of heavy metals in MSWI fly ash using silica fume', *Waste Management,* 34(12), pp. 2494-2504.

Li, Y., Wu, D., Zhang, J., Chang, L., Wu, D., Fang, Z. and Shi, Y. (2000) 'Measurement and statistics of single pellet mechanical strength of differently shaped catalysts', *Powder Technology,* 113(1), pp. 176-184.

Li, Y., Zhang, H., Shao, L.-M. and He, P.-J. (2017) 'Tracing source and migration of Pb during waste incineration using stable Pb isotopes', *Journal of Hazardous Materials,* 327, pp. 28-34.

Lindberg, D., Molin, C. and Hupa, M. (2015) 'Thermal treatment of solid residues from WtE units: A review', *Waste Management,* 37, pp. 82-94.

Liu, D. H. F. and Lipták, B. l. G. (1999) *Environmental engineers' handbook.* Boca Raton, Fla.: CRC Press.

Liu, W. and Cao, C. (2009) 'Artificial neural network prediction of glass transition temperature of polymers', *Colloid and Polymer Science,* 287(7), pp. 811-818.

Liu, Y., Sellmyer, D. J. and Shindo, D. (2005) *Handbook of Advanced Magnetic Materials: Vol 1. Nanostructural Effects. Vol 2. Characterization and Simulation. Vol 3. Fabrication and Processing. Vol 4. Properties and Applications. Developments in Hydrobiology Series*: Springer.

Lopez-Fernandez, X. M., Penabad-Duran, P. and Turowski, J. (2012) 'Three-Dimensional Methodology for the Overheating Hazard Assessment on Transformer Covers', *IEEE Transactions on Industry Applications,* 48, pp. 1549-1555.

Luna Galiano, Y., Fernández Pereira, C. and Vale, J. (2011) 'Stabilization/solidification of a municipal solid waste incineration residue using fly ash-based geopolymers', *Journal of Hazardous Materials,* 185(1), pp. 373-381.

Lura, P., Wyrzykowski, M., Tang, C. and Lehmann, E. (2014) 'Internal curing with lightweight aggregate produced from biomass-derived waste', *Cement and Concrete Research,* 59, pp. 24-33.

Lutz, M. (2006) *Programming Python.* 3rd edn. Beijing; Farnham: O'Reilly Media.

Luukkonen, T., Abdollahnejad, Z., Yliniemi, J., Kinnunen, P. and Illikainen, M. (2018) 'One-part alkali-activated materials: A review', *Cement and Concrete Research,* 103, pp. 21-34.

MacKay, D. J. C. (2004) *Information theory, inference, and learning algorithms.* Cambridge: Cambridge University Press.

Macleod, C., Duarte-Davidson, R., Fisher, B., Ng, B., Willey, D., Shi, J. P., Martin, I., Drew, G. and Pollard, S. (2006) 'Modeling human exposures to air pollution control (APC) residues released from landfills in England and Wales', *Environment International,* 32(4), pp. 500-509.

Maghsoodloorad, H., Amiri, H. K., Allahverdi, A., Lachemi, M. and Hossain, K. M. A. (2014) 'Recycling phosphorus slag as a precursor for alkali-activated binder; impact of type and dosage of activator', *Ceramics - Silikaty,* 58(3), pp. 227-236.

Maglogiannis, I. G. (2007) *Emerging artificial intelligence applications in computer engineering: real word AI systems with applications in eHealth, HCI, information retrieval and pervasive technologies.* Amsterdam; Oxford: IOS Press.

Malinauskaite, J., Jouhara, H., Czajczyńska, D., Stanchev, P., Katsou, E., Rostkowski, P., Thorne, R. J., Colón, J., Ponsá, S., Al-Mansour, F., Anguilano, L., Krzyżyńska, R., López, I. C., A.Vlasopoulos and Spencer, N. (2017) 'Municipal solid waste management and waste-to-energy in the context of a circular economy and energy recycling in Europe', *Energy,* 141, pp. 2013-2044.

Margallo, M., Taddei, M. B. M., Hernández-Pellón, A., Aldaco, R. and Irabien, Á. (2015) 'Environmental sustainability assessment of the management of municipal solid waste incineration residues: a review of the current situation', *Clean Technologies and Environmental Policy,* 17(5), pp. 1333-1353.

Marghussian, V. (2015) '1 - Glass Crystallization', in Marghussian, V. (ed.) *Nano-Glass Ceramics*. Oxford: William Andrew Publishing, pp. 1-62.

Margui, E. and Van Grieken, R. (2013) *X-Ray Fluorescence Spectrometry and Related Techniques: An Introduction.* New York: Momentum Press.

Matthys, J. H. (1990) *Masonry : components to assemblages : Symposium : Papers.* Philadelphia, PA: ASTM.

McCulloch, W. S. and Pitts, W. (1943) 'A logical calculus of the ideas immanent in nervous activity', *The bulletin of mathematical biophysics,* 5(4), pp. 115-133.

McKay, G. (2002) 'Dioxin characterisation, formation and minimisation during municipal solid waste (MSW) incineration: review', *Chemical Engineering Journal,* 86(3), pp. 343-368.

Meddah, M. S., Zitouni, S. and Belâabes, S. (2010) 'Effect of content and particle size distribution of coarse aggregate on the compressive strength of concrete', *Construction and Building Materials,* 24(4), pp. 505-512.

Mellado, A., Catalan, C., Bouzon, N., Borrachero, M. V., Monzo, J. M. and Paya, J. (2014) 'Carbon footprint of geopolymeric mortar: study of the contribution of the alkaline activating solution and assessment of an alternative route', *RSC Advances,* 4(45), pp. 23846-23852.

Merikallio, T., Mannonen, R. and Penttala, V. (1996) 'Drying of lightweight concrete produced from crushed expanded clay aggregates', *Cement and Concrete Research,* 26(9), pp. 1423-1433.

Miller, B. G. (2005) *Coal energy systems.* Amsterdam ; London: Elsevier Academic Press.

Mohammed, M., Khan, M. B. and Bashier, E. B. M. (2016) *Machine Learning: Algorithms and Applications.* Boca Raton, Florida: CRC Press.

Mohseni, E. (2018) 'Assessment of Na2SiO3 to NaOH ratio impact on the performance of polypropylene fiber-reinforced geopolymer composites', *Construction and Building Materials,* 186, pp. 904-911.

Mohseni, O., Stefan, H. G. and Erickson, T. R. (1998) 'A nonlinear regression model for weekly stream temperatures', *Water Resources Research,* 34(10), pp. 2685-2692.

Moon, D. H. and Dermatas, D. (2007) 'Arsenic and lead release from fly ash stabilized/solidified soils under modified semi-dynamic leaching conditions', *Journal of Hazardous Materials,* 141(2), pp. 388-394.

Morita, A., Fukui, H., Tadano, H., Hayashi, S., Hasegawa, J. and Niinomi, M. (2000) 'Alloying titanium and tantalum by cold crucible levitation melting (CCLM) furnace', *Materials Science and Engineering: A,* 280(1), pp. 208-213.

Mukerjee, A. K. and Thakur, N. (2011) *Photovoltaic Systems: Analysis and Design.* PHI Learning.

Nazari, A., Milani, A. A. and Zakeri, M. (2011) 'Modeling ductile to brittle transition temperature of functionally graded steels by artificial neural networks', *Computational Materials Science,* 50(7), pp. 2028-2037.

Neizel, B. W., Beukes, J. P., van Zyl, P. G. and Dawson, N. F. (2013) 'Why is CaCO3 not used as an additive in the pelletised chromite pre-reduction process?', *Minerals Engineering,* 45, pp. 115-120.

Niknejad, A. M. and Meyer, R. G. (2000) *Design, Simulation and Applications of Inductors and Transformers for Si RF ICs.* Springer.

Nikolić, V., Komljenović, M., Džunuzović, N. and Miladinović, Z. (2018) 'The influence of Pb addition on the properties of fly ash-based geopolymers', *Journal of Hazardous Materials,* 350, pp. 98-107.

Nilsson, N. J. (2010) *The quest for artificial intelligence: a history of ideas and achievements.* Cambridge: Cambridge University Press.

Nochaiya, T., Wongkeo, W. and Chaipanich, A. (2010) 'Utilization of fly ash with silica fume and properties of Portland cement–fly ash–silica fume concrete', *Fuel,* 89(3), pp. 768-774.

Noor ul, A., Nawab, L. and Ghani, U. (2017) 'Synthesis and characterization of chloride resistant cement from industrial waste through geopolymerization', *Journal of Cleaner Production,* 156, pp. 577-580.

Ogundiran, M. B. and Kumar, S. (2015) 'Synthesis and characterisation of geopolymer from Nigerian Clay', *Applied Clay Science,* 108, pp. 173-181.

Ojovan, M. I. and Lee, W. E. (2005) 'Chapter 17 - Immobilisation of Radioactive Wastes in Glass', in Ojovan, M.I. & Lee, W.E. (eds.) *An Introduction to Nuclear Waste Immobilisation*. Oxford: Elsevier, pp. 213-249.

Oka, Y. and Majima, H. (1970) 'A theory of size reduction involving fracture mechanics', *Canadian Metallurgical Quarterly,* 9(2), pp. 429-439.

Onori, R., Will, J., Hoppe, A., Polettini, A., Pomi, R. and Boccaccini, A. R. (2011) 'Bottom ash-based geopolymer materials: Mechanical and environmental properties', *Ceramic Engineering and Science Proceedings,* 32, pp. 71-82.

Pan, J. R., Huang, C., Kuo, J.-J. and Lin, S.-H. (2008) 'Recycling MSWI bottom and fly ash as raw materials for Portland cement', *Waste Management,* 28(7), pp. 1113-1118.

Park, Y. J. and Heo, J. (2002) 'Conversion to glass-ceramics from glasses made by MSW incinerator fly ash for recycling', *Ceramics International,* 28(6), pp. 689-694.

Parker, K. R. (1997) 'Why an electrostatic precipitator?', in Parker, K.R. (ed.) *Applied Electrostatic Precipitation*. Dordrecht: Springer Netherlands, pp. 1-10.

Patel, J., Patil, H., Patil, Y. and Vesmawala, G. (2018) 'Production and performance of alkali-activated cold-bonded lightweight aggregate in concrete', *Journal of Building Engineering*.

Patterson, J. and Gibson, A. (2017) *Deep learning: a practitioner's approach.* Sebastopol, CA: O'Reilly.

Pedamonti, D. (2018) 'Comparison of non-linear activation functions for deep neural networks on MNIST classification task', *arXiv preprint arXiv:1804.02763*.

Pejchal, V., Žagar, G., Charvet, R., Dénéréaz, C. and Mortensen, A. (2017) 'Compression testing spherical particles for strength: Theory of the meridian crack test and implementation for microscopic fused quartz', *Journal of the Mechanics and Physics of Solids,* 99, pp. 70-92.

Pels, J. R. and Sarabèr, A. J. (2011) 'Utilization of Biomass Ashes', in Grammelis, P. (ed.) *Solid Biofuels for Energy: A Lower Greenhouse Gas Alternative*. London: Springer London, pp. 219-235.

Periathamby, A. (2011) 'Chapter 8 - Municipal Waste Management', in Letcher, T.M. & Vallero, D.A. (eds.) *Waste*. Boston: Academic Press, pp. 109-125.

Phoo-Ngernkham, T., Maegawa, A., Mishima, N., Hatanaka, S. and Chindaprasirt, P. (2015) 'Effects of sodium hydroxide and sodium silicate solutions on compressive and

shear bond strengths of FA-GBFS geopolymer', *Construction and Building Materials,* 91, pp. 1-8.

Pietsch, W. (2008) *Agglomeration processes: phenomena, technologies, equipment.* Weinheim; Cambridge: Wiley-VCH.

Pimraksa, K., Chindaprasirt, P., Rungchet, A., Sagoe-Crentsil, K. and Sato, T. (2011) 'Lightweight geopolymer made of highly porous siliceous materials with various Na2O/Al2O3 and SiO2/Al2O3 ratios', *Materials Science and Engineering: A,* 528(21), pp. 6616-6623.

Plant, J. A., Ragnarsdottir, K. V. and Voulvoulis, N. (2012) *Pollutants, human health, and the environment: a risk based approach.* Oxford: Wiley-Blackwell.

Platt, C. (2014) *Make: More Electronics Learning Through Discovery.* Sebastopol, CA: O'Reilly.

Podgorsak, E. B. (2016) *Radiation physics for medical physicists. Graduate texts in physics* Switzerland: Springer,.

Poole, D. L. and Mackworth, A. K. (2010) *Artificial intelligence: foundations of computational agents.* New York: Cambridge University Press.

Provis, J. L., Lukey, G. C. and van Deventer, J. S. J. (2005) 'Do Geopolymers Actually Contain Nanocrystalline Zeolites? A Reexamination of Existing Results', *Chemistry of Materials,* 17(12), pp. 3075-3085.

Provis, J. L. and Van Deventer, J. S. J. (2009) '1 - Introduction to geopolymers', in Provis, J.L. & van Deventer, J.S.J. (eds.) *Geopolymers*: Woodhead Publishing, pp. 1-11.

Prytz, K. (2015) *Electrodynamics: The Field-Free Approach: Electrostatics, Magnetism, Induction, Relativity and Field Theory. Undergraduate Lecture Notes in Physics*: Springer International Publishing.

Purgar, A., Winter, F., Blasenbauer, D., Hartmann, S., Fellner, J., Lederer, J. and Rechberger, H. (2016) 'Main drivers for integrating zinc recovery from fly ashes into the Viennese waste incineration cluster', *Fuel Processing Technology,* 141, pp. 243-248.

Quina, M. J., Bordado, J. C. and Quinta-Ferreira, R. M. (2008) 'Treatment and use of air pollution control residues from MSW incineration: An overview', *Waste Management,* 28(11), pp. 2097-2121.

Quina, M. J., Bordado, J. M. and Quinta-Ferreira, R. M. (2014) 'Recycling of air pollution control residues from municipal solid waste incineration into lightweight aggregates', *Waste Management,* 34(2), pp. 430-438.

Ramezanianpour, A. A. (2013) *Cement replacement materials: properties, durability, sustainability. Springer-Verlag* Heidelberg: Springer.

Rand, T., Haukohl, J. and Marxen, U. (2000) *Municipal solid waste incineration: requirements for a successful project.* Washington, D.C.: World Bank.

Rapoport, E. and Pleshivtseva, Y. (2006) *Optimal Control of Induction Heating Processes. Mechanical Engineering*: CRC Press.

Raschka, S. (2015) *Python machine learning: unlock deeper insights into machine learning with this vital guide to cutting-edge predictive analytics.* Birmingham, UK: Packt Publishing Ltd.

Raschka, S., Julian, D. and Hearty, J. (2016) *Python: Deeper Insights into Machine Learning.* Packt Publishing.

Raschka, S. and Mirajalili, V. (2017) *Python machine learning: machine learning and deep learning with Python, scikit-learn, and TensorFlow.* 2nd edn. Birmingham, UK: Packt Publishing.

Rashidian-Dezfouli, H., Rangaraju, P. R. and Kothala, V. S. K. (2018) 'Influence of selected parameters on compressive strength of geopolymer produced from ground glass fiber', *Construction and Building Materials,* 162, pp. 393-405.

Reddy, P. J. (2016) *Energy recovery from municipal solid waste by thermal conversion technologies.* London, UK; Boca Raton: CRC Press.

Reimer, L. (1998) *Scanning electron microscopy: physics of image formation and microanalysis. Springer series in optical sciences* 2nd edn. Berlin; New York: Springer.

Rendek, E., Ducom, G. and Germain, P. (2006) 'Carbon dioxide sequestration in municipal solid waste incinerator (MSWI) bottom ash', *Journal of Hazardous Materials,* 128(1), pp. 73-79.

Riello, P., Canton, P., Comelato, N., Polizzi, S., Verità, M., Fagherazzi, G., Hofmeister, H. and Hopfe, S. (2001) 'Nucleation and crystallization behavior of glass-ceramic materials in the Li2O–Al2O3–SiO2 system of interest for their transparency properties', *Journal of Non-Crystalline Solids,* 288(1), pp. 127-139.

Roether, J. A., Daniel, D. J., Amutha Rani, D., Deegan, D. E., Cheeseman, C. R. and Boccaccini, A. R. (2010) 'Properties of sintered glass-ceramics prepared from plasma vitrified air pollution control residues', *Journal of Hazardous Materials,* 173(1), pp. 563-569.

Rogoff, M. J. and Screve, F. (2011) *Waste-to-energy: technologies and project implementation.* 2nd edn. Waltham, MA; Oxford: William Andrew.

Rojas, R. (1996) *Neural networks: a systematic introduction* Berlin; New York: Springer-Verlag.

Rosenblatt, F. (1958) 'The perceptron: a probabilistic model for information storage and organization in the brain', *Psychological review,* 65(6), pp. 386-408.

Rowat, S. C. (1999) 'Incinerator toxic emissions: a brief summary of human health effects with a note on regulatory control', *Medical Hypotheses,* 52(5), pp. 389-396.

Rożek, P., Król, M. and Mozgawa, W. (2018) 'Spectroscopic studies of fly ash-based geopolymers', *Spectrochimica Acta Part A: Molecular and Biomolecular Spectroscopy,* 198, pp. 283-289.

Rudnev, V., Loveless, D. and Cook, R. (2017) *Handbook of induction heating. Manufacturing engineering and materials processing* 2nd edn. Boca Raton, FL: CRC Press, Taylor & Francis Group.

Rumelhart, D. E., Hinton, G. E. and Williams, R. J. (1986) 'Learning representations by back-propagating errors', *Nature,* 323, pp. 533.

Runde, M., Magnusson, N., Fulbier, C. and Buhrer, C. (2011) 'Commercial Induction Heaters With High-Temperature Superconductor Coils', *IEEE Transactions on Applied Superconductivity,* 21, pp. 1379-1383.

Sabbas, T., Polettini, A., Pomi, R., Astrup, T., Hjelmar, O., Mostbauer, P., Cappai, G., Magel, G., Salhofer, S., Speiser, C., Heuss-Assbichler, S., Klein, R. and Lechner, P. (2003) 'Management of municipal solid waste incineration residues', *Waste Management,* 23(1), pp. 61-88.

Sakai, S.-i. and Hiraoka, M. (2000) 'Municipal solid waste incinerator residue recycling by thermal processes', *Waste Management,* 20(2), pp. 249-258.

Sammut, C. and Webb, G. I. (2010) *Encyclopedia of machine learning.* New York; London: Springer.

Santoleri, J. J., Theodore, L. and Reynolds, J. (2000) *Introduction to hazardous waste incineration.* 2nd edn. New York; Chichester: Wiley.

Sarıdemir, M. (2009) 'Prediction of compressive strength of concretes containing metakaolin and silica fume by artificial neural networks', *Advances in Engineering Software,* 40(5), pp. 350-355.

Sarkar, D., Bali, R. and Sharma, T. (2018) *Practical machine learning with Python: a problem-solver's guide to building real-world intelligent systems* New York, NY: Apress.

Sawyer, R. K. (2006) *The Cambridge handbook of the learning sciences.* Cambridge: Cambridge University Press.

Saxena, N. (2010) *Electrical Engineering.* University Science Press.

Sear, L. K. A. (2002) *Properties and use of coal fly ash, a valuable industrial by-product: coal fly ash, or pulverised fuel ash, from coal-fired power stations: the production, properties and applications of the material.* London: Thomas Telford.

Sen, S. and Mukerji, T. (1999) 'A generalized classical nucleation theory for rough interfaces: application in the analysis of homogeneous nucleation in silicate liquids', *Journal of Non-Crystalline Solids,* 246(3), pp. 229-239.

Serway, R. A. and Vuille, C. (2011) *College Physics.* Cengage Learning.

Shalev-Shwartz, S. and Ben-David, S. (2014) *Understanding machine learning: from theory to algorithms.* New York, USA: Cambridge University Press.

Shinohara, N., Katori, S., Okumiya, M., Hotta, T., Nakahira, K., Naito, M., Cho, Y.-I. and Uematsu, K. (2002) 'Effect of heat treatment of alumina granules on the compaction behavior and properties of green and sintered bodies', *Journal of the European Ceramic Society,* 22(16), pp. 2841-2848.

Siddique, R. and Khan, M. I. (2011) *Supplementary cementing materials.* Berlin; London: Springer.

Silva, I. N. D., Spatti, D. H., Andrade Flauzino, R., Liboni, L. H. B. and Reis Alves, S. F. d. (2016) *Artificial neural networks: a practical course.* Switzerland: Springer.

Silva, L. M., Ribeiro, R. A., Labrincha, J. A. and Ferreira, V. M. (2010) 'Role of lightweight fillers on the properties of a mixed-binder mortar', *Cement and Concrete Composites,* 32(1), pp. 19-24.

Silva, R. V., de Brito, J., Lynn, C. J. and Dhir, R. K. (2017) 'Use of municipal solid waste incineration bottom ashes in alkali-activated materials, ceramics and granular applications: A review', *Waste Management,* 68, pp. 207-220.

Singh, T. S. and Pant, K. K. (2006) 'Solidification/stabilization of arsenic containing solid wastes using portland cement, fly ash and polymeric materials', *Journal of Hazardous Materials,* 131(1), pp. 29-36.

Singh, Y. (2011) *Electro Magnetic Field Theory.* Dorling Kindersley India.

Skansi, S. (2018) *Introduction to Deep Learning From Logical Calculus to Artificial Intelligence. Undergraduate Topics in Computer Science,* Cham: Springer International Publishing.

Skoog, D. A., Holler, F. J. and Crouch, S. R. (2007) *Principles of instrumental analysis.* 6th edn. Belmont, CA: Thomson Brooks.

Somani, A. K. and P. Rostykus (1991) 'Hypercube-based Compact Neural Networks and Their Comparison with other Artificial Neural Networks', in Omidvar, O. (ed.) *Progress in Neural Networks*. Norwood, New Jersey: Ablex Publishing Company.

Somna, K., Jaturapitakkul, C., Kajitvichyanukul, P. and Chindaprasirt, P. (2011) 'NaOH-activated ground fly ash geopolymer cured at ambient temperature', *Fuel,* 90(6), pp. 2118-2124.

Sousa, S. I. V., Martins, F. G., Alvim-Ferraz, M. C. M. and Pereira, M. C. (2007) 'Multiple linear regression and artificial neural networks based on principal components to predict ozone concentrations', *Environmental Modelling & Software,* 22(1), pp. 97-103.

Spiess, A.-N. and Neumeyer, N. (2010) 'An evaluation of R2 as an inadequate measure for nonlinear models in pharmacological and biochemical research: a Monte Carlo approach', *BMC pharmacology,* 10, pp. 6-6.

SUEZ Recycling and Recovery Isle of Man (2018) *SUEZ Isle of Man: Annual Public Report 2017*. Available at: http://www.suez.co.im/downloads/SUEZIOM-AnnualPublicReport-2017-web.pdf (Accessed: 09/03/2018).

Sugilal, G. (2008) 'Experimental analysis of the performance of cold crucible induction glass melter', *Applied Thermal Engineering,* 28(14), pp. 1952-1961.

Sugilal, G., Jha, J., Shashikumar, H. Rao, M., Banerjee, K. and K. Dey, G. (2016) 'Indigenous development of induction skull melting technology for electromagnetic processing of refractory and reactive metals and alloys', *Materials Today: Proceedings,* 3(9, Part B), pp. 2942-2950.

Suksiripattanapong, C., Horpibulsuk, S., Boongrasan, S., Udomchai, A., Chinkulkijniwat, A. and Arulrajah, A. (2015a) 'Unit weight, strength and microstructure of a water treatment sludge-fly ash lightweight cellular geopolymer', *Construction and Building Materials,* 94, pp. 807-816.

Suksiripattanapong, C., Horpibulsuk, S., Chanprasert, P., Sukmak, P. and Arulrajah, A. (2015b) 'Compressive strength development in fly ash geopolymer masonry units manufactured from water treatment sludge', *Construction and Building Materials,* 82, pp. 20-30.

Sun, X., Li, J., Zhao, X., Zhu, B. and Zhang, G. (2016) 'A Review on the Management of Municipal Solid Waste Fly Ash in American', *Procedia Environmental Sciences,* 31, pp. 535-540.

Suryanarayana, C. and Norton, M. G. (1998) *X-Ray Diffraction: A Practical Approach.* Boston, MA: Springer US.

Sutton, R. S. and Barto, A. G. (1998) *Reinforcement learning: an introduction.* Cambridge, Mass.; London: MIT Press.

Tajra, F., Elrahman, M. A., Chung, S.-Y. and Stephan, D. (2018) 'Performance assessment of core-shell structured lightweight aggregate produced by cold bonding pelletization process', *Construction and Building Materials,* 179, pp. 220-231.

Tanaka, S., Pin, C. C. and Uematsu, K. (2006) 'Effect of Organic Binder Segregation on Sintered Strength of Dry-Pressed Alumina', *Journal of the American Ceramic Society,* 89(6), pp. 1903-1907.

Tang, J. and Steenari, B.-M. (2016) 'Leaching optimization of municipal solid waste incineration ash for resource recovery: A case study of Cu, Zn, Pb and Cd', *Waste Management,* 48, pp. 315-322.

Tang, P. and Brouwers, H. J. H. (2017) 'Integral recycling of municipal solid waste incineration (MSWI) bottom ash fines (0–2mm) and industrial powder wastes by cold-bonding pelletization', *Waste Management,* 62, pp. 125-138.

Tang, P. and Brouwers, H. J. H. (2018) 'The durability and environmental properties of self-compacting concrete incorporating cold bonded lightweight aggregates produced from combined industrial solid wastes', *Construction and Building Materials,* 167, pp. 271-285.

Tang, P., Florea, M. V. A. and Brouwers, H. J. H. (2017) 'Employing cold bonded pelletization to produce lightweight aggregates from incineration fine bottom ash', *Journal of Cleaner Production,* 165, pp. 1371-1384.

Thermo Fisher Scientific (2016) *Dionex Aquion Ion Chromatography System Operator's Manual.* Thermo Fisher Scientific

Thomson, V. E. (2009) *Garbage In, Garbage Out: Solving the Problems with Long-Distance Trash Transport.* University of Virginia Press.

Tian, S., Zhu, Y., Meng, B., Guan, J., Nie, Z., Die, Q., Xu, W., Yu, M. and Huang, Q. (2018) 'Chemical speciation of lead in secondary fly ash using X-ray absorption spectroscopy', *Chemosphere,* 197, pp. 362-366.

Tippayasam, C., Boonsalee, S., Sajjavanich, S., Ponzoni, C., Kamseu, E. and Chaysuwan, D. (2011) 'Geopolymer Development by Powders of Metakaolin and Wastes in Thailand', *Advances in Science and Technology,* 69, pp. 63-68.

Tome, S., Etoh, M.-A., Etame, J. and Sanjay, K. (2018) 'Characterization and Leachability Behaviour of Geopolymer Cement Synthesised from Municipal Solid Waste Incinerator Fly Ash and Volcanic Ash Blends', *Recycling,* 3(4).

Toniolo, N. and Boccaccini, A. R. (2017) 'Fly ash-based geopolymers containing added silicate waste. A review', *Ceramics International,* 43(17), pp. 14545-14551.

Toniolo, N., Rincón, A., Avadhut, Y. S., Hartmann, M., Bernardo, E. and Boccaccini, A. R. (2018) 'Novel geopolymers incorporating red mud and waste glass cullet', *Materials Letters,* 219, pp. 152-154.

Totten, G. E. (2006) *Steel Heat Treatment: Equipment and Process Design. Steel Heat Treatment Handbook* 2nd edn.: CRC Press.

Tsai, W.-T., Chang, J.-H., Hsien, K.-J. and Chang, Y.-M. (2009) 'Production of pyrolytic liquids from industrial sewage sludges in an induction-heating reactor', *Bioresource Technology,* 100, pp. 406-412.

Tzanakos, K., Mimilidou, A., Anastasiadou, K., Stratakis, A. and Gidarakos, E. (2014) 'Solidification/stabilization of ash from medical waste incineration into geopolymers', *Waste Management,* 34(10), pp. 1823-1828.

Ul-Hamid, A. (2018) *A Beginners' Guide to Scanning Electron Microscopy* Cham, Switzerland: Springer.

Vafaei, M. and Allahverdi, A. (2017) 'High strength geopolymer binder based on waste-glass powder', *Advanced Powder Technology,* 28(1), pp. 215-222.

Van Damme, H. (2018) 'Concrete material science: Past, present, and future innovations', *Cement and Concrete Research,* 112, pp. 5-24.

Van der Heide, P. (2012) *X-ray photoelectron spectroscopy an introduction to principles and practices* Hoboken, N.J.: Wiley.

van der Wegen, G. J. L. and Bijen, J. M. J. M. (1985) 'Properties of concrete made with three types of artificial PFA coarse aggregates', *International Journal of Cement Composites and Lightweight Concrete,* 7(3), pp. 159-167.

Van Jaarsveld, J. G. S., Van Deventer, J. S. J. and Lorenzen, L. (1997) 'The potential use of geopolymeric materials to immobilise toxic metals: Part I. Theory and applications', *Minerals Engineering,* 10(7), pp. 659-669.

Verma, C. L., Handa, S. K., Jain, S. K. and Yadav, R. K. (1998) 'Techno-commercial perspective study for sintered fly ash light-weight aggregates in India', *Construction and Building Materials,* 12(6), pp. 341-346.

Vernaz, É. and Bruezière, J. (2014) 'History of Nuclear Waste Glass in France', *Procedia Materials Science,* 7, pp. 3-9.

Videla, C. and Martinez, P. M. (2002) 'FLY ASH LIGHTWEIGHT AGGREGATES PRODUCED BY COLD BONDING FOR SUSTAINABLE CONCRETE CONSTRUCTION', *Challenges of Concrete Construction: Volume 5, Sustainable Concrete Construction*: Thomas Telford Publishing, pp. 363-372.

Vutchkov, M., Lalor, G. and Macko, S. (2013) 'Inorganic and Organic Geochemistry Techniques', in Selinus, O. (ed.) *Essentials of Medical Geology: Revised Edition*. Dordrecht: Springer Netherlands, pp. 689-716.

Wächter, M. R. and Ionel, I. 'Integration of the solid waste incineration residues into dense slurry technology'. *2013 4th International Youth Conference on Energy (IYCE)*, 6-8 June 2013, 1-6.

Wagh, A. S. 2005. Chemically bonded phosphate ceramics - A novel class of geopolymers. *In:* Singh, J.P., Bansal, N.P. & Kriven, W.M. (eds.) *106th Annual Meeting of the American Ceramic Society.* Indianapolis, IN.

Wan, Q., Rao, F., Song, S., García, R. E., Estrella, R. M., Patiño, C. L. and Zhang, Y. (2017) 'Geopolymerization reaction, microstructure and simulation of metakaolin-based geopolymers at extended Si/Al ratios', *Cement and Concrete Composites,* 79, pp. 45-52.

Wan, X., Wang, W., Ye, T., Guo, Y. and Gao, X. (2006) 'A study on the chemical and mineralogical characterization of MSWI fly ash using a sequential extraction procedure', *Journal of Hazardous Materials,* 134(1), pp. 197-201.

Wang, J. and Cheng, T. 'Production geopolymer materials by coal fly ash'. *Proceedings of the 7th International Symposium on East Asian Resources Recycling Technology*, 2003, 266.

Wang, L., Chen, Q., Jamro, I. A., Li, R. D. and Baloch, H. A. (2016) 'Accelerated co-precipitation of lead, zinc and copper by carbon dioxide bubbling in alkaline municipal solid waste incinerator (MSWI) fly ash wash water', *RSC Advances,* 6(24), pp. 20173-20186.

Wang, L. K., Taricska, J. R., Hung, Y.-T., Eldridge, J. E. and Li, K. H. (2004) 'Wet and Dry Scrubbing', in Wang, L.K., Pereira, N.C. & Hung, Y.-T. (eds.) *Air Pollution Control Engineering*. Totowa, NJ: Humana Press, pp. 197-305.

Wang, W. (2006) *Stochasticity, nonlinearity and forecasting of streamflow processes.* Amsterdam; Fairfax, VA: IOS Press.

Wang, X., Jin, B., Xu, B., Lan, W. and Qu, C. (2017) 'Melting characteristics during the vitrification of MSW incinerator fly ash by swirling melting treatment', *Journal of Material Cycles and Waste Management,* 19(1), pp. 483-495.

Waseda, Y., Matsubara, E. and Shinoda, K. (2011) *X-Ray Diffraction Crystallography: Introduction, Examples and Solved Problems.* Berlin, Heidelberg: Springer Berlin Heidelberg.

Wesche, K. (2004) *Fly Ash in Concrete: Properties and performance.* London: Taylor & Francis.

Wheeler, H. A. (1928) 'Simple Inductance Formulas for Radio Coils', *Proceedings of the Institute of Radio Engineers,* 16, pp. 1398-1400.

Williams, P. T. (1994) 'Pollutants from Incineration: An Overview', in Hester, R.E. & Harrison, R.M. (eds.) *Waste Incineration and the Environment*: The Royal Society of Chemistry, pp. 27-52.

Williams, P. T. (2005) *Waste treatment and disposal.* 2nd edn. Chichester: Wiley.

Witten, I. H. a., Frank, E. a. and Hall, M. A. a. (2011) *Data mining: practical machine learning tools and techniques.* 3rd edn. Burlington, MA: Morgan Kaufmann.

Wong, Y. L., Lam, L., Poon, C. S. and Zhou, F. P. (1999) 'Properties of fly ash-modified cement mortar-aggregate interfaces', *Cement and Concrete Research,* 29(12), pp. 1905-1913.

Worrell, W. A., Vesilind, P. A. and Gupta, T. (2012) *Solid waste engineering.* 2nd edn. Stamford, Conn.: Cengage Learning.

Xu, N., Li, S., Li, Y., Xue, Z., Yuan, L., Zhang, J. and Wang, L. (2015) 'Preparation and properties of porous ceramic aggregates using electrical insulators waste', *Ceramics International,* 41(4), pp. 5807-5811.

Yang, J., Xiao, B. and Boccaccini, A. R. (2009) 'Preparation of low melting temperature glass–ceramics from municipal waste incineration fly ash', *Fuel,* 88(7), pp. 1275-1280.

Yang, Y. B., Goh, Y. R., Zakaria, R., Nasserzadeh, V. and Swithenbank, J. (2002) 'Mathematical modelling of MSW incineration on a travelling bed', *Waste Management,* 22(4), pp. 369-380.

Yang, Z., Ji, R., Liu, L., Wang, X. and Zhang, Z. (2018a) 'Recycling of municipal solid waste incineration by-product for cement composites preparation', *Construction and Building Materials,* 162, pp. 794-801.

Yang, Z., Tian, S., Ji, R., Liu, L., Wang, X. and Zhang, Z. (2017) 'Effect of water-washing on the co-removal of chlorine and heavy metals in air pollution control residue from MSW incineration', *Waste Management,* 68, pp. 221-231.

Yang, Z., Tian, S., Liu, L., Wang, X. and Zhang, Z. (2018b) 'Application of washed MSWI fly ash in cement composites: long-term environmental impacts', *Environmental Science and Pollution Research*.

Yashima, S., Kanda, Y. and Sano, S. (1987) 'Relationships between particle size and fracture energy or impact velocity required to fracture as estimated from single particle crushing', *Powder Technology,* 51(3), pp. 277-282.

Ye, N., Chen, Y., Yang, J., Liang, S., Hu, Y., Xiao, B., Huang, Q., Shi, Y., Hu, J. and Wu, X. (2016) 'Co-disposal of MSWI fly ash and Bayer red mud using an one-part geopolymeric system', *Journal of Hazardous Materials,* 318, pp. 70-78.

Yliniemi, Paiva, Ferreira, Tiainen and Illikainen (2017) 'Development and incorporation of lightweight waste-based geopolymer aggregates in mortar and concrete', *Construction and Building Materials,* 131, pp. 784-792.

Yoon, I.-H., Moon, D. H., Kim, K.-W., Lee, K.-Y., Lee, J.-H. and Kim, M. G. (2010) 'Mechanism for the stabilization/solidification of arsenic-contaminated soils with Portland cement and cement kiln dust', *Journal of Environmental Management,* 91(11), pp. 2322-2328.

Yoon, S., Monteiro, P. J. M., Macphee, D. E., Glasser, F. P. and Imbabi, M. S.-E. (2014) 'Statistical evaluation of the mechanical properties of high-volume class F fly ash concretes', *Construction and Building Materials,* 54, pp. 432-442.

You, K.-s. and Ahn, J.-W. (2012) 'Performance of sintering process to synthesize cementitious materials and to stabilize heavy metals from MSWI fly ash and water sludge', *Geosystem Engineering,* 15(4), pp. 261-268.

Zacco, A., Borgese, L., Gianoncelli, A., Struis, R. P. W. J., Depero, L. E. and Bontempi, E. (2014) 'Review of fly ash inertisation treatments and recycling', *Environmental Chemistry Letters,* 12(1), pp. 153-175.

Zafar, I., Tzanidou, G., Burton, R., Patel, N. and Araujo, L. (2018) *Hands-On Convolutional Neural Networks with TensorFlow: Solve computer vision problems with modeling in TensorFlow and Python.* Packt Publishing.

Žagar, G., Pejchal, V., Kissling, M. and Mortensen, A. (2018) 'On the diametric compression strength test of brittle spherical particles', *European Journal of Mechanics - A/Solids,* 72, pp. 148-154.

Zhang, R. and Hu, Y. 2012. Feasibility of reutilizing municipal solid waste incineration residues as construction materials. *Applied Mechanics and Materials.*

Zheng, L., Wang, C., Wang, W., Shi, Y. and Gao, X. (2011) 'Immobilization of MSWI fly ash through geopolymerization: Effects of water-wash', *Waste Management,* 31(2), pp. 311-317.

Zhu, W., Jiang, H., Zhang, H., Jia, S. and Liu, Y. (2018) 'Effect of TiO2 and CaF2 on the crystallization behavior of Y2O3-Al2O3-SiO2 glass ceramics', *Ceramics International,* 44(6), pp. 6653-6658.

Appendices

Appendix A

The CD supplied with this thesis contains the folders shown in the table below.

Folder name	Description
ANN Model for APC residues geopolymer	This folder contains all ANN models developed and tested in chapter 6
APC residues classification model	This folder contains the final ANN model tested in chapter 7.
Multivariate nonlinear regression model	This folder contains all Multivariate nonlinear regression models tested in chapter 6
Unwashed APCr graph	This folder contains the code that was used to draw graphs for unwashed APC residues based geopolymer material
Washed APCr graph	This folder contains the code that was used to draw graphs for washed APC residues based geopolymer material
Circuit for induction heating system	This folder contains NI multisim file for induction heating system
Pan Pelletiser automation code	This folder contains Arduino microcontroller code used for the automation of pan pelletiser

Appendix B

Sample number for multivariate regression model for unwashed APC residues

Sample Number	S:L	SS:SH	ln(days)	$(S:L)^2$	$(SS:SH)^2$	Compressive strength (kPa)
1	0.50	4.00	1.95	0.25	16.00	188.34
2	0.50	3.00	1.95	0.25	9.00	224.42
3	0.50	2.00	1.95	0.25	4.00	238.90
4	0.50	1.50	1.95	0.25	2.25	221.67
5	0.50	1.00	1.95	0.25	1.00	170.08
6	0.50	0.50	1.95	0.25	0.25	79.10
7	0.33	4.00	1.95	0.11	16.00	133.40
8	0.33	3.00	1.95	0.11	9.00	196.23
9	0.33	2.00	1.95	0.11	4.00	217.89
10	0.33	1.50	1.95	0.11	2.25	148.54
11	0.33	1.00	1.95	0.11	1.00	61.99
12	0.33	0.50	1.95	0.11	0.25	48.27
13	0.50	4.00	2.64	0.25	16.00	640.20
14	0.50	3.00	2.64	0.25	9.00	721.05
15	0.50	2.00	2.64	0.25	4.00	848.49
16	0.50	1.50	2.64	0.25	2.25	684.33
17	0.50	1.00	2.64	0.25	1.00	456.44
18	0.50	0.50	2.64	0.25	0.25	194.71
19	0.33	4.00	2.64	0.11	16.00	299.30
20	0.33	3.00	2.64	0.11	9.00	442.90
21	0.33	2.00	2.64	0.11	4.00	456.20
22	0.33	1.50	2.64	0.11	2.25	276.48
23	0.33	1.00	2.64	0.11	1.00	177.49
24	0.33	0.50	2.64	0.11	0.25	112.76
25	0.50	4.00	3.33	0.25	16.00	745.08
26	0.50	3.00	3.33	0.25	9.00	874.53
27	0.50	2.00	3.33	0.25	4.00	984.33
28	0.50	1.50	3.33	0.25	2.25	806.73
29	0.50	1.00	3.33	0.25	1.00	632.99
30	0.50	0.50	3.33	0.25	0.25	292.69
31	0.33	4.00	3.33	0.11	16.00	490.46
32	0.33	3.00	3.33	0.11	9.00	510.44
33	0.33	2.00	3.33	0.11	4.00	571.49
34	0.33	1.50	3.33	0.11	2.25	366.48
35	0.33	1.00	3.33	0.11	1.00	272.75
36	0.33	0.50	3.33	0.11	0.25	162.41

Appendix C

Sample number for multivariate regression model for washed APC residues

Sample Number	S:L	SS:SH	ln(days)	$(S:L)^2$	$(SS:SH)^2$	Compressive strength (kPa)
1	0.33	4.00	3.33	0.11	16.00	187.63
2	0.33	4.00	2.64	0.11	16.00	110.75
3	0.33	4.00	1.95	0.11	16.00	68.03
4	0.33	3.00	3.33	0.11	9.00	201.57
5	0.33	3.00	2.64	0.11	9.00	123.43
6	0.33	3.00	1.95	0.11	9.00	76.60
7	0.33	2.00	1.95	0.11	4.00	108.02
8	0.33	2.00	2.64	0.11	4.00	522.26
9	0.33	2.00	3.33	0.11	4.00	1089.83
10	0.33	1.50	3.33	0.11	2.25	1186.26
11	0.33	1.50	2.64	0.11	2.25	605.73
12	0.33	1.50	1.95	0.11	2.25	154.63
13	0.33	1.00	1.95	0.11	1.00	35.64
14	0.33	1.00	2.64	0.11	1.00	204.65
15	0.33	1.00	3.33	0.11	1.00	286.43
16	0.33	0.50	1.95	0.11	0.25	33.57
17	0.33	0.50	2.64	0.11	0.25	192.44
18	0.33	0.50	3.33	0.11	0.25	252.78
19	0.50	2.00	1.95	0.25	4.00	427.07
20	0.50	1.00	1.95	0.25	1.00	104.10
21	0.50	0.50	1.95	0.25	0.25	49.87
22	0.50	2.00	2.64	0.25	4.00	1294.48
23	0.50	1.00	2.64	0.25	1.00	303.29
24	0.50	0.50	2.64	0.25	0.25	131.46
25	0.50	2.00	3.33	0.25	4.00	2185.56
26	0.50	1.00	3.33	0.25	1.00	840.25
27	0.50	0.50	3.33	0.25	0.25	261.82
28	0.50	4.00	3.33	0.25	16.00	1422.34
29	0.50	4.00	2.64	0.25	16.00	991.13
30	0.50	4.00	1.95	0.25	16.00	174.28
31	0.50	3.00	3.33	0.25	9.00	1717.17
32	0.50	3.00	2.64	0.25	9.00	986.43
33	0.50	3.00	1.95	0.25	9.00	168.77
34	0.50	1.50	3.33	0.25	2.25	2348.53
35	0.50	1.50	2.64	0.25	2.25	1518.52
36	0.50	1.50	1.95	0.25	2.25	1030.14

Appendix D

Training dataset used for all ANN models in chapter 6

Ash type	Days	S to L	SS to SH	Compressive strength
1	7	0.50	4.00	188.34
1	7	0.50	3.00	224.42
1	7	0.50	2.00	238.90
1	7	0.50	1.50	221.67
1	7	0.50	1.00	170.08
1	7	0.50	0.50	79.10
1	7	0.33	4.00	133.40
1	7	0.33	3.00	196.23
1	7	0.33	2.00	217.89
1	7	0.33	1.50	148.54
1	7	0.33	1.00	61.99
1	7	0.33	0.50	48.27
1	14	0.50	4.00	640.20
1	14	0.50	3.00	721.05
1	14	0.50	2.00	848.49
1	14	0.50	1.50	684.33
1	14	0.50	1.00	456.44
1	14	0.50	0.50	194.71
1	14	0.33	4.00	299.30
1	14	0.33	3.00	442.90
1	14	0.33	2.00	456.20
1	14	0.33	1.50	276.48
1	14	0.33	1.00	177.49
1	14	0.33	0.50	112.76
1	28	0.50	4.00	745.08
1	28	0.50	3.00	874.53
1	28	0.50	2.00	984.33
1	28	0.50	1.50	806.73
1	28	0.50	1.00	632.99
1	28	0.50	0.50	292.69
1	28	0.33	4.00	490.46
1	28	0.33	3.00	510.44
1	28	0.33	2.00	571.49
1	28	0.33	1.50	366.48
1	28	0.33	1.00	272.75
1	28	0.33	0.50	162.41
2	28	0.33	4.00	187.63
2	14	0.33	4.00	110.75

2	7	0.33	4.00	68.03
2	28	0.33	3.00	201.57
2	14	0.33	3.00	123.43
2	7	0.33	3.00	76.60
2	7	0.33	2.00	108.02
2	14	0.33	2.00	522.26
2	28	0.33	2.00	1089.83
2	28	0.33	1.50	1186.26
2	14	0.33	1.50	605.73
2	7	0.33	1.50	154.63
2	7	0.33	1.00	35.64
2	14	0.33	1.00	204.65
2	28	0.33	1.00	286.43
2	7	0.33	0.50	33.57
2	14	0.33	0.50	192.44
2	28	0.33	0.50	252.78
2	7	0.50	2.00	427.07
2	7	0.50	1.00	104.10
2	7	0.50	0.50	49.87
2	14	0.50	2.00	1294.48
2	14	0.50	1.00	303.29
2	14	0.50	0.50	131.46
2	28	0.50	2.00	2185.56
2	28	0.50	1.00	840.25
2	28	0.50	0.50	261.82
2	28	0.50	4.00	1422.34
2	14	0.50	4.00	991.13
2	7	0.50	4.00	174.28
2	28	0.50	3.00	1717.17
2	14	0.50	3.00	986.43
2	7	0.50	3.00	168.77
2	28	0.50	1.50	2348.53
2	14	0.50	1.50	1518.52
2	7	0.50	1.50	1030.14

Appendix E

Evaluation dataset used for all ANN models in chapter 6

Ash type	Days	S to L	SS to SH	Compressive strength
2	28	0.4	4	253.57
2	14	0.4	4	134.62
2	7	0.4	4	104.56
2	28	0.4	3	277.40
2	14	0.4	3	156.02
2	7	0.4	3	124.60
2	7	0.4	2	290.83
2	14	0.4	2	766.79
2	28	0.4	2	1152.21
2	28	0.4	1.5	1335.42
2	14	0.4	1.5	875.35
2	7	0.4	1.5	361.71
2	7	0.4	1	259.05
2	14	0.4	1	661.21
2	28	0.4	1	931.60
2	7	0.4	0.5	0.00
2	14	0.4	0.5	0.00
2	28	0.4	0.5	0.00
2	28	0.6	4	420.30
2	14	0.6	4	312.24
2	7	0.6	4	161.88
2	28	0.6	3	523.65
2	14	0.6	3	434.55
2	7	0.6	3	170.54
2	28	0.6	2	1429.56
2	14	0.6	2	837.73
2	7	0.6	2	536.45
2	28	0.6	1.5	2276.66
2	14	0.6	1.5	2201.32
2	7	0.6	1.5	2120.59

Appendix F

Prediction dataset used for all ANN models in chapter 6

Ash type	Days	S to L	SS to SH
1	28	0.33	4
1	28	0.40	4
1	28	0.50	4
1	28	0.60	4
1	28	0.70	4
1	28	0.33	3
1	28	0.40	3
1	28	0.50	3
1	28	0.60	3
1	28	0.70	3
1	28	0.33	2
1	28	0.40	2
1	28	0.50	2
1	28	0.60	2
1	28	0.70	2
1	28	0.33	1.5
1	28	0.40	1.5
1	28	0.50	1.5
1	28	0.60	1.5
1	28	0.70	1.5
1	28	0.33	1
1	28	0.40	1
1	28	0.50	1
1	28	0.60	1
1	28	0.70	1
1	28	0.33	0.5
1	28	0.40	0.5
1	28	0.50	0.5
1	28	0.60	0.5
1	28	0.70	0.5
2	28	0.33	4
2	28	0.40	4
2	28	0.50	4
2	28	0.60	4
2	28	0.70	4
2	28	0.33	3
2	28	0.40	3
2	28	0.50	3

2	28	0.60	3
2	28	0.70	3
2	28	0.33	2
2	28	0.40	2
2	28	0.50	2
2	28	0.60	2
2	28	0.70	2
2	28	0.33	1.5
2	28	0.40	1.5
2	28	0.50	1.5
2	28	0.60	1.5
2	28	0.70	1.5
2	28	0.33	1
2	28	0.40	1
2	28	0.50	1
2	28	0.60	1
2	28	0.70	1
2	28	0.33	0.5
2	28	0.40	0.5
2	28	0.50	0.5
2	28	0.60	0.5
2	28	0.70	0.5
1	14	0.33	4
1	14	0.40	4
1	14	0.50	4
1	14	0.60	4
1	14	0.70	4
1	14	0.33	3
1	14	0.40	3
1	14	0.50	3
1	14	0.60	3
1	14	0.70	3
1	14	0.33	2
1	14	0.40	2
1	14	0.50	2
1	14	0.60	2
1	14	0.70	2
1	14	0.33	1.5
1	14	0.40	1.5
1	14	0.50	1.5
1	14	0.60	1.5
1	14	0.70	1.5
1	14	0.33	1
1	14	0.40	1

1	14	0.50	1
1	14	0.60	1
1	14	0.70	1
1	14	0.33	0.5
1	14	0.40	0.5
1	14	0.50	0.5
1	14	0.60	0.5
1	14	0.70	0.5
2	14	0.33	4
2	14	0.40	4
2	14	0.50	4
2	14	0.60	4
2	14	0.70	4
2	14	0.33	3
2	14	0.40	3
2	14	0.50	3
2	14	0.60	3
2	14	0.70	3
2	14	0.33	2
2	14	0.40	2
2	14	0.50	2
2	14	0.60	2
2	14	0.70	2
2	14	0.33	1.5
2	14	0.40	1.5
2	14	0.50	1.5
2	14	0.60	1.5
2	14	0.70	1.5
2	14	0.33	1
2	14	0.40	1
2	14	0.50	1
2	14	0.60	1
2	14	0.70	1
2	14	0.33	0.5
2	14	0.40	0.5
2	14	0.50	0.5
2	14	0.60	0.5
2	14	0.70	0.5
1	7	0.33	4
1	7	0.40	4
1	7	0.50	4
1	7	0.60	4
1	7	0.70	4
1	7	0.33	3

1	7	0.40	3
1	7	0.50	3
1	7	0.60	3
1	7	0.70	3
1	7	0.33	2
1	7	0.40	2
1	7	0.50	2
1	7	0.60	2
1	7	0.70	2
1	7	0.33	1.5
1	7	0.40	1.5
1	7	0.50	1.5
1	7	0.60	1.5
1	7	0.70	1.5
1	7	0.33	1
1	7	0.40	1
1	7	0.50	1
1	7	0.60	1
1	7	0.70	1
1	7	0.33	0.5
1	7	0.40	0.5
1	7	0.50	0.5
1	7	0.60	0.5
1	7	0.70	0.5
2	7	0.33	4
2	7	0.40	4
2	7	0.50	4
2	7	0.60	4
2	7	0.70	4
2	7	0.33	3
2	7	0.40	3
2	7	0.50	3
2	7	0.60	3
2	7	0.70	3
2	7	0.33	2
2	7	0.40	2
2	7	0.50	2
2	7	0.60	2
2	7	0.70	2
2	7	0.33	1.5
2	7	0.40	1.5
2	7	0.50	1.5
2	7	0.60	1.5
2	7	0.70	1.5

2	7	0.33	1
2	7	0.40	1
2	7	0.50	1
2	7	0.60	1
2	7	0.70	1
2	7	0.33	0.5
2	7	0.40	0.5
2	7	0.50	0.5
2	7	0.60	0.5
2	7	0.70	0.5

Appendix G

Training dataset used in chapter 7

X^1 *is* Al_2O_3 *composition in percentage*

X^2 *is* CaO *composition in percentage*

X^3*is* K_2O *composition in percentage*

X^4 *is* MgO *composition in percentage*

X^5 *is* Na_2O *composition in percentage*

X^6 *is* SiO_2 *composition in percentage*

X^7*is* $(100 - (X^1 + X^2 + X^3 + X^4 + X^5))$

X^1	X^2	X^3	X^4	X^5	X^6	X^7	Ash type
27.04	3.32	1.29	1.23	1.15	52.31	18.66	1
34.94	1.65	3.02	1.26	0.91	50.58	7.64	1
36.4	1.4	2	1.2	1	50.7	7.3	1
21.5	3.94	1.67	1.84	0.68	63.9	6.47	1
7.2	28.8	4.3	2.2	6.5	15.4	35.6	2
1.4	47.8	0	1.9	0	3.5	45.4	2
1.2	41.8	4.2	1.7	7.3	3.1	40.7	2
0.92	45.42	3.85	3.16	4.16	13.6	28.89	2
4.7	31.5	0	0	0	16.4	47.4	2
5.88	26.28	2.24	1.87	6.42	8.7	48.61	2
1.11	7.46	1.16	0.43	22.08	2.63	65.13	2
4.02	48.35	4.33	1.73	4.28	6.64	30.65	2
1.26	50.39	1.78	2.26	12.66	13.44	18.21	3
8.7	14.3	1.1	1.9	11.7	53.8	8.5	3
5.8	16.9	1.11	2.22	7.58	44.3	22.09	3
12.037	43.115	0.848	2.116	2.359	19.122	20.403	3
12.96	5.79	2.83	2.94	2.83	49.32	23.33	4
13.14	30.24	1.63	0	0.41	47.51	7.07	4

Appendix H

This section contains 8 matrices.

Weight matrix layer 1 for model 4-35-35-35-1

matrix 4 x 35	**n1**	**n2**	**n3**	**n4**	**n5**	**n6**	**n7**	**n8**
m1	-0.22514	0.389496	0.772536	-0.1236	0.309	0.492	0.175072	0.296064
m2	0.014392	0.013025	0.60698	-0.15037	-0.10419	0.224029	-0.31331	-0.22743
m3	2.036866	1.103322	0.315744	0.382393	-0.24482	0.542365	-0.14342	0.028639
m4	1.94741	1.677673	0.467027	-0.2258	0.044327	-0.11875	-0.07578	0.231877
matrix 4 x 35	**n9**	**n10**	**n11**	**n12**	**n13**	**n14**	**n15**	**n16**
m1	0.198447	0.454508	1.166521	-0.11915	0.351191	-0.00516	0.174746	0.41168
m2	-0.15481	0.320641	0.029801	0.28671	0.1077	-0.3087	0.156725	0.08413
m3	-0.21098	0.324163	0.473786	2.025473	0.130847	0.141058	0.563831	1.30714
m4	-0.31936	1.726161	-0.63803	-0.91139	0.03047	0.263415	0.1619	0.615547
matrix 4 x 35	**n17**	**n18**	**n19**	**n20**	**n21**	**n22**	**n23**	**n24**
m1	0.22816	-0.00268	-0.24268	0.709298	0.361624	-0.20288	-1.02437	0.046209
m2	-0.15829	0.351684	-0.36808	0.577197	0.230139	0.296701	-0.25846	-0.05171
m3	-0.24226	1.763622	-0.106	0.931146	1.056138	1.046985	-0.99653	0.368799
m4	-0.05829	-1.61471	-0.09513	0.075028	-0.25908	0.454857	1.840134	-0.24947
matrix 4 x 35	**n25**	**n26**	**n27**	**n28**	**n29**	**n30**	**n31**	**n32**
m1	-0.11134	0.150845	0.747776	0.635857	1.608394	1.057937	-0.17505	0.887034
m2	-0.02411	-0.23789	0.474853	0.44778	-0.39686	-0.0388	-0.24	0.310564
m3	-0.37246	-0.26845	0.22712	-0.41668	-2.3544	2.738486	0.110681	0.082806
m4	-0.05353	-0.02277	0.329369	0.655466	1.309471	-0.28551	-0.39212	0.005825
matrix 4 x 35	**n33**	**n34**	**n35**					
m1	0.145072	0.556165	0.619023					
m2	-0.37721	0.006134	0.063096					
m3	-0.36777	2.637909	1.374757					
m4	0.274845	0.153642	-0.05054					

Weight matrix layer 2 for model 4-35-35-35-1

matrix 35 x 35	n1	n2	n3	n4	n5	n6	n7	n8
m1	-0.15277	1.257491	1.454923	-0.0159	1.443156	0.004812	0.249894	0.676368
m2	-0.2221	2.066864	1.572345	0.035637	2.325857	0.179784	0.631306	1.647432
m3	0.204123	0.068339	-0.06329	-0.05618	0.227779	-0.25685	0.431118	0.38498
m4	0.244502	0.143057	0.154461	0.133754	0.243568	0.229559	-0.01532	-0.11031
m5	0.168444	-0.11166	0.118565	-0.02191	0.252687	-0.12756	-0.02135	0.092926
m6	-0.04357	0.415643	0.010285	0.172586	0.290894	-0.20407	0.556564	0.297134
m7	0.24212	-0.18845	-0.05789	0.07811	-0.05441	0.070569	0.024579	0.047204
m8	0.068441	-0.20081	0.019379	-0.05037	0.087604	0.089637	0.248063	0.133001
m9	-0.2628	-0.29082	0.138585	0.14502	0.270263	-0.29084	-0.04491	0.147417
m10	-0.0709	0.468184	0.78394	-0.27324	0.473948	0.010438	0.256707	0.233883
m11	-0.22495	0.63025	-0.42986	-0.11489	-0.30795	0.274739	0.916268	1.451463
m12	-0.10366	-0.22147	-1.08701	0.245139	-0.16059	0.170433	-0.21691	-0.15022
m13	-0.02174	0.203013	0.188022	0.071212	0.1206	0.237417	0.557544	0.103344
m14	-0.26834	-0.0771	0.039908	0.178851	-0.26135	-0.16996	0.076798	-0.15898
m15	0.25194	-0.13909	0.543295	0.105572	0.345983	0.157861	-0.00681	-0.06618
m16	0.207905	-0.09015	0.555135	0.03145	0.148641	0.199752	0.805191	0.069654
m17	-0.09478	0.074351	0.188838	-0.08307	0.270064	-0.17391	-0.03157	-0.21101
m18	-0.233	0.19639	-1.3504	-0.19333	0.320507	-0.20144	-0.22428	0.278976
m19	-0.22976	-0.17684	0.031383	0.272912	0.031568	-0.24195	-0.24946	-0.218
m20	0.243378	0.223122	-0.29694	-0.17662	0.448518	-0.27244	0.246607	0.220691
m21	-0.1636	0.287207	-0.34733	-0.22701	-0.18403	-0.23253	0.166773	-0.03139
m22	0.079861	0.361906	-0.16168	-0.24299	0.378737	-0.01251	0.44001	-0.10457
m23	0.16608	-0.9157	0.715716	0.214067	-0.2831	0.107595	-1.45686	-1.85087
m24	0.018051	-0.18937	0.201242	0.072892	-0.00266	0.004662	0.037633	0.181247
m25	-0.07455	0.204577	0.064047	-0.12645	-0.17928	0.025143	0.096701	-0.21333
m26	-0.20333	-0.00928	0.206763	-0.03911	-0.02769	-0.00653	0.010553	-0.21795
m27	-0.29417	0.374239	0.168491	0.144879	0.005293	-0.22901	0.423332	0.353913
m28	-0.03229	0.055823	0.23437	-0.12066	0.491151	-0.27529	0.307735	0.213193
m29	-0.14584	-0.13579	-1.40967	-0.16093	0.197182	-0.23574	-3.07098	-0.37022
m30	0.084699	-0.70276	-1.02361	-0.25787	-0.97801	-0.28174	3.583467	0.966527
m31	0.144383	-0.21146	0.279834	-0.19373	-0.15766	0.105931	0.252925	-0.16043
m32	-0.22426	0.386862	0.431569	-0.2266	0.063701	-0.29168	0.361699	0.302798
m33	0.245351	0.182233	0.078093	0.10706	0.203517	0.123696	0.216895	-0.22787
m34	0.181442	2.988852	2.620192	0.265275	3.794421	0.192135	2.791117	3.247696
m35	-0.25934	-0.29337	0.124006	-0.10157	-0.31882	0.251063	0.567469	0.179023
matrix 35 x 35	**n9**	**n10**	**n11**	**n12**	**n13**	**n14**	**n15**	**n16**
m1	0.104013	1.734064	0.265437	0.260426	-0.14933	0.544328	1.039733	-1.03685
m2	0.143889	2.174358	-0.14301	-0.13895	-0.01625	1.13306	2.102401	-1.63735
m3	0.243628	0.130925	-0.04324	-0.17332	-0.24685	0.450928	0.262473	0.513785
m4	0.241076	0.029593	0.054378	-0.13164	0.207025	0.268227	0.029832	0.025991
m5	0.008618	0.16525	0.041786	0.24208	-0.19743	-0.23096	-0.02575	-0.18452

m6	-0.24073	-0.05429	0.047506	-0.22765	-0.06104	0.184006	0.346051	0.40019
m7	-0.28785	0.244909	0.206169	-0.07279	0.258161	0.206021	-0.10507	0.254003
m8	0.096276	0.236345	-0.2165	-0.23249	-0.20116	0.10799	0.030436	-0.19246
m9	-0.00884	0.107729	-0.14457	-0.07666	-0.21244	0.207151	-0.03065	-0.14771
m10	-0.04833	0.591038	-0.1775	-0.28391	0.064094	0.42449	0.303503	0.419668
m11	-3.28816	-0.33573	0.251403	0.28612	0.157796	0.90629	0.316273	1.037252
m12	-0.50493	-0.52793	-0.31713	-0.09176	0.043755	0.098853	-0.04072	0.26311
m13	-0.34166	0.253286	-0.30107	-0.01072	-0.1208	0.030221	0.296972	0.491556
m14	-0.16848	-0.10827	-0.19647	0.243701	-0.15204	-0.22682	0.208157	-0.09476
m15	-0.21864	0.316325	-0.09387	-0.203	-0.23098	0.12463	0.11453	0.61973
m16	-0.34819	0.346558	-0.29913	0.185616	0.280995	0.466249	0.179616	0.847618
m17	-0.12011	0.119883	-0.03786	-0.01916	-0.1169	-0.23355	0.227228	-0.04419
m18	0.098462	-0.19393	-0.17624	-0.07989	-0.01798	0.620928	0.390999	0.594946
m19	-0.15668	-0.02007	-0.19297	-0.21636	-0.19861	0.03835	0.217125	-0.08129
m20	-0.02957	0.182782	-0.18114	-0.03649	-0.27371	0.300825	0.098541	0.448783
m21	-0.34609	0.060675	-0.1631	0.17448	-0.1919	0.123589	-0.06616	0.532059
m22	0.472329	0.233376	0.127861	0.187052	-0.23866	0.380166	0.460211	0.156364
m23	0.249435	-0.69703	0.073618	0.120721	-0.28022	1.191289	-0.18563	-1.34607
m24	0.172381	0.265515	0.001151	-0.24636	-0.21409	0.097151	0.150214	0.275808
m25	-0.07473	-0.07739	-0.06347	-0.23857	0.051056	-0.09088	0.272067	0.011698
m26	-0.27558	-0.15852	-0.09102	-0.22135	0.266519	0.113207	-0.20883	-0.24483
m27	0.210724	0.266692	0.243857	0.202357	-0.26942	0.559045	0.035745	-0.00051
m28	-0.08559	0.288299	0.041585	0.181393	0.104442	0.05925	0.302218	0.44277
m29	-0.27965	-0.59048	-0.2497	-0.1243	-0.21316	1.803111	0.083124	-1.05743
m30	-2.50642	-0.58718	0.037781	0.118286	0.138192	0.32192	-0.22896	1.920732
m31	0.25917	0.057003	0.040103	0.109645	0.099965	-0.27273	0.083024	-0.05384
m32	-0.04254	-0.04234	0.230431	-0.27418	-0.24929	0.711963	0.451663	0.552041
m33	-0.24005	-0.29041	-0.2677	0.016228	-0.03918	0.11147	0.288213	-0.00345
m34	3.90639	4.340934	-0.22406	0.114972	0.225813	0.809769	2.855963	-1.53794
m35	-0.825	-0.02018	0.01452	-0.1636	-0.15505	0.56328	0.054138	1.148431
matrix 35 x 35	**n17**	**n18**	**n19**	**n20**	**n21**	**n22**	**n23**	**n24**
m1	0.98502	0.057878	-0.2565	-0.12776	0.949904	-0.21243	-0.09524	1.893162
m2	1.346409	0.240548	0.123962	-0.15922	1.51413	-0.26479	-0.23493	2.147404
m3	0.341891	-0.28433	-0.05739	-0.01607	0.35612	-0.22268	-0.18867	0.333696
m4	-0.20226	0.109179	0.120641	-0.20271	0.250019	-0.12275	-0.22644	-0.23736
m5	-0.11415	-0.18047	-0.1352	0.048073	0.178622	-0.15666	-0.05052	-0.12984
m6	-0.33261	0.122368	0.277753	0.291465	0.285005	-0.11735	-0.11935	0.156185
m7	0.212205	-0.20408	0.202264	0.078828	0.148257	0.227279	0.207997	-0.25804
m8	-0.17149	0.152423	-0.17627	-0.1515	-0.11008	0.013051	0.118953	-0.246
m9	-0.19514	0.039896	-0.0129	0.278638	0.279343	-0.03791	0.271154	-0.0549
m10	0.526299	-0.21987	-0.1258	0.007246	0.210289	-0.3198	-0.18487	0.165298
m11	-2.13116	-0.03178	-0.15862	0.793877	0.955927	0.235868	-0.26811	0.108947
m12	-1.15985	0.157381	-0.15837	-3.52372	-0.06214	-0.30022	-0.19127	0.145646
m13	0.04044	-0.21461	-0.15057	-0.0783	-0.07353	0.199436	-0.07259	0.326083

m14	-0.184	-0.22774	-0.06265	0.011696	0.013697	0.002532	0.048325	0.245309
m15	-0.00256	-0.22061	0.250729	0.348121	0.171813	-0.30244	-0.23029	0.015765
m16	0.312874	0.204153	-0.1048	0.115794	-0.03389	0.013326	0.220106	-0.0837
m17	0.180589	-0.06391	-0.08338	0.120007	0.077639	0.06892	0.106351	-0.12038
m18	-0.84186	-0.28913	0.232373	-0.926	0.439154	0.206366	0.07841	0.255788
m19	0.290455	-0.12803	-0.15214	0.158382	0.026874	-0.00288	0.240477	-0.12773
m20	0.141087	-0.2773	0.051727	-0.483	0.062265	-0.05939	-0.26216	0.214857
m21	-0.35534	-0.02556	-0.09608	0.088813	0.31978	-0.28459	-0.19545	0.227669
m22	-0.18267	-0.15862	-0.27388	0.051331	0.170148	0.078083	-0.2614	0.466352
m23	-2.78277	0.057851	-0.28336	1.103944	-1.59612	0.14626	-0.23365	-0.82298
m24	-0.06401	0.237554	-0.28742	-0.05244	-0.22614	-0.24925	-0.21057	-0.12993
m25	-0.01823	-0.19725	0.210233	0.133723	0.21284	-0.16234	0.167549	0.099052
m26	-0.13709	-0.00426	0.221802	-0.11622	0.08375	0.003731	0.190368	0.153059
m27	0.301442	-0.07958	-0.20535	-0.04234	0.03172	0.127065	-0.13796	0.126957
m28	0.503986	0.097462	-0.26108	-0.32367	0.349062	0.247651	0.207014	0.244738
m29	-0.59396	0.027238	-0.05059	0.492182	-0.69946	-0.12717	0.243941	-0.19977
m30	-2.54331	0.221838	-0.23688	1.290586	-0.62577	0.015292	-0.15226	-1.15268
m31	0.225716	0.017177	0.283387	0.230805	0.176177	-0.22467	0.072506	-0.12804
m32	-0.08496	-0.22851	-0.09923	0.157773	0.277382	0.056326	0.056982	0.179539
m33	-0.07444	-0.26909	0.203917	-0.25629	-0.07201	0.03942	0.047016	0.260753
m34	-3.31945	-0.03582	0.004366	1.219744	3.63731	0.223982	-0.04341	4.310286
m35	-0.36272	-0.12352	-0.0028	-0.09859	-0.28525	0.042862	-0.19182	-0.38039
matrix 35 x 35	**n25**	**n26**	**n27**	**n28**	**n29**	**n30**	**n31**	**n32**
m1	-0.25273	-0.22631	0.079435	0.769006	-0.16418	1.60765	-1.70781	-0.27316
m2	0.218791	-0.24505	-0.14214	0.862389	0.159927	1.977322	-3.30926	-0.08593
m3	-0.01375	0.032633	0.247834	0.321202	0.096358	0.188915	1.568842	0.16373
m4	0.188603	0.020545	0.170761	-0.02557	0.069429	-0.01294	-0.29207	0.203134
m5	0.267143	-0.00029	-0.11264	0.181157	-0.20022	-0.00242	0.094416	0.186395
m6	0.154288	-0.24172	0.032405	0.468842	0.617573	0.076792	-0.42817	-0.1559
m7	-0.0554	0.270923	0.283954	0.07752	0.009753	-0.07256	0.030949	-0.11194
m8	-0.27329	-0.15114	-0.10407	-0.01497	-0.18852	-0.19168	0.145821	-0.06831
m9	0.018454	-0.00043	-0.16239	0.11096	0.134486	-0.26017	-0.05122	0.262106
m10	0.123495	0.096318	-0.04933	0.145613	0.676322	0.481362	-0.19368	0.140245
m11	-0.15323	-0.15474	0.147536	3.613995	0.993389	-0.2761	-1.16756	-0.19931
m12	-0.27605	-0.28938	-0.10074	0.398687	0.118205	-0.44275	-0.58558	-0.26824
m13	-0.15427	0.098548	-0.2481	0.137857	0.554148	0.077269	-0.56	-0.08367
m14	-0.14919	0.282501	0.135008	-0.21522	0.067344	0.123619	0.050787	-0.08049
m15	-0.14777	0.276896	-0.12205	0.324983	0.140987	0.001639	-0.98124	-0.03936
m16	-0.07424	-0.04012	-0.03069	0.024933	0.465485	0.000589	-1.42948	-0.24356
m17	-0.02203	-0.02785	-0.20447	-0.19389	-0.20809	0.215976	-0.23739	-0.15602
m18	0.096459	0.043538	0.022455	0.166921	0.011741	-0.25263	0.206034	-0.0811
m19	-0.28878	-0.05229	-0.13917	-0.07909	-0.23894	-0.07909	-0.03104	-0.04008
m20	0.159013	-0.14122	-0.07954	0.205619	0.435741	0.394437	0.95414	0.138747
m21	-0.20878	0.144525	-0.00725	-0.08393	0.453649	-0.00837	-0.42421	-0.28133

m22	-0.15369	-0.13255	-0.10142	-0.25712	0.482736	0.355335	-0.55664	-0.28955
m23	0.07322	-0.2406	0.150345	-3.01349	-1.79986	0.037063	0.108717	-0.22756
m24	-0.07172	0.207224	0.042662	-0.09162	-0.16201	-0.086	-0.08044	-0.17837
m25	0.006435	-0.19837	0.126801	-0.21072	0.063247	-0.068	0.124692	0.228414
m26	-0.09764	0.012114	-0.03336	-0.28454	0.011898	-0.06328	-0.1837	0.093445
m27	-0.19768	-0.09327	-0.02123	0.235693	0.361192	0.357786	1.498995	-0.20136
m28	-0.00151	0.068881	-0.17984	-0.0887	0.093218	0.431331	1.352108	0.152641
m29	0.031034	0.052289	-0.04489	-3.81065	-2.41537	-0.31602	0.073269	0.257856
m30	-0.0542	-0.14103	-0.31258	3.441243	1.686694	-0.87961	-0.34001	0.13967
m31	-0.19987	0.263976	-0.11089	-0.09566	0.168097	-0.15706	0.041234	-0.22574
m32	-0.13051	-0.14633	0.107224	0.065519	0.608052	0.552637	-0.1792	-0.24394
m33	-0.16525	0.045028	-0.05488	-0.23995	0.257429	-0.09028	0.034792	0.096166
m34	-0.09664	0.116002	-0.08117	2.442722	2.926764	3.829328	-5.45711	-0.29078
m35	0.183972	-0.11275	0.068945	0.386577	0.793411	0.111405	-1.02895	0.132749
matrix 35 x 35	**n33**	**n34**	**n35**					
m1	-0.13875	1.89275	0.919964					
m2	-0.12551	2.362984	1.777212					
m3	-0.15892	0.360373	0.270516					
m4	-0.18654	0.182795	-0.10119					
m5	0.163564	0.182809	-0.20638					
m6	-0.00812	0.330207	0.384342					
m7	0.253843	-0.28103	0.173425					
m8	0.252425	0.169786	-0.24855					
m9	-0.26012	0.197906	0.120557					
m10	-0.11585	0.309987	0.453021					
m11	0.082526	-0.24576	0.511788					
m12	-0.03468	-0.26739	0.205756					
m13	0.1061	0.133966	0.442995					
m14	0.116394	0.224059	0.202661					
m15	-0.12957	-0.20894	0.012857					
m16	0.17306	0.198964	-0.07877					
m17	0.163148	-0.13304	-0.21031					
m18	-0.21279	0.260476	0.556517					
m19	0.169841	-0.27667	0.187508					
m20	-0.03976	0.304829	0.038868					
m21	-0.0031	-0.25912	0.05912					
m22	-0.27131	0.021777	0.273702					
m23	-0.07331	-0.6587	-1.26936					
m24	-0.13187	-0.12064	0.074615					
m25	0.288346	0.069187	-0.05329					
m26	-0.28672	0.032469	-0.26233					
m27	-0.00409	0.137497	0.308389					
m28	0.145798	0.359738	0.414846					
m29	0.161801	0.01214	-1.41039					

m30	-0.30557	-1.2885	-0.03366					
m31	0.262488	0.216748	-0.04705					
m32	0.044669	0.003003	0.420984					
m33	-0.01203	0.003198	0.139153					
m34	0.266481	4.174869	2.139916					
m35	-0.1076	-0.10203	0.138549					

Weight matrix layer 3 for model 4-35-35-35-1

matrix 35 x 35	**n1**	**n2**	**n3**	**n4**	**n5**	**n6**	**n7**	**n8**
m1	0.188771	-0.16491	-0.09392	0.098611	-0.17497	-0.15834	0.243967	-0.10015
m2	0.101878	0.576874	-0.38894	0.727085	0.23462	0.530296	-0.40764	-0.30437
m3	2.579852	-2.43243	2.467299	-1.96501	2.711235	-2.40443	2.459478	2.116692
m4	0.2195	-0.21506	0.240842	0.169747	0.094231	-0.23989	-0.04492	-0.09057
m5	0.328745	0.738698	-0.30408	0.766998	0.731559	0.484142	-0.31018	-0.37377
m6	-0.28049	0.155987	-0.05296	-0.05027	0.078433	-0.10789	-0.17271	0.078171
m7	-0.18484	0.25674	0.035273	0.420435	-0.12975	0.099569	0.043364	0.203227
m8	-0.28005	0.302569	-0.24814	0.38488	-0.71184	0.620102	-0.137	-0.2308
m9	-3.74632	3.806585	-4.03005	4.079146	-0.91578	4.118302	-3.21693	-3.68495
m10	0.219914	0.426654	-0.57455	0.817624	0.520996	0.499625	-0.75033	-0.65342
m11	-0.10598	0.156364	-0.09282	-0.29982	0.222742	0.175904	-0.2503	-0.05651
m12	0.278733	0.184386	0.002133	0.118873	-0.05259	-0.1314	-0.16703	0.219024
m13	0.251006	-0.25076	-0.2342	0.158859	0.173566	0.233348	-0.03606	0.19514
m14	0.378445	0.476119	0.103218	0.539333	0.088839	0.360965	0.015185	-0.08066
m15	0.467314	0.611099	-0.33378	0.575969	0.280029	0.635314	-0.13208	-0.21484
m16	-0.45912	0.078347	0.466043	0.333637	-0.71941	0.008243	0.449344	0.277631
m17	0.459713	-3.9245	4.126009	-3.66007	-1.12139	-3.60967	4.261082	4.342973
m18	-0.12608	0.131389	0.102648	0.209123	-0.08586	-0.11581	0.131116	-0.24533
m19	-0.23596	0.001154	0.138747	0.125275	-0.18401	0.242757	0.136929	0.161116
m20	4.41701	-2.79188	6.692652	-4.75717	4.315235	-3.22693	2.1367	3.445723
m21	-0.57853	0.449528	0.074788	0.267934	-0.02981	0.602823	-0.12024	-0.2175
m22	-0.22538	0.116535	0.181216	0.174663	0.122613	0.21203	-0.10923	0.046076
m23	-0.02814	-0.0568	-0.19502	-0.05165	-0.10987	0.041536	0.193086	0.285491
m24	0.088006	0.310056	-0.60595	0.874044	0.186288	0.518576	-0.6512	-0.5054
m25	-0.04208	-0.22322	0.042299	0.280799	0.017173	0.041204	-0.14221	-0.08823
m26	0.050971	0.015431	-0.12725	-0.29168	-0.24731	-0.20588	0.262187	0.086315
m27	-0.30301	-0.09157	-0.26032	-0.03553	0.233745	0.163282	0.174026	-0.25476
m28	-1.83952	0.413744	-0.20421	0.487121	-2.49392	0.284595	0.117781	0.21695
m29	-0.34159	0.417147	0.184662	0.520629	-0.52078	0.158853	0.170996	0.337802
m30	0.667602	0.250954	-0.50907	0.889555	0.69315	0.515294	-0.37223	-0.3234
m31	-0.77509	-1.55889	1.787189	-2.00038	0.022191	-1.81157	1.893944	1.921382
m32	0.323781	-0.33308	-0.10254	0.197385	-0.09992	0.152929	0.241758	0.265315
m33	0.197312	-0.00063	0.092865	0.175366	-0.08645	0.044243	0.123885	-0.01097

m34	0.288783	0.595707	-0.68453	0.550441	0.534879	0.51858	-0.72743	-0.51892
m35	0.067787	0.237664	0.193088	0.319526	0.046291	0.464783	0.099726	-0.12661
matrix 35 x 35	**n9**	**n10**	**n11**	**n12**	**n13**	**n14**	**n15**	**n16**
m1	0.172082	-0.02756	-0.13949	0.226514	0.034968	0.081096	0.2284	0.241432
m2	0.525658	-0.24381	-0.24118	0.708286	-0.35084	0.762292	0.685916	-0.23118
m3	-1.88028	-0.26801	-0.24013	-1.79565	2.10813	-1.94922	-1.60436	0.152321
m4	-0.24613	-0.21634	0.156516	-0.02707	0.243821	-0.20379	-0.11983	0.149147
m5	0.288958	0.231857	-0.22944	0.848962	-0.20797	0.532104	0.549052	-0.22728
m6	0.101848	0.151093	0.257247	0.060058	-0.07684	-0.02826	0.146585	0.108909
m7	0.019751	0.016343	0.133109	0.486771	-0.12588	0.433847	0.311606	-0.10928
m8	0.322352	-0.16388	0.007019	0.780419	0.046461	0.357316	0.536164	-0.23284
m9	3.589816	0.253637	-0.17127	3.919746	-3.34558	3.622254	3.334655	-0.14285
m10	0.793289	-0.28976	-0.26097	0.412202	-0.48878	0.310245	0.310577	0.163756
m11	0.140466	-0.01102	0.168376	-0.2041	-0.16501	0.26302	0.037594	0.231594
m12	-0.04457	0.145614	0.002696	0.16566	-0.12155	0.052553	-0.06944	0.12508
m13	0.252985	-0.12624	-0.27196	-0.23153	0.166771	-0.21146	-0.10222	-0.2499
m14	0.410004	-0.05303	0.07653	0.223049	-0.07642	0.181191	0.450937	0.021631
m15	0.526889	-0.23554	-0.15299	0.289795	-0.49296	0.761764	0.536239	0.126683
m16	0.176376	0.147557	-0.17062	0.343766	0.569317	-0.06646	0.38849	0.242831
m17	-4.03646	0.237763	0.082087	-3.4484	4.499234	-3.40366	-3.18442	0.171089
m18	0.287124	0.268759	-0.27087	-0.01166	0.066396	-0.05474	-0.22456	-0.23952
m19	0.151884	-0.19431	0.11776	-0.09711	0.082502	0.092522	0.2185	-0.13486
m20	-3.74173	-0.25763	0.246103	-3.97748	3.978812	-3.23755	-2.18321	-0.10033
m21	0.349833	0.174817	-0.04542	0.256766	-0.14375	0.239192	0.332425	-0.13816
m22	0.04873	0.25494	0.173737	-0.02154	0.232839	-0.19662	0.109391	-0.10076
m23	0.13527	-0.23715	-0.2838	-0.08042	-0.25758	-0.15048	-0.28842	0.111518
m24	0.527411	0.231079	-0.19164	0.716035	-0.63282	0.681597	0.231121	0.174514
m25	-0.21633	0.196325	-0.11477	-0.01401	0.063286	0.277168	-0.25366	-0.20244
m26	-0.08858	0.204495	0.093243	-0.29129	0.165504	0.273965	-0.11219	0.284913
m27	-0.04832	0.133752	-0.11127	0.009266	0.144836	0.234716	-0.21092	-0.03176
m28	0.447137	-0.19576	-0.16547	0.618094	-0.01138	0.47886	0.391331	0.11448
m29	0.437504	-0.1648	0.237265	0.503069	0.302104	0.190146	0.531881	0.050813
m30	0.257683	-0.12994	0.144578	0.799428	-0.4163	0.799042	0.615401	0.020608
m31	-2.01347	0.034466	0.246898	-2.17173	1.946672	-1.80953	-1.96531	0.003292
m32	-0.04953	-0.0866	0.051589	-0.26566	-0.05278	-0.11377	0.205911	0.019514
m33	-0.30655	-0.06119	0.133662	0.243219	0.204445	0.24113	0.129391	-0.02056
m34	0.295828	-0.27231	-0.31654	0.793173	-0.5739	0.930459	0.425296	-0.12559
m35	0.346943	-0.19468	-0.21797	0.430059	-0.03437	0.558708	0.372945	-0.2215
matrix 35 x 35	**n17**	**n18**	**n19**	**n20**	**n21**	**n22**	**n23**	**n24**
m1	-0.23363	-0.12954	0.327656	0.042363	0.062951	0.155707	-0.25668	-0.13632
m2	-0.16165	-0.30233	0.399552	0.223889	-0.40284	0.251742	-0.18427	-0.31913
m3	0.181139	2.209991	-1.47287	0.255974	3.534766	0.033631	-0.19409	2.336363
m4	0.268074	0.072967	0.103126	0.261778	-0.21451	-0.20184	-0.10222	0.146702
m5	0.029198	-0.47212	0.813981	0.075661	-0.63242	-0.30603	-0.17269	0.607014

m6	-0.03108	0.017958	0.097444	0.254258	0.159004	-0.24975	-0.04568	0.044215
m7	-0.21105	-0.01841	0.067834	-0.19368	0.652283	-0.20236	0.012659	-0.94143
m8	0.195781	-0.22576	0.547698	0.207011	0.246962	-0.17569	-0.1785	-0.93632
m9	0.209125	-2.40836	3.310748	0.044711	-5.69552	0.085496	0.047031	-3.75309
m10	-0.21685	-0.87296	0.653753	0.03442	-0.17083	-0.202	-0.07279	0.747718
m11	0.222658	-0.14939	0.142596	-0.15957	-0.14431	-0.1308	-0.08621	0.093583
m12	0.043504	-0.17502	0.103977	-0.06087	0.04129	0.281901	0.023988	0.030287
m13	0.14712	-0.18508	0.008391	-0.26167	-0.08939	0.110555	-0.27875	-0.2768
m14	0.205547	0.333223	0.411746	-0.08494	-0.02983	0.092085	-0.05837	-0.21888
m15	0.051456	-0.27252	0.561925	-0.28546	-0.2531	0.105984	0.005141	0.404599
m16	-0.0785	0.852729	0.344821	-0.2719	0.721745	-0.13128	0.192671	-1.98149
m17	0.048371	3.36599	-3.25649	-0.085	-1.12136	-0.24244	0.279071	0.03964
m18	0.005046	0.194478	-0.27778	-0.19234	-0.03377	-0.20897	-0.13412	-0.02226
m19	-0.25829	-0.05655	0.17817	-0.19269	-0.28769	-0.0725	0.0085	-0.05797
m20	0.212223	3.552074	-2.37728	-0.25956	5.650837	-0.11385	0.220371	3.769798
m21	0.055254	-0.58379	0.670345	0.098502	-0.24613	-0.29836	-0.08685	-1.41084
m22	0.275283	-0.06085	-0.12284	-0.13125	-0.1068	-0.14884	0.286879	-0.23812
m23	0.081349	-0.16892	0.268063	0.261663	-0.036	0.165678	0.154014	-0.04705
m24	-0.12968	-0.73433	0.53858	-0.17916	-0.80568	0.142456	-0.06027	0.343901
m25	0.007551	-0.22705	0.199466	-0.06097	0.289267	0.083113	0.182428	0.044241
m26	0.179585	0.108189	-0.01678	-0.0043	-0.16545	0.168149	-0.14691	-0.09495
m27	-0.1241	-0.02495	0.244323	-0.13265	0.123126	-0.28013	0.2278	-0.30045
m28	0.022056	-0.0446	0.430039	-0.15349	0.466418	0.230587	-0.29669	-1.14183
m29	0.104401	-0.18169	0.281128	-0.12738	0.372043	-0.2488	-0.07905	-2.0866
m30	-0.30236	-0.39347	0.239285	-0.14564	0.017011	-0.21426	-0.27035	0.405576
m31	0.113406	2.199328	-2.02592	0.081093	-0.17526	0.229444	-0.04215	-1.70555
m32	0.124424	-0.02049	-0.2028	-0.2113	-0.01282	-0.21311	0.203254	-0.27043
m33	-0.1532	-0.09391	-0.23031	-0.23362	0.128478	-0.08295	-0.144	0.090202
m34	-0.27302	-0.79634	0.859375	-0.08577	-0.82882	0.230619	0.037293	0.876387
m35	-0.11179	-0.34788	0.287046	-0.28904	-0.13267	-0.01283	0.193633	-0.97788
matrix 35 x 35	**n25**	**n26**	**n27**	**n28**	**n29**	**n30**	**n31**	**n32**
m1	-0.14993	0.109103	0.071361	-0.05987	0.203332	0.005023	-0.20745	-0.01186
m2	0.507303	-0.42828	-0.17618	0.300974	0.496935	0.864736	0.364949	0.532378
m3	-1.38211	2.263382	0.019629	-1.74467	-1.61408	-2.05388	-1.87384	-1.51382
m4	-0.04362	-0.23156	-0.23002	0.056827	0.279453	-0.17147	-0.18903	0.029776
m5	0.282541	-0.50181	-0.18069	0.387131	0.597038	0.559707	0.835976	0.499633
m6	-0.11908	0.146728	0.256594	-0.28174	-0.26464	-0.10421	0.226818	0.2326
m7	0.358479	0.318802	-0.28803	0.115679	0.532073	0.185135	0.361247	0.311549
m8	0.647429	-0.09312	0.022913	0.314206	0.544531	0.378461	0.289847	0.361472
m9	3.072106	-3.51807	-0.23011	3.66257	3.474807	3.981755	3.398062	3.052369
m10	0.70957	-0.86239	-0.22064	0.57062	0.758947	0.698007	0.323757	0.59385
m11	-0.07113	-0.04609	-0.04635	0.07625	-0.08968	0.209319	-0.27511	0.129734
m12	0.18696	0.211178	0.096024	-0.03761	0.079702	-0.09699	-0.25627	0.007362
m13	-0.15883	0.207506	0.232913	-0.24662	0.267315	-0.06612	0.238484	0.059392

m14	0.186359	-0.23364	0.113828	0.587516	0.58918	0.581181	0.294074	0.626448
m15	0.305568	-0.0887	0.160236	0.555191	0.623312	0.844873	0.315548	0.570534
m16	0.386805	0.471635	0.099927	0.227062	0.024607	0.107842	-0.09043	0.379558
m17	-2.85304	4.704044	0.025704	-2.82672	-2.78277	-4.01021	-2.95836	-2.7069
m18	-0.19949	0.171036	0.24281	-0.19134	-0.21588	-0.20026	-0.12407	-0.04886
m19	-0.06402	0.044807	0.168325	0.288768	0.122094	-0.13893	0.021434	-0.20049
m20	-1.71781	4.225916	-0.09778	-2.35171	-1.76061	-5.84529	-2.94634	-1.98501
m21	0.658315	-0.27375	0.097688	0.555938	0.465443	0.782355	0.168596	0.68483
m22	0.294925	-0.15606	0.011581	0.272051	-0.13948	0.104205	-0.20769	-0.22915
m23	-0.17256	-0.26222	0.065361	0.068896	-0.03649	0.00644	0.183409	-0.04348
m24	0.565246	-0.39357	-0.07689	0.705929	0.47114	0.612784	0.809894	0.389464
m25	-0.11314	0.173103	-0.06075	-0.13893	0.181276	-0.25782	-0.26173	0.082455
m26	-0.2037	0.198702	-0.25411	0.205176	-0.03497	-0.21142	0.166723	-0.13886
m27	-0.23263	0.179619	0.253202	-0.09148	0.236294	0.053387	-0.14844	-0.12044
m28	0.522387	-0.04147	0.19198	0.638078	0.335777	0.28464	0.627148	0.508592
m29	0.533212	0.255279	-0.26034	0.421973	0.408724	0.523379	0.444026	0.399191
m30	0.547877	-0.39527	0.110366	0.693768	0.399995	0.816887	0.403448	0.49699
m31	-2.09796	2.045578	-0.19986	-1.69742	-1.86424	-1.88618	-2.00817	-1.57094
m32	-0.16096	-0.08216	-0.17281	-0.32856	0.120746	-0.0132	0.165624	0.212663
m33	-0.1916	-0.25171	-0.03004	0.252697	0.254311	-0.27829	-0.02712	0.050695
m34	0.756908	-0.54434	0.038574	0.696413	0.440393	0.838906	0.873244	0.467375
m35	0.560853	0.000565	-0.31131	0.414932	0.354013	0.333517	0.637445	0.243495
matrix 35 x 35	**n33**	**n34**	**n35**					
m1	-0.20986	-0.15184	-0.15149					
m2	-0.39318	0.541547	-0.55066					
m3	2.193157	-1.44095	1.086874					
m4	-0.09686	0.235395	0.223994					
m5	-0.43081	0.719738	-0.39963					
m6	0.067466	0.285235	-0.09367					
m7	-0.06775	0.573168	-0.00588					
m8	-0.34856	0.683958	-0.32619					
m9	-3.8472	3.518658	-1.37247					
m10	-0.31445	0.675727	-0.97944					
m11	-0.24841	0.096128	-0.00524					
m12	-0.11931	0.122639	0.092761					
m13	-0.01797	0.027741	-0.13237					
m14	0.213191	0.365415	0.212268					
m15	-0.26496	0.626041	-0.392					
m16	0.419358	0.266051	0.724975					
m17	4.418972	-3.27083	4.319343					
m18	0.046256	-0.22793	-0.00175					
m19	0.172042	-0.12761	0.163906					
m20	6.5014	-2.20597	4.844643					
m21	-0.40988	0.592096	-0.3116					

m22	0.017582	0.152578	0.186226					
m23	-0.20068	-0.016	-0.09281					
m24	-0.27357	0.414406	-0.67567					
m25	-0.15915	0.20459	0.175779					
m26	-0.0414	0.118711	-0.08347					
m27	0.132706	-0.06816	-0.10296					
m28	0.117311	0.63071	-0.19163					
m29	0.276599	0.245599	0.2388					
m30	-0.42736	0.493908	-0.42417					
m31	1.219085	-2.05456	2.87124					
m32	-0.1835	-0.07417	-0.04505					
m33	0.015004	0.00709	0.171478					
m34	-0.65132	0.715375	-1.0611					
m35	0.291282	0.473063	-0.25896					

Bias weight matrices for layer 1 and 2.

Bias weight matrix layer 1				**Bias weight matrix layer 2**			
Matrix 1 x35	**n1**	**Matrix 1 x35**	**n1**	**Matrix 1 x35**	**n1**	**Matrix 1 x35**	**n1**
m1	-2.5798	**m19**	0	**m1**	-0.03135	m19	0
m2	-3.19062	**m20**	-0.62129	**m2**	0.275883	m20	0.041304
m3	-0.16994	**m21**	0.132172	**m3**	-0.9152	m21	0.157256
m4	0	**m22**	0.488851	**m4**	0	m22	-0.02909
m5	0	**m23**	2.640195	**m5**	0.182766	m23	0
m6	0.406598	**m24**	0	**m6**	0	m24	0.006056
m7	0	**m25**	0	**m7**	1.297112	m25	-0.0271
m8	-0.03934	**m26**	0	**m8**	0.404285	m26	0
m9	0	**m27**	-0.07014	**m9**	2.312984	m27	-0.02164
m10	-0.97033	**m28**	-0.3527	**m10**	0.280087	m28	-0.39473
m11	-1.28038	**m29**	1.157786	**m11**	-0.02726	m29	0.270068
m12	-1.06561	**m30**	-1.08605	**m12**	0	m30	0.409273
m13	0.000582	**m31**	0	**m13**	0	m31	1.344869
m14	0	**m32**	0.654166	**m14**	1.009776	m32	-0.05693
m15	-0.27175	**m33**	0	**m15**	0.422556	m33	-0.03014
m16	-0.33221	**m34**	-2.66359	**m16**	-0.23929	m34	0.093013
m17	0	**m35**	-0.03088	**m17**	-1.29561	m35	0.168731
m18	0.901005			**m18**	0		

Bias weight matrices for layer 1 and output layer matrix. The output layer Bias weight is 0.274139.

Bias weight matrix layer 3				**Output matrix layer**			
Matrix 1 x 35	**n1**	**Matrix 1 x 35**	**n1**	**matrix 1 x 35**	**n1**	**matrix 1 x 35**	**n1**
m1	0.976292	**m19**	0.448143	**m1**	-3.16011	**m19**	1.062632
m2	0.457201	**m20**	-0.03114	**m2**	1.412862	**m20**	0.0521
m3	0.451368	**m21**	1.881423	**m3**	-4.36042	**m21**	-8.35572
m4	0.441789	**m22**	-0.01735	**m4**	0.926316	**m22**	-0.02953
m5	0.977707	**m23**	-0.02229	**m5**	-4.9583	**m23**	-0.01988
m6	0.46065	**m24**	-0.64671	**m6**	1.372081	**m24**	2.272057
m7	-0.20383	**m25**	0.380069	**m7**	-3.97275	**m25**	0.950001
m8	0.559915	**m26**	0.579196	**m8**	-4.50563	**m26**	-4.25948
m9	0.471903	**m27**	-0.03173	**m9**	1.689671	**m27**	0.30745
m10	0	**m28**	0.423424	**m10**	-0.34182	**m28**	0.945415
m11	-0.03176	**m29**	0.39454	**m11**	-0.26191	**m29**	0.995423
m12	0.47042	**m30**	0.33384	**m12**	0.900153	**m30**	1.224801
m13	0.557637	**m31**	0.466197	**m13**	-4.5172	**m31**	1.145303
m14	0.47951	**m32**	0.377283	**m14**	1.034418	**m32**	1.000689
m15	0.433162	**m33**	0.598264	**m15**	1.013498	**m33**	-4.52895
m16	-0.02099	**m34**	0.426134	**m16**	-0.08696	**m34**	0.851175
m17	-0.02291	**m35**	0.40748	**m17**	-0.23668	**m35**	-4.80461
m18	1.323557			**m18**	-5.63529		

Appendix I

This section contains two weight matrices - Weight Matrix 1 and Weight Matrix 2:

Weight Matrix 1 of the final model used in the classification of ashes (chapter 7). It is a 530 by 8 (m by n) matrix.

Matrix 530 x 8	n1	n2	n3	n4	n5	n6	n7	n8
m1	-0.10397	-0.15658	0.016755	0.067048	-0.03738	0.18015	0.000609	0.20263
m2	-0.06694	0.125749	-0.00394	0.047097	0.031552	0.065834	-0.00504	0.114856
m3	-0.06384	-0.08211	0.03345	0.012922	0.008243	-0.03492	0.099048	-0.06509
m4	-0.08153	-0.05949	0.009612	-0.04379	-0.10982	-0.08532	-0.05925	0.080703
m5	-0.01368	0.085353	0.092626	-0.09705	0.056336	0.12166	-0.03178	-0.12994
m6	0.11664	0.050781	0.102881	0.011152	-0.07483	-0.07434	0.005175	0.034053
m7	0.051087	-0.09119	-0.00586	0.08117	-0.09975	-0.0312	0.035772	0.056547
m8	-0.08233	-0.00897	-0.13949	0.072584	-0.05384	-0.05185	0.112859	0.098656
m9	-0.08227	0.013752	-0.0899	0.10917	-0.06126	-0.13676	-0.14287	0.219527
m10	0.104842	0.085225	0.039612	0.067745	0.074474	0.012924	0.04411	-0.12896
m11	-0.04378	0.005177	-0.00236	0.045874	-0.10446	0.018682	-0.04807	-0.12548
m12	0.08359	-0.03075	-0.16848	-0.06398	0.075628	-0.15966	-0.08816	-0.0674
m13	0.100942	-0.06473	-0.01719	-0.05713	-0.10578	-0.05567	0.050474	-0.04034
m14	-0.11047	0.10624	-0.02444	-0.0901	0.022345	-0.0278	0.116923	-0.00795
m15	-0.07402	0.055459	0.094132	-0.0798	-0.11588	0.043946	0.033658	-0.03622
m16	0.033912	0.16926	-0.03383	-0.02207	-0.02365	0.086257	0.021908	0.049065
m17	0.086843	0.002069	0.036045	0.000989	0.004966	-0.12169	0.065518	0.006641
m18	0.098479	-0.02365	-0.08031	0.02869	-0.06851	0.00643	-0.03982	0.004241
m19	0.004539	0.136652	0.003025	0.032831	-0.00985	0.067532	-0.00526	-0.14115
m20	0.072954	0.126791	-0.11235	0.004249	-0.09045	-0.11429	-0.02319	-0.01561
m21	0.009958	0.052036	-0.06889	-0.05221	0.058054	-0.06481	0.023989	-0.00525
m22	-0.05195	0.035616	-0.05496	-0.05453	0.015125	0.098728	0.037609	-0.1101
m23	0.119829	-0.08529	0.031784	-0.10316	0.068102	0.112965	-0.01075	-0.16891
m24	-0.02878	0.091341	-0.13189	0.053918	-0.09709	0.15301	0.040187	-0.04917
m25	-0.0398	0.083985	-0.16499	-0.01337	-0.06893	-0.05045	-0.03249	-0.12783
m26	0.038087	-0.1172	0.05183	0.132614	-0.06119	-0.02062	-0.10224	0.016637
m27	0.015909	0.120582	-0.01935	-0.01523	-0.05162	0.114936	-0.01519	-0.09067
m28	-0.10401	0.036405	-0.00124	0.072835	-0.11294	0.037528	-0.04183	-0.12954
m29	0.021556	0.078772	-0.05126	0.084164	-0.04826	-0.11775	0.026788	-0.08221
m30	-0.0565	-0.00103	0.068673	0.027414	-0.06481	0.085527	-0.05333	-0.06682
m31	-0.06584	-0.1368	0.026293	-0.05028	0.003235	0.028895	0.052483	-0.08237
m32	-0.07872	0.091512	-0.21968	0.103283	-0.05529	-0.07409	-0.06304	0.086454
m33	0.019579	-0.05209	0.067185	0.072575	-0.08125	0.030542	0.07968	-0.25235
m34	-0.02204	0.127312	-0.19903	-0.07385	0.096653	0.045146	0.070293	0.119387
m35	0.05096	-0.12581	-0.04552	0.063418	-0.09824	0.108237	-0.0603	0.087866

m36	0.024094	-0.08848	0.025883	0.03618	0.008869	0.009316	-0.07548	-0.05289
m37	0.01269	0.142543	-0.03132	0.020016	0.063536	-0.11892	-0.01156	0.036433
m38	-0.11398	-0.00909	-0.00297	0.001606	0.050081	-0.02879	0.074968	0.016727
m39	0.019281	-0.12429	0.11735	0.029286	0.060031	0.124419	-0.12005	0.209435
m40	0.118267	-0.11725	0.113289	-0.12334	-0.08727	0.005845	0.097601	-0.31479
m41	-0.00301	-0.10029	-0.12468	0.116318	0.005909	-0.11213	-0.00699	0.010007
m42	-0.05359	-0.11391	0.016058	-0.11781	0.119769	-0.02002	0.138038	-0.19114
m43	0.045521	-0.01985	0.142768	-0.0064	0.000259	0.051472	-0.01897	-0.02349
m44	-0.00498	-0.18948	0.070162	0.092173	-0.09711	0.065384	-0.13609	0.221964
m45	0.027496	0.257152	0.046015	-0.02698	-0.00362	0.00618	0.100453	-0.08477
m46	0.080476	-0.02031	0.094481	0.032011	-0.02725	-0.08476	0.077614	0.047496
m47	0.002107	-0.05138	0.076683	0.011301	0.116164	0.020933	0.103215	-0.04853
m48	-0.05946	-0.07577	0.008369	0.058381	0.03517	0.009448	0.047231	-0.03269
m49	-0.04316	0.147107	0.096488	0.005025	0.065093	0.088243	-0.03644	0.03869
m50	-0.10735	-0.11396	0.026734	0.022436	0.058913	0.076814	0.030467	-0.09194
m51	0.067316	-0.09664	0.109478	-0.03177	-0.00456	0.116398	-0.10061	0.09036
m52	0.037463	0.047139	-0.09283	-0.07309	-0.03858	0.060624	-0.11281	0.148245
m53	-0.08261	-0.10807	0.019078	0.008873	0.062135	-0.00832	-0.0499	0.048359
m54	0.07592	0.060039	0.139542	0.136428	0.012828	-0.09086	-0.20499	0.285556
m55	-0.03354	0.017865	-0.04743	-0.00491	0.084274	-0.10819	-0.10198	0.014899
m56	0.118227	0.020021	-0.13377	0.016406	-0.12399	-0.06354	-0.03109	0.053437
m57	0.054051	0.066254	-0.06719	-0.07615	0.069296	-0.11566	0.015563	0.115257
m58	0.103313	-0.06027	-0.12905	-0.08523	-0.03054	0.091815	0.001323	-0.12589
m59	0.11802	0.036499	0.020551	0.001076	0.100888	-0.04727	-0.12572	0.107148
m60	0.04071	0.024375	0.024852	0.054349	-0.10221	0.11919	-0.03625	0.128999
m61	-0.06991	-0.04651	-0.09844	-0.01212	0.06379	-0.14647	-0.04237	0.134622
m62	0.092301	0.019386	-0.06165	-0.09429	-0.03118	0.031503	0.043175	-0.04188
m63	0.060599	0.061587	-0.04256	0.060874	0.086454	-0.10997	-0.00185	-0.15385
m64	0.003814	-0.17239	0.135452	-0.00285	0.068783	0.109188	0.060062	-0.14971
m65	-0.01349	0.054293	0.066416	0.043496	0.109767	0.073066	0.138699	-0.04247
m66	0.119423	-0.04357	-0.08381	0.071992	-0.01263	0.152899	0.025257	0.006486
m67	0.116676	-0.16354	0.148429	-0.00576	-0.08101	-0.04481	-0.05697	0.111452
m68	0.096727	0.04434	0.104741	0.080129	0.069961	0.040992	-0.019	-0.04696
m69	-0.05962	-0.02697	0.09322	-0.06262	-0.01618	-0.04949	-0.00352	-0.01672
m70	-0.07383	0.045755	0.063843	-0.02643	-0.07849	-0.07383	-0.15279	0.177875
m71	-0.11252	0.025184	-0.07723	-0.07238	0.004262	-0.03684	0.130701	-0.09268
m72	-0.0882	0.023729	-0.06537	0.071745	-0.09022	0.14786	0.105687	-0.09164
m73	-0.07787	0.038577	0.035587	0.048257	-0.09288	0.076342	0.02075	-0.06198
m74	-0.09121	-0.07948	0.145832	0.033976	-0.06013	0.186573	0.144611	-0.07135
m75	-0.11316	-0.09812	0.004285	0.062047	-0.06321	0.142309	0.059013	0.045833
m76	-0.11059	-0.09475	-0.04441	-0.08635	0.078506	-0.03995	-0.1266	0.010356
m77	0.024147	0.018758	0.120608	0.10057	-0.08418	-0.11315	0.129187	-0.03218
m78	-0.08429	0.202351	-0.09088	-0.06586	-0.0443	0.047955	0.162884	-0.16746
m79	-0.0192	0.129534	-0.15636	0.000708	0.049079	-0.02277	0.093469	0.027419

m80	0.082728	-0.05537	-0.14858	-0.08606	0.052608	-0.16639	0.008458	0.15225
m81	-0.00807	0.111324	0.043162	-0.0837	0.057444	0.000482	0.0461	-0.06979
m82	0.009485	0.003117	-0.14928	-0.05723	-0.01881	-0.00875	-0.03965	-0.14405
m83	0.05577	0.008916	0.002467	0.063735	-0.04708	-0.03669	0.083706	-0.12993
m84	-0.10908	0.057223	-0.06735	-0.03854	0.050572	-0.00709	-0.19911	0.201876
m85	-0.09102	0.166721	-0.12025	-0.03855	0.050295	-0.08753	0.149809	-0.04806
m86	-0.12095	-0.052	-0.02816	0.106492	0.031284	-0.18811	0.070877	-0.03354
m87	-0.07578	-0.04736	-0.03758	-0.01982	0.102522	0.029783	-0.0339	-0.04648
m88	-0.12079	0.043322	-0.18185	-0.10961	-0.03748	0.054643	-0.00531	0.114801
m89	0.057531	-0.01825	-0.01519	-0.10647	0.114778	0.016364	0.056459	-0.17139
m90	0.101349	0.040633	-0.04539	-0.03178	0.095667	0.015777	-0.1431	0.026858
m91	-0.08128	-0.08775	0.10879	-0.11664	-0.08626	0.132678	-0.04839	0.120107
m92	0.007545	0.077861	-0.04297	0.104106	-0.06324	0.003034	0.053974	-0.11726
m93	-0.06683	0.08184	0.146878	-0.01054	-0.03582	-0.01019	-0.11569	0.164198
m94	0.059424	-0.0536	0.021976	-0.02096	-0.00557	-0.12679	-0.02561	0.204676
m95	0.029178	-0.08334	0.156222	0.065312	-0.0498	-0.0502	-0.18746	0.209888
m96	0.026538	-0.14251	-0.00905	-0.02785	0.089179	0.009365	0.006642	0.076946
m97	-0.03217	-0.06972	0.019193	-0.05051	0.023543	0.020722	0.044338	0.058681
m98	0.092606	-0.1804	0.129092	0.094195	0.032475	0.090637	-0.12893	0.174113
m99	0.049825	-0.0586	0.033923	-0.0911	0.043446	0.076758	-0.15108	0.191162
m100	-0.09597	0.074065	-0.0344	0.0198	0.068966	-0.00695	0.025578	-0.07318
m101	-0.05015	-0.00231	-0.07027	0.082585	0.021787	-0.02908	0.00243	0.006746
m102	-0.11258	-0.12429	0.135736	0.08398	-0.03843	0.085734	-0.12381	-0.07179
m103	-0.03027	0.141311	0.070473	0.088029	-0.05643	0.033492	-0.00879	-0.07081
m104	-0.05604	0.211456	-0.08441	0.064379	-0.06786	-0.1546	0.214083	-0.25354
m105	-0.0132	0.167072	-0.07014	0.011323	0.079471	-0.02041	-0.09991	0.084052
m106	-0.09716	-0.1408	0.048901	-0.05433	0.100821	0.04874	-0.06713	-0.00636
m107	-0.07101	-0.05348	-0.02348	-0.0884	0.026173	0.120708	-0.06182	0.019118
m108	0.038903	-0.01942	-0.07547	0.002218	-0.05732	0.120257	-0.03762	-0.08006
m109	0.050981	-0.15587	-0.04203	0.032513	0.075534	0.160594	-0.13158	0.055311
m110	-0.10869	-0.1367	-0.13462	-0.04799	-0.00322	0.10946	-0.08706	-0.05506
m111	-0.07474	0.05	0.111723	-0.0528	0.001157	-0.06404	0.000863	0.064737
m112	0.029634	0.007462	0.033793	0.032293	-0.08124	0.037871	0.080676	-0.09784
m113	-0.00031	0.153901	0.019171	0.094579	0.092863	-0.1122	-0.11913	0.102429
m114	0.086506	-0.14533	0.071715	0.090224	-0.02712	0.025204	0.133166	-0.07661
m115	0.088245	-0.01462	-0.14858	0.030476	-0.08806	-0.13792	0.160196	-0.15043
m116	0.041038	-0.23777	0.033593	-0.00099	-0.02756	-0.02518	0.06814	-0.06071
m117	0.078541	0.062643	-0.17862	0.00476	0.067277	-0.02556	-0.06622	-0.13032
m118	-0.10406	0.184303	0.070375	0.112808	0.090081	0.062741	-0.03825	0.08479
m119	-0.08654	0.010384	-0.08001	-0.04442	0.107746	0.029664	0.130012	-0.07051
m120	-0.00242	-0.02705	0.061134	0.070688	-0.07168	-0.00167	0.071694	-0.14254
m121	-0.07776	-0.05346	0.161848	-0.03027	-0.04195	0.199045	-0.02489	0.115914
m122	0.084188	0.149897	-0.16714	0.034788	-0.07953	0.048709	-0.00064	-0.04388
m123	0.08239	-0.01854	-0.01346	0.036584	-0.06533	-0.03612	-0.18445	0.168758

m124	-0.021	-0.10939	0.119197	0.002644	-0.05514	-0.05509	0.008986	0.196378
m125	-0.03813	0.072041	0.102579	-0.12259	0.100221	0.110721	0.128086	-0.05926
m126	-0.04183	-0.09169	0.093277	0.02351	-0.08196	-0.02739	0.043176	-0.02727
m127	-0.0939	-0.00628	0.1265	-0.02294	0.055119	0.072345	-0.12903	0.00451
m128	-0.11465	0.193323	0.005	0.023752	0.045681	-0.00106	0.04884	-0.00923
m129	0.086419	0.009555	0.042335	-0.00495	-0.05548	-0.05927	-0.04976	-0.05628
m130	0.117094	-0.00535	-0.04805	-0.07763	-0.00882	0.028064	0.088599	-0.0011
m131	0.090938	-0.03458	-0.05202	-0.02736	0.063038	-0.04259	0.051659	-0.00193
m132	-0.04654	0.096698	-0.03803	0.065152	0.062924	-0.00746	0.089805	-0.11299
m133	-0.04471	0.082291	-0.04344	-0.07371	0.069569	-0.06006	0.07081	-0.0045
m134	0.083886	0.054539	0.065067	0.043919	0.059493	0.058677	0.138154	-0.08621
m135	0.016551	-0.11994	0.138859	0.062444	-0.1036	-0.06375	-0.0307	0.074014
m136	-0.00771	-0.06978	0.163147	0.087453	0.051993	0.160643	-0.04773	-0.01188
m137	0.08563	-0.1122	0.06181	-0.07693	0.019716	-0.01531	-0.10929	0.120121
m138	-0.08273	0.031797	-0.04789	0.021665	-0.09834	-0.10796	-0.05752	0.111522
m139	-0.01914	-0.01318	0.041089	-0.05715	0.061134	0.012501	0.003003	-0.02938
m140	-0.05159	0.050605	0.093844	-0.0802	0.049846	0.101934	0.099436	8.00E-06
m141	0.010853	0.150127	-0.08643	0.076065	0.04779	0.144138	0.150598	-0.13196
m142	0.013081	-0.04756	0.05266	-0.06628	-0.00854	0.013138	0.098811	-0.1042
m143	-0.0745	-0.01389	-0.0081	0.035947	0.080089	0.190345	0.13403	-0.08468
m144	0.078348	-0.14846	0.104201	-0.0309	0.020167	0.220525	-0.02499	-0.06407
m145	-0.11088	-0.00608	0.02408	-0.06376	0.02286	0.113302	-0.02169	0.08155
m146	-0.09176	-0.03626	-0.00433	0.001701	-0.10898	-0.0504	-0.13361	0.129239
m147	0.089353	-0.06121	0.013872	-0.08444	-0.02997	0.052459	0.13968	-0.04255
m148	0.109552	0.002106	0.01018	0.086845	-0.0532	-0.08796	0.000757	-0.02549
m149	-0.0524	-0.03404	-0.05632	-0.02729	0.100767	-0.15185	0.044943	0.104247
m150	0.106185	-0.13386	0.074587	-0.05527	-0.03412	0.052918	-0.07303	0.153259
m151	-0.06613	-0.08775	0.067397	0.085977	-0.04971	-0.07403	0.057181	0.069637
m152	-0.00694	-0.04498	0.104031	0.04118	0.018208	-0.02146	0.071563	-0.08961
m153	-0.04039	-0.01899	0.095736	-0.12407	-0.01494	0.211567	-0.0417	-0.10655
m154	-0.10515	-0.13336	0.04089	-0.07532	-0.03158	-0.05835	0.002238	-0.01447
m155	0.102504	-0.11864	-0.03959	0.103873	-0.0162	0.052708	0.062626	0.055582
m156	0.008976	0.147279	-0.07134	0.065976	-0.06542	-0.02095	-0.03107	-0.02666
m157	-0.03799	-0.00748	0.091412	-0.04899	-0.00367	0.164482	-0.06872	-0.11732
m158	0.03164	-0.09098	-0.00557	0.107128	-0.07852	0.005436	-0.0694	0.068533
m159	-0.09404	-0.08249	0.085009	0.105063	-0.00469	-0.05401	-0.19505	0.099084
m160	-0.03058	-0.08948	0.051322	-0.01413	-0.02758	-0.02258	-0.06778	0.074009
m161	-0.00675	0.06796	-0.15253	0.018185	0.00086	-0.04564	0.079316	-0.09922
m162	-0.11178	0.086091	0.082702	0.07898	-0.07515	0.018436	-0.02085	0.130221
m163	-0.05199	-0.03408	0.132344	0.042243	0.034463	0.102202	0.033097	-0.0658
m164	-0.01991	0.000363	-0.1025	0.052658	-0.10142	0.007888	-0.12609	0.122167
m165	0.037444	-0.0922	0.039321	-0.02644	0.004581	-0.0218	0.086421	-0.05033
m166	0.109235	0.051357	-0.06135	0.078811	-0.08694	-0.09012	0.06306	0.196015
m167	-0.00893	-0.12796	-0.01438	0.093675	-0.05671	-0.02022	-0.03823	0.094373

m168	-0.00531	0.002407	-0.06055	-0.01901	0.054756	0.035993	-0.06451	0.196188
m169	0.06155	0.041929	-0.16933	-0.00023	0.044379	-0.07991	-0.07497	0.034276
m170	-0.00773	0.068398	-0.02846	0.053574	0.069459	0.091944	0.021441	-0.08682
m171	0.062975	-0.11827	0.078751	-0.09223	0.085041	-0.11715	-0.0496	0.140521
m172	0.056312	0.005246	-0.0994	-0.01556	0.041978	0.012865	-0.12067	0.147475
m173	-0.06291	0.011801	-0.05263	0.092024	0.010947	0.026079	0.04617	-0.07359
m174	-0.09282	-0.03204	0.03129	-0.05953	0.091248	0.15952	0.023895	-0.0242
m175	-0.02116	-0.0405	-0.08191	-0.06083	-0.04587	-0.1466	0.023969	-0.03254
m176	0.024744	-0.09014	0.0867	0.094142	0.075605	0.013513	-0.04549	0.063626
m177	-0.00538	0.098362	0.018043	0.010002	0.052819	-0.06013	-0.04214	-0.06352
m178	-0.02395	0.004281	-0.05254	0.086375	-0.03791	-0.13315	0.123951	-0.02337
m179	0.026742	-0.18394	0.0775	0.048976	-0.09465	-0.16733	-0.17441	0.178207
m180	-0.08385	-0.06655	0.025996	-0.089	0.052687	-0.06532	-0.00155	-0.15494
m181	0.013696	-0.05974	-0.04683	0.098497	-0.04163	0.018111	-0.03313	-0.02593
m182	-0.07167	0.050256	0.059243	-0.08153	-0.07143	-0.00316	-0.06044	-0.04605
m183	-0.09979	-0.07736	-0.05977	0.104516	-0.09795	-0.09099	0.043167	0.075002
m184	-0.1162	0.185614	-0.07255	0.052322	-0.0155	-0.07084	0.103459	0.046562
m185	-0.00676	-0.05893	0.04142	-0.06691	0.107566	0.024315	0.126715	-0.10408
m186	-0.0323	-0.07583	0.057719	0.041203	0.075128	-0.09458	-0.10237	0.068298
m187	0.106982	0.001854	0.036146	0.00733	-0.03103	0.05988	0.095286	-0.09517
m188	0.047101	0.146475	0.050695	0.104768	0.062167	-0.15612	0.029016	-0.11282
m189	-0.07975	-0.03836	-0.03283	0.006341	0.079114	0.061125	-0.01407	0.03431
m190	-0.05874	-0.14111	0.024055	-0.06081	0.027658	-0.04011	0.001282	0.058581
m191	0.051246	-0.13955	0.105102	0.00745	-0.06343	0.073804	-0.01359	0.046266
m192	0.080128	-0.01828	0.007853	-0.0962	0.015385	-0.00402	0.143126	-0.02092
m193	-0.01232	0.054162	-0.01086	0.10682	-0.11151	-0.03514	0.122043	0.044188
m194	-0.11953	-0.07853	0.039391	0.071692	0.078647	-0.01762	-0.04882	-0.05419
m195	0.098966	-0.01398	0.029419	0.010998	0.099532	0.074233	-0.12481	-0.11483
m196	0.093465	0.024142	0.019355	0.104805	0.056078	0.092681	-0.19045	0.064846
m197	0.014712	-0.04078	0.004324	-0.07377	0.085761	-0.16507	0.032513	-0.04874
m198	0.070144	-0.06969	-0.07729	-0.01125	-0.1105	-0.06535	-0.06502	-0.05606
m199	-0.11841	0.026322	-0.07618	-0.00452	-0.09312	-0.21341	0.017056	0.050623
m200	0.054784	0.127839	0.009438	0.077583	0.069672	0.025299	-0.03954	0.009425
m201	0.09846	0.097808	0.137241	-0.10938	-0.03417	-0.05615	-0.02717	-0.00837
m202	-0.05779	-0.08967	0.099921	-0.05406	-0.01686	0.027353	0.031675	0.089508
m203	-0.1092	0.038321	-0.08907	0.053397	-0.01105	0.057994	-0.02151	-0.21118
m204	-0.02701	-0.04776	-0.05299	0.023251	-0.05781	-0.04079	-0.06508	0.114715
m205	0.09067	-0.03612	0.050748	-0.09035	0.029943	-0.05312	-0.11772	0.154026
m206	-0.11485	-0.06976	-0.03082	0.036569	0.092021	0.136844	0.154222	-0.12076
m207	-0.01416	0.068178	0.037258	-0.04499	0.009055	0.028473	0.15861	-0.18437
m208	-0.03762	0.11644	0.003845	-0.08426	-0.02981	0.043491	-0.07288	-0.03241
m209	0.069773	-0.02605	-0.02258	0.094457	0.042422	0.033535	0.017578	0.156171
m210	0.021114	-0.12861	0.165283	0.050426	-0.10087	0.072673	-0.03616	0.119457
m211	-0.03959	0.0199	-0.01833	-0.06187	-0.03177	0.086334	0.124698	-0.01722

m212	0.039688	-0.19074	-0.01019	-0.08629	0.044636	0.093276	-0.02565	-0.05872
m213	0.093188	-0.03106	-0.02531	-0.02727	0.092391	-0.1422	0.123937	0.01428
m214	0.056095	0.016039	0.036139	-0.01641	0.087823	0.107564	-0.00704	-0.01975
m215	0.118753	0.181771	-0.07817	0.105875	0.054105	-0.09059	-0.02773	0.199007
m216	0.088059	0.167192	-0.11196	0.117699	0.076319	-0.10229	-0.01062	-0.06058
m217	0.117362	0.045981	-0.0004	-0.05596	0.013751	-0.07535	-0.09869	0.033783
m218	0.061232	-0.01973	0.024342	-0.05304	-0.09878	-0.01711	-0.12411	0.242383
m219	-0.04896	0.054499	-0.09229	0.006557	-0.00117	0.033718	-0.04825	0.06933
m220	-0.0964	0.053514	0.097939	0.110915	0.106884	0.102169	-0.01165	0.132233
m221	-0.10655	-0.07347	0.094946	0.050048	-0.02591	-0.1285	0.18818	-0.10478
m222	0.116116	-0.13154	0.106265	0.046316	-0.05645	0.078777	0.108011	-0.05106
m223	0.112623	0.005476	0.139876	0.026418	-0.04168	0.107216	0.038154	0.173371
m224	-0.00626	-0.07826	-0.08224	0.075811	0.042523	0.027832	0.032622	-0.0513
m225	0.015892	0.057042	0.125268	-0.01648	0.056712	0.001856	0.066322	-0.16366
m226	0.016206	0.075996	-0.00928	0.001545	0.022062	0.00875	0.089718	-0.01831
m227	-0.05881	-0.02479	0.018164	0.098949	0.015536	0.145555	-0.14116	0.077786
m228	-0.11724	0.222357	0.001876	-0.09864	0.085033	-0.08122	-0.0071	-0.05011
m229	0.108857	0.090116	-0.05741	-0.05532	0.051711	0.103046	-0.00089	-0.09986
m230	-0.00817	0.070343	0.146516	0.104237	-0.07534	0.010526	0.031583	0.154874
m231	0.001017	0.10975	0.071509	-0.07212	0.092851	-0.08414	0.006062	0.093683
m232	-0.11562	-0.00459	0.021244	0.09833	0.083921	0.096738	0.064782	-0.03008
m233	0.049234	0.020528	-0.04566	-0.08623	0.066447	-0.07935	0.045723	-0.01872
m234	-0.00604	-0.09019	0.08231	-0.06285	-0.01957	0.155656	-0.03994	-0.06207
m235	-0.04875	-0.07493	0.064629	0.017138	0.018304	0.066406	0.094539	0.016671
m236	0.112071	-0.12509	0.048111	-0.00264	0.066909	0.070341	-0.16722	0.009897
m237	0.032022	-0.01258	-0.06845	-0.02719	0.044783	0.063548	-0.05767	-0.00576
m238	-0.01885	0.023176	-0.0782	0.043912	-0.04835	-0.09093	-0.0206	0.017709
m239	-0.0714	-0.04349	0.057587	0.065753	0.034039	-0.00346	0.004729	-0.01947
m240	0.11971	-0.03994	0.124199	0.062001	0.016267	-0.01749	0.095455	-0.07194
m241	-0.03739	-0.14396	0.134213	-0.03899	0.0477	-0.07879	-0.04796	0.058814
m242	-0.0327	-0.01927	0.201293	0.020318	0.060467	0.131893	0.042221	-0.0246
m243	0.104027	0.161656	-0.10229	-0.00743	-0.00531	-0.05539	0.023073	-0.05018
m244	0.013315	-0.1114	-0.00121	0.092365	-0.06	0.022818	0.01515	-0.18324
m245	0.109056	0.030226	0.092159	-0.04681	-0.04432	-0.07733	0.009708	-0.00965
m246	-0.05513	0.181948	-0.10679	-0.05618	0.099784	-0.10301	0.002771	-0.10301
m247	0.070564	-0.01189	-0.02731	-0.07338	-0.09694	-0.07928	-0.08045	0.039215
m248	-0.09606	0.069971	0.051416	-0.08876	-0.06873	-0.08563	0.185387	-0.15207
m249	-0.09968	0.10929	-0.11383	-0.07982	0.078341	-0.18205	0.011021	0.134106
m250	0.120165	-0.04191	0.134462	-0.10436	-0.03458	0.183372	0.018593	-0.06154
m251	0.013826	0.016684	-0.02525	0.030479	0.07656	-0.09275	0.134881	0.063879
m252	-0.0099	-0.12295	-0.06926	-0.13001	0.006729	-0.00383	0.101897	-0.22359
m253	-0.06684	-0.01776	-0.0859	0.057289	0.054937	0.008876	0.073758	-0.06223
m254	-0.04286	0.03246	0.048177	-0.06027	-0.11594	-0.04249	-0.09099	0.007273
m255	-0.09252	0.141708	-0.15465	-0.12832	-0.06605	0.15052	-0.10098	-0.02541

m256	-0.07374	-0.24876	0.127073	-0.0249	-0.02613	-0.03023	-0.02186	0.141687
m257	0.102711	0.115203	-0.05811	0.029553	0.078701	-0.06263	-0.02067	-0.04089
m258	0.010365	-0.03635	0.066143	0.095774	0.023384	0.018824	0.103834	0.059977
m259	-0.08052	-0.22168	0.083868	-0.0112	0.121158	-0.00743	-0.11285	0.153709
m260	0.030269	0.096823	-0.00622	0.001839	-0.01678	0.103639	0.086854	-0.24036
m261	-0.04012	0.03835	-0.07156	-0.02812	-0.05828	-0.12343	-0.19024	0.081853
m262	-0.03835	-0.0044	-0.20084	0.103101	-0.07632	-0.10777	0.084754	0.0678
m263	0.094357	-0.01289	0.149662	-0.08727	-0.00918	-0.02209	0.007634	0.045246
m264	-0.094	0.069091	-0.0592	-0.01671	-0.02937	-0.20595	-0.09009	-0.03805
m265	-0.1065	-0.09783	-0.01855	0.018934	-0.02874	0.00521	0.149569	-0.15696
m266	-0.00808	-0.00093	-0.12728	0.082183	0.094941	-0.04599	0.09025	-0.03813
m267	-0.01859	0.167594	0.016047	0.02436	0.037189	0.011014	-0.01436	0.052834
m268	0.09832	0.002822	-0.1816	0.022177	-0.08769	-0.12862	0.064638	0.071541
m269	-0.1105	-0.02802	0.132203	0.034972	-0.03564	0.025554	-0.02979	-0.16557
m270	0.031357	-0.11421	-0.03778	-0.10371	-0.04818	0.139014	-0.07942	0.05801
m271	0.022611	-0.17031	0.074465	-0.04588	0.100061	-0.02513	-0.11816	0.035952
m272	-0.0697	0.002131	0.020829	-0.07408	0.071317	0.073916	0.002573	0.16965
m273	-0.11581	0.013315	-0.12067	-0.03314	0.046101	0.034335	-0.00341	-0.05682
m274	-0.09219	-0.03618	0.085598	0.019481	0.049912	-0.06312	-0.02947	-0.07897
m275	0.062094	-0.05816	-0.01547	-0.03405	0.053347	0.028504	-0.05425	0.018962
m276	0.073422	-0.01513	0.083386	0.020736	-0.03365	0.08345	-0.08096	0.095547
m277	0.08542	0.0682	0.034886	-0.07673	0.093969	-0.06387	0.059712	-0.01437
m278	0.113852	0.168628	-0.10398	0.010584	0.074845	-0.11183	-0.09323	0.133498
m279	-0.09028	-0.01801	-0.16602	0.068675	0.062285	-0.01057	-0.0506	-0.04308
m280	0.087555	-0.07561	-0.00204	-0.00302	0.108224	0.079399	-0.1553	0.127853
m281	-0.04679	-0.00215	0.061976	0.060044	0.001924	0.048996	0.159912	-0.03563
m282	0.096162	-0.12613	0.152249	-0.03306	0.069166	0.048158	0.127113	0.018433
m283	-0.0153	0.036733	-0.02533	0.016533	0.095334	-0.01985	0.033334	0.187679
m284	-0.04223	-0.11032	0.10632	0.02024	0.082449	-0.00285	-0.07408	0.215856
m285	-0.0407	0.041288	-0.04225	-0.10095	0.017028	0.128156	0.015745	0.068581
m286	-0.04912	0.093074	-0.00353	-0.03462	0.089324	0.160007	-0.14604	0.05697
m287	0.115533	0.161537	0.042027	0.030013	0.060981	-0.08764	-0.14864	0.160963
m288	-0.00391	0.0198	-0.03927	0.046486	-0.05527	0.116929	-0.13715	0.140137
m289	-0.01131	0.023653	-0.05682	-0.10915	-0.06695	-0.05797	-0.00387	-0.0843
m290	-0.10837	-0.16104	0.153876	-0.07934	-0.06628	0.051153	0.098871	-0.13148
m291	0.10029	0.151137	0.042693	-0.07473	-0.06439	-0.083	0.114148	-0.20305
m292	0.083258	-0.17366	0.16717	-0.06633	-0.07321	-0.02531	0.016249	-0.00761
m293	-0.07149	0.031997	-0.03395	-0.02087	0.054143	0.111393	-0.03378	-0.05813
m294	0.102966	0.133254	0.107415	0.024686	0.067482	-0.03562	0.010343	-0.00894
m295	-0.06353	0.004572	-0.07918	0.102829	0.071568	-0.02114	0.057103	-0.06039
m296	0.028838	-0.0583	0.107998	0.048635	-0.02823	0.093952	0.076638	-0.0957
m297	0.000422	-0.07588	-0.03726	0.11693	0.098247	0.014202	0.00957	0.099484
m298	0.009365	0.14729	-0.058	0.059593	-0.10146	-0.03288	-0.11813	0.088106
m299	0.014229	3.11E-05	-0.11831	-0.09693	-0.06235	-0.08073	-0.05126	-0.0547

m300	-0.09113	0.224715	-0.03481	-0.05153	0.055378	-0.09228	0.147498	-0.19674
m301	0.109273	-0.00029	-0.06547	-0.02908	0.00301	-0.08071	-0.04397	-0.06106
m302	-0.09113	0.112552	-0.08809	-0.00604	-0.07837	-0.02909	0.002982	-0.01412
m303	0.032915	-0.07784	-0.01193	0.106693	-0.08865	-0.011	-0.08616	0.115649
m304	0.024318	-0.08488	0.090957	-0.01677	-0.10766	0.029079	0.123983	-0.08446
m305	-0.09214	-0.01751	0.050122	0.103907	0.011888	-0.05836	-0.08145	0.098823
m306	0.098773	0.015174	-0.03412	0.03274	-0.03415	0.092658	-0.05798	-0.09872
m307	0.106728	-0.02537	0.081697	0.088464	-0.10046	-0.08882	0.020795	0.119355
m308	-0.11526	0.005914	-0.16123	-0.03598	-0.09567	0.049919	0.013763	-0.0624
m309	-0.10855	-0.00258	-0.04549	-0.05959	-0.0621	0.107798	0.118632	-0.00655
m310	0.090097	0.008082	0.031993	-0.0962	0.03401	-0.09474	0.05078	0.16141
m311	0.042364	-0.04821	0.011449	0.100784	0.05612	-0.14185	-0.11177	0.106664
m312	0.092235	0.215741	-0.09746	-0.03543	-0.09284	-0.0465	-0.00053	0.181321
m313	0.052287	0.038863	0.106748	-0.04998	-0.07275	0.14918	-0.03727	-0.1959
m314	0.045426	-0.01109	0.125665	0.099848	0.053362	-0.0659	0.018112	-0.08612
m315	-0.11806	0.013275	-0.08799	-0.05103	-0.09539	0.022763	-0.03998	0.162691
m316	0.034867	0.093831	-0.11096	-0.01831	-0.08018	0.084922	0.083852	-0.08885
m317	0.090328	0.119016	-0.05749	-0.0203	0.086611	0.063092	0.093733	-0.06412
m318	-0.08768	-0.10366	0.104097	0.073823	-0.03722	-0.00364	-0.06388	0.092139
m319	0.061741	-0.09582	-0.00918	0.016037	0.018196	0.041395	0.04459	0.060923
m320	0.012829	0.015471	-0.06862	-0.02421	0.010684	0.010997	-0.06594	0.110737
m321	-0.10216	-0.0291	0.086624	0.077731	0.093558	0.043916	0.049617	0.04948
m322	0.070225	-0.05311	-0.16788	-0.01544	-0.0396	-0.12671	0.046224	-0.03417
m323	-0.05426	-0.00844	0.001085	0.117997	-0.11212	-0.1031	-0.00183	0.023126
m324	-0.11656	0.055699	0.053037	0.075623	0.080561	-0.1559	-0.0122	0.135336
m325	-0.08146	-0.01897	0.029125	0.017755	0.046997	0.013472	0.072506	-0.08488
m326	0.058114	-0.09357	-0.00876	-0.11643	-0.00814	-0.04556	0.022078	-0.16082
m327	-0.04061	0.083753	-0.08668	-0.06152	0.017432	-0.04955	0.020474	-0.09196
m328	0.114445	0.106987	0.071111	-0.04427	-0.0323	0.014715	0.102615	-0.01654
m329	0.093837	0.109443	-0.10479	-0.01054	0.063363	-0.21126	-0.08163	0.110117
m330	0.118981	-0.0532	-0.09596	-0.00547	-0.06026	0.125064	-0.07647	0.086671
m331	-0.11193	0.008716	-0.01274	-0.10833	0.113038	0.005531	0.002036	-0.05327
m332	-0.09344	-0.1712	-0.03398	0.005566	0.02403	-0.01726	-0.16746	0.046488
m333	0.078999	-0.12201	-0.04182	0.101618	0.050844	-0.08617	0.087905	-0.0833
m334	0.088104	0.180521	0.102491	-0.08121	0.07677	0.081633	-0.01564	0.052512
m335	0.020535	0.047884	-0.11898	-0.09233	-0.11401	0.031834	-0.12183	0.149748
m336	-0.03183	0.050608	-0.08219	-0.02792	0.044934	-0.01862	0.138645	-0.01798
m337	0.063307	-0.02968	-0.11612	0.125657	-0.03895	-0.10852	-0.07933	0.086316
m338	0.118056	0.047778	0.088834	-0.0503	0.057941	0.04883	-0.15878	0.187501
m339	-0.0517	-0.04727	-0.08524	-0.01208	0.046399	0.031422	0.06892	-0.015
m340	0.085244	0.010346	-0.01512	0.098105	-0.05538	-0.02896	-0.03117	0.167117
m341	-0.00121	0.020499	-0.09541	0.13023	0.035024	-0.17233	-0.18537	0.141468
m342	-0.02776	-0.02409	0.004716	-0.0644	0.070494	0.049825	0.132041	-0.0238
m343	0.105119	-0.06776	-0.08262	-0.1147	-0.01432	0.03504	-0.07367	-0.10411

m344	0.105995	-0.17237	0.230131	-0.09709	-0.01622	0.005846	0.138732	-0.09194
m345	-0.02766	-0.07189	-0.14183	0.022177	0.022557	-0.07774	0.054382	0.028565
m346	-0.02135	-0.19663	-0.04135	-0.04125	0.060007	0.034026	0.031511	-0.04447
m347	-0.05092	0.037096	-0.00725	-0.01094	-0.04635	-0.03887	-0.09467	0.024501
m348	0.105579	-0.05257	-0.03134	-0.05795	-0.10985	-0.13952	-0.01445	0.008714
m349	0.053614	-0.07582	-0.14134	-0.11503	-0.03083	0.005992	0.04217	-0.07412
m350	0.08668	0.034436	0.003968	-0.09702	0.014889	0.103465	-0.17694	0.153449
m351	-0.01351	-0.07976	0.023387	0.026013	0.030382	0.11509	0.059301	-0.01843
m352	0.076601	0.033262	0.023968	-0.02137	0.057682	0.090736	-0.06648	-0.05206
m353	0.001579	-0.21252	0.059744	0.076438	0.04781	0.13743	0.034316	0.045432
m354	-0.06088	-0.18344	0.113477	-0.03314	-0.00832	-0.01749	0.061304	-0.05897
m355	-0.01405	-0.05193	0.034163	-0.10048	0.028143	-0.02488	0.06464	0.036715
m356	-0.11368	0.042478	0.029377	0.079145	0.037307	-0.2086	-0.09813	0.161089
m357	-0.09305	-0.04249	0.186438	-0.09995	-0.03184	0.024029	-0.01396	0.158401
m358	-0.03149	-0.08911	-0.05522	0.104332	-0.02622	0.07142	0.051174	0.161515
m359	-0.07892	0.060885	-0.01574	-0.10823	-0.05351	0.157818	0.040788	0.038312
m360	-0.0159	-0.03863	-0.03552	-0.05156	-0.03182	-0.15554	-0.12762	0.129231
m361	0.096881	0.013259	-0.12153	-0.13196	-0.04393	0.068056	0.018218	-0.05488
m362	-0.08272	-0.01233	0.151827	0.010718	-0.04896	-0.09481	0.011139	0.044057
m363	-0.02972	0.033401	0.083864	-0.03576	0.049219	0.000668	0.002188	0.04659
m364	-0.05153	0.063914	0.012235	-0.02255	0.007867	-0.15914	0.117123	-0.07805
m365	0.03005	0.006956	-0.13589	0.027208	0.056625	0.016679	-0.15945	0.043432
m366	-0.05809	0.12108	-0.10407	-0.06634	-0.10773	-0.02832	-0.02499	-0.04159
m367	0.030953	0.117831	-0.16321	0.02167	0.084178	-0.08475	-0.05964	0.03281
m368	-0.09127	0.087561	0.158214	0.083752	0.112691	0.179214	-0.00472	0.017458
m369	-0.02649	0.130105	0.001862	0.1268	0.060296	0.055189	0.074503	0.096626
m370	-0.0157	0.085846	0.041911	-0.07639	-0.06131	-0.01407	-0.00082	0.115488
m371	-0.09137	0.095349	0.135256	0.100131	-0.10982	0.027652	0.04441	0.202002
m372	-0.11101	-0.10709	-0.01881	0.012571	0.0591	-0.13305	0.017111	0.077032
m373	-0.07481	-0.00312	0.020318	0.074332	-0.06862	0.025187	0.053117	0.083595
m374	0.106286	0.002266	-0.14811	0.028077	-0.02587	-0.08547	0.070137	0.011135
m375	-0.08836	-0.02585	0.13896	0.072177	-0.02207	-0.00621	0.059991	0.009761
m376	0.092511	0.045987	0.053545	0.099331	-0.0911	0.037787	-0.06387	-0.10538
m377	0.048089	-0.01366	0.087094	0.00561	0.114138	0.006507	-0.00413	-0.03834
m378	0.105312	0.035945	-0.11669	0.001356	0.021853	-0.05691	0.055478	-0.0015
m379	0.104454	-0.04723	0.101415	0.067631	-0.01789	0.105007	-0.09454	0.111611
m380	0.007269	0.110585	-0.11895	-0.06999	-0.02064	0.020861	-0.09824	-0.10908
m381	0.084419	-0.11663	0.01701	-0.00469	0.106434	0.025533	-0.14022	0.019963
m382	-0.08489	-0.18212	0.139581	0.099155	0.104618	0.100887	-0.0122	0.188926
m383	0.117483	-0.05899	0.001484	0.088597	0.115493	-0.02741	-0.02968	-0.02827
m384	0.002514	-0.09026	0.0461	-0.03598	-0.09449	0.057916	0.063211	-0.17321
m385	0.016257	0.07237	0.042442	-0.01283	0.041256	-0.06342	0.103304	0.021127
m386	0.114216	-0.01855	-0.06392	0.123723	0.004282	-0.14953	0.113273	0.044717
m387	0.051058	0.047532	-0.03785	-0.08727	0.002503	0.100857	-0.10328	-0.03254

m388	-0.0704	-0.12939	-0.09375	0.084735	0.018899	0.066737	0.000482	0.084912
m389	-0.08482	-0.08466	0.011783	0.105029	-0.07995	-0.16426	-0.09388	0.044492
m390	-0.04931	0.053683	-0.03867	0.079174	-0.04449	-0.20708	-0.08905	0.012384
m391	0.003625	0.057974	-0.1173	0.015561	-0.08959	-0.07997	-0.11332	0.071023
m392	0.003485	0.081667	0.077106	-0.00721	-0.0747	-0.08165	0.120774	0.060746
m393	0.064629	0.010114	0.06008	0.002122	-0.01045	-0.02177	0.08818	-0.1186
m394	-0.0084	-0.12419	-0.05499	-0.0826	-0.04048	-0.04988	-0.16518	0.035044
m395	0.061533	-0.11454	0.157574	0.081102	-0.02863	-0.02877	0.129427	0.00701
m396	0.082896	0.14936	-0.0201	0.097096	0.077805	0.10989	-0.12187	0.011535
m397	-0.07019	-0.04121	-0.02351	0.084322	-0.11575	0.056968	-0.01968	-0.01151
m398	0.08647	0.019124	-0.13752	0.008742	0.060551	-0.03712	-0.02446	0.12246
m399	-0.01403	0.113881	-0.07062	0.020076	-0.0254	-0.14317	0.037455	-0.01622
m400	0.085873	-0.09187	-0.0446	0.055275	-0.05578	-0.00829	-0.15977	0.002962
m401	-0.09851	-0.12542	0.091824	-0.02301	0.066801	0.043938	-0.02982	0.052016
m402	0.048423	0.117366	-0.02585	0.007246	-0.00939	0.039329	0.051091	0.056556
m403	-0.01705	0.096106	-0.0734	0.060185	0.092819	-0.01172	0.011321	-0.18145
m404	-0.03881	-0.09113	0.065523	0.002944	-0.10924	0.052234	-0.08868	0.107822
m405	0.063298	-0.06355	0.051948	-0.01918	-0.03609	-0.04528	0.074381	-0.11893
m406	0.014156	-0.12328	0.172858	-0.08639	0.079385	0.009831	0.042688	-0.02236
m407	0.023665	0.007465	-0.02207	0.04128	0.068644	-0.07994	0.072304	-0.12842
m408	-0.03207	0.082076	-0.02871	-0.00231	-0.05292	-0.02657	0.129919	0.021093
m409	0.083771	-0.15246	0.180614	-0.00154	0.033185	0.083887	-0.07715	0.152108
m410	-0.02648	-0.20789	0.050882	0.051335	0.108206	0.047181	-0.05795	0.06857
m411	0.081101	0.051877	-0.10351	0.029464	-0.11054	-0.04362	0.044086	-0.17
m412	0.117506	0.146362	-0.06025	0.080347	0.10284	-0.00701	0.012327	-0.05701
m413	0.092336	-0.05801	0.081955	-0.03614	-0.08757	0.063306	0.004892	-0.03524
m414	0.100022	0.073075	0.023634	0.100853	-0.06393	-0.07817	0.099639	-0.02961
m415	0.05194	-0.11207	0.014545	-0.05469	-0.02303	0.004062	0.121806	-0.14114
m416	0.110002	-0.13737	0.011762	0.053913	-0.00552	-0.03256	0.086	-0.08898
m417	-0.04983	0.039815	0.053355	-0.1144	0.002262	0.029692	0.112983	0.029479
m418	0.037424	0.122707	-0.10362	0.009232	-0.06186	-0.09294	0.032045	-0.06635
m419	0.108374	-0.08435	-0.09988	0.106745	-0.04057	-0.0349	-0.06233	0.05419
m420	-0.02091	0.11854	-0.03429	-0.08939	-0.03283	-0.09601	-0.13879	0.142643
m421	-0.01463	-0.15074	0.066666	-0.00852	0.028522	0.091022	-0.12927	0.097515
m422	-0.10007	-0.12987	0.0923	-0.02821	-0.04277	-0.03745	-0.05094	-0.06021
m423	0.085365	0.054562	0.129449	-0.05397	0.044016	0.055893	-0.08732	0.137795
m424	0.091827	0.015764	-0.01284	0.001525	-0.07612	-0.0599	-0.04405	0.155697
m425	0.03017	-0.08723	0.051968	-0.07052	-0.06821	-0.04292	-0.08003	0.037269
m426	-0.04419	0.07201	0.044534	-0.03933	0.088815	-0.03358	0.046096	-0.14662
m427	-0.02518	-0.09869	-0.0388	-0.06552	0.057363	0.105748	0.045846	-0.27628
m428	-0.10213	0.048525	-0.17154	-0.00959	0.03494	-0.1128	-0.16016	0.033681
m429	-0.10902	0.069545	0.002655	-0.06407	-0.00109	0.148772	-0.10924	-0.06836
m430	0.001131	0.038037	-0.05769	0.082339	-0.10424	-0.09423	0.131643	-0.04042
m431	-0.03615	0.070162	0.075927	-0.02794	-0.11271	0.006858	-0.12587	0.11503

m432	0.018514	-0.05917	-0.03093	-0.0408	-0.07506	0.038839	-0.02594	0.09993
m433	0.086619	0.022923	0.030247	-0.02333	-0.06473	-0.16738	-0.03724	0.002487
m434	0.111081	0.040221	-0.0242	0.093132	0.061976	0.040836	-0.0629	-0.04637
m435	0.113705	0.143958	-0.1354	0.015532	0.095948	-0.01743	-0.0727	-0.07589
m436	0.077632	0.174629	-0.0564	0.07727	-0.01564	-0.00921	-0.0531	0.116625
m437	0.002268	-0.05703	-0.10291	0.008448	-0.02793	-0.01134	0.033412	0.226603
m438	-0.0064	0.134545	-0.00435	-0.0525	-0.05839	-0.10888	-0.06379	-0.04937
m439	-0.04293	0.0333	-0.05547	0.028347	-0.08984	-0.13216	-0.10768	0.075975
m440	-0.00148	0.040295	-0.04641	-0.04915	-0.10454	-0.07955	0.009291	0.024053
m441	0.053227	-0.02388	0.041195	0.077003	-0.04078	-0.00304	-0.1008	0.039142
m442	-0.04422	-0.10829	0.148618	0.010915	0.00761	0.060705	-0.0379	0.074107
m443	0.001026	0.111533	-0.13561	0.045801	-0.01329	0.052881	-0.07908	-0.04672
m444	-0.08165	0.022077	0.055003	0.129642	-0.0083	0.003914	-0.22063	0.236478
m445	-0.06157	0.02847	-0.06854	-0.0608	0.027849	-0.01668	0.088949	-0.10127
m446	-0.04653	-0.04202	-0.00462	0.090775	0.049145	-0.02745	0.012376	0.01841
m447	-0.04415	-0.01059	-0.07659	-0.0395	0.049185	0.044565	-0.12757	0.184042
m448	-0.02938	0.110644	-0.08285	0.002798	0.103898	-0.08591	-0.04738	0.213733
m449	0.096095	-0.05009	0.017427	0.051991	-0.07474	0.037008	0.059423	-0.24496
m450	-0.01654	-0.14598	0.091957	-0.10948	-0.0549	0.115913	0.019718	-0.11902
m451	0.0795	-0.0639	-0.03622	-0.01227	0.073221	-0.04164	-0.12248	0.02961
m452	-0.01672	-0.04744	-0.07799	0.060136	0.049434	-0.07696	-0.10122	-0.01711
m453	-0.09251	0.090948	-0.0496	-0.10578	-0.00388	0.088116	-0.02981	-0.0036
m454	-0.01773	-0.1496	0.050661	0.030827	0.064376	0.072518	-0.18301	0.181275
m455	0.109827	-0.09935	0.057901	0.091723	0.050992	0.155911	0.025259	-0.0934
m456	0.015563	-0.06436	0.014049	-0.08686	0.094638	0.165259	-0.04457	-0.06531
m457	0.01868	-0.07843	0.037163	0.020942	-0.06417	0.050003	-0.04659	0.155321
m458	-0.09669	0.058797	0.060933	0.068294	-0.0889	-0.14484	0.005653	0.010102
m459	0.001701	0.003058	-0.06415	-0.07107	0.100933	-0.0115	-0.01125	-0.06427
m460	-0.11529	0.09366	-0.00053	0.091372	-0.02439	0.038428	-0.00799	0.092409
m461	-0.09533	-0.08857	0.084056	-0.0028	0.102105	0.082553	-0.03882	0.097687
m462	-0.06947	0.155838	0.039476	0.077341	0.080926	-0.03665	0.014735	0.026493
m463	0.077724	-0.02842	0.036052	-0.00903	-0.04216	0.107841	-0.15514	-0.02316
m464	0.116816	0.083271	-0.11148	0.06165	0.046556	-0.00261	-0.10046	0.104947
m465	0.057906	0.050213	0.04761	-0.08792	0.057266	0.173338	0.130845	-0.09167
m466	-0.07285	0.052879	-0.03722	-0.04895	-0.02061	0.046595	-0.00597	0.196994
m467	-0.02042	-0.12137	0.099508	0.060556	-0.05416	-0.05855	-0.1706	0.158453
m468	-0.10528	0.014798	0.021288	0.07437	0.053544	0.181852	-0.02563	0.057842
m469	-0.04672	0.027789	0.157416	0.024783	0.113755	0.137468	-0.00305	-0.09821
m470	0.113502	0.062962	-0.12875	0.026166	0.006049	-0.01836	-0.0958	0.066174
m471	0.103054	0.018651	-0.08994	0.041538	0.061872	-0.06345	-0.04988	0.029967
m472	-0.05503	-0.11125	0.142	-0.03502	0.011961	0.01186	-0.12159	0.141394
m473	0.098129	-0.04483	0.084403	0.041243	0.084743	0.177956	0.08535	-0.15316
m474	0.118834	-0.12251	0.095393	-0.06306	0.011488	0.21417	-0.03805	-0.01237
m475	0.072818	-0.00996	0.06186	0.013696	0.047982	-0.14036	0.091385	-0.06769

m476	0.038266	0.064797	-0.09046	-0.01094	-0.08179	-0.01935	-0.09586	-0.0306
m477	-0.11367	-0.03219	-0.09648	-0.07195	0.088854	0.035939	0.106508	-0.16559
m478	-0.08331	0.035087	-0.10526	-0.04498	0.033541	-0.13683	-0.12358	0.225708
m479	-0.00637	-0.16885	0.019482	0.095335	-0.03523	-0.05316	0.03865	0.146835
m480	-0.07405	0.033154	-0.03871	-0.0775	-0.07217	-0.21603	-0.06476	-0.02617
m481	-0.02966	0.047632	0.052712	0.03257	-0.08925	-0.13323	0.021575	-0.00291
m482	0.070589	0.141208	-0.10452	0.040679	-0.07636	-0.10608	0.123315	-0.04532
m483	-0.03606	0.121368	-0.07488	0.115723	0.008375	0.062617	-0.0168	0.046656
m484	0.007905	-0.04037	0.103686	-0.04405	0.009327	0.192323	-0.12572	-0.0483
m485	-0.02076	-0.01587	0.088749	-0.07061	0.101607	-0.02178	-0.01614	-0.11394
m486	-0.04609	-0.08068	0.116397	-0.01936	0.023394	0.174617	0.02403	0.085033
m487	-0.01164	0.005439	-0.06654	-0.03822	0.061596	0.042509	0.108417	-0.12088
m488	-0.09101	-0.24119	0.047386	0.080407	-0.10074	0.015106	0.13061	-0.18515
m489	0.02001	0.030301	0.077037	0.079497	-0.02133	-0.10439	-0.04667	0.135394
m490	0.013729	0.031129	-0.12045	0.022744	0.064401	-0.03773	0.046848	-0.00479
m491	0.062114	0.101187	-0.10166	-0.06426	-0.02173	-0.12481	-0.09591	0.152162
m492	0.108861	0.030383	0.046376	0.10705	0.083629	-0.10426	-0.14415	0.155891
m493	-0.03616	0.01302	0.162038	0.0119	-0.02819	0.189354	0.11764	-0.09591
m494	-0.05455	-0.11953	0.154307	-0.09221	-0.04068	0.170692	-0.04797	-0.12114
m495	0.058998	0.014686	-0.09227	-0.01265	-0.03954	0.088056	-0.00217	-0.17477
m496	0.007327	-0.12307	0.126925	-0.08925	-0.03447	-0.11532	0.143985	0.054412
m497	0.014464	0.078907	0.085945	-0.00586	0.057875	0.065487	0.0315	0.120459
m498	-0.01884	0.02802	-0.04778	0.058204	-0.01226	0.107548	-0.00299	0.160373
m499	-0.08647	-0.11416	-0.08937	-0.09907	0.043816	0.115651	-0.00494	0.140217
m500	-0.03902	0.083918	0.097579	0.040371	0.026144	-0.06609	0.079086	-0.00223
m501	-0.08178	0.027589	-0.08097	0.063435	-0.0998	-0.00125	-0.06908	-0.01733
m502	0.108663	0.188099	-0.13941	0.082069	-0.11303	-0.02304	-0.08046	0.048454
m503	0.021906	-0.06707	-0.11704	-0.10806	0.04694	0.020105	-0.08452	-0.11086
m504	0.11531	-0.05672	0.129293	0.052301	0.027591	0.009888	-0.02218	-0.08709
m505	0.03564	0.189479	-0.01717	-0.00965	0.040249	0.041759	0.138527	0.019852
m506	-0.04844	-0.00316	0.092123	0.062503	0.056942	0.086807	0.106091	-0.09043
m507	0.060318	0.116042	-0.04416	-0.12033	0.012873	-0.0422	-0.01169	-0.09939
m508	0.02286	-0.14046	0.032876	0.013737	-0.10041	-0.08014	0.001163	-0.12976
m509	0.082818	-0.15364	-0.03095	-0.098	-0.00364	-0.01186	-0.13869	0.127975
m510	0.085582	-0.02734	-0.06421	-0.08196	0.011382	0.014352	-0.11639	0.028559
m511	0.05062	-0.01022	0.15299	0.086805	0.039165	-0.01897	-0.11384	0.116763
m512	0.050387	-0.07064	0.211571	-0.03057	-0.09273	0.11637	0.005995	0.002515
m513	0.082994	-0.00347	0.000758	0.002413	-0.09597	0.044664	-0.02066	0.194306
m514	-0.00078	0.140339	0.020043	-0.07077	0.096269	-0.02585	0.051998	0.02622
m515	0.000662	-0.17879	0.089367	-0.0773	0.032803	0.14158	-0.06255	0.234544
m516	-0.01494	-0.23832	0.099586	0.06363	-0.06136	-0.06366	-0.05465	-0.00369
m517	-0.04078	0.092949	-0.03202	-0.04726	0.049552	0.001746	-0.06225	0.037305
m518	0.096978	-0.13406	0.071744	-0.04405	-0.03685	-0.12814	-0.04245	0.016817
m519	-0.06383	0.12751	-0.03443	0.041551	0.043973	-0.00951	0.024248	-0.1202

m520	0.059714	0.050357	-0.09402	-0.04625	0.011883	-0.00135	-0.05805	-0.11752
m521	-0.11319	-0.05677	0.066692	-0.0962	0.006722	-0.0789	0.112625	-0.05938
m522	0.081665	-0.01797	0.167805	-0.09789	0.087696	0.102045	-0.00572	-0.02553
m523	-0.08216	-0.03223	-0.09587	-0.07347	0.064892	-0.09392	-0.03881	0.010104
m524	0.043922	0.06178	0.043418	-0.08355	0.040213	-0.04363	0.077866	-0.114
m525	-0.01126	0.038319	-0.00354	0.050955	-0.0449	0.027616	-0.02393	-0.0619
m526	0.04405	-0.11284	0.033271	0.081853	0.049273	0.097085	-0.10019	0.086111
m527	0.048786	-0.17701	0.144393	-0.03193	0.073979	0.00875	0.076757	-0.05244
m528	-0.01851	-0.28006	-0.04898	0.069979	0.028119	-0.02007	-0.01143	-0.00018
m529	0.117298	-0.11841	0.028154	0.076319	-0.01257	0.032019	-0.10538	-0.04741
m530	0.110899	-0.10295	-0.01663	-0.03397	0.077951	-0.03332	-0.05279	-0.05392

Weight Matrix 2 of the final model used in the classification of ashes (chapter 7). It is a 4 by 531 (m by n) matrix.

Matrix 4 x 531	**n1**	**n2**	**n3**	**n4**	**n5**	**n6**	**n7**	**n8**
m1	-0.06797	-0.10678	-0.0514	-0.06773	0.045064	0.003441	-0.05059	0.041287
m2	-0.0906	0.092771	-0.06083	-0.09236	0.056607	-0.02007	-0.10513	0.071304
m3	-0.06592	0.121753	-0.10177	-0.04284	0.005493	0.113669	-0.04343	0.064908
m4	0.014781	-0.09205	-0.0777	0.026355	-0.00176	-0.09086	0.041203	-0.03467
Matrix 4 x 531	**n9**	**n10**	**n11**	**n12**	**n13**	**n14**	**n15**	**n16**
m1	0.013931	0.070319	0.006669	0.073715	0.089637	0.077926	0.055069	0.013905
m2	-0.00203	0.136188	-0.10931	0.086529	0.055308	0.068196	-0.06194	-0.06876
m3	-0.09872	-0.10326	-0.07886	0.081652	-0.04458	0.021551	-0.01191	-0.10284
m4	0.088428	-0.08781	0.008998	0.047736	0.091963	0.107634	-0.00507	-0.01419
Matrix 4 x 531	**n17**	**n18**	**n19**	**n20**	**n21**	**n22**	**n23**	**n24**
m1	8.29E-05	0.010666	0.013489	0.015844	0.064782	0.033436	0.071166	-0.11206
m2	-0.00176	0.049393	0.014341	-0.08154	-0.04652	-0.02337	-0.02693	-0.10509
m3	-0.05883	-0.03634	0.055197	0.057734	-0.06789	-0.11314	-0.02124	0.037467
m4	-0.08486	0.018442	-0.00605	-0.11573	-0.06423	0.062976	-0.06472	0.063654
Matrix 4 x 531	**n25**	**n26**	**n27**	**n28**	**n29**	**n30**	**n31**	**n32**
m1	0.063319	0.090587	-0.09705	0.016633	0.103812	0.044675	0.011921	-0.10691
m2	0.008082	0.015823	-0.01703	-0.11006	0.064668	-0.04303	-0.04909	-0.05882
m3	0.053502	0.053681	-0.11434	-0.04583	0.058883	-0.06353	0.049367	0.030955
m4	-0.07851	-0.04848	0.037972	-0.07833	0.105676	-0.03597	-0.01772	0.045275
Matrix 4 x 531	**n33**	**n34**	**n35**	**n36**	**n37**	**n38**	**n39**	**n40**
m1	0.108035	0.069515	0.101443	0.066568	-0.03268	0.094603	-0.04932	-0.06547
m2	0.079	-0.08045	0.062983	0.12163	-0.0141	0.090786	0.022056	0.10004
m3	-0.09768	0.062304	-0.01141	0.088588	0.02423	0.016741	-0.01659	0.08334
m4	0.065886	0.036217	-0.06597	0.033332	-0.10387	-0.02996	0.013508	-0.05108
Matrix 4 x 531	**n41**	**n42**	**n43**	**n44**	**n45**	**n46**	**n47**	**n48**
m1	0.041267	0.014247	-0.00299	-0.08134	-0.11723	0.101756	-0.04262	-0.04803
m2	-0.12187	0.097295	-0.09723	0.054628	0.088502	-0.11152	-0.03984	-0.07511
m3	0.082006	-0.00099	0.073503	0.087113	0.014216	-0.07966	-0.04911	0.065445

m4	0.088609	0.105376	-0.01429	-0.05849	-0.01918	-0.11296	0.05383	-0.01471
Matrix 4 x 531	**n49**	**n50**	**n51**	**n52**	**n53**	**n54**	**n55**	**n56**
m1	-0.00155	-0.0076	-0.06731	-0.10107	0.022696	-0.07885	-0.11846	0.024665
m2	0.078782	-0.09111	-0.06057	-0.03505	0.123312	0.041746	0.054092	0.066641
m3	-0.04079	0.006987	0.099443	-0.00428	-0.00866	0.009321	-0.10257	0.01146
m4	0.105481	-0.04646	-0.07704	-0.00696	-0.06399	-0.00565	-0.08235	0.082142
Matrix 4 x 531	**n57**	**n58**	**n59**	**n60**	**n61**	**n62**	**n63**	**n64**
m1	0.030782	0.097566	0.109608	-0.05157	0.022591	0.056421	0.067472	0.091351
m2	0.078292	0.079311	0.036941	0.091261	0.066191	0.095219	-0.1013	-0.02593
m3	-0.10452	-0.09162	0.109369	-0.10806	0.034598	-0.11254	0.042474	-0.03489
m4	0.068359	0.092328	-0.01054	-0.02672	-0.0273	0.094209	-0.08234	0.056611
Matrix 4 x 531	**n65**	**n66**	**n67**	**n68**	**n69**	**n70**	**n71**	**n72**
m1	-0.0624	-0.07914	-0.01289	-0.11543	-0.02708	0.031129	-0.05299	-0.01294
m2	-0.06556	-0.10143	0.035474	0.049274	0.00174	-0.09969	0.019243	-0.08545
m3	0.089973	0.067311	0.091913	-0.03931	-0.02715	-0.05264	-0.07924	-0.04316
m4	0.105114	-0.06089	-0.06044	0.040645	0.016291	0.08744	-0.13217	-0.00373
Matrix 4 x 531	**n73**	**n74**	**n75**	**n76**	**n77**	**n78**	**n79**	**n80**
m1	0.053352	0.022751	-0.01537	-0.11303	-0.0518	-0.06764	0.110348	0.092615
m2	-0.07278	-0.09644	-0.08116	-0.04692	0.013997	-0.09534	-0.0988	-0.04473
m3	0.048882	-0.00362	0.109909	0.03243	-0.0198	-0.0434	0.019396	-0.10298
m4	-0.0861	0.084591	0.02437	-0.03759	-0.0732	0.092469	-0.00218	-0.08379
Matrix 4 x 531	**n81**	**n82**	**n83**	**n84**	**n85**	**n86**	**n87**	**n88**
m1	0.023151	-0.00772	0.086858	0.064305	-0.05852	0.101766	-0.01788	0.021281
m2	0.091143	-0.0939	0.014029	-0.08943	0.083746	-0.09327	0.060543	-0.05676
m3	-0.07263	0.079196	0.074836	-0.10247	-0.10352	-0.08569	-0.0636	0.035853
m4	-0.03699	-0.07908	0.102766	0.08512	-0.09348	-0.04773	0.113086	0.055109
Matrix 4 x 531	**n89**	**n90**	**n91**	**n92**	**n93**	**n94**	**n95**	**n96**
m1	0.077471	0.007335	-0.05537	-0.10068	0.005255	-0.0902	-0.04456	-0.10766
m2	0.111681	-0.05378	0.039675	0.069666	-0.09303	-0.00881	0.06885	0.105621
m3	0.048754	0.020792	-0.07937	0.112733	-0.04665	-0.07239	-0.05791	0.025599
m4	-0.01945	-0.01051	0.023797	-0.08116	-0.00283	-0.04726	-0.04998	-0.02626
Matrix 4 x 531	**n97**	**n98**	**n99**	**n100**	**n101**	**n102**	**n103**	**n104**
m1	-0.04781	-0.026	-0.0816	-0.10308	0.044479	-0.00027	-0.0935	0.052034
m2	0.078108	0.037245	0.107492	0.005113	0.011814	0.001021	0.025094	-0.03213
m3	0.054229	-0.07222	0.071772	-0.06405	0.053387	-0.06315	0.108006	0.00836
m4	0.097536	0.091291	-0.07172	-0.11945	0.019173	-0.00964	0.035096	-0.00222
Matrix 4 x 531	**n105**	**n106**	**n107**	**n108**	**n109**	**n110**	**n111**	**n112**
m1	0.100855	0.069498	-0.03517	-0.04882	0.048951	-0.02715	0.056866	-0.02311
m2	-0.12066	0.010269	0.054181	-0.0644	0.072068	0.103021	0.084846	0.053293
m3	-0.07952	-0.12106	0.085219	0.041371	0.101285	0.070899	0.111476	0.03694
m4	0.090251	-0.04437	0.06903	-0.10503	0.024731	-0.10377	0.05148	-0.00306
Matrix 4 x 531	**n113**	**n114**	**n115**	**n116**	**n117**	**n118**	**n119**	**n120**
m1	0.068583	0.057972	-0.09967	0.112251	-0.06414	0.102696	-0.00221	0.08458
m2	0.012978	0.058537	-0.11347	-0.03074	0.030719	-0.0057	-0.04096	-0.0673

m3	0.037734	-0.05796	0.046318	0.001392	0.098999	-0.01251	-0.09797	0.098927
m4	0.036562	-0.08987	0.014398	0.08845	0.114411	0.012188	-0.03305	-0.05459
Matrix 4 x 531	**n121**	**n122**	**n123**	**n124**	**n125**	**n126**	**n127**	**n128**
m1	-0.08548	-0.08772	0.131852	-0.0013	-0.0935	0.002334	-0.00042	-0.09031
m2	-0.07925	-0.01649	0.024846	0.123104	0.03606	-0.09557	0.043715	0.044879
m3	0.078571	0.088739	0.028615	-0.06138	-0.07764	0.075732	0.108212	-0.03192
m4	-0.0449	-0.06555	-0.00492	-0.01188	-0.00268	0.001307	-0.04553	0.002303
Matrix 4 x 531	**n129**	**n130**	**n131**	**n132**	**n133**	**n134**	**n135**	**n136**
m1	0.041239	-0.0276	0.003382	-0.04705	-0.01616	-0.04236	-0.00817	-0.118
m2	-0.10298	-0.05014	-0.00612	-0.04994	-0.09726	-0.07441	-0.11628	0.060629
m3	-6.24E-05	-0.0878	0.050788	0.015888	0.04607	-0.11054	-0.02033	-0.03792
m4	-0.09143	-0.05962	-0.08135	0.077928	-0.03484	0.083723	0.089562	0.029856
Matrix 4 x 531	**n137**	**n138**	**n139**	**n140**	**n141**	**n142**	**n143**	**n144**
m1	-0.0983	-0.04911	0.028252	-0.08056	-0.02235	0.03796	0.07986	-0.02658
m2	-0.02876	0.073231	0.047345	-0.03943	-0.06666	-0.11822	-0.07605	-0.04958
m3	-0.00103	-0.09361	-0.10633	0.008781	-0.0013	0.076291	0.048274	0.127431
m4	-0.10882	0.07919	-0.09394	0.05567	-0.03309	-0.08833	0.019	-0.00442
Matrix 4 x 531	**n145**	**n146**	**n147**	**n148**	**n149**	**n150**	**n151**	**n152**
m1	-0.11187	-0.0925	-0.08255	-0.06206	-0.01651	0.06833	-0.12182	-0.02278
m2	-0.05262	0.085413	0.123638	-0.06958	-0.03388	0.086	0.021775	0.016867
m3	0.097884	-0.00301	-0.0133	-0.02339	-0.02842	-0.06687	-0.06829	-0.06019
m4	-0.08108	-0.051	0.068847	0.114859	0.013296	-0.03403	0.018811	0.038584
Matrix 4 x 531	**n153**	**n154**	**n155**	**n156**	**n157**	**n158**	**n159**	**n160**
m1	0.005296	0.003458	-0.07702	-0.0336	0.101447	0.005998	-0.10683	-0.08129
m2	-0.02411	0.012096	0.036491	0.038502	-0.00841	-0.07877	0.05403	0.077804
m3	0.052403	0.11938	0.024746	-0.00811	-0.00849	0.082358	-0.01136	-0.10833
m4	0.01455	-0.08028	0.042055	0.067447	-0.08366	-0.07667	-0.03132	-0.09841
Matrix 4 x 531	**n161**	**n162**	**n163**	**n164**	**n165**	**n166**	**n167**	**n168**
m1	-0.08224	0.107998	-0.06934	-0.07146	-0.0022	-0.05159	-0.05251	-0.00872
m2	0.060266	-0.04688	-0.00477	-0.10205	0.023288	-0.02781	0.068062	0.101878
m3	-0.05746	-0.11345	-0.07751	-0.00177	0.001397	0.04263	-0.09213	-0.10146
m4	-0.0842	0.088925	-0.07943	-0.04053	-0.03685	0.067106	0.100032	0.081156
Matrix 4 x 531	**n169**	**n170**	**n171**	**n172**	**n173**	**n174**	**n175**	**n176**
m1	-0.02079	0.088378	0.06563	-0.06466	-0.03441	0.012407	-0.02835	0.085309
m2	0.048268	0.109843	-0.08695	0.048932	0.086678	-0.01644	-0.07835	-0.00746
m3	-0.00186	0.10045	0.044461	-0.04747	-0.11892	-0.05813	0.116324	-0.04558
m4	-0.10818	0.050464	-0.02758	0.019982	-0.10623	0.045625	0.008536	0.064685
Matrix 4 x 531	**n177**	**n178**	**n179**	**n180**	**n181**	**n182**	**n183**	**n184**
m1	-0.01719	0.08496	0.01505	-0.11142	-0.03883	0.010676	0.084086	-0.05125
m2	0.08994	-0.05289	-0.07922	0.118286	-0.00568	0.054003	-0.05835	0.084486
m3	0.115558	-0.07328	-0.00042	-0.11237	0.069334	0.000441	0.005588	-0.0521
m4	-0.02421	0.058835	0.110282	0.058798	0.099209	-0.0784	-0.10088	0.097008
Matrix 4 x 531	**n185**	**n186**	**n187**	**n188**	**n189**	**n190**	**n191**	**n192**
m1	0.073972	0.06371	-0.05546	-0.02947	0.055686	0.071484	-0.03616	-0.11672

m2	-0.04998	-0.0499	0.059235	-0.05886	-0.06386	0.055961	0.048077	0.068636
m3	0.009463	0.105561	-0.11262	0.127445	-0.10751	0.093214	0.029024	0.096415
m4	-0.0903	0.032035	-0.05219	-0.0124	0.062694	-0.03706	0.103162	0.091336
Matrix 4 x 531	**n193**	**n194**	**n195**	**n196**	**n197**	**n198**	**n199**	**n200**
m1	0.072487	0.053631	0.008545	0.054435	0.061339	-0.09962	0.065864	-0.00718
m2	-0.0146	0.002503	0.028618	0.09427	0.111799	-0.09396	0.097016	0.091155
m3	0.047934	-0.05751	-0.02644	0.09434	0.02602	-0.11926	0.001829	-0.13137
m4	0.085745	0.026865	0.072026	0.079403	-0.12253	0.072203	0.030634	0.055451
Matrix 4 x 531	**n201**	**n202**	**n203**	**n204**	**n205**	**n206**	**n207**	**n208**
m1	0.092701	-0.0672	-0.07147	0.058265	0.014599	-0.08184	-0.00559	0.011885
m2	0.002464	-0.03937	0.012812	0.009793	0.117622	0.055588	-0.08841	-0.10465
m3	-0.07592	-0.03296	0.021657	0.088915	-0.01272	-0.05715	0.052568	0.126948
m4	0.002414	-0.04532	0.035949	0.079466	0.037322	-0.0493	0.048448	0.030388
Matrix 4 x 531	**n209**	**n210**	**n211**	**n212**	**n213**	**n214**	**n215**	**n216**
m1	-0.04973	0.004774	-0.10253	0.010038	-0.08687	-0.04149	0.088774	0.0646
m2	-0.07412	0.025304	-0.01364	-0.10181	0.014873	-0.06254	0.014191	0.096732
m3	-0.10776	-0.10146	0.018212	0.030343	0.071804	-0.10037	0.069337	-0.08841
m4	0.008331	-0.04876	-0.03751	0.009975	-0.01715	-0.017	0.014626	-0.03128
Matrix 4 x 531	**n217**	**n218**	**n219**	**n220**	**n221**	**n222**	**n223**	**n224**
m1	0.118474	0.006607	-0.01081	0.027748	-0.04472	-0.09394	-0.11084	-0.10839
m2	0.074078	0.020241	0.113242	-0.00055	0.072521	-0.1301	-0.10525	0.009317
m3	-0.06728	-0.08114	-0.0879	0.039564	-0.00853	-0.07802	0.05521	-0.04275
m4	-0.00654	-0.05301	-0.01577	-0.07059	-0.02594	0.107164	0.047892	-0.00774
Matrix 4 x 531	**n225**	**n226**	**n227**	**n228**	**n229**	**n230**	**n231**	**n232**
m1	-0.0026	-0.00487	-0.03201	0.001969	0.089805	0.040524	-0.10723	-0.02309
m2	-0.08431	-0.0583	-0.05397	0.098342	-0.05179	0.032795	-0.08834	-0.02431
m3	-0.00579	0.036344	-0.06705	0.064024	-0.05814	0.074741	-0.0632	-0.0837
m4	0.019249	0.003489	0.005707	-0.0978	-0.09096	-0.10518	-0.08641	-0.09875
Matrix 4 x 531	**n233**	**n234**	**n235**	**n236**	**n237**	**n238**	**n239**	**n240**
m1	0.003836	0.089128	-0.00614	-0.05772	-0.01519	-0.0036	0.069944	0.028845
m2	-0.081	0.024203	-0.09336	0.000955	0.08473	0.045664	0.025896	0.093768
m3	-0.04478	0.074689	0.074924	0.008649	0.078202	0.025205	-0.05402	0.053882
m4	-0.07968	0.074615	-0.04955	0.005593	-0.12617	-0.04538	-0.02998	-0.02459
Matrix 4 x 531	**n241**	**n242**	**n243**	**n244**	**n245**	**n246**	**n247**	**n248**
m1	-0.08581	-0.06658	-0.08626	0.119255	0.07888	-0.00375	0.059517	-0.05682
m2	-0.06174	0.096482	-0.0843	-0.09298	0.069	-0.00106	-0.06216	0.067832
m3	0.039748	0.083588	0.068663	-0.01008	0.10401	-0.02287	-0.12895	-0.08453
m4	0.032598	0.087372	-0.0729	-0.0158	0.093087	-0.03968	-0.07574	0.03992
Matrix 4 x 531	**n249**	**n250**	**n251**	**n252**	**n253**	**n254**	**n255**	**n256**
m1	0.029291	0.08332	-0.09696	-0.00797	0.036953	0.073006	0.013995	0.10488
m2	-0.13007	0.114184	-0.10299	-0.07763	-0.07275	0.001689	0.093389	0.108055
m3	-0.04168	-0.08793	0.111364	-0.10293	0.102923	-0.07969	-0.06386	0.100065
m4	0.047533	-0.00616	-0.08372	-0.03909	0.039821	0.021274	0.073149	-0.11959
Matrix 4 x 531	**n257**	**n258**	**n259**	**n260**	**n261**	**n262**	**n263**	**n264**

m1	-0.13916	0.023151	-0.08633	-0.10381	0.103687	0.011152	0.081167	-0.11748
m2	0.098342	-0.05258	-0.04761	0.109538	-0.12174	0.095848	0.040598	0.02199
m3	0.012372	-0.10053	-0.10576	0.087806	0.098764	-0.10315	-0.09614	0.064781
m4	0.086847	0.01715	0.019534	0.035589	-0.05647	-0.00801	0.018402	-0.0374
Matrix 4 x 531	**n265**	**n266**	**n267**	**n268**	**n269**	**n270**	**n271**	**n272**
m1	0.064095	0.024367	0.101118	0.062929	0.098659	-0.04577	-0.06632	-0.05349
m2	0.03859	-0.07194	-0.02607	-0.00377	0.006312	-0.03806	0.064177	0.075142
m3	-0.10569	0.06314	0.054182	0.052681	-0.04085	0.048809	0.080202	-0.00608
m4	0.024665	-0.01169	-0.06915	-0.10986	-0.07089	0.078637	0.066359	0.021251
Matrix 4 x 531	**n273**	**n274**	**n275**	**n276**	**n277**	**n278**	**n279**	**n280**
m1	-0.04783	0.0353	0.020886	0.064626	-0.06909	0.061846	0.111998	0.047598
m2	-0.0024	0.023307	-0.00468	0.082429	0.08825	0.015857	0.091637	0.070018
m3	-0.07211	0.073866	0.000214	0.068461	0.042006	-0.02278	-0.09002	-0.00241
m4	-0.0606	0.084311	-0.01142	0.06802	0.085763	-0.02633	0.051371	0.095118
Matrix 4 x 531	**n281**	**n282**	**n283**	**n284**	**n285**	**n286**	**n287**	**n288**
m1	-0.07276	-0.00971	-0.07446	-0.00919	-0.1336	0.048334	-0.04156	0.023632
m2	0.121177	-0.06745	-0.05911	0.07867	0.030542	0.055376	0.018841	0.042469
m3	0.03484	-0.06654	0.044364	-0.05339	0.004902	0.106972	0.036957	-0.10423
m4	-0.08514	0.071165	0.055236	-0.0069	-0.07967	-0.01476	-0.10531	-0.10834
Matrix 4 x 531	**n289**	**n290**	**n291**	**n292**	**n293**	**n294**	**n295**	**n296**
m1	-0.02805	0.063994	-0.08623	0.099874	-0.13169	0.006296	0.026265	-0.02524
m2	0.072865	-0.08542	-0.02855	-0.13769	-0.0159	-0.08462	-0.04294	-0.06982
m3	0.024141	0.053037	0.128677	-0.02957	0.078742	0.104332	0.052627	-0.09052
m4	-0.11122	-0.0399	0.072371	-0.06453	0.035186	-0.03894	-0.10012	0.034723
Matrix 4 x 531	**n297**	**n298**	**n299**	**n300**	**n301**	**n302**	**n303**	**n304**
m1	-0.0434	-0.07067	-0.02121	0.048291	0.075139	0.015063	0.081441	-0.07201
m2	-0.11388	0.048965	0.014325	0.025641	-0.12866	-0.01787	0.020162	0.069806
m3	-0.01374	-0.07032	-0.09956	-0.01434	-0.09999	-0.04487	-0.08153	-0.00162
m4	-0.07708	0.065915	-0.0863	0.044886	0.036267	0.084082	-0.05669	-0.0396
Matrix 4 x 531	**n305**	**n306**	**n307**	**n308**	**n309**	**n310**	**n311**	**n312**
m1	0.04221	-0.09803	-0.00304	-0.0795	0.068911	-0.02225	-0.06674	-0.0641
m2	-0.05684	0.104093	-0.05652	0.055845	0.023186	-0.07441	0.063431	0.049388
m3	0.032624	-0.09161	-0.04655	-0.05653	-0.00384	0.099947	-0.01982	-0.08664
m4	0.049226	0.070312	-0.0411	0.073548	-0.11631	-0.0813	0.100675	0.084491
Matrix 4 x 531	**n313**	**n314**	**n315**	**n316**	**n317**	**n318**	**n319**	**n320**
m1	0.024906	0.048946	-0.04011	-0.0254	0.100558	0.097996	-0.0353	-0.01239
m2	0.060332	-0.09222	0.001682	0.041749	-0.00932	-0.02037	0.084074	0.012724
m3	-0.11791	0.075739	-0.01211	-0.11708	0.002935	0.008137	0.081438	0.006424
m4	-0.11827	-0.06619	0.033748	-0.00326	-0.03279	-0.03463	-0.08646	-0.02474
Matrix 4 x 531	**n321**	**n322**	**n323**	**n324**	**n325**	**n326**	**n327**	**n328**
m1	0.08372	-0.10159	0.121622	-0.00336	-0.00358	0.069863	0.031731	0.092342
m2	0.080025	-0.03325	0.080444	0.043393	0.089718	-0.0461	-0.10931	-0.0345
m3	-0.02946	-0.08476	0.054173	-0.03099	-0.1144	0.00852	0.053859	-0.10151
m4	0.010234	-0.05932	0.100265	0.003759	-0.09968	0.035454	0.038016	-0.07215

Matrix 4 x 531	n329	n330	n331	n332	n333	n334	n335	n336
m1	-0.05545	0.103928	0.002505	-0.00168	-0.06443	-0.04044	0.006478	0.029935
m2	-0.08212	0.025101	0.061642	-0.02611	0.096575	-0.01014	-0.10241	0.100056
m3	-0.1041	-0.12605	0.035498	-0.00031	-0.05064	-0.01387	-0.07023	-0.03084
m4	-0.09966	-0.0088	-0.05495	-0.05639	0.07586	0.08666	-0.04576	0.042227
Matrix 4 x 531	**n337**	**n338**	**n339**	**n340**	**n341**	**n342**	**n343**	**n344**
m1	0.051905	0.014531	-0.0457	-0.0026	-0.09815	0.059736	0.056522	-0.01804
m2	-0.01896	0.045539	0.071245	-0.02863	0.05334	0.101142	-0.03966	0.024861
m3	-0.00903	-0.10084	-0.07501	0.076855	-0.03047	-0.11754	0.004593	0.061144
m4	0.048616	0.035241	-0.04729	0.052381	-0.11144	-0.04679	0.078751	0.027497
Matrix 4 x 531	**n345**	**n346**	**n347**	**n348**	**n349**	**n350**	**n351**	**n352**
m1	-0.11675	0.069511	-0.07201	0.054757	0.055422	0.086075	-0.04098	-0.00114
m2	-0.11422	-0.0015	0.006949	0.008539	0.06012	0.023196	0.056672	-0.07677
m3	0.073303	0.051936	0.107802	-0.1106	-0.02811	0.030793	-0.05717	0.079669
m4	0.000586	0.020078	0.089382	-0.06538	0.029444	0.071386	-0.09182	-0.02103
Matrix 4 x 531	**n353**	**n354**	**n355**	**n356**	**n357**	**n358**	**n359**	**n360**
m1	0.066523	-0.0984	-0.10476	0.017061	-0.00567	-0.11732	-0.02711	0.007393
m2	0.071735	0.001628	-0.09235	0.00835	0.110656	0.054126	0.040364	-0.03949
m3	0.090756	0.09376	0.062342	-0.02975	-0.07091	0.061655	-0.0132	0.056461
m4	-0.06774	0.040419	0.043923	-0.06352	0.092896	-0.05999	-0.04615	-0.03857
Matrix 4 x 531	**n361**	**n362**	**n363**	**n364**	**n365**	**n366**	**n367**	**n368**
m1	0.071106	0.083963	-0.08623	-0.03075	0.04983	0.005883	0.033733	0.065529
m2	0.110779	-0.0843	-0.02789	-0.00646	-0.0501	0.11143	-0.00131	0.018642
m3	-0.13421	0.046903	-0.03878	0.032693	-0.07737	-0.0001	-0.10663	-0.08962
m4	0.024441	-0.12099	-0.00197	-0.09644	0.020663	0.043803	-0.02729	-0.10017
Matrix 4 x 531	**n369**	**n370**	**n371**	**n372**	**n373**	**n374**	**n375**	**n376**
m1	-0.04217	-0.07614	-0.00577	-0.09872	0.041121	-0.07574	0.066316	-0.06317
m2	-0.05216	-0.11352	0.008308	-0.01386	0.10935	-0.10452	-0.00986	-0.1006
m3	0.06877	-0.11489	-0.08489	-0.10681	0.058293	-0.09426	-0.01766	-0.08505
m4	-0.08799	0.012272	-0.00925	-0.11421	0.112035	-0.04865	0.063196	-0.0366
Matrix 4 x 531	**n377**	**n378**	**n379**	**n380**	**n381**	**n382**	**n383**	**n384**
m1	-0.00093	-0.05754	0.079069	-0.04865	0.070571	0.029156	-0.13458	-0.02223
m2	-0.02586	-0.05123	0.043065	0.086403	0.032979	0.081781	0.104108	0.083427
m3	-0.02513	-0.00922	-0.05161	0.086247	0.064245	-0.00504	0.084493	0.085651
m4	0.049898	-0.03786	-0.04254	-0.0174	-0.0178	0.027923	0.080352	-0.02293
Matrix 4 x 531	**n385**	**n386**	**n387**	**n388**	**n389**	**n390**	**n391**	**n392**
m1	0.050198	-0.09864	-0.01431	-0.03288	-0.04655	-0.01415	0.04406	0.030738
m2	-0.11558	-0.06172	-0.02728	0.007465	0.104774	0.052892	0.089048	0.087776
m3	0.053148	-0.0231	-0.08261	0.022615	0.041355	-0.11124	-0.07759	-0.10481
m4	0.078818	-0.02812	-0.00279	-0.11	-0.04871	0.062736	0.082433	0.093258
Matrix 4 x 531	**n393**	**n394**	**n395**	**n396**	**n397**	**n398**	**n399**	**n400**
m1	0.026798	0.022476	-0.08999	-0.10299	0.035439	-0.09766	0.046046	-0.00077
m2	-0.00933	-0.09028	0.095266	-0.10671	0.003076	-0.07246	0.080248	-0.03985
m3	-0.03822	0.056978	0.050172	-0.06479	-0.01147	-0.08309	-0.07835	-0.06294

m4	0.092516	0.010525	0.102274	0.087416	-0.09119	0.069811	0.011197	0.051154
Matrix 4 x 531	**n401**	**n402**	**n403**	**n404**	**n405**	**n406**	**n407**	**n408**
m1	-0.04918	-0.04337	0.041772	0.055452	-0.09525	0.049452	-0.12718	0.049914
m2	0.09664	0.034503	-0.02462	-0.05768	0.063063	-0.06393	-0.09661	-0.00621
m3	0.087684	0.107393	-0.07991	0.054972	-0.05072	-0.00525	0.039494	-0.0432
m4	0.04089	0.101184	-0.08327	-0.04281	-0.04723	0.079878	0.019384	0.042018
Matrix 4 x 531	**n409**	**n410**	**n411**	**n412**	**n413**	**n414**	**n415**	**n416**
m1	-0.02596	-0.13114	-0.08631	0.11058	0.094099	-0.11122	0.038012	0.03187
m2	-0.07682	0.037133	0.103462	-0.07656	-0.02133	-0.06685	0.012984	-0.05916
m3	0.044681	0.017107	-0.02268	0.004007	-0.03598	-0.05306	-0.04455	0.107122
m4	-0.00529	0.060273	0.085782	-0.12277	0.009791	-0.02924	0.096285	0.07564
Matrix 4 x 531	**n417**	**n418**	**n419**	**n420**	**n421**	**n422**	**n423**	**n424**
m1	0.006483	-0.08043	0.092428	0.007862	0.018943	-0.09589	-0.07568	-0.06548
m2	0.014982	-0.11175	0.032431	0.083443	0.064968	0.016772	-0.02985	-0.00174
m3	0.075888	0.032933	-0.07639	-0.06595	-0.03232	0.05181	0.022884	-0.07149
m4	-0.00457	-0.10494	0.080587	0.109138	-0.10387	-0.02822	-0.04231	-0.02133
Matrix 4 x 531	**n425**	**n426**	**n427**	**n428**	**n429**	**n430**	**n431**	**n432**
m1	-0.04996	-0.06082	0.052223	0.041199	0.080744	0.069123	-0.00287	-0.07078
m2	0.001185	-0.00962	-0.12879	-0.10893	0.101865	0.056499	-0.0604	0.032991
m3	-0.07984	-0.00733	0.001303	0.112404	-0.08868	0.09652	0.004981	-0.09383
m4	-0.09893	-0.05461	-0.07209	-0.00325	-0.09823	-0.0517	0.12132	-0.05747
Matrix 4 x 531	**n433**	**n434**	**n435**	**n436**	**n437**	**n438**	**n439**	**n440**
m1	-0.11664	0.028518	0.066536	0.079536	0.037676	-0.0052	0.095472	-0.05155
m2	-0.01732	-0.05025	-0.04896	-0.0086	0.038526	0.109919	0.06901	0.09129
m3	-0.10635	-0.10816	0.001887	0.041666	-0.02691	-0.11147	-0.00733	-0.06477
m4	0.056985	0.031358	-0.11954	-0.08775	-0.10317	0.046803	-0.00013	0.048425
Matrix 4 x 531	**n441**	**n442**	**n443**	**n444**	**n445**	**n446**	**n447**	**n448**
m1	-0.02993	0.020997	-0.11302	0.112308	-0.05013	0.079966	-0.08779	0.024174
m2	-0.03819	0.070451	0.001939	0.013905	0.101294	0.043569	0.038188	0.122767
m3	-0.04296	0.069189	-0.03277	-0.00036	-0.07769	-0.03517	-0.0126	-0.00351
m4	0.084217	0.023076	0.011866	-0.10704	-0.13846	0.067574	0.049051	-0.04097
Matrix 4 x 531	**n449**	**n450**	**n451**	**n452**	**n453**	**n454**	**n455**	**n456**
m1	-0.03145	0.100081	-0.05425	-0.04879	0.071277	-0.00475	-0.09913	-0.1179
m2	0.07227	-0.10936	0.027576	0.024684	0.100626	-0.07413	0.085987	-0.11109
m3	-0.09057	0.068496	0.131721	-0.05099	-0.10543	-0.06328	0.017671	0.047401
m4	-0.10434	0.102674	0.047092	-0.01915	0.078953	-0.06904	-0.11287	-0.06874
Matrix 4 x 531	**n457**	**n458**	**n459**	**n460**	**n461**	**n462**	**n463**	**n464**
m1	-0.07346	-0.11943	-0.00139	0.013371	0.028478	-0.09997	0.001273	-0.0368
m2	0.044901	-0.02314	0.056081	-0.09733	0.020687	0.015673	-0.08804	0.008895
m3	0.100528	0.060731	-0.06092	0.047322	-0.02257	0.103978	-0.01774	0.010993
m4	-0.01226	-0.09782	0.080175	-0.00286	0.06853	-0.07129	-0.08826	-0.11341
Matrix 4 x 531	**n465**	**n466**	**n467**	**n468**	**n469**	**n470**	**n471**	**n472**
m1	0.023191	0.067895	-0.06732	-0.03942	-0.0488	-0.0427	0.005522	0.064346
m2	0.090702	-0.04621	0.078188	0.095623	0.047009	-0.10885	-0.00698	0.065309

m3	0.03296	0.096655	-0.07296	0.024075	0.107024	0.070244	-0.08287	-0.02229
m4	-0.03078	-0.09504	0.007099	-0.01021	-0.08106	-0.02351	0.034492	0.069292
Matrix 4 x 531	**n473**	**n474**	**n475**	**n476**	**n477**	**n478**	**n479**	**n480**
m1	-0.12075	0.003429	-0.09438	0.028835	0.071432	0.111402	0.005827	-0.08073
m2	0.069947	-0.06069	-0.0097	-0.01044	0.108228	-0.05241	0.116793	0.048797
m3	0.088068	0.115379	0.112978	-0.01929	0.068922	0.100303	-0.12999	0.019462
m4	-0.0523	-0.00942	-0.05621	0.070096	-0.10109	0.042094	0.057226	0.078783
Matrix 4 x 531	**n481**	**n482**	**n483**	**n484**	**n485**	**n486**	**n487**	**n488**
m1	0.094413	-0.00331	0.090773	0.032123	-0.07083	0.023002	-0.10826	0.080522
m2	-0.00492	-0.03451	-0.02571	-0.04903	0.049516	-0.02845	-0.0151	-0.08419
m3	-0.07994	-0.01876	0.005279	-0.06412	0.11351	0.042841	0.026422	0.021368
m4	0.075536	0.068557	-0.04154	-0.11768	-0.05821	-0.08689	-0.07302	-0.02112
Matrix 4 x 531	**n489**	**n490**	**n491**	**n492**	**n493**	**n494**	**n495**	**n496**
m1	-0.06077	-0.04631	0.085471	0.034978	-0.01009	-0.06614	-0.07785	0.027595
m2	-0.0119	0.048914	-0.06838	0.017336	0.082534	-0.10691	-0.00887	-0.05174
m3	0.109983	-0.08963	-0.00527	-0.13163	-0.04745	0.095385	0.109784	0.070755
m4	0.098321	0.061478	-0.01148	0.009074	0.019493	-0.08526	0.028828	-0.08992
Matrix 4 x 531	**n497**	**n498**	**n499**	**n500**	**n501**	**n502**	**n503**	**n504**
m1	-0.07377	-0.011	-0.06844	-0.03267	-0.01671	0.036256	0.066723	0.055882
m2	-0.08753	0.053462	-0.01726	0.101812	-0.07108	-0.01579	0.074697	-0.00611
m3	-0.04271	0.030961	-0.02815	0.110731	-0.03821	-0.04484	-0.09186	0.081076
m4	0.03062	-0.04898	-0.1222	-0.0846	-0.09252	-0.06428	-0.11494	-0.08144
Matrix 4 x 531	**n505**	**n506**	**n507**	**n508**	**n509**	**n510**	**n511**	**n512**
m1	-0.04409	0.08169	-0.03048	0.075052	-0.00959	0.010294	0.021876	-0.10836
m2	-0.05302	-0.06488	-0.10589	-0.01406	-0.0759	0.131829	0.082854	0.09245
m3	0.067813	-0.00575	0.028388	0.010955	0.057753	0.059249	0.010692	-0.01015
m4	0.031879	-0.06525	0.03937	-0.04259	0.092268	0.035935	0.071008	-0.09262
Matrix 4 x 531	**n513**	**n514**	**n515**	**n516**	**n517**	**n518**	**n519**	**n520**
m1	-0.13436	-0.05891	0.066258	-0.08406	-0.06279	0.027628	-0.10964	0.030052
m2	-0.06317	0.069843	0.004528	0.106586	0.042846	0.030239	0.021691	-0.1009
m3	0.050275	-0.02182	-0.05225	0.060806	0.049933	0.003095	-0.10741	-0.0928
m4	0.034642	0.015624	0.011864	-0.03174	0.091168	-0.02196	0.069589	0.036974
Matrix 4 x 531	**n521**	**n522**	**n523**	**n524**	**n525**	**n526**	**n527**	**n528**
m1	0.07585	0.048133	-0.0538	0.068045	0.083992	0.004157	-0.09077	-0.08715
m2	-0.05602	-0.07317	-0.10285	0.098969	-0.02975	-0.09568	0.023425	-0.08029
m3	0.016945	-0.05208	0.029054	0.097379	0.02719	-0.09769	-0.00071	0.035523
m4	-0.03222	0.096564	-0.05683	0.06167	-0.00763	0.0012	-0.00485	0.085826
Matrix 4 x 531	**n529**	**n530**	**n531**					
m1	-0.09673	0.026564	-0.0101					
m2	0.093332	0.035145	0.003714					
m3	0.074387	-0.00234	-0.03758					
m4	0.092099	0.04274	0.039344					